



Theses and Dissertations

2019-04-01

Design and Synthesis of Ceragenins–Cationic Steroid Antimicrobial Compounds, Structural Improvement and Synthesis of Cyclopentenone Prostaglandins and Modification and Synthesis of Derivatives of Ribityllumazines: Potential Antigens for Activation of MAIT Cells

Yubo Li
Brigham Young University

Follow this and additional works at: <https://scholarsarchive.byu.edu/etd>

BYU ScholarsArchive Citation

Li, Yubo, "Design and Synthesis of Ceragenins–Cationic Steroid Antimicrobial Compounds, Structural Improvement and Synthesis of Cyclopentenone Prostaglandins and Modification and Synthesis of Derivatives of Ribityllumazines: Potential Antigens for Activation of MAIT Cells" (2019). *Theses and Dissertations*. 8283.

<https://scholarsarchive.byu.edu/etd/8283>

This Dissertation is brought to you for free and open access by BYU ScholarsArchive. It has been accepted for inclusion in Theses and Dissertations by an authorized administrator of BYU ScholarsArchive. For more information, please contact scholarsarchive@byu.edu, ellen_amatangelo@byu.edu.

Design and Synthesis of Ceragenins–Cationic Steroid Antimicrobial Compounds,
Structural Improvement and Synthesis of Cyclopentenone Prostaglandins
and Modification and Synthesis of Derivatives of Ribityllumazines:
Potential Antigens for Activation of MAIT Cells

Yubo Li

A dissertation submitted to the faculty of
Brigham Young University
in partial fulfillment of the requirements for the degree of

Doctor of Philosophy

Paul Savage, Chair
Steven Castle
Matt Peterson
Merritt Andrus
Scott Burt

Department of Chemistry and Biochemistry
Brigham Young University

Copyright © 2019 Yubo Li

All Rights Reserved

ABSTRACT

Design and Synthesis of Ceragenins–Cationic Steroid Antimicrobial Compounds, Structural Improvement and Synthesis of Cyclopentenone Prostaglandins and Modification and Synthesis of Derivatives of Ribityllumazines: Potential Antigens for Activation of MAIT Cells

Yubo Li

Department of Chemistry and Biochemistry, BYU
Doctor of Philosophy

Antimicrobial peptides (AMPs) are ubiquitous and display broad-spectrum antimicrobial activity that can control bacterial colonization of surfaces. Ceragenins are small-molecule mimics of AMPs and have several advantages over AMPs, including cost of manufacture and stability. A ceragenin, CSA-120, modified with an acrylamide group was directly incorporated into fluoropolymer coatings as a means of inhibiting bacterial biofilm formation. The ceragenin-containing coatings displayed improved performance. By conjugating a copper chelating group to the ceragenin, chelation of ^{64}Cu by the conjugate was effective and provided a stable complex that allowed *in vivo* imaging. This conjugate may provide a means of identifying infection sites in patients presenting general signs of infection without localized symptoms. A combination nanoparticle comprised of a maghemite core for enhanced T2 MRI contrast diagnostics, a colloidal silver shell acting as an antimicrobial and therapeutic vehicle, and a ceragenin (CSA-124) surfactant providing microbial adhesion was synthesized and characterized by multiple methods. Silver nanoparticles conjugated with ceragenin, CSA-124, as a potential Gram-positiveselective antimicrobial were synthesized and termed as CSA-SNPs. Herein, CSA-SNPs are characterized using multiple methods and the antimicrobial properties are determined through minimum inhibitory concentration/minimum bactericidal concentration (MIC/MBC) and time-kill studies.

Prostanoids are a natural subclass of eicosanoids generated mainly from metabolic oxidation of arachidonic acid. Cyclopentenone prostaglandins (cyPGs) contain a highly reactive α,β -unsaturated carbonyl group in their cyclopentenone ring and possess three main potentially therapeutic properties: anti-inflammatory, antiproliferative and antiviral. We designed and synthesized EC and its derivatives in reducing secretion of pro-inflammatory cytokines IL-6 and IL-12. Mucosal-Associated Invariant T (MAIT) Cells are unique innate-like T cells and play a key role in host defense against bacterial and fungal infection as well as in human autoimmune diseases. The MAIT cells are activated through T-cell receptor $\alpha\beta$ chain (TCR- $\alpha\beta$) binding with the MR1-ligand, which is vitamin B metabolites presented on MR1. Ribityllumazines, one of important MR1-ligand was synthesized in my study.

Keywords: antimicrobial peptides, ceragenin, cationic steroid antimicrobial, nanoparticle, cyclopentenone prostaglandins, ribityllumazines.

ACKNOWLEDGEMENTS

First and foremost, I want to acknowledgement my advisor, Dr. Savage, for his serious and patient direction and I appreciate everything he did for me. Since day one of my doctoral study, Dr. Savage took every opportunity to help me develop the proper attitude and vision toward science, which I think is extremely important for a Ph.D. student. Additionally, Dr. Savage trained me how to read, write, think and present my work. Also, Dr. Savage is the best teacher I have ever observed and I am grateful to have had the opportunity to learn from his teaching style.

Next I would like to thank the committee members Dr. Merritt B. Andrus, Dr. Matt A. Peterson, Dr. Steven L. Castle, and Dr. Scott R. Burt. Each gave me nice suggestions on my research plan, research proposals and dissertation. They are always willing to help and teach me whenever I come to their offices. I am grateful for everything they have ever done for me.

I also want to acknowledge our lab's role at teaching me the essential tools of organic chemistry. Dr. Deng and Dr. Feng, especially, have been excellent mentors. I have gotten to know a lot of synthetic knowledge, skills and experiences which I could not learn from text books. Along with them, I also want to thank Dr. Anderson, Dr. Gu, Sara Mata, Tianyao Meng and many others have helped me along the way.

I also want to acknowledge my wife and my family for their support all the time. During the course of my graduate study I endured many really difficult times, but because of you my efforts and insistence are especially meaningful.

Table of Contents

Appendix.....	viii
Chapter 1.....	1
Design and Synthesis of Ceragenins--Cationic Steroid Antimicrobial Compounds.....	1
1.1 Introduction.....	1
1.1.1 Origin of Ceragenins.....	1
1.1.2 Design of Ceragenins.....	3
1.1.3 Development and Applications of Ceragenins	5
1.1.4 References.....	9
1.2 Ceragenin-Containing Coatings for Use in Inhibiting marine Biofouling.....	14
1.2.1 Introduction.....	14
1.2.2 Materials and Methods.....	16
1.2.3 Synthesis of CSA-120.....	17
1.2.4 Application of Coatings	22
1.2.5 Biofouling Testing	23
1.2.6 Methods of Analysis	24
1.2.7 Results and Discussion	25
1.2.8 Conclusions.....	31

1.2.9 Experimental Section.....	33
1.2.10 References.....	45
1.3 Translation of Ceragenin Affinity for Bacteria to an Imaging Reagent for Infection.....	48
1.3.1 Introduction.....	48
1.3.2 Synthesis of Ceragenin-NOTA Conjugates and Structural Variants	50
1.3.3 Results and Discussion	52
1.3.4 Conclusions.....	56
1.3.5 Experiment Section.....	57
1.3.6 References.....	71
1.4 Maghemite, Silver, Ceragenin Conjugate Particles for Selective Binding and Contrast of Bacteria.....	74
1.4.1 Introduction.....	74
1.4.2 Synthesis of CSA-124.....	77
1.4.3 Synthesis, characteristic and bioactivity of DANs	78
1.4.4 Results and discussion	79
1.4.5 Conclusions.....	90
1.4.6 Experiment Section.....	90
1.4.7 References.....	93
1.5 Ceragenin mediated selectivity of Antimicrobial silver nanoparticles	95
1.5.1 Introduction.....	95

1.5.2 Synthesis of CSA. 124	97
1.5.3 Characteristic and Bioactivity of CSA-SNP.....	97
1.5.4 Results and Discussion	97
1.5.5 Conclusions.....	106
1.5.6 References.....	108
Chapter 2.....	114
Structural Improvement and Synthesis of Cyclopentenone Prostaglandins	114
2.1 Introduction.....	114
2.1.1 Prostaglandins.....	114
2.1.2 Functions of Cyclopentenone Prostaglandins.....	117
2.1.3 Regulation of Inflammation	117
2.1.4 Antiproliferative Activity and Antitumoral Activity	118
2.1.5 Antiviral Properties	118
2.1.6 Synthesis of Cyclopentenone Prostaglandins	119
2.2 Synthesis and Modification of Cyclopentenone Prostaglandins.....	120
2.2.1 The Target Cyclopentenone Prostaglandin to Synthesize and Modify	120
2.2.2 Synthesis of EC.....	120
2.2.3 Modification and Synthesis of Cyclopentenone Prostaglandin.....	123
2.3 Study of Bioactivities of EC and Its Derivatives in Reducing Secretion of Pro-inflammatory Cytokines IL-6 and IL-12	126

2.4 Results and Discussion	127
2.5 Conclusions.....	128
2.6 Experiment Section.....	128
2.7 References.....	146
Chapter 3.....	151
Modification and Synthesis of Derivatives of Ribityllumazines: Potential Antigens for Activation of MAIT cells.....	151
3.1 Introduction.....	151
3.1.1 Mucosal-Associated Invariant T (MAIT) Cells.....	151
3.1.2 Activation of MAIT cells.....	152
3.1.3 MR1–Antigen Structures	154
3.1.4 Synthesis of Ligands of MR1.....	157
3.2 Synthesis of Ligands of MR1.....	158
3.3 Results.....	160
3.4 Collusions	160
3.5 Experiment Section.....	160
3.6 References.....	168

Appendix:

A	List of Abbreviations	172
B	NMR spectra	173

Chapter 1

Design and Synthesis of Ceragenins--Cationic Steroid Antimicrobial Compounds

1.1 Introduction

1.1.1 Origin of Ceragenins

Infectious diseases are a continuous challenge to higher organisms. Antimicrobial peptides (AMPs), small peptides isolated from organisms ranging from insects to plants to mammals, are one of the primary means of protecting their hosts from multiple kinds of microorganisms. AMPs inhibit biofilm formation, display a wide antimicrobial spectrum, and play an important position in the innate immune system of multicellular organisms.¹⁻⁵ Human antimicrobial cathelicidin LL37 and magainins, from amphibians are the best-studied endogenous antimicrobial peptides.

AMPs share common features: small size and either linear or cyclic structure. A linear structure includes amphipathic α -helices while a cyclic structure contains β -sheet secondary structure with one or more disulfide bridges.⁶ They demonstrate the same structural properties, with cationic and facially amphiphilic morphology, as shown in Figure 1.1. One face presents cationic residues and the other face hydrophobic groups.⁷

Researchers have studied the mechanisms of action of AMPs. Two basic types of mechanisms have been proposed. One is a disruptive mechanism, embodied in membrane lysis, and the other one is undisruptive mechanism, associated with intracellular targets.^{8,9} In the disruptive mechanism, one basic important role of AMPs is their interaction with cytoplasmic membranes via electrostatic interactions.¹⁰ Several permeabilization mechanisms have been proposed to explain their disruption activities, including the toroidal model, the carpet model, the aggregate model, the barrel model and so on.¹¹ A description of the “carpet model” as an example to

demonstrate how cathelicidins or magainins traverse the membranes of Gram-negative bacteria. There are 3 layers in Gram-negative bacterial membranes: an outer membrane (OM) with a lipid bilayer, made up mostly of lipopolysaccharide (LPS) interlocked with teichoic acid; a peptidoglycan cell wall; an inner membrane (cytoplasmic membrane), made up of phospholipid bilayer. The first important activity is disruption of the OM. Lipopolysaccharide (LPS), the primary component of the OM (which has a major role in protection against the environment), is composed of three main regions: O-antigen, core polysaccharide and lipid A. As shown in Figure 1.2, the cationic face of AMPs binds to the negative membrane surface by electrostatic interactions. When the concentration of the AMPs is increased to the critical point, the peptides cause membrane reorienting and depolarize the membrane, which is sufficient to cause cell death.

However, AMPs also have some serious drawbacks that limit their applications in therapeutic areas. The complex structure and large size of AMPs make them difficult to isolate and prepare and result in a high manufacturing cost. They are salt-sensitive and susceptible to degradation in a short time when met with proteases.^{12,13} Because of AMPs' limitations, researchers designed and synthesized novel compounds to mimic the activities of antibacterial peptides. Ceragenins are one kind of these non-peptide mimics.

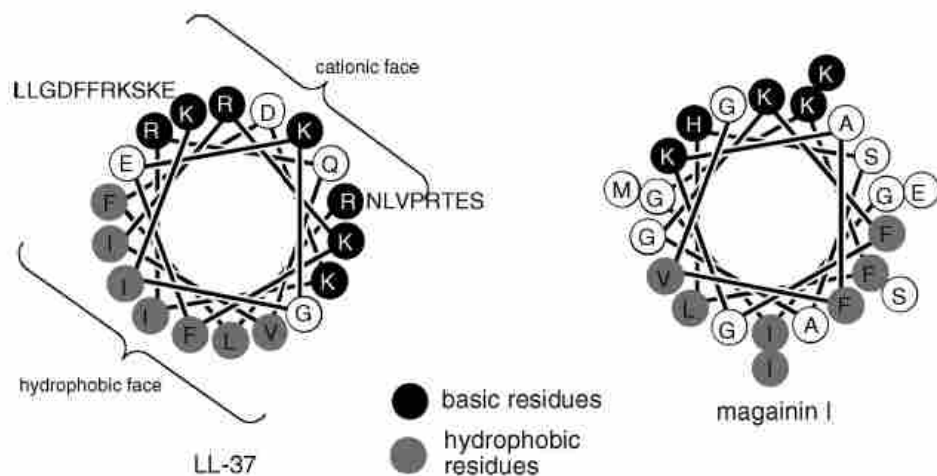


Figure 1.1 Helix-wheel representations of antimicrobial peptides cathelicidin LL-37 and magainin I showing facial amphiphilicity (Adapted from ref [23]).

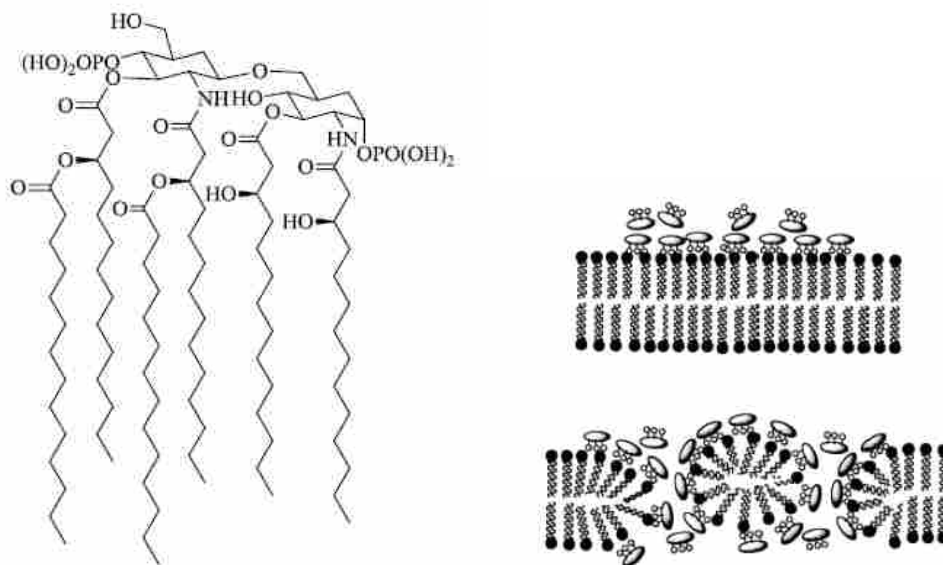


Figure 1.2 One typical structure of LPS (lipid A) and “Carpet model” of bactericidal activity of AMPs.

1.1.2 Design of Ceragenins

Early in the research with ceragenins, Li et al. designed a series of new sensitizers of Gram-negative bacteria based on the consideration of bactericidal behavior of *polymyxin B* and its

derivatives. They synthesized several series of cholic acid derivatives, such as amine- and guanidine-functionalized derivatives, and found these compounds had good antibacterial activity against Gram-negative and Gram-positive bacteria, and also had the ability to inhibit bacterial growth.¹⁴⁻¹⁹ Later, these series of cholic acid derivatives were termed cationic steroid antimicrobials (CSAs) or ceragenins.²⁰⁻²³

Shown in Figure 1.3, ceragenins, cationic steroid antimicrobials (CSAs), are derived from cholic acid, which is inherently facially amphiphilic with three hydroxyl groups on one face of the steroid. To mimic the bactericidal behavior of AMPs, amine groups are covalently attached through the hydroxyl groups on the cholic acid. As a result, the ceragenins have a net cationic charge and can electrostatically attract negatively charged bacterial membranes. They also have a hydrophobic face, giving them their facially amphiphilic character. Position C-24 is also very important and the groups attached at this point substantially influence CSAs' bactericidal activity against Gram-negative bacteria. Ceragenins are not peptide based, so they are not substrates of proteases and are therefore very stable under physiological conditions. Furthermore, their structures are simple and easily prepared at a large scale.

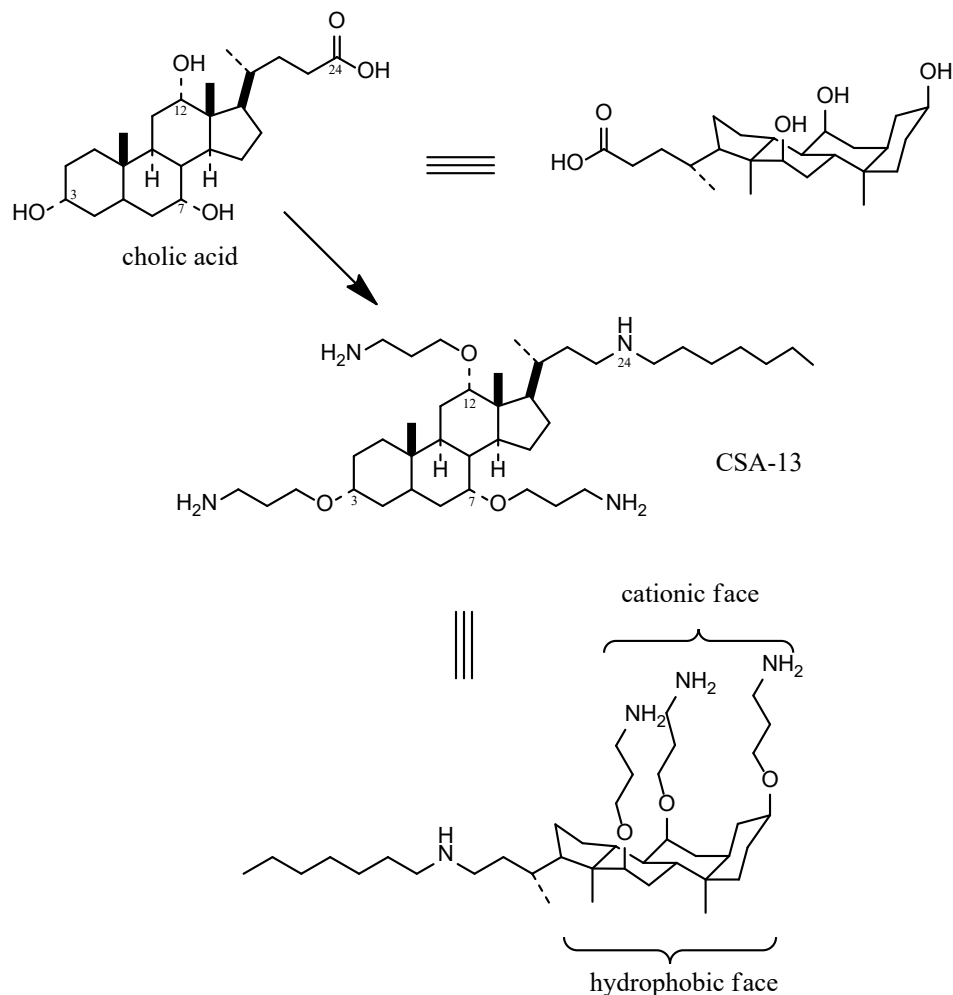


Figure 1.3 Structures of cholic acid and CSA-13 showing facial amphiphilicity character of CSAs.

1.1.3 Development and Applications of Ceragenins

More than one hundred CSAs have been prepared so far. CSAs have demonstrated broad-spectrum activity against viruses, multidrug-resistant bacteria, fungi and parasites, and have the potential ability to kill both Gram-negative and Gram-positive organisms. CSAs can also permeabilize the outer membrane of Gram-negative bacteria. The antibacterial activities of these agents are typically characterized via measurement of minimum inhibition concentrations (MICs) and minimum bactericidal concentrations (MBCs). Membrane selectivity is determined by MIC

and minimum hemolytic concentration (MHC). Many studies have been carried out to investigate the antibacterial activities of these ceragenins. For example, Ding et al. studied CSAs' cell selectivity and their association with lipid A by appending a fluorophore on these antibiotics. The experimental results showed that CSAs have higher selectivity for *Escherichia coli* (Gram-negative) over both *Staphylococcus aureus* (Gram-positive bacteria) and Chinese hamster ovary (eukaryotic cell) membranes. The results also suggested that CSAs with higher affinity for lipid A display greater antibacterial activity and greater cell selectivity.²⁴

Paying attention to the issue of increasing multidrug resistance in microbes, Chin et al. compared the antibacterial activities of CSA-8 and CSA-13 to those of daptomycin, linezolid, and vancomycin against clinical isolates of VISA (vancomycin-intermediate *S. aureus*), hVISA (heterogeneous VISA), and VRSA (vancomycin-resistant *S. aureus*). Their results demonstrated that ceragenins have therapeutic implications for infections caused by strains of VISA and hVISA.²⁵ Leszczyńska et al. demonstrated the anti-*Helicobacter pylori* potential of ceragenin CSA-13, as it yielded much lower MBC values than those of cathelicidin LL-37 and WLBU2 (synthetic analog of LL-37). Furthermore, at low pH, only CSA-13 kept its antibacterial activity.²⁶

To evaluate the potential of ceragenins as antiviral agents and antimicrobial agents, Howell et al. demonstrated the CSA-13 had antiviral activity against vaccinia virus (VV) under *in vitro* or *in vivo* models and protected the KC cells against VV-mediated cell death. Therefore, ceragenins may be a potential intervention for disseminated VV skin infection.²⁷ Isogai et al. confirmed that CSA-13 has antimicrobial activities against oral pathogens, including cariogenic and periodontopathic bacteria.²⁸ Leszczyńska et al. also demonstrated the ceragenins CSA-13, CSA-90 and CSA-92 have antibacterial activity against oral and upper respiratory tract bacteria

comparable to that of LL-37 and exhibit less resistance.²⁹ Durnas et al. demonstrated that when compared with LL-37, ceragenins, including CSA-13, CSA-131 and CSA-192, have better fungicidal activity against four fluconazole-resistant *Candida* strains and showed an increased ability to kill DNA-induced *Candida* biofilm.³⁰

To confirm the utility of ceragenins on medical devices, due to their ability to prevent biofilm formation, Williams et al. investigated the *in vivo* efficacy of a silicon-ceragenin coating to prevent biofilm implant-related infections and the results indicated that CSA-13 had the ability to prevent biofilm implant-related osteomyelitis, which may indicate promise for clinical application of ceragenins.³¹ Zahoor et al. illustrated that when another ceragenin, CSA-107, was labeled with ^{99m}Tc via transchelating agent Na-K tartrate, it showed good human serum stability and binding activity with *S. aureus* bacteria. This result makes CSAs promising in radiopharmaceuticals for infection imaging.³² Hoppens et al. successfully synthesized novel nanoparticles with an iron oxide core, reduced silver shell and CSA-124 as surfactant. Their characterization results suggest this nanoparticle could be a good potential candidate for diagnostic use.³³ Niemirowicz et al. prepared CSA-13-coated magnetic nanoparticles (MNP-CSA-13) and characterized their physicochemical properties. They further demonstrated MNP-CSA-13 could increase antimicrobial properties and decrease hemolytic activity. These results implied a promising future of ceragenins' applications in a drug delivery system.³⁴ To further explore MNP-ceragenins' applications, they illustrated the combination of core-shell MNPs with membrane-active compounds, including ceragenins and other classical antibiotics, to show a novel method to treat and overcome infections caused by multidrug resistant (MDR) pathogens.³⁵

To evaluate the safety of ceragenins, Leszczynska et al. illustrated that although CSA-13 would cause lysis of erythrocytes at high concentration, when CSA-13 was mixed with pluronic F-127, the hemolytic activity of CSA-13 decreased in the presence of pluronic F-127. This finding suggests there is a useful way to reduce ceragenins' toxicity.³⁶ They further demonstrated the mixture was also a good solution for the toxicity of CSA-13 to eukaryotic cells.³⁷

1.1.4 References

1. Lehrer, R. I.; Ganz, T. Antimicrobial peptides in mammalian and insect host defense, *Curr. Opin. Immunol.* **1999**, *11*, 23–27.
2. Marr, A. K.; Gooderham, W. J. Hancock REW: Antibacterial peptides for therapeutic use: obstacles and realistic outlook. *Curr. Opin. Pharmacol.* **2006**, *6*, 468-472.
3. Overhage, J.; Campisano, A.; Bains, M.; Torfs, ECW.; Rehm, B. H .A. Hancock REW: Human host defense peptide LL-37 prevents bacterial biofilm formation. *Infect Immun.* **2008**, *76*, 4176-4182.
4. Nijnik, A.; Hancock. *REW*: The roles of cathelicidin LL-37 in immune defences and novel clinical applications. *Curr Opin Hematol.* **2009**, *16*, 41-47.
5. Gryllos, I.; Tran-Winkler, H. J.; Cheng, M-F.; Chung, H. Bolcome.; Lehrer, R. I.; Wessels. MR: Induction of group A Streptococcus virulence by a human antimicrobial peptide. *Proc Natl Acad Sci U S A.* **2008**, *105*, 16755-16760.
6. Boman, H.G. Peptide antibiotics and their role in innate immunity, *Annu. Rev. Immunol.* **1995**, *13*, 61–92.
7. Giuliani, A.; Rinaldi, A. C. Antimicrobial peptides: Methods and protocols (Methods in molecular biology), Humana Press, New York, **2010**, 618-625.
8. Malanovic, N.; Lohner, K. Antimicrobial peptides targeting Gram-positive bacteria. *Pharmaceuticals* **2016**, *9*, 59-62.
9. Cunha, D.; Nicolau, B.; Cobacho, N. B.; Viana, J.; Lima, Loiane.; Sampaio, A.; Kamila, B. O.; Dohms, S. M.; Ferreira, A.C. R.; Cesar, de la Fuente-Nunez.; Costa, F.; Franco, O. L.; Dias, S. C. The next generation of antimicrobial peptides (AMPs) as molecular therapeutic tools for

the treatment of diseases with social and economic impacts. *Drug Discovery Today*. **2017**, *22*, 234-248.

10. Epanand, R. M.; Vogel, H. J. Diversity of antimicrobial peptides and their mechanisms of action, *Biochim. Biophys. Acta*. **1999**, *1462*, 11–28.

11. Nguyen, L.T.; et al. The expanding scope of antimicrobial peptide structures and their modes of action. *Trends Biotechnol.* **2011**, *29*, 464–472.

12. Hof, W. V.; Veerman, E. C.; Helmerhorst, E. J.; Amerongen, A. V. Antimicrobial peptides: properties and applicability. *Biol Chem*. **2001**, *382*, 597–619.

13. Jenssen, H.; Hamill, P. Hancock. *REW*. Peptide antimicrobial agents. *Clin. Microbiol. Rev.* **2006**, *19*, 491–511.

14. Li, C.; Peters, A. S.; Meredith, E. L.; Allman, G. H.; Savage, P. B. Design and synthesis of potent sensitizers of Gram-negative bacteria based on a cholic acid scaffolding. *J. Am. Chem. Soc.* **1998**, *120*, 2961–2962.

15. Li, C.; Lewis, M. R.; Gilbert, A. B.; Noel, M. D.; Scoville, D. H.; Allman, G. W.; Savage, P. B. Antimicrobial activities of amine- and guanidine-functionalized cholic acid derivatives. *Antimicrob. Agents Chemother.* **1999**, *43*, 1347–1351.

16. Li, C.; Budge, L. P.; Driscoll, C. D.; Willardson, B. M.; Allman, G. W.; Savage, P. B. Incremental conversion of outer-membrane permeabilizers into potent antibiotics for Gram-negative bacteria. *J. Am. Chem. Soc.* **1999**, *121*, 931–940.

17. Rehman, A., Li, C., Budge, L.P., Street, S.E. and Savage, P.B. Preparation of amino acid-appended cholic acid derivatives as sensitizers of Gram-negative bacteria. *Tetrahedron Lett.* **1999**, *40*, 1865-1869.

18. Guan, Q.; Schmidt, E.J.; Boswell, S.R.; Li, C.; Allman, G.W. and Savage, P.B. Preparation and characterization of cholic acid-derived antimicrobial agents with controlled stabilities. *Org. Lett.* **2000**, *2*, 2837-2840.
19. Schmidt, E. J.; Boswell, S. R.; Walsh, J. P.; Schellenberg, M. M.; Winter, T. W.; Li, C.; Allman, G. W.; Savage, P. B. Activities of cholic acid-derived antimicrobial agents against multidrug-resistant bacteria. *J. Antimicrob. Chemother.* **2001**, *47*, 671–674.
20. Savage, P. B.; Li, C.; Taotafa, U.; Ding, B.; Guan, Q. Antibacterial properties of cationic steroid antibiotics. *FEMS Lett.* **2002**, *217*, 1–7.
21. Savage, P. B. Cationic steroid antibiotics. *Curr. Med. Chem. Anti-Infective Agents* **2002**, *3*, 293–304.
22. Savage, P. B. Design, synthesis and characterization of cationic peptide and steroid antibiotics. *Eur. J. Org. Chem.* **2002**, 759–768.
23. Lai, X.; Feng, Y.; Pollard J.; Chin, J. N.; Rybak, M. J.; Bucki, R.; Epand R. F.; Epand, R. M.; Savage, P. B. *Accounts Chem. Res.* **2008**, *41*, 1233-1240.
24. Ding, B.; Yin, N.; Liu, Y.; Cardenas-Garcia, J.; Evanson, R.; Orsak, R.; Fan, M.; Turin, G.; Savage, P. B. Origins of cell selectivity of cationic steroid antibiotics. *J. Am. Chem. Soc.* **2004**, *126*, 13642–13648.
25. Chin, J. N.; Rybak, M. J.; Cheung, C. M.; Savage, P. B. Antimicrobial activities of ceragenins against clinical isolates of resistant *Staphylococcus aureus*. *Antimicrob. Agents. Chemother.* **2007**, *51*, 1268–1273.
26. Leszczyńska, K.; Namiot, A.; Fein, DE.; Wen, Q.; Namiot, Z.; Savage, P.B.; Diamond, S.; Janmey, P.A.; Bucki, R. Bactericidal activities of the cationic steroid CSA-13 and the

- cathelicidin peptide LL-37 against *Helicobacter pylori* in simulated gastric juice. *BMC Microbiol.* **2009**, *9*, 187-197.
27. Howell, M. D.; Streib, J. E.; Kim, B. E.; Lesley, L. J.; Dunlap, A. P.; Geng, D. et al. Ceragenins: a class of antiviral compounds to treat orthopox infections. *J. Invest. Dermatol.* **2009**, *129*, 2668–75.
28. Isogai, E.; Isogai, H.; Takahashi, K.; Okumura, K.; Savage, P. B. Ceragenin CSA-13 exhibits antimicrobial activity against cariogenic and periodontopathic bacteria. *Oral Microbiol Immunol.* **2009**, *24*, 170-172.
29. Leszczynska, K.; Namiot, D.; Byfield, F. J.; Cruz, K.; Zendzian-Piotrowska, M.; Fein, D. E.; et al. Antibacterial activity of the human host defense peptide LL-37 and selected synthetic cationic lipids against bacteria associated with oral and upper respiratory tract infections. *J Antimicrob Chemother.* **2013**; *68(3)*:610–618.
30. Durnaś, B.; Wnorowska, U.; Pogoda, K.; Deptuła, P.; Wątek, M.; Piktel, E.; Głuszek, S.; Gu, X.; Savage, P. B.; Niemirowicz, K.; Bucki, R. Candidacidal activity of selected ceragenins and human cathelicidin LL-37 in experimental settings mimicking infection Sites. *PLoS One.* **2016**, *11*, 157242-157262.
31. Williams, D.L.; Haymond, B. S.; Beck, J. P.; Savage, P. B.; et al. In vivo efficacy of a silicone–cationic steroid antimicrobial coating to prevent implant-related infection. *Biomaterials* **2012**, *33*, 8641-8656.
32. Zahoor, R.; Roohi, S.; Ahmad, M.; et al. Synthesis of ^{99m}Tc-cationic steroid antimicrobial-107 and in vitro evaluation. *J Radioanal Nucl Chem* **2013**, *295*, 841-844.

33. Hayes, M. A.; Wheeler, Z. E. W.; Qureshi, A. T.; et al. Maghemite, silver, ceragenin conjugate particles for selective binding and contrast of bacteria. *J. Colloid. Interf. Sci.* **2014**, *413*, 167-174.
34. Niemirowicz, K.; Surel, U.; Wilczewska, A. Z.; et al. Bactericidal activity and biocompatibility of ceragenin-coated magnetic nanoparticles. *J. Nanobiotechno.* **2015**, *13*, 32-43.
35. Niemirowicz, K.; Piktel, E.; Wilczewska, A. Z.; et al. core-shell magnetic nanoparticles display synergistic antibacterial effects against *Pseudomonas aeruginosa* and *Staphylococcus aureus* when combined with cathelicidin ll-37 or selected ceragenins. *Int J. Nanomed.* **2016**, *11*, 5443-5455.
36. Leszczyńska, K.; Namiot, A.; Cruz, K.; et al. Potential of ceragenin CSA-13 and its mixture with pluronic F-127 as treatment of topical bacterial infections. *J. Appl. Microbio.* **2011**, *110*, 229-238.
37. Nagant, C.; Savage, P. B.; Dehaye, J. P. Effect of pluronic acid F-127 on the toxicity towards eukaryotic cells of CSA-13, a cationic steroid analogue of antimicrobial peptides. *J. Appl. Microbio.* **2012**, *112*, 1173-1183.

1.2 Ceragenin-Containing Coatings for Use in Inhibiting Marine Biofouling

1.2.1 Introduction

The economic impacts of marine biofouling are well established (Yebra et al. 2004; Callow and Callow 2011) and with increasing efforts to harness marine hydrokinetic (MHK) energy through wave motion and tidal flows, these impacts are likely to grow. Marine biofouling occurs in stages, with formation of bacterial biofilms on surfaces believed to be a key initial step leading to biofouling with higher organisms (Dang and Lovell 2016). Controlled release of cytotoxic metals proved to be successful in controlling biofouling; however, use of these metals has been discontinued due to concerns over effects on the marine environment (Callow and Callow 2011). MHK energy deployment projects must also adhere to these environmental policies, thus there is a need to investigate metal free antifouling coatings for these renewable energy technologies. More recent efforts have turned to naturally-occurring biocides as a means of controlling biofouling initiated by bacterial biofilm formation (Trepas et al. 2015 and references cited therein). In general, efforts have been placed on incorporation of these biocides into coatings from which the biocides leach over time.

The activities of antimicrobial peptides (AMPs) are one of the most common means by which bacterial growth is controlled by higher organisms, and AMPs are found in organisms ranging from mammals to plants (Lai and Gallo 2009). The diversity of their primary sequences argues that they have evolved independently at least dozens of times. Due to their bactericidal activity and their suggested unlikelihood of engendering bacterial resistance (Mangoni et al. 2016), substantial efforts have been made to develop AMPs for clinical use. They have also been applied in antimicrobial coatings, demonstrating that AMPs retain antibacterial activities after covalent attachment to surfaces (Gao et al. 2011). It has also been suggested that AMPs could

find use in preventing marine biofouling (Trepos et al. 2015). However, there are impediments to the use of AMPs for many applications, including their relatively high cost of manufacturing relative to small molecules and their susceptibility to hydrolysis by ubiquitous proteases (Afacan et al. 2012).

We have developed small molecules that mimic the antibacterial activities of AMPs, termed ceragenins (Lai et al. 2008). These molecules are based on a bile acid scaffolding, and due to their simplicity, they can be produced at large scale. Also because they are not peptide based, ceragenins are not substrates for proteases. Nevertheless, ceragenins retain the broad-spectrum antibacterial activities of AMPs and are active against Gram-negative and positive bacteria. They selectively target bacterial membranes, causing depolarization and cell death (Epanand et al. 2010 and Ding et al. 2004).

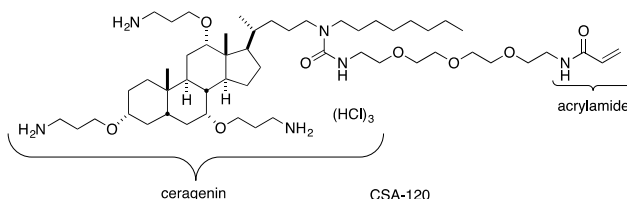


Figure 1.2.1 Structure of Ceragenin CSA-120

Recently, we demonstrated that ceragenins, even when covalently attached to a polymer, are capable of preventing bacterial colonization of surfaces (Gu et al. 2013). Immobilization required appending the ceragenin with an acrylamide group to allow radical polymerization (e.g., CSA-120, Figure 1.2.1). A short tether was used between the acrylamide group and the ceragenin to allow flexibility with how the ceragenin interacts with microbial membranes.

Because many coating materials polymerize via radical-based reactions, CSA-120 is well suited for incorporation into multiple different types of coatings, including those designed to

inhibit biofouling in marine environments. The fluoropolymer-based coating IS970 (International InterSleek 970) is well recognized as a fouling-release coating (Watson et al. 2015), and we reasoned that the combination of fouling-release by IS970 with the antibiofilm activities of CSA-120 would provide a novel and effective coating for prevention of biofouling. A key aspect of this combination is that the ceragenin is covalently (i.e., permanently) attached to the coating, so material is not leaching into the environment.

To test this combination, we incorporated CSA-120 at two concentrations into commercially available Intersleek formulation IS970 and coated primed aluminum coupons. Coated coupons were tested for biofilm formation and compared to the parent coating in open water testing at Pacific Northwest National Laboratory's (PNNL) Marine Sciences Laboratory under low and high velocity flows. Coating of the coupons with the combination coating (IS970 and CSA-120) resulted in a decrease in biofouling relative to controls, and we attribute this to inhibition of initial bacterial biofilm formation on the coating.

1.2.2 Materials and Methods

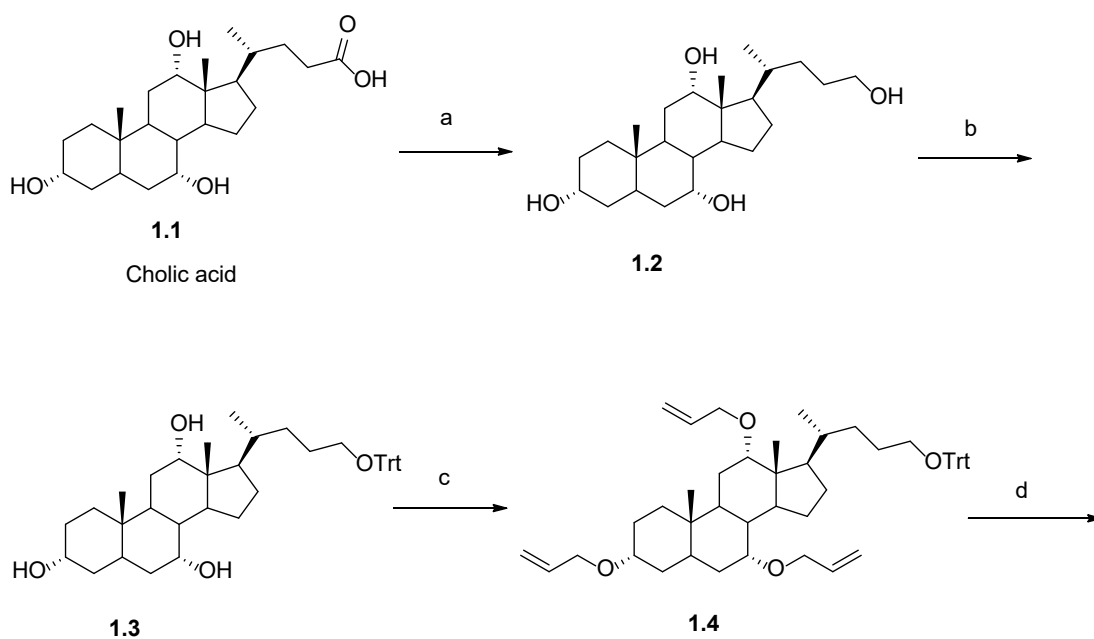
Chemical reagents and materials

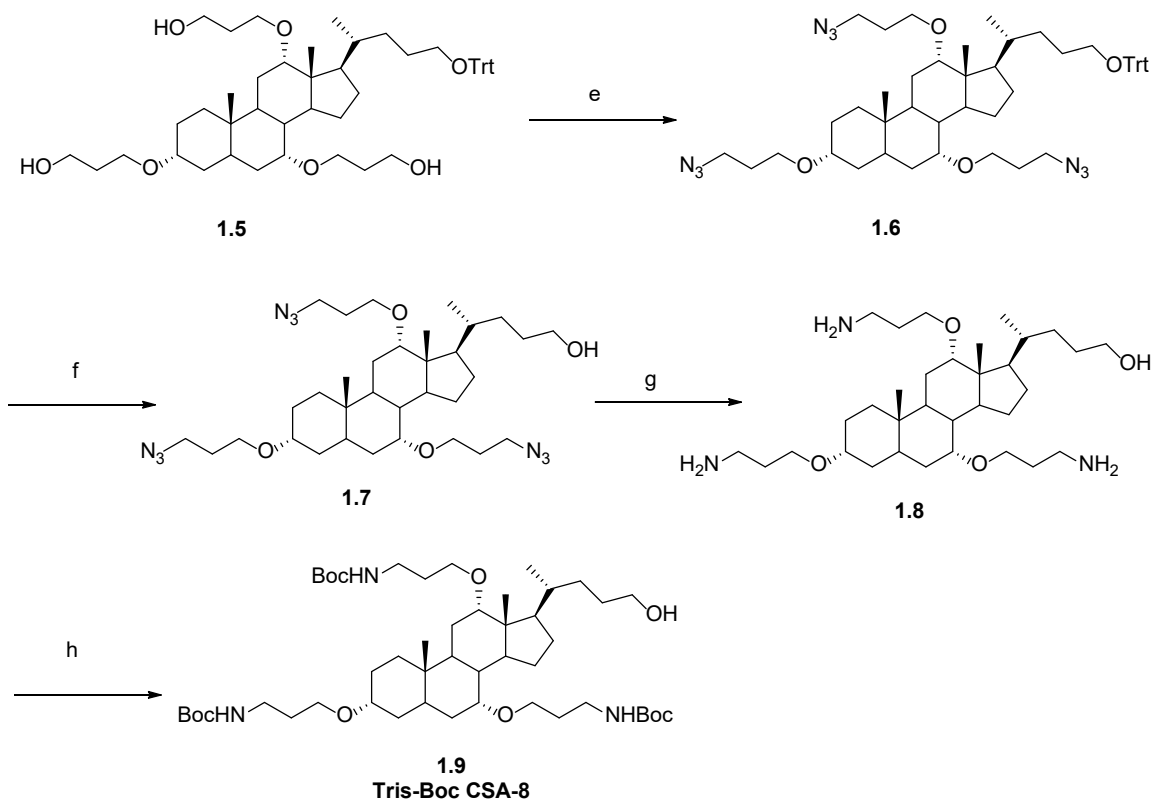
Intergard®264, Intersleek® 900 (IS 900) and IS730 coating systems were purchased from International Paint, Houston, TX, USA. Aluminum test coupons, painted on all sides with an epoxy-based primer (Intergard 264), were used as substrates for the coatings. Coupons were 1" x 1", 3" x 3" and 8" x 8" squares. Coupons had holes drilled in each corner for use in mounting the coupons during testing.

1.2.3 Synthesis of CSA-120

Synthesis of Tris-Boc CSA-8

After a few decade studies for CSAs in our group, we developed a general effective and efficient synthetic pathway to prepare all CSAs. Among these intermediates, Tris-Boc CSA.8 played key role in whole synthetic pattern of various CSAs including CSA-120. The scheme 1.2.1 presents synthetic route for Tris-Boc CSA.8.



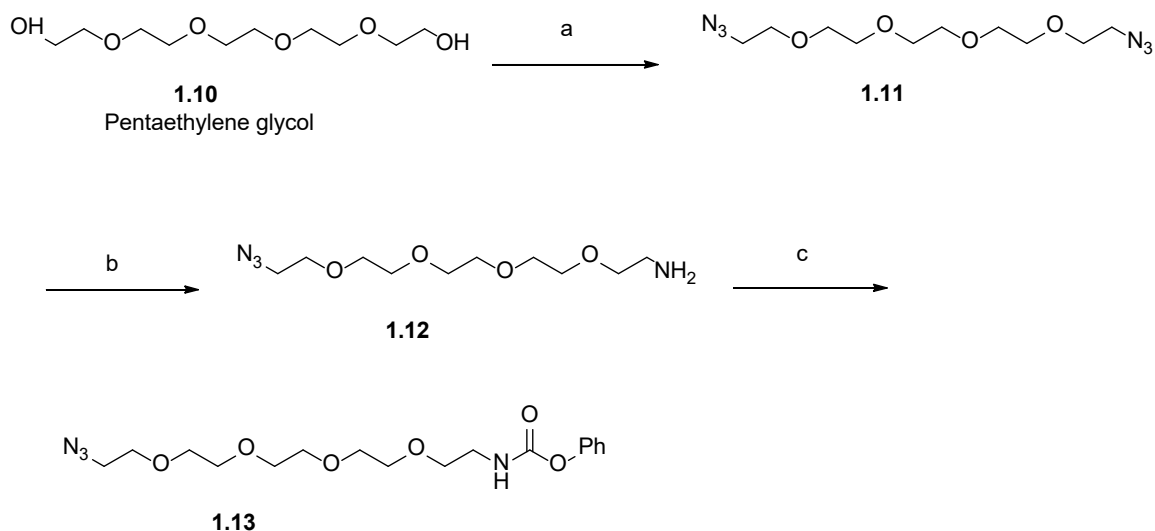


Scheme 1.2.1 Synthesis of Tris-Boc CSA-8

Reagents: a) LAH, THF, reflux, 93%; b) Triphenylmethyl chloride, pyridine, Acetonitrile, 70%; c) allyl bromide, KHMDS, THF, 81%; d) 9-BBN, THF, r.t, NaOH, H₂O₂, 50%; e) i) MsCl, TEA, DCM; ii) NaN₃, DMSO, 80 °C, 92%; f) p-TSA, MeOH/DCM(1:1), 82%; g) Triphenyl phosphine, THF,H₂O, 78%; h) (Boc)₂O, TEA, DCM, 95%.

Cholic acid **1.1** was reduced by LAH to obtain compound **1.2**. The primary hydroxyl group of **1.2** was then protected by trityl group giving compound **1.3**. Treatment of compound **1.3** with allyl bromide and strong base KHMDS provided compound **1.4**. Hydroboration-oxidation of compound **1.4** yielded alcohol compound **1.5**. The compound **1.5** was converted to azide **1.6**, followed by removal of trityl group of compound **1.6** giving compound **1.7**. Amine **1.8** was obtained by reduction of azide compound **1.7**. Protection of the primary amine groups of **1.8** afforded compound **1.9** (Tris-Boc CSA-8).

Synthesis of PEG tether side chain (Compound 1.13)

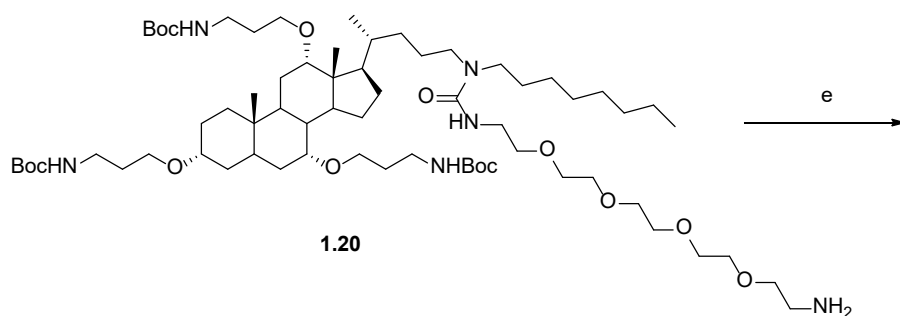
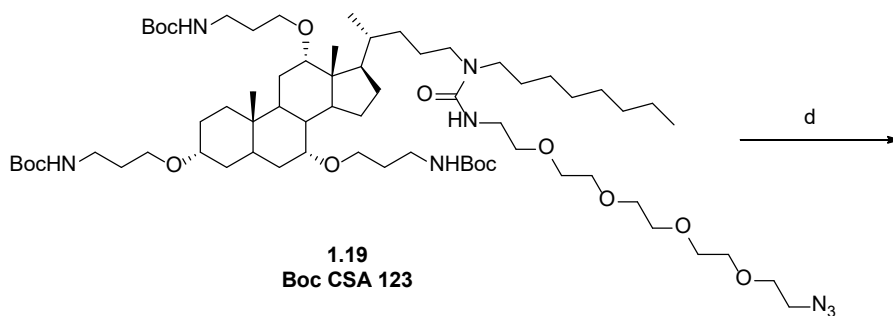
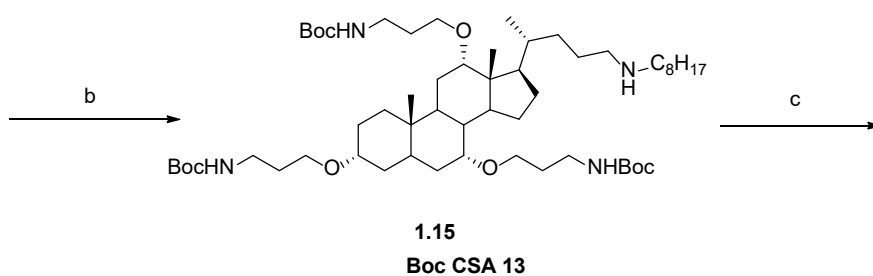
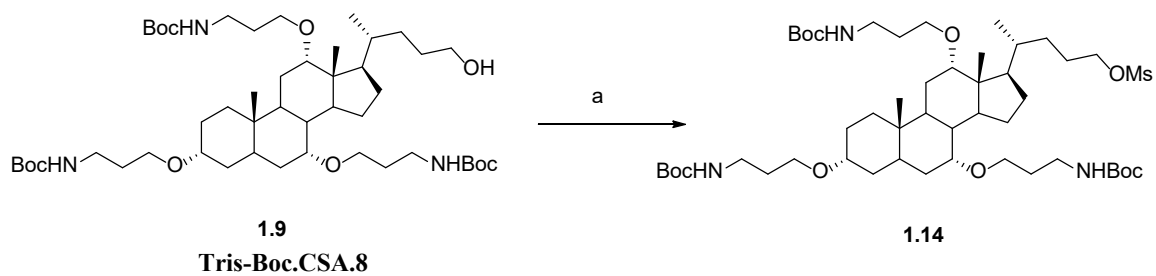


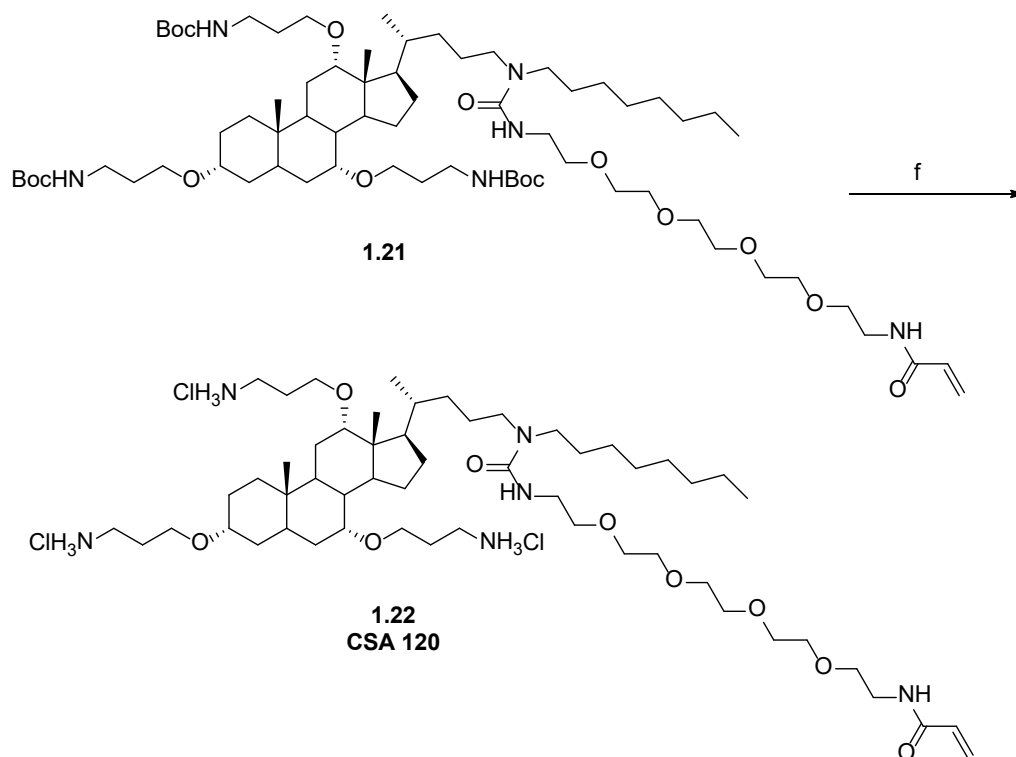
Scheme 1.2.2 Synthesis of compound **1.13**

Reagents: a) i) MsCl, TEA, DCM; ii) NaN₃, DMSO, 80 °C, 82%; b) H₃PO₄, PPh₃, Et₂O, EtOAc, 72%; c) phenyl chloroformate, TEA, DCM, 0 °C, 94%.

Compound **1.13** is an important synthetic block as a short tether which was used between the functional group such as acrylamide group and the ceragenin to allow flexibility with how the ceragenin interacts with microbial membranes. Pentaethylene glycol **1.10** was converted to the corresponding di-azide **1.11** by reacting with MsCl and TEA first and then NaN₃ in DMSO. Reduction of compound **1.11** by triphenyl phosphine in the presence of phosphorus acid afforded compound **1.12**. The primary amine of compound **1.12** was coupling with phenyl chloroformate in presence of basic condition to give the compound **1.13**.

Synthesis of CSA.120 HCl salt





Scheme 1.2.3 Synthesis of CSA-120

Reagents: a) MsCl, TEA, DCM; b) Octyl amine, 85%; c) **1.13**, K₂CO₃, acetonitrile, 80 °C, 12 hrs, 64%; d) Triphenyl phosphine, THF/H₂O (3:1), 73%; e) EDC, HOBt, acrylic acid, DCM, 100%; f) HCl/Dioxane, 91%.

With the important intermediate **Tris-Boc CSA.8** in hand, compound **1.14** was converted with MsCl and TEA at 0 °C, followed treatment of octyl amine without any solvent at 80 °C for 1 hour afforded compound **1.15**. Then the amine **1.15** was reacted with compound **1.13** in presence of base at 80 °C for 12 hours to obtain the coupling product compound **1.19**. Reduction of azide group afforded the corresponding amine **1.20**, which was coupled with acrylic acid providing compound **1.21** in reasonable yield. Deprotection of the remaining amines gave the target compound **1.22** as **CSA.120** HCl salt form.

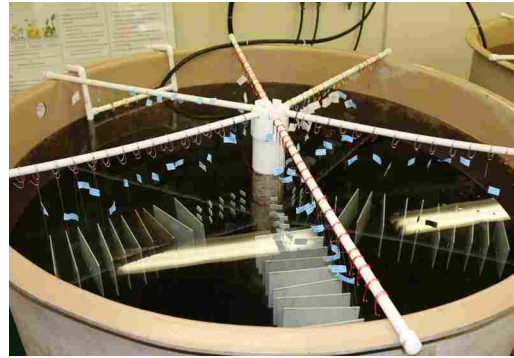
1.2.4 Application of Coatings

All coupons were primed with IS730 prior to final coating according to manufacturer instructions. For the ceragenin/fluoropolymer coating, **CSA-120** was added as either 1 or 2.5% of the total solids in the coating. Application of the IS970 coating requires use of three components: A, B and C. **CSA-120** was added to component B before mixing by first dissolving **CSA-120** in isopropanol (10% solution (w/v)). The three components were then mixed according to manufacturer instructions and applied on lateral sides using a nylon roller designed for smooth surfaces. Solvents in the coating solution were allowed to evaporate at room temperature for 15 min, and then coupons were exposed to direct sunlight for a minimum of 1 h, per side. Coupons were soaked in water for 1 h and washed with flowing water for 5 min to remove any non-covalently linked material. Coupons were dried and subjected to biofouling testing.

To determine the effectiveness of incorporation of **CSA-120** into the coatings, primed 3" x 3" coupons were coated on one side with IS970 alone and with IS970 (120 mg cured weight) containing 2.5% **CSA-120** (3.0 mg). The coatings were cured as described above, and the coupons were immersed in deionized water (120 mL) for 24 h. The water was removed by lyophilization. From the IS970 alone, 0.59 mg μg of a white solid was recovered; from the IS970 coating containing **CSA-120**, 0.97 mg of a white solid was recovered. If the difference between the IS970 alone and the **CSA-120**-containing coating (0.38 mg) were **CSA-120** or a derivative thereof (**CSA-120** is clear oil), covalent attachment is greater than 85%. Material recovered from the **CSA**-containing coating was subjected to mass spectrometry, and **CSA-120** was not detected (detection limit of ca. 10 μg). This result suggests that >99% of the **CSA-120** was covalently immobilized in the coating.

1.2.5 Biofouling Testing

Tests were conducted using two different flow velocity systems in tanks filled with unfiltered seawater to simulate the marine environment where currents are dynamic ranging from 0 to 5 knots (0.0 ~ 2.5 m/s). The low-flow velocity environment used circular 500 gal tanks (Figure 1.2.2) with rotational currents < 0.5 knots. The high flow environment used a raceway tank with a flow velocity of 2.5-4 knots (Figure 1.2.2). The low velocity tanks were located indoors and used ambient temperatures and a diurnal light cycle.



The raceway flume was located outdoors and also used ambient conditions.



For the indoor, low-flow rate tank tests, water exchange rates were maintained at 30% volume

Figure 1.2.2 Top: One of the 500 gal tanks used for the low-velocity studies. Bottom left: Raceway flume used for the high-velocity studies. Bottom right: Frames (empty) used to hold coupons in the raceway.

per hour or greater. Salinity and temperature were monitored and recorded. For the outdoor, high-flow rate tests in the flume shown in Figure 1.2.2; the flow velocity was set at a single (non-varying) rate and measured at the location of each coupon. The coupons were held vertically and at a 45-degree angle relative to the direction of flow such that one coupon surface faced the flow and the backside of the coupon was exposed to turbulence and back eddies. The coupons were arranged in a staggered pattern through the tank.

For each antifouling coating, PNNL tested a total of six 1" x 1" coupons, two 3" x 3" coupons, and two 8" x 8" coupons per time period. The 1" x 1" coupons were used for total organic carbon (TOC) measurements. The 3" x 3" coupons were used to assess changes in weight during the exposure period. The 8" x 8" coupons were used for visual analysis, staining, and for molecular characterization. Coupons were submerged in the tanks and recovered after 30 (short-term), 60 (mid-term), and 90 (long-term) days. Primer control, SN1, IS970 coatings were used as reference standards.

1.2.6 Methods of Analysis

Total Organic Carbon (TOC)

Each 1" x 1" coupon was transferred to a sterile 50 mL polypropylene centrifuge tube and hydrogen peroxide (3%, 30 mL) was added. Tubes incubated in 55 °C (water bath) for an hour. Tubes were vortexed vigorously and then attached to a Vial Tweeter sonication unit and oriented such that one face of the coupon faced the Vial Tweeter horn. Following one-minute sonication, the tube was rotated 180° so the other side of coupon faced the horn for one-minute sonication. The resulting suspension was transferred and analyzed for TOC.

Weight Analysis

Each 3" x 3" coupon was weighed prior to testing. After exposure to seawater, coupons were removed and passed through a Dyson Airblade hand dryer unit to remove bulk water and then weighed. Wet biomass weights were determined by subtraction of initial weights from final weights.

Visual Analysis

Each 8" x 8" coupon was photographed and assessed to determine percent coverage by slime and macrobiota species. One edge of the coupon was wiped clean (approximately ½ inch wide) and the coupon was then stained with mixture of three different dyes. Erythrosine B is a general red dye for biomass, rhodamine stains nucleic acids and coomassie brilliant blue is used to detect proteins. The coupon was photographed and analyzed (Matlab) to quantify biofilm growth intensities.

1.2.7 Results and Discussion

Fluoropolymer coatings (e.g., IS970) are effective fouling-release coatings; however, these coatings perform best in flowing systems in which shear forces cause loss of adhered organisms. We reasoned that anti-biofouling performance of these coatings under conditions with lower shear forces could be improved by incorporation of a means to inhibit the first stages in biofouling. Based on operation, not all MHK Wave and Tidal energy devices will reach or experience the required velocity and shear rates necessary for foul release coatings. AMPs are one of Nature's primary means of controlling microbial growth (Lai and Gallo 2009). And AMPs maintain antimicrobial activity even when covalently attached to a surface (Gao et al. 2011). Use of AMPs to inhibit biofouling has been reported with good results (Trepos et al. 2015). However, due to the cost of AMPs and their susceptibility to degradation by proteases, it is unlikely that they will find wide-spread use in coatings. As mimics of AMPs, ceragenins offer the same antimicrobial mechanism without the cost and stability issues.

AMPs and ceragenins are membrane active; consequently, it is not surprising that they retain antimicrobial activity when immobilized on a solid surface. However, design of a means of incorporating this type of molecule in a polymer must take into account the need for the molecules to attack microbial membranes at optimal angles. This need can be met by using a

sufficiently flexible tether between the immobilized ceragenin and the polymer, and CSA-120 a short span of polyethyleneglycol (PEG) is used as a tether. The acrylamide group at the end of the PEG tether is for incorporation into the polymer. Acrylamides, like related acrylates found in acrylic paints (Bao et al. 2015), readily engage in radical polymerizations that can be initiated via UV light and/or atmospheric oxygen. To ensure complete radical polymerization, CSA-120, added to the components of IS970 was exposed to both atmospheric oxygen and UV light. And to approximate conditions likely to be used in practical applications, sunlight was used as the UV source.

Once polymerization occurred, little or no unpolymerized starting material remained. No CSA-120 was observed after soaking coatings in water. CSA-120 is highly soluble in water (> 5% w/v), so unreacted CSA-120 would have been readily removed upon exposure to water. Furthermore, anti-biofouling testing was performed over extended periods, so any unreacted ceragenin would be washed from the coupons well before it had any impact on adhesion of microorganisms.

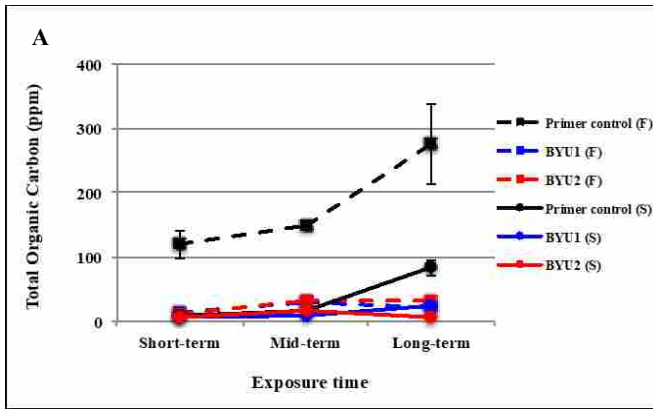
Two different amounts of CSA-120 were incorporated into IS970 to determine the impact of local concentration of the ceragenin. Previously, we observed antibacterial activity of CSA-120 immobilized in a hydrogel at a concentration of 1% (Gu et al. 2013), so one of the concentrations used was 1% and a high concentration of 2.5% was included in the study. Both concentrations were obtained by dissolving CSA-120 in isopropanol and then mixing it with component B of IS970, which employs ethylbenzene as a solvent. The resulting stable solution was then mixed with the remaining components of IS970 and immediately applied to the coupons.

To quantify biofouling, coupons were placed in either the static tank (S) or raceway flume (F) shown in Figure 1.2.2. Comparators were primer control and IS970-coated coupons. By each

measure (total carbon, added weight, and biofilm growth intensity) a small amount of biofouling was observed in the static tank relative to the raceway flume, and larger amounts of biofouling allowed more meaningful distinction among the coated coupons.

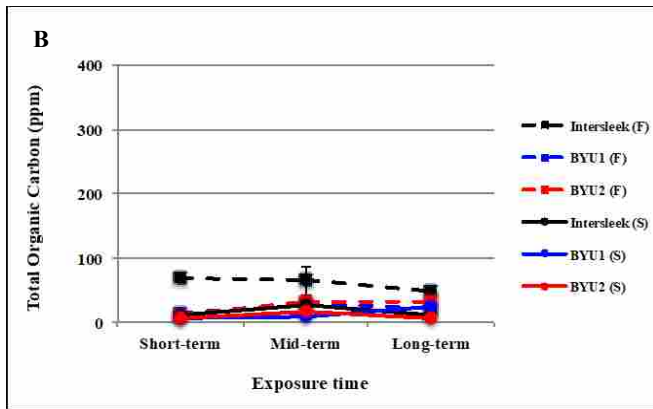
For determination of total carbon adhered to the coatings, 1" x 1" coupons were used, and the measurement (parts per million) reflects adherence of both bacteria and other, higher organisms (Figure 1.2.3). Substantially greater amounts of carbon were found on the primer control coupons in the flume as compared to coupons with coatings containing differing amounts of CSA-120 (BYU1 with 1.0% CSA-120, and BYU2 with 2.5% CSA-120) (Figure 1.2.3A). Notably, lower amounts of carbon accumulated on BYU1 and BYU2 coupons as compared to the IS970-coated coupons; with one exception (long-term, static tank with BYU1), all of the amounts of adhered carbon with BYU1 and BYU 2 were below those with the IS970 coupons (Figure 1.2.3B).

In measurement of total attached carbon there were not substantial differences between BYU1 and BYU2 coupons. As mimics of AMPs, ceragenins are membrane active and require a threshold concentration for activity. It is likely that this threshold is met with 1% CSA-120. The idea that if some is good then more is better may not hold with molecules of this type. It is likely that if CSA-120 is too densely packed on a surface that the compounds may be unable to obtain the necessary orientation for antibacterial activities. This idea may explain why there is not a significant difference between coatings containing different amounts of CSA-120 by this measure of biofouling.



Total Organic Carbon (ppm)

	Short-term	Mid-term	Long-term
Primer control (F)	119.48	149.78	275.71
BYU1 (F)	13.90	29.32	22.80
BYU2 (F)	11.88	32.30	31.72
Primer control (S)	8.35	16.51	83.28
BYU1 (S)	6.93	9.92	25.82
BYU2 (S)	6.45	17.56	7.52



Total Organic Carbon (ppm)

	Short-term	Mid-term	Long-term
Intersleek (F)	69.34	65.23	48.64
BYU1 (F)	13.90	29.32	22.80
BYU2 (F)	11.88	32.30	31.72
Intersleek (S)	12.81	28.08	11.73
BYU1 (S)	6.93	9.92	25.82
BYU2 (S)	6.45	17.56	7.52

Figure 1.2.3 Total organic carbon measurements for coated coupons. (S) indicates coupons tested in the static tank; (F) indicates coupons tested in the raceway flume (2.5-4 knots). Short-term-30 days; Mid-term-60 days; Long-term-90 days; 3A: Primer control, IS970 containing 1% CSA-120 (BYU1) and IS970 containing 2.5% CSA-120 (BYU2). 3B: IS970 (Intersleek), BYU1 and BYU2.

The intermediate-sized coupons (3" x 3") were used for determination of wet biomass weight accumulation (Figure 1.2.4). As expected, substantial amounts of biomass accumulated on the primer coupons in the static tank and in the raceway flume (Figure 4A). BYU1 and BYU2 coupons accumulated less biomass in all measurements. As seen with measurement of total organic carbon (Figure 1.2.3A), the BYU1 coupons accumulated less biofouling as compared to BYU2.

As compared to the IS970-coated coupons, BYU1 and BYU2 were comparable in the static tank. In the flume, these coupons accumulated more biomass than the IS970-coupons at short

and intermediate time points. However at the long time point (90 days), there was a substantial difference; BYU1 and BYU2 lost most of the accumulated biomass. There are multiple possible explanations for this difference, and a possibility is that the immobilized CSA-120 interfered with formation of the initial bacterial biofilm layer, which in turn interfered with the strength of adherence of higher organisms; with a longer exposure to higher velocity flows accumulated biofouling was lost.

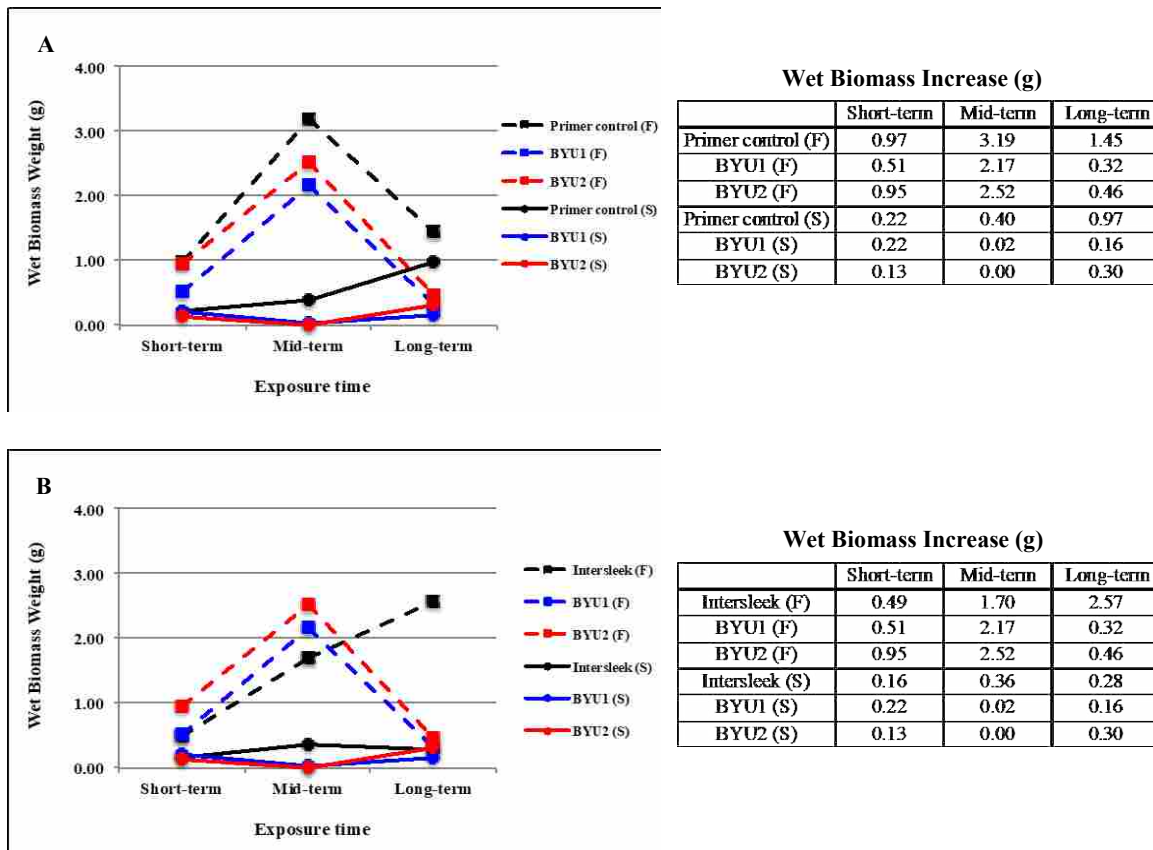


Figure 1.2.4 Wet biomass accumulated on coated coupons. (S) indicates coupons tested in the static tank; (F) indicates coupons tested in the raceway flume (2.5-4 knots). Short-term- 30 days; Mid-term- 60 days; Long-term- 90 days; 1.3.4A: Primer control, IS970 containing 1% CSA-120 (BYU1) and IS970 containing 2.5% CSA-120 (BYU2). 1.3.3B: IS970 (Intersleek), BYU1 and BYU2.

The 8" x 8" coupons were used to determine biofilm growth intensities (Figure 1.2.5). As compared to primer-coated coupons, less biofouling was observed on BYU1 and BYU2 (Figure 1.2.3A) at both mid and long-term exposure in the raceway flume. A small difference was observed between the BYU1 and BYU2, and as with other measures of inhibition of biofouling, BYU1 proved to be better than BYU2.

A comparable amount of biofilm formation was observed on the BYU1 and BYU2 coupons in the static tank; however, at 90 days, both supported less biofilm growth than the IS970-coated coupons (Figure 1.2.5B). In contrast, in the raceway flume, a substantially greater amount of biofouling was observed on both BYU1 and BYU2 relative to the IS970-coated coupons at the short- and mid-term time points. At 90 days, BYU1 and Intersleek coupons had comparable amounts of biofilm.

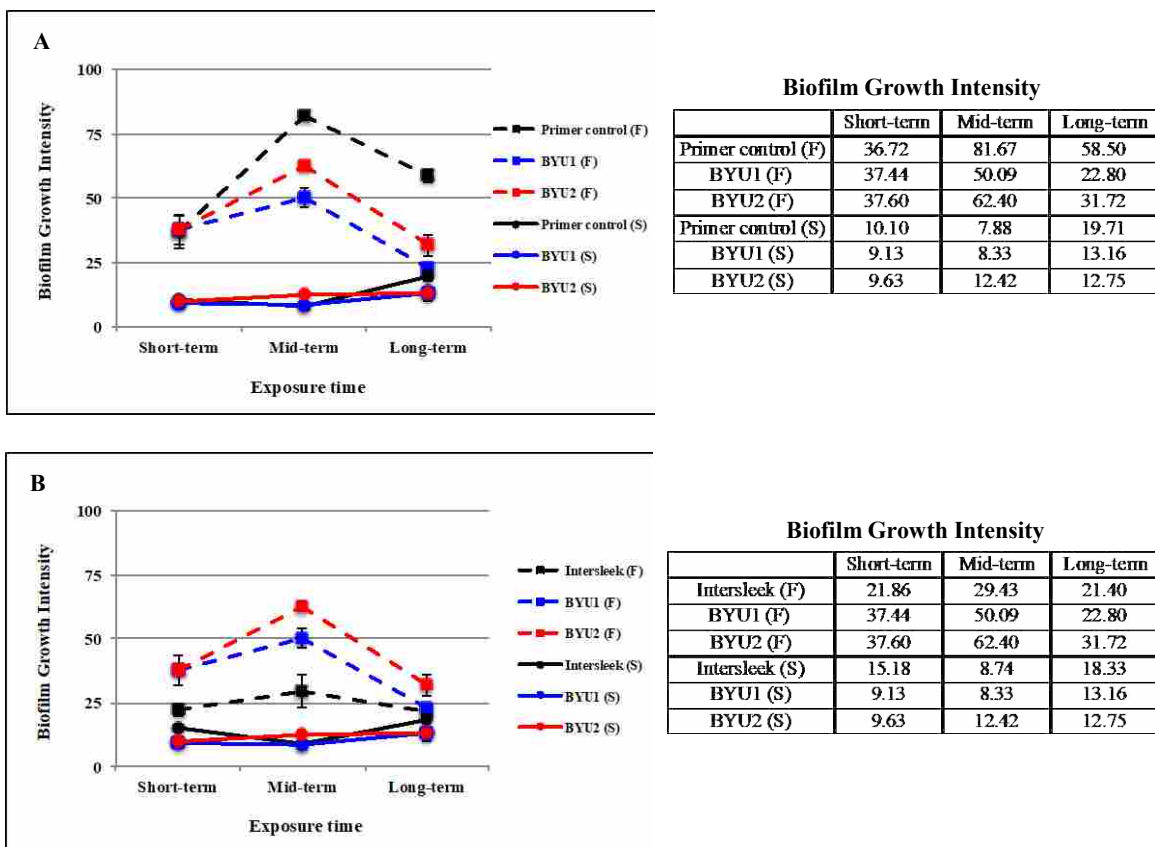


Figure 1.2.5 Biofilm growth intensity on coated coupons. (S) indicates coupons tested in the static tank; (F) indicates coupons tested in the raceway flume (2.5-4 knots). Short-term- 30 days; Mid-term- 60 days; Long-term- 90 days; 1.3.4A: Primer control, IS970 containing 1% CSA-120 (BYU1) and IS970 containing 2.5% CSA-120 (BYU2). 3B: IS970 (Intersleek), BYU1 and BYU2.

1.2.8 Conclusions

Inhibition of biofouling in marine environments is a daunting challenge given the number of types of organisms that can adhere to surfaces and the variety of conditions under which surfaces can be colonized (e.g., variations in temperature, shear forces, exposure to light, etc.). Consequently, optimization of ant biofouling coatings may require combinations of strategies to inhibit colonization. Fluoropolymer coatings have proven useful in inhibiting biofouling, especially under conditions in which shear forces aid in removing adhered organisms from the

coating. Under conditions lacking shear forces, fluoropolymer coatings are left vulnerable to biofouling (Watson et al. 2015). Since biofouling follows a progression of colonization by bacteria to adherence of higher organisms, adding a method of preventing bacterial biofilm formation on coatings was expected to provide added antifouling protection to fluoropolymer coatings.

The prevalence of AMPs in organisms ranging from mammals to amphibians to insects to plants argues that AMPs are one of the primary ways in which these organisms control and prevent bacterial growth. This prevalence also argues that bacteria are unlikely to generate high resistance to AMPs. These observations have led to efforts to use AMPs in coatings for prevention of bacterial colonization of surfaces, include efforts to inhibit marine biofouling (Trepas et al. 2015). These efforts are complicated by the high costs of AMP synthesis and sensitivity of AMPs to degradation. Ceragenins offer the same broad-spectrum antimicrobial activities as AMPs with substantially lower production costs and no sensitivity to proteases.

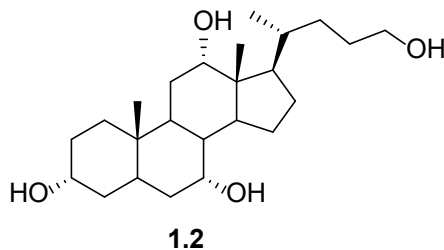
Ceragenin CSA-120 can be copolymerized in a fluoropolymer coating at varied concentrations, and the resulting coatings differ from the parent coating. By measures total adhered organic carbon and wet biomass, CSA-120 containing coatings displayed some improvements over the parent fluoropolymer coating. Only in long-term exposure to flowing sea water was one of the ceragenin coatings comparable to the parent coating. Results from these studies suggest that combination of strategies, in this case use of a fluoropolymer and an AMP mimic, may improve inhibition of biofouling. Further optimization of relative concentrations of ceragenin and use of alternative tethering groups may lead to incremental improvements in the antibiofouling properties of this type of coating.

1.2.9 Experimental Section

General: Reagents were purchased from Aldrich Chemical Co. unless otherwise noted. Methylene chloride, THF, DMF, pyridine, and DMSO were dried by passage through a Glass Contour solvent drying system containing a cylinder of activated alumina. Silica gel was used for chromatography unless otherwise noted.

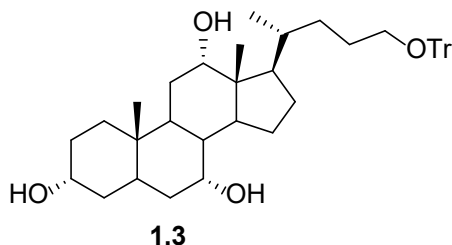
Instrumentation: ^1H and ^{13}C NMR spectra were recorded on a Varian Gemini 500 (500 MHz) spectrometer. Proton chemical shift were referenced to tetramethylsilane (TMS). Carbon chemical shifts were referenced to carbon resonance of solvents (CDCl_3 , CD_3OD). High resolution electron impact mass spectra (HR-MS) were obtained on a JOEL SX 102A spectrometer.

Experiment:

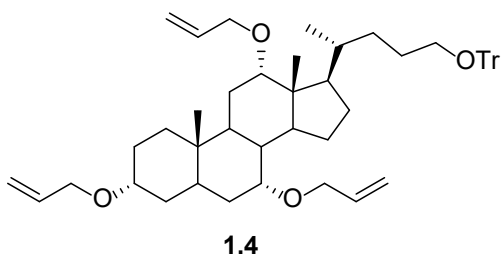


Compound 1.2 To a suspension of LiAlH_4 (9 g, 236.8 mmol) in 1 L of THF, cholic acid (50 g, 122.5 mmol) was added at 0 °C. The mixture was refluxed 24 hrs. 120 mL of saturated Na_2SO_4 was added to quench the reaction at 0 °C. The filter cake was washed with 100 mL of cold MeOH. 42 g of **1.2** was obtained as a white powder, after the trace amount of water was removed under 120 °C. The yield was 95%. ^1H NMR (CDCl_3 / 30% CD_3OD , 200 MHz) δ 3.98 (br, 1 H), 3.83 (br, 1 H), 3.60-3.46 (m, 2 H), 3.38 (br, 5 H), 2.30-2.10 (m, 2 H), 2.05-1.05 (m, 22 H), 1.03 (br, 2H), 0.92 (s, 3 H), 0.71 (s, 3 H); ^{13}C NMR (CDCl_3 , 50 MHz) δ 73.89, 72.44,

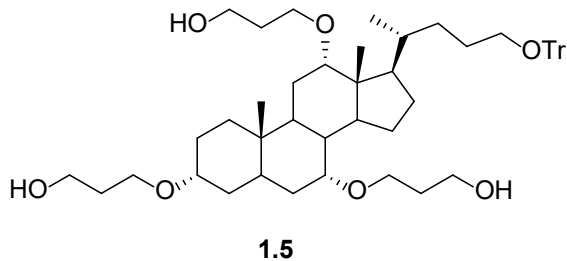
68.99, 63.51, 48.05, 47.12, 42.49, 40.37, 39.99, 36.62, 36.12, 35.58, 35.40, 32.77, 30.69, 30.04, 29.02, 28.43, 27.27, 23.96, 23.08, 18.00, 13.02; HRMS (ESI) calcd for C₂₄H₄₂O₄ [M+H]⁺: 566.4889, found: 566.4898.



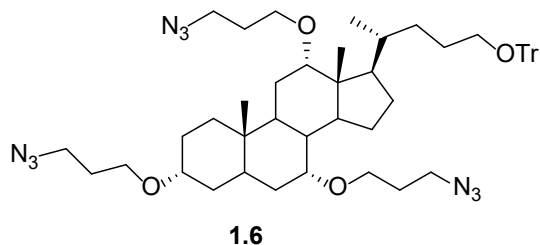
Compound 1.3 To a suspension of **1.2** (42 g, 106.5 mmol) in 400 mL of MeCN, TrCl (41.5 g, 149 mmol) and dry pyridine (12.6 g, 159.75 mmol) was added. The suspension was heated at 65 °C for 16 hrs. After the temperature was cooled down to room temperature, 240 mL of MeCN was added. The mixture was stirred for 2 hrs. The solid was washed with 100 mL of MeCN. 61 g of **1.3** was obtained as a white powder, after the trace amount of the solvent was removed under 120 °C. The yield was 92%. ¹H NMR (CDCl₃, 200 MHz) δ 7.46-7.42 (m, 6 H), 7.32-7.17 (m, 9H), 3.97 (br, 1 H), 3.83 (br, 1 H), 3.50-3.38 (m, 1 H), 3.01 (br, 1 H), 2.94 (dd, *J* = 14.2, 12.2 Hz, 2H), 2.64 (br, 1 H), 2.51 (br, 1 H), 2.36-2.10 (m, 2 H), 2.00-1.05 (m, 22 H), 0.96 (d, *J* = 5.8 Hz, 3H), 0.87 (s, 3 H), 0.64 (s, 3 H); ¹³C NMR (CDCl₃, 50 MHz) δ 144.77, 128.93, 127.91, 127.01, 86.43, 73.35, 72.06, 68.66, 64.28, 47.47, 46.53, 41.74, 41.62, 39.64, 35.57, 35.46, 34.91, 34.82, 32.40, 30.55, 28.21, 27.69, 26.80, 26.45, 23.36, 22.59, 17.83, 12.61; HRMS (ESI) calcd for C₄₃H₅₆O₄ [M+H]⁺: 637.4179, found: 637.4183.



Compound 1.4 To a solution of **1.3** (41.5 g, 65.2 mmol) in 400 mL of dry THF, NaH (8 g, 326 mmol), tetrabutylammonium iodide (802.4 mg, 2.17 mmol), and allyl bromide (39.4 g, 326 mmol) were added. The mixture was refluxed overnight. 20 mL of MeOH was added to quench the reaction at 0 °C. After the solvent was removed, 100 mL of water was added. Hexanes were used to extract the mixture. The combined organic layer was dried over Na₂SO₄. After the solvent was removed, 44.4 g of the crude product was obtained and used in the next step directly. ¹H NMR (CDCl₃, 200 MHz) δ 7.48-7.30 (m, 6 H), 7.32-7.14 (m, 9H), 6.04-5.80 (m, 3 H), 5.36-5.04 (m, 6H), 4.14-3.94 (m 4 H), 3.74 (dt, *J* = 13.8, 5.8 Hz, 2 H), 3.53 (br, 1 H), 3.20-2.94 (m 3 H), 3.31 (br, 1 H), 2.38-1.90 (m, 4 H), 1.90-0.96 (m, 20 H), 0.90 (d, *J* = 5.4 Hz, 3 H), 0.89 (s, 3 H), 0.64 (s, 3 H); ¹³C NMR (CDCl₃, 50 MHz) δ 144.83, 136.27, 136.08, 128.94, 127.90, 126.98, 116.46, 115.40, 86.42, 80.94, 79.29, 74.98, 69.52, 69.39, 68.86, 64.39, 46.51, 46.42, 42.67, 42.14, 39.92, 35.63, 35.51, 35.13, 32.45, 28.98, 28.09, 27.66, 27.57, 26.72, 23.32, 23.11, 17.92, 12.69; HRMS (ESI) calcd for C₅₂H₆₈O₄ [M+H]⁺: 757.5118, found: 757.5123.

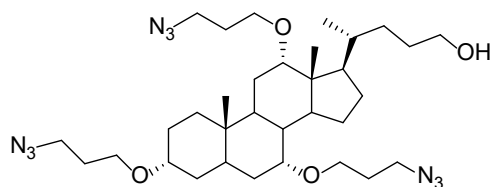


Compound 1.5 To a 100 mL of 1 M BH₃ in THF, cyclohexene (16 g, 200 mmol) in 50 mL of THF was added 0 °C. The mixture was stirred 30 mins. **1.4** (22 g, 30 mmol) in 200 mL of THF was added, and the solution was refluxed for 6 hrs. After the temperature was cooled down to 0 °C, 70 mL of 20% NaOH and 70 mL of H₂O₂ was added dropwise carefully. The reaction mixture was refluxed overnight. Before the THF was removed, KI / starch test paper was used to make sure that no peroxide remained. EtOAc was used to extract the mixture and after dried over Na₂SO₄, the solvent and the cyclohexanol were removed under vacuum. The resulting sticky oil was used in the next step without purification. The crude yield was 90%. ¹H NMR (CDCl₃, 200MHz) δ 7.50-7.42 (m, 6 H), 7.32-7.14 (m, 9H), 3.90-3.65 (m, 8 H), 3.50 (br, 6 H), 3.40-2.96 (m, 6 H), 2.30-0.94 (m, 30 H), 0.90 (s, 3 H), 0.88 (d, *J* = 5.4 Hz, 3 H), 0.64 (s, 3 H); ¹³C NMR (CDCl₃, 50 MHz) δ 144.73, 128.88, 127.85, 126.94, 86.36, 80.52, 78.90, 76.36, 66.82, 66.18, 65.77, 64.22, 61.53, 61.41, 61.34, 46.89, 46.04, 42.60, 41.59, 39.60, 35.37, 35.27, 34.88, 32.75, 32.44, 32.31, 28.82, 27.65, 27.48, 27.13 26.77, 23.35, 22.74, 22.38, 18.08, 12.48; HRMS (ESI) calcd for C₅₂H₇₄O₇ [M+H]⁺: 811.5435, found: 811.5440.



Compound 1.6 To a solution of crude **1.5** in 100 mL of THF, MsCl (3.8 g, 33 mmol) and Et₃N (3.4 g, 33.5 mmol) were added at 0 °C. The solution was stirred for 30 mins. After removing the solvent, 50 mL of water was added. The mixture was extracted with EtOAc.

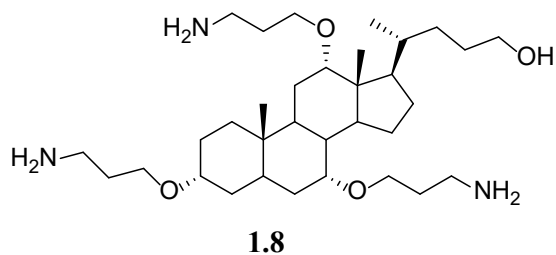
The combined organic phase was dried over Na₂SO₄. After the solvent was removed, 100 mL of DMSO was used to dissolve the residue. Sodium Azide (6.6 g, 100 mmol) was added, and the mixture was stirred at 80 °C for 12 hrs. The reaction was allowed to cool down to RT. 150 mL cold DI water was used to quench reaction. Then the mixture was extracted with EtOAc (100mL×4). The combined organic layer was dried over Na₂SO₄. After the solvent was removed, 7.3 g of the product was isolated through a column chromatography (SiO₂). The yield was 75%. ¹H NMR (CDCl₃, 200 MHz) δ 7.50-7.42 (m, 6 H) 7.32-7.14 (m, 9H), 3.90-3.65 (m, 5H), 3.50 (br, 6 H), 2.30-0.94 (m, 30 H), 1.49-1.6 (m, 6H), 0.90 (s, 3 H), 0.88 (d, *J* = 5.4 Hz, 3H), 0.64 (s, 3 H); ¹³C NMR (CDCl₃, 50 MHz) δ 144.73, 128.88, 127.85, 126.94, 86.36, 80.52,78.90, 76.36, 66.82, 66.18, 65.77, 64.22, 46.89, 46.53, 46.41, 46.34, , 46.04, 42.60, 41.59, 39.60,35.37, 35.27, 34.88, 32.75, 32.44, 32.31, 28.82, 27.65, 27.48, 27.13, 26.77, 23.35, 22.74, 22.38, 18.08, 12.48; HRMS (ESI) calcd for C₅₂H₇₁N₉O₄ [M+H]⁺: 886.56290, found:886.56410.



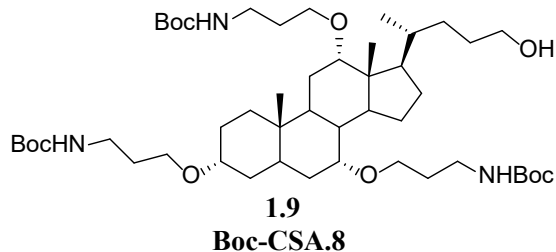
1.7

Compound 1.7 To a solution of **1.6** (23 g, 26 mmol) in 240 mL of DCM and MeOH (1:1), p-toluenesulfonic acid (1.3g, 6.5mmol) was added. The mixture was stirred at RT for 2hrs. A solution of saturated NaHCO₃ was used to quench reaction. Then the mixture was extracted with EtOAc. The combined organic layer was dried over Na₂SO₄. After the solution was removed,

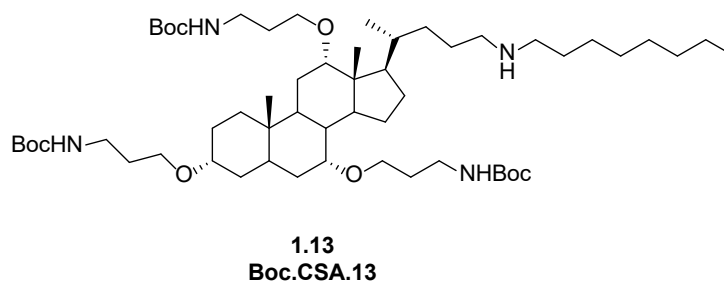
15g of the product was isolated through a column chromatography (SiO₂). The yield was 90%. ¹H NMR (CDCl₃, 200 MHz) δ 3.90-3.65 (m, 6H), 3.50 (br, 6 H), 2.30-0.94 (m, 30 H), 1.49-1.6 (m, 6 H), 0.90 (s, 3 H), 0.88 (d, J = 5.4 Hz, 3H), 0.64 (s, 3 H); ¹³C NMR (CDCl₃, 50 MHz) δ 80.52, 78.90, 76.36, 66.82, 66.18, 65.77, 64.22, 46.89, 46.53, 46.41, 46.34, 46.04, 42.60, 41.59, 39.60, 35.37, 35.27, 34.88, 32.75, 32.44, 32.31, 28.82, 27.65, 27.48, 27.13, 26.77, 23.35, 22.74, 22.38, 18.08, 12.48; HRMS (ESI) calcd for C₃₃H₅₇N₉O₄ [M+H]⁺: 644.45335, found: 644.46143.



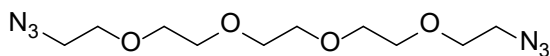
Compound 1.8 To a solution of 1.7 (16.73g, 26mmol) in 400 mL of THF and H₂O (3:1), Triphenyl phosphine (68.2g, 260mmol) was added. The reaction was stirred at RT overnight. Then the mixture was exacted with EtOAc, the combined organic layer was dried over Na₂SO₄. After the solvent was removed, 11.5g of the product was isolated through a column chromatography (SiO₂). The yield was 78%. ¹H NMR (CDCl₃ / 30% CD₃OD, 300 MHz) δ 4.43 (bs, 7 H), 3.74-3.68 (m, 1 H), 3.66-3.60 (m, 1 H), 3.50-3.57 (m, 5 H), 3.25-3.34 (m, 2 H), 3.06-3.17 (m, 2 H), 2.74-2.84 (m, 6 H), 2.01-2.19 (m, 3 H), 0.96-1.97 (m, 27H), 0.94 (d, J = 7.2 Hz, 3 H), 0.92 (s, 3 H), 0.69 (s, 3 H); ¹³C NMR (CDCl₃, 75 MHz) δ 80.44, 79.27, 75.77, 66.59, 66.53, 65.86, 62.51, 46.21, 45.84, 42.55, 41.53, 40.09, 39.43, 39.31, 39.02, 35.16, 34.93, 34.86, 34.57, 32.93, 32.71, 31.57, 28.66, 28.33, 27.64, 27.22, 23.04, 22.40, 22.29, 17.06, 11.98; HRMS (ESI) calcd for C₃₃H₆₃N₃O₄ [M+H]⁺: 566.4889, found: 566.4898.



Tris-Boc CSA-8 To a solution of 1.8 (11.5g, 20mmol) in 300 ml of DCM, (Boc)₂O (19.7g, 86mmol) was added. The reaction was stirred at RT overnight. 50 ml of MeOH was used to quench reaction. After the solvent was removed, 16.4g of the product was isolated through a column chromatography (SiO₂). The yield was 95%. ¹H NMR (CDCl₃, 500 MHz) δ 4.82-5.34 (m, 3 H), 3.41-3.56 (m, 4 H), 3.25-3.40 (m, 3 H), 2.81-3.20 (m, 8 H), 2.40-2.58 (m, 2 H), 1.84-2.20 (m, 2 H), 1.41-1.82 (m, 17 H), 1.18- 1.40 (m, 36 H), 0.81-0.89 (m, 2 H), 0.79 (d, J= 6.4 Hz, 3 H), 0.72 (s, 3 H), 0.51 (s, 3 H). ¹³C NMR (CDCl₃, 125 MHz) δ 155.9, 155.75, 80.23, 78.88, 78.24, 75.37, 66.11, 65.40, 63.48, 46.28, 45.78, 42.34, 41.49, 39.39, 39.16, 38.25, 38.02, 35.20, 34.90, 34.53, 32.77, 30.25, 29.82, 28.47, 28.19, 28.16, 27.31, 27.16, 23.02, 22.55, 22.17, 17.67, 12.11; HRMS (ESI) calcd for C₄₈H₈₇N₃O₁₀ [M+H]⁺: 866.6391, found: 866.7021.

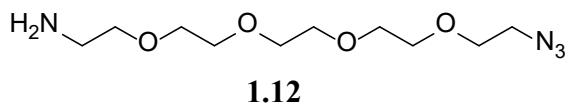


Compound 1.15 To a solution of **Boc-CSA-8** (20.5 g, 23.7 mmol) in 200 mL of THF, MsCl (2.98 g, 26.1 mmol) and Et₃N (2.64 g, 26.1 mmol) were added at 0 °C. The temperature was allowed to rise up to room temperature. The solution was stirred for 30 mins. Then, 100 mL of water was used to wash the solution. The aqueous layer was extracted with DCM three times. The combined organic layer was dried over Na₂SO₄. After the solvent was removed, 50 mL of octylamine was added to dissolve the residue. The mixture was stirred at 80 °C overnight. The temperature was cooled to room temperature then, 200 mL of water and 200 mL of DCM were added. The aqueous layer was extract with DCM three times and the combined organic phase was dried over Na₂SO₄. After removing the solvent, 19.32g of the product was isolated through a column chromatography (SiO₂). The yield was 85%. ¹H NMR (CDCl₃, 500 MHz) δ 4.82-5.34 (m, 3 H), 3.41-3.56 (m, 2 H), 3.25-3.40 (m, 3 H), 2.81-3.20 (m, 8 H), 2.40-2.58 (m, 6 H), 1.84-2.20 (m, 2 H), 1.41-1.82 (m, 29 H), 1.18- 1.40 (m, 36 H), 0.81-0.89 (m, 2 H), 0.88 (t, 3H), 0.79 (d, J= 6.4 Hz, 3 H), 0.72 (s, 3 H), 0.51 (s, 3 H). ¹³C NMR (CDCl₃, 125 MHz) δ 155.9, 155.75, 80.23, 78.88, 78.24, 75.37, 66.11, 65.40, 48.71, 47.86, 46.28, 45.78, 42.34, 41.49, 39.39, 39.16, 38.25, 38.02, 35.20, 34.90, 34.53, 32.77, 32.23, 30.25, 29.82, 29.31, 29.12, 28.47, 28.19, 28.16, 27.31, 27.16, 27.10, 23.17, 23.02, 22.55, 22.17, 17.67, 14.63, 12.11; HRMS (ESI) calcd for C₅₆H₁₀₄N₄O₉ [M+H]⁺: 977.7803, found: 977.8023.



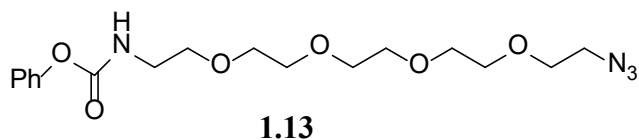
1.11

Compound 1.11. To a solution of pentaethylene glycol (50g, 210 mmol) in 300 ml of DCM, MsCl (49 ml, 630 mmol) and Et₃N (102 ml, 740mmol) were added sequentially at °C. The reaction was allowed to stir at RT for 1 hour. Then 150 ml of cold DI water was used to quench. The mixture was exacted with DCM and washed with Brine (150 ml), the combined organic layer was dried over Na₂SO₄. After removing the solvent, the crude compound was dissolved in 150 ml of DMSO (dry). 48g of NaN₃ was added and the mixture was stirred at 80 °C overnight. Then the cold DI water (200ml) was used to quench. The mixture was exacted with EtOAc (100ml ×4). The combined organic layer was dried over Na₂SO₄. After removing the solvent, 49g of the product was isolated through a column chromatography (SiO₂). The yield was 82%. ¹H NMR (200 MHz, CDCl₃): d 3.62–3.60 (m, 16H), 3.34 (t, 4H, J = 5.1 Hz). ¹³C NMR (50 MHz, CDCl₃): d 70.5, 69.9, 50.5 (10· CH₂). ; HRMS (ESI) calcd for C₁₀H₂₀N₆O₄ [M+H]⁺: 289.1546, found: 289.1632.

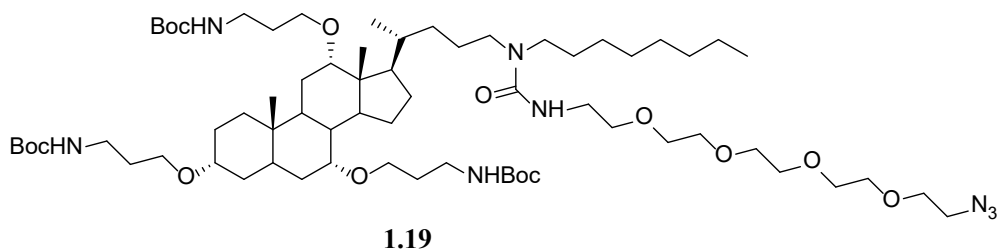


Compound 1.12 To a solution of **1.11** (49g, 172mmol) in 240 ml of Et₂O and EtOAc (1:1), 210 ml of H₃PO₄ (2M) and 52 g of triphenyl phosphine were added sequentially. The reaction was stirred at RT overnight. After washing the aqueous layer with DCM, the combined organic layer was dried over Na₂SO₄. 32g of the product was isolated through a column chromatography (SiO₂). The yield was 72%. ¹H NMR (CDCl₃, 400 MHz) δ 3.6-3.7 (m, 16 H), 3.40 (t, 2 H), 3.36

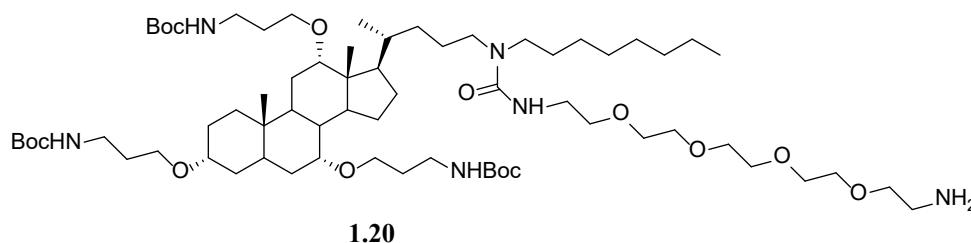
(t, 2 H); ^{13}C NMR (CDCl_3 , 125 MHz) δ 70.70, 70.67, 70.62, 70.61, 70.57, 70.31, 70.02, 69.85, 50.63, 40.84; HRMS (ESI) calcd for $\text{C}_{10}\text{H}_{22}\text{N}_4\text{O}_4$ $[\text{M}+\text{H}]^+$:263.1641, found: 263.1657.



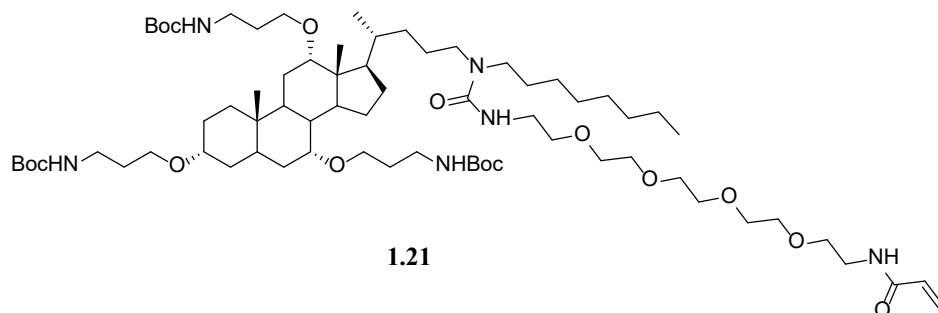
Compound 1.13. To a solution of **1.12** (23g, 88mmol) in 150 ml of DCM, Et_3N (17ml, 125 mmol) and phenyl chloroformate (12ml, 96.5 mmol) were added at 0 °C. The reaction was stirred for 1 hour. Then 100 ml of cold DI water was used to quench the reaction. The aqueous layer was extracted with DCM (3×50 ml) and the combined organic layer was dried over Na_2SO_4 . After removing the solvent, 32g of the product was isolated through a column chromatography (SiO_2). The yield was 94%. ^1H NMR (CDCl_3 , 400 MHz) δ 7.35 (t, 2 H), 7.19 (t, 1 H), 7.12 (d, 2 H), 3.6-3.7 (m, 16 H), 3.47 (t, 2 H), 3.36 (t, 2 H). ^{13}C NMR (CDCl_3 , 125 MHz) δ 154.88, 151.10, 129.24, 125.21, 121.63, 70.70, 70.67, 70.62, 70.61, 70.57, 70.31, 70.02, 69.85, 50.63, 41.04. HRMS (ESI) calcd for $\text{C}_{17}\text{H}_{26}\text{N}_4\text{O}_6$ $[\text{M}+\text{H}]^+$:383.1852, found: 383.2053.



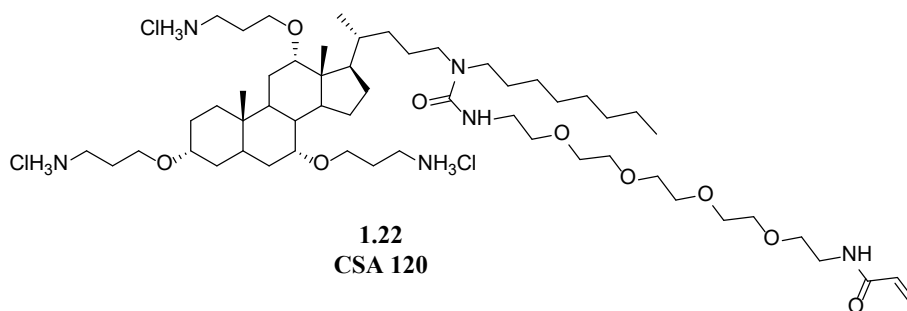
Compound 1.19 To a solution of compound **1.15** (5.25g, 5.4 mmol) in 100 ml of MeCN (dry), K_2CO_3 (2.1g, 5.4 mmol) and compound **1.13** (0.75g, 5.4 mmol) were added sequentially. The reaction was allowed to reflux overnight. After cooled down to RT, 50 ml of DI water was used to quench. The mixture was extracted with EtOAc, and the combined organic layer was dried over Na_2SO_4 . After removing the solvent, 4.4g of the product was isolated through a column chromatography (SiO_2). The yield was 64%. 1H NMR ($CDCl_3$, 500 MHz): δ 4.79 (br, 1 H), 3.6-3.7 (m, 18 H), 3.03-3.58 (m, 24 H), 1.55-2.11 (m, 17 H), 1.43 (s, 27 H), 1.20-1.31 (m, 21 H), 0.98-1.03 (m, 2 H), 0.88-0.94 (m, 11 H), 0.69 (s, 3 H). ^{13}C NMR ($CDCl_3$, 125 MHz): δ 158.02, 156.23, 156.07, 80.56, 79.26, 78.89, 78.63, 70.70, 70.67, 70.63, 70.61, 70.57, 70.52, 70.15, 70.02, 66.40, 65.76, 50.61, 47.78, 47.37, 47.05, 46.15, 42.60, 41.88, 41.84, 39.68, 39.43, 38.64, 38.35, 35.66, 35.21, 34.91, 34.86, 33.16, 31.83, 30.57, 30.11, 29.69, 29.47, 29.27, 28.72, 28.61, 28.54, 28.48, 27.61, 27.04, 25.63, 23.31, 22.95, 22.87, 22.48, 17.89, 14.11, 12.49. HRMS (ESI) calcd for $C_{67}H_{124}N_8O_{14}$ $[M+H]^+$: 1264.9237, found: 1264.9648.



Compound 1.20 To a solution of **1.19** (18.3g, 14.5 mmol) in 200 ml of THF and H_2O (3:1), triphenyl phosphine (7.6g, 29 mmol) was added. The reaction was stirred at RT overnight. Then THF was removed, the aqueous layer was extracted with DCM (3×100 ml). The mixture was dried over Na_2SO_4 following to dry off the solvent. 13g of the target compound was isolated through a column chromatography. The yield was 73%.



Compound 1.21 To a solution of **1.20** (6.5 g, 5.2 mmol) in dichloromethane (100 mL), triethyl amine (1.4ml, 10mmol) was cooled to 0 °C. Acryloyl chloride (0.6 mL, 7.5mmol) was added dropwise over 10 minutes, and the mixture was stirred at room temperature for 15 min. Water (50 mL) was added, and the aqueous layer was extracted dichloromethane (3 x 50mL). The combined organic extracts were dried over sodium sulfate. The solvent was removed under vacuum, and 1.18 was recovered as clear oil (6.8 g, 100% yield). ¹H NMR (CDCl₃, 500 MHz): δ 6.51 (br, 1 H), 6.32 (d, 1 H), 6.16 (dd, 1 H), 5.63 (d, 1 H), 5.12 (br, 1 H), 4.8 (br, 1 H), 3.6-3.7 (m, 18 H), 3.03-3.58 (m, 24 H), 1.55-2.11 (m, 17 H), 1.43 (s, 27 H), 1.20-1.31 (m, 21 H), 0.98-1.03 (m, 2 H), 0.88-0.94 (m, 11 H), 0.69 (s, 3 H). ¹³C NMR (CDCl₃, 125 MHz): δ 165.37, 158.02, 156.23, 156.07, 130.82, 126.51, 80.56, 79.26, 78.89, 78.63, 70.70, 70.67, 70.63, 70.61, 70.57, 70.52, 70.15, 70.02, 66.40, 65.76, 47.78, 47.37, 47.05, 46.15, 42.60, 41.88, 41.84, 39.68, 39.43, 39.41, 38.64, 38.35, 35.66, 35.21, 34.91, 34.86, 33.16, 31.83, 30.57, 30.11, 29.69, 29.47, 29.27, 28.72, 28.61, 28.54, 28.48, 27.61, 27.04, 25.63, 23.31, 22.95, 22.87, 22.48, 17.89, 14.11, 12.49. HRMS (ESI) calcd for C₇₀H₁₂₈N₆O₁₅ [M+H]⁺: 1292.9438, found: 1292.9715.



CSA 120. 4.6g of **1.21** was dissolved into 40 mL of 4 M HCl/Dioxane solution. The solution was stirred overnight at RT. After removing the solvent, 200 mL of toluene was poured into the residue. 4.2g of **CSA-120** was obtained by azeotropic removing the solvent in 91% yield. ^1H NMR (CDCl_3 , 500 MHz): δ 8.26 (br, 4 H), 8.12 (br, 2 H), 6.32 (d, 1 H), 6.16 (dd, 1 H), 5.63 (d, 1 H), 4.79 (br, 1 H), 3.6-3.7 (m, 18 H), 3.03-3.58 (m, 24 H), 1.55-2.11 (m, 17 H), 1.20-1.31 (m, 21 H), 0.98-1.03 (m, 2 H), 0.88-0.94 (m, 11 H), 0.69 (s, 3 H); ^{13}C NMR (CDCl_3 , 100 MHz): δ 165.37, 158.02, 130.82, 126.51, 80.56, 79.26, 78.89, 78.63, 70.70, 70.67, 70.63, 70.61, 70.57, 70.52, 70.15, 70.02, 66.40, 65.76, 47.78, 47.37, 47.05, 46.15, 42.60, 41.88, 41.84, 39.68, 39.43, 39.41, 39.22, 39.21, 38.35, 35.66, 35.21, 34.91, 34.86, 33.16, 31.83, 30.57, 30.11, 29.69, 29.47, 29.27, 28.72, 28.61, 27.61, 27.04, 25.63, 23.31, 22.95, 22.87, 22.48, 17.89, 14.11, 12.49. HRMS (ESI) calcd for $\text{C}_{55}\text{H}_{104}\text{N}_6\text{O}_9$ $[\text{M}+\text{H}]^+$: 992.7865, found: 992.8021.

1.2.10 References

1. Afacan, N. J.; Yeung, A. T. Y.; Pena, OM. Hancock REW. Therapeutic potential of host defense peptides in antibiotic-resistant infections. *Curr. Pharm. Design.* **2012**, *18*, 807-819.
2. Bao, Y.; Ma, J.; Zhang, X.; Shi, C. Recent advances in modification of polyacrylate latexes. *J. Mater. Sci.* **2015**, *50*, 6839-6863.
3. Callow, J. A.; Callow, M.E. Trends in the development of environmentally friendly fouling-resistant marine coatings. *Nat. Commun.* **2011**, *2*, 1-10.

4. Dang, H.; Lovell, C. R. Microbial surface colonization and biofilm development in marine environments. *Microb. Mol. Biol. Rev.* **2016**, *80*, 91-138.
5. Ding, B.; Yin, N.; Liu, Y.; Cardenas-Garcia, J.; Evanson, R.; Orsak, R.; Fan, M.; Turin, G.; Savage, P. B. Origins of cell selectivity of cationic steroid antibiotics. *J. Am. Chem. Soc.* **2004**, *126*, 13642-13648.
6. Epanand, R. F.; Pollard, J. E.; Wright, J. O.; Savage, P. B.; Epanand, R. M. Depolarization, bacterial membrane composition and the antimicrobial action of ceragenins. *Antimicrob. Agents. Chemother.* **2010**, *54*, 3708-3717.
7. Gao, G.; Yu, K.; Kindrachuk, J.; Brooks, D. E.; Hancock REW, Kizhakkedathu, J.N. Antibacterial surfaces based on polymer brushes: Investigation on the influence of brush properties on antimicrobial peptide immobilization and antimicrobial activity. *Biomacromol.* **2011**, *12*, 3715-3727.
8. Gu, X.; Jennings, J. D.; Snarr, J.; Chaudhary, V.; Pollard, J. E.; Savage, P. B. Optimization of ceragenins for prevention of bacterial colonization of hydrogel contact lenses. *Invest. Ophthalm. Vis. Sci.* **2013**, *54*, 6217-6223.
9. Lai, X. Z.; Feng, Y.; Pollard, J.; Chin, J.N.; Rybak, M.J.; Bucki, R.; Epanand, R. F.; Epanand, R. M.; Savage, P. B. Ceragenins: Cholic acid-based mimics of antimicrobial peptides. *Acc. Chem. Res.* **2008**, *4*, 1233-1240.
10. Lai, Y.; Gallo, R. AMPed up immunity: how antimicrobial peptides have multiple roles in immune defense. *Trends Immunol.* **2009**, *30*, 131-141.
11. Mangoni, M. L.; DmDermott, A.M.; Zasloff, M. Antimicrobial peptides and wound healing: biological and therapeutic considerations. *Exper. Dermatol.* **2016**, *25*, 167-173.

12. Trepos, R.; Cervin, G.; Pile, C.; Pavia, H.; Hellio, C.; Svenson, J. Evaluation of cationic micropeptides derived from the innate immune system as inhibitors of marine biofouling. *Biofouling*. **2015**, *31*, 393-403.
13. Watson, M. G.; Scardino, A. J.; Zalizniak, L.; Shimetam J. Colonization and succession of marine biofilm-dwelling ciliate assemblages on biocidal antifouling and fouling-release coatings in temperate Australia. *Biofouling*. **2015**, *31*, 709-720.
14. Yebra, D. M.; Kiil, S.; Dam-Johansen, K. Antifouling technology- past, present and future steps towards efficient and environmentally friendly antifouling coatings. *Prog. Org. Coat.* **2004**, *50*, 75-104.

1.3 Translation of Ceragenin Affinity for Bacteria to an Imaging Reagent for Infection

1.3.1 Introduction

Identification of sites of bacterial infection is important for proper clinical care of patients manifesting general signs of infection (e.g., fever and elevated white blood cell counts). This is especially true with patients that are immunocompromised because they often have reduced symptoms of infection and consequently it may be difficult to pinpoint these sites.^{1,2} Signs of inflammation can be used to identify sites of infection at superficial sites or in the extremities; however, infection in internal structures (i.e., abdomen, chest and brain) can be difficult to localize at early stages.³ Only after infection has progressed to tissue necrosis and/or abscess formation can it be observed via X-ray computed tomography and ultrasound. Consequently, a method of imaging infections at their initial stages would be useful for diagnosis and treatment.

A key element for imaging infections is a targeting motif in a molecule that provides for selective association with bacteria. Multiple small molecules are known to associate with bacteria; for example, polymyxins bind the lipid A portion of lipopolysaccharides found in the outer membranes of Gram-negative bacteria⁴. Similarly, endogenous antimicrobial peptides (AMPs) associate with Gram-negative⁵ and Gram-positive bacteria.⁶ Ceragenins are small molecule mimics of AMPs, and they also display affinity for Gram-negative and positive bacteria, specifically bacterial membrane components lipid A⁶⁻⁸ and lipotechoic acid.⁶ Due to the relatively simple structures of ceragenins, they can be readily modified, and one such modification has allowed them to be attached to silver nanoparticles.^{9,10} Silver nanoparticles, coated with a ceragenin, were placed in the presence of bacteria, and confocal imaging showed the ceragenin-appended nanoparticles associated with bacteria. This association was attributed to the affinity of the appended ceragenin for the bacterial membrane components. In a related

study, the association of a fluorophore-appended ceragenin with intact cells showed that the ceragenin displayed selectivity for bacterial cells over eukaryotic cells.⁷

Nuclear medicine techniques such as positron emission tomography (PET) and single photon computed tomography (SPECT) have become a primary means of visualizing tumors and inflammation due to their high levels of sensitivity, low background interference and the three-dimensionality of their images. Some SPECT agents have been developed that allow imaging of infection. For example, Ga-citrate^{6, 7} binds to bacteria, but it does not discriminate between bacterial infections and proteins that accumulate at sites of inflammation^{11, 12}. Similarly, ^{99m}Tc-labeled compounds have been used to label leukocytes for infection/inflammation imaging; however, these have been shown to be non-specific for bacterial infections.^{13, 14} The use of radiolabeled antibiotics such as ciprofloxacin and kanamycin has also suffered from a lack of specificity to date.¹⁵ Radiolabeled AMPs, such as ubiquicidin, human lactoferrin, and human defensin-3, also appear promising.¹⁵

As mimics of AMPs and due to their simplicity and insensitivity to proteases, we reasoned that ceragenins might be well suited for imaging of infections. By conjugating a ceragenin (bacteria targeting) to an appropriate metal chelating group (positron emission), we generated compounds with features necessary for selectively imaging infections. In initial studies of infection imaging, ceragenins were non-specifically labeled with ^{99m}Tc and successfully imaged an infection (*Staphylococcus aureus*) model in rats¹⁶. However, the nature of the ceragenin-technetium complex was not well established. Additionally, ceragenins display higher cell selectivity for Gram-negative bacteria (e.g., *Escherichia coli*) over Gram-positive organisms (e.g., *S. aureus*). Consequently, we anticipated that Gram-negative infections would be preferentially labeled by ceragenin conjugates.

Conjugates of a ceragenin with 1, 4, 7-triazacyclononane-1, 4, 7-triacetic acid (NOTA) were prepared, along with structural variants, and these were stably labeled with ^{64}Cu and injected into mice. Distribution of the labeled compounds was determined in un-infected mice and in mice with a local thigh infection. ^{64}Cu -labeled conjugates derived from a ceragenin accumulated in the infected muscle in significantly greater amounts than structural variants lacking a ceragenin. The presence of a C8 lipid chain on a ceragenin-containing conjugate increased the lipophilicity of the compound but did not significantly alter accumulation of the conjugate in infected muscle.

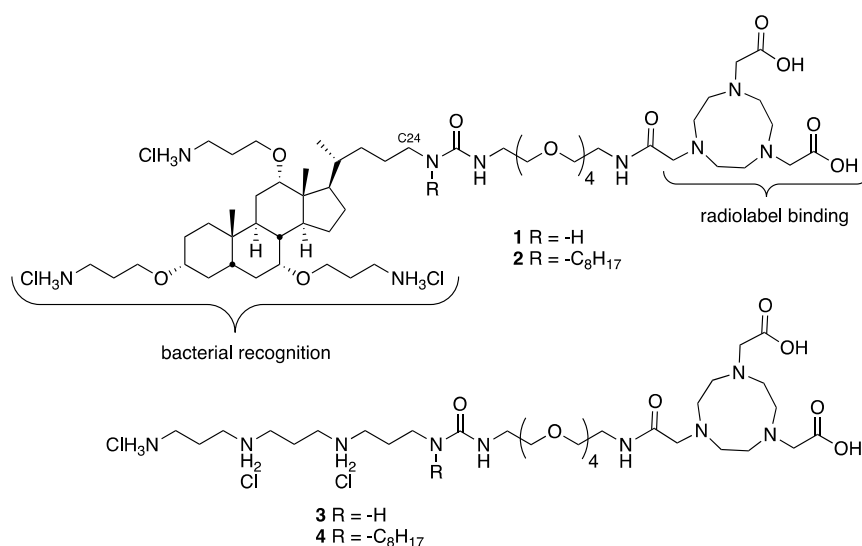
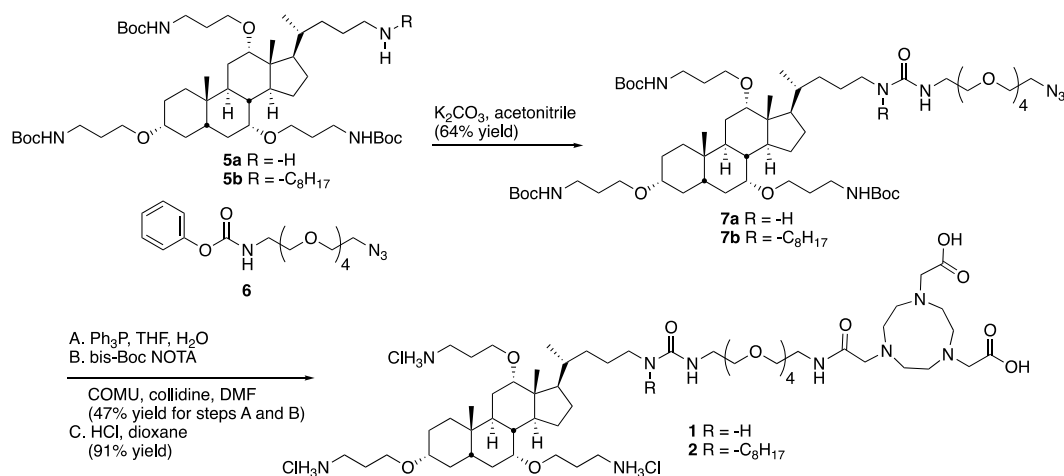


Figure 1.3.1 Structures of ceragenin-NOTA conjugates 1 and 2 and structural variants 3-5

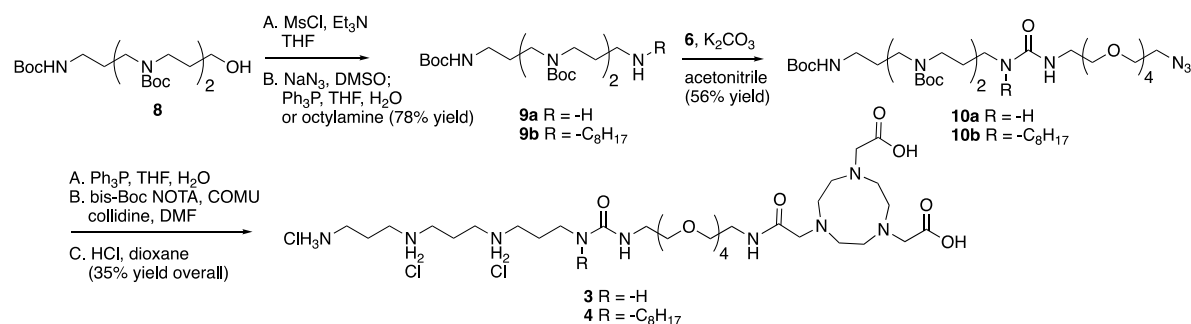
1.3.2 Synthesis of Ceragenin-NOTA Conjugates and Structural Variants

To generate desired conjugates **1** and **2**, amines **5a** and **5b** (Scheme 1.3.1) were reacted with phenylcarbamate **6** to give **7a** and **7b** in reasonable yields. The azide groups in **7a** and **7b** were reduced to the corresponding amines, which were reacted with bis-Boc NOTA, using COMU as a coupling agent. Deprotection of both the carbamates and the t-butyl esters with hydrogen chloride in dioxane gave **1** and **2**.



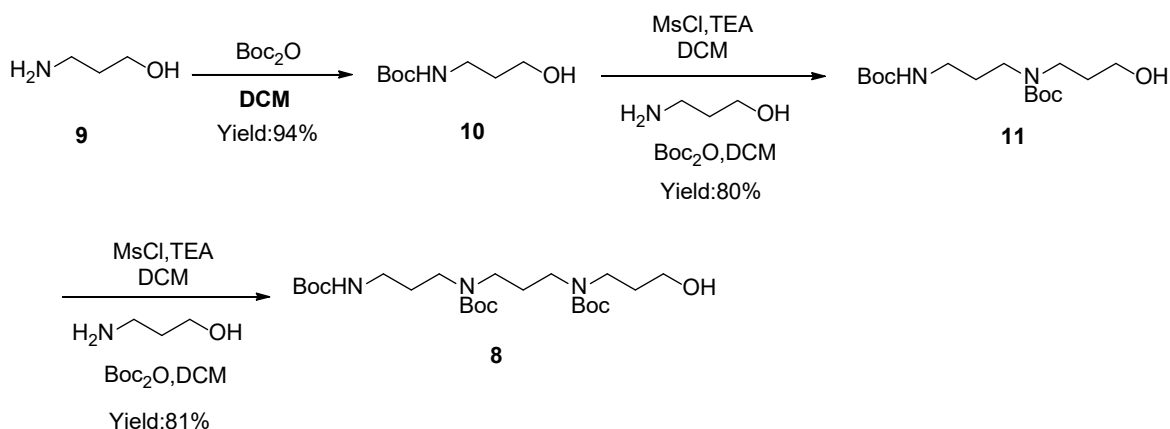
Scheme 1.3.1 Preparation of ceragenin-NOTA conjugates **1** and **2**

For generation of **3** and **4** the steps outlined in Scheme 1.3.2 were followed. Alcohol in compound **8** was converted to the mesylate and then to either the corresponding amine **9a** or octylamine **9b**. Coupling with the PEG tether **6** gave **10a** and **10b**, which were reduced and coupled with NOTA to give **3** and **4**.



Scheme 1.3.2 Preparation of tri-ammonium-NOTA conjugates **3** and **4**

For generation of **8** the steps outlined in Scheme 1.3.3 were followed. 3-amino-1-propanol was treated with Boc_2O to obtain **10**, which was converted to mesylate and then to the corresponding amine, finally to Boc-protected alcohol **11**. The same procedure as last step was followed to generate **8**.



Scheme 1.3.2 Preparation of **8**

1.3.3 Results and Discussion

We have found that lipid chains extending from the nitrogen on C24 of ceragenins impact their antimicrobial properties.¹⁷ Consequently, two different forms of ceragenin were used as bacterial membrane recognition elements: one without a lipid chain (**1**) and one with an octyl chain (**2**) (Figure 1.3.1). NOTA was used for binding ^{64}Cu , which is a positron emitter with a 12.7 hour half-life. NOTA has been well characterized as a thermodynamically and kinetically stable copper binding ligand suitable for radiolabeling a variety of targeting groups.¹⁸ An oligoethylene glycol linker was used to separate the ceragenin and NOTA to ensure that the bound copper ion did not interfere with interactions with bacterial membranes. In efforts to determine the structural features of conjugates **1** and **2** that impact bacterial labeling and imaging, structural variants **3** and **4** were prepared. Variants **3** and **4** retain three positive charges and lack the bile acid backbone found in **1** and **2**. The absence (**1**, **3**) or presence (**2**, **4**) of an octyl lipid chain was used to determine its role in association with bacteria. Conjugates **1-4** were loaded with $^{64}\text{Cu}^{2+}$ (CuCl_2) to give the corresponding complexes, which were analyzed via reversed-phase HPLC. Radiochemical purity was determined as $98 \pm 1.3\%$, and specific activity was maintained at ca. $20 \mu\text{Ci}/\mu\text{g}$ for all compounds. As shown in Figure 1.3.2, copper-labeled, ceragenin-NOTA

conjugates 1 and 2 (^{64}Cu -1 and ^{64}Cu -2) gave retention times of 12.0 and 15.4 min, respectively, without loss of the copper label (i.e., free copper was not detected). To the extent that retention times on a C18 silica chromatography column provide information about the lipophilicity of analytes, labeled structural variants 3 and 4 (^{64}Cu -3 and ^{64}Cu -4) proved to have lipophilicities comparable to and less than those of ^{64}Cu -1 and ^{64}Cu -2.

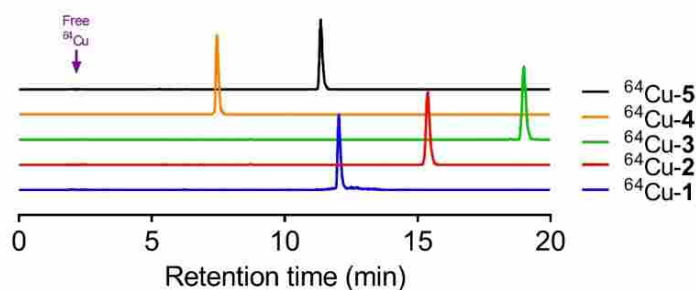


Figure 1.3.2 HPLC chromatograms of ^{64}Cu radiolabeled compounds. Retention times were 12.02, 15.4, 7.5 and 11.3 min for ^{64}Cu -1, ^{64}Cu -2, ^{64}Cu -3 and ^{64}Cu -4, respectively. If present, free copper would appear at 2.5 min.

To further demonstrate the stability of the complexes, studies were conducted in human serum to investigate potential degradation of the radiolabeled compounds. The stability of ceragenin complexes was determined by measuring the radioactive fraction of the parent compound at incubation intervals in human serum at 37 °C. No unbound metal was observed over the evaluation time indicating that the complex remained 100% intact up to 4 h.

To determine the relative uptake and retention of the conjugates, biodistribution experiments were conducted in CD-1 mice with labeled 1-4. The most substantial differences in uptake and retention among the conjugates were that ^{64}Cu -1 and ^{64}Cu -2 were retained in the liver in higher relative amounts than ^{64}Cu -3 and ^{64}Cu -4, and that ^{64}Cu -1 was retained in the kidney in higher relative amounts than ^{64}Cu -2.

We used a model of thigh muscle infection with *Escherichia coli* (TG1) in CD-1 mice to evaluate the impact of infection on distribution of the conjugates. The infection was established 24 h before injection of the conjugates. The primary measure of uptake was percentage of injected dose per gram in each type of tissue (%ID/g). We previously observed high affinity of ceragenins for the outer membranes of Gram-negative bacteria, including the lipid A portion of lipopolysaccharide,^{6,7} and it was anticipated that this affinity would result in accumulation of the conjugates at the site of infection. Similar to the uninfected mice ⁶⁴Cu-1 and ⁶⁴Cu-2 accumulated in the liver and kidney, relative to ⁶⁴Cu-3 and ⁶⁴Cu-4 (Figure 1.3.3) of infected mice. Uptake values for labeled conjugates in the left thigh muscle (control, no bacteria) were not significantly different (Figure 1.3.3B). Uptake in the right thigh muscle, containing the bacterial infection, was highest with ⁶⁴Cu-1 (1.86 ± 0.78 %ID/g) and was lowest with ⁶⁴Cu-3 (0.26 ± 0.07 %ID/g) with a p value of 0.008. The uptake of ⁶⁴Cu-2 was also significantly increased relative to ⁶⁴Cu-3 and ⁶⁴Cu-4.

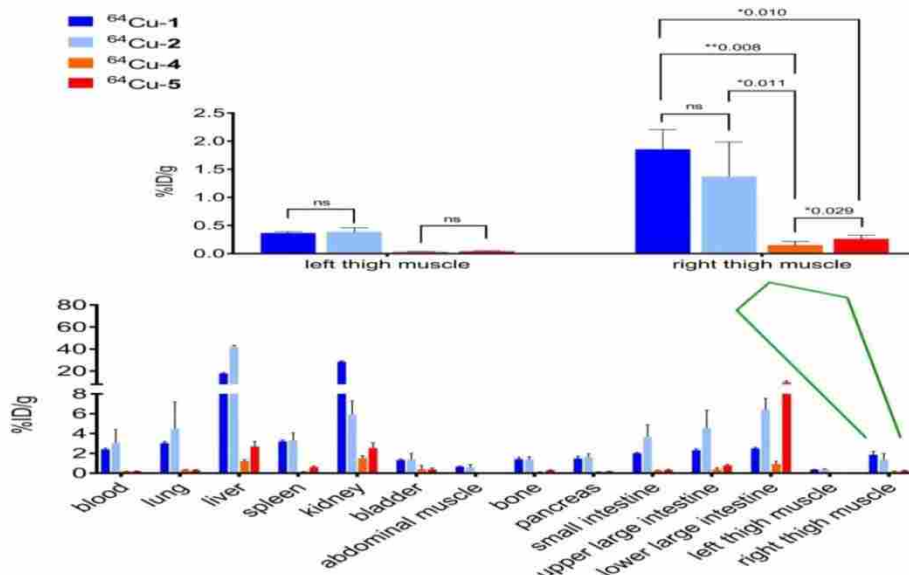


Figure 1.3.3 Overall biodistribution results (%ID/g) of ⁶⁴Cu-1, ⁶⁴Cu-2, ⁶⁴Cu-3 and ⁶⁴Cu-4 in CD-1 mice with intramuscular infection in right thigh muscle at 4 h post injection

Based on the biodistribution results, ^{64}Cu -1 was selected for more detailed autoradiography studies of infections sites. Thigh infections (*E. coli*) were generated in mice as described above, and muscles were removed, sectioned, and imaged. Uptake of ^{64}Cu -1 was much higher in the infected thigh muscles compared to the control left thigh (Figure 1.3.4). This significant difference ($p < 0.0001$) was quantified by recording the number of counts per mm^2 from the sections and these values are given in Figure 1.3.5A. A comparison of the %ID/g of ^{64}Cu -1 in abdominal and thigh muscles is given in Figure 1.3.5B. Further comparison was from in vivo measurement of standardized uptake values (SUVs), which are ratios of the image-derived radioactivity concentration and the whole-body concentration of injected radioactivity. With this measurement, there is no significant difference between the uptake of ^{64}Cu -1 in uninfected thigh muscle and peripheral muscle, while the difference between uptake in infected and uninfected muscle is significant ($p = 0.0064$) (Figure 1.3.5C).

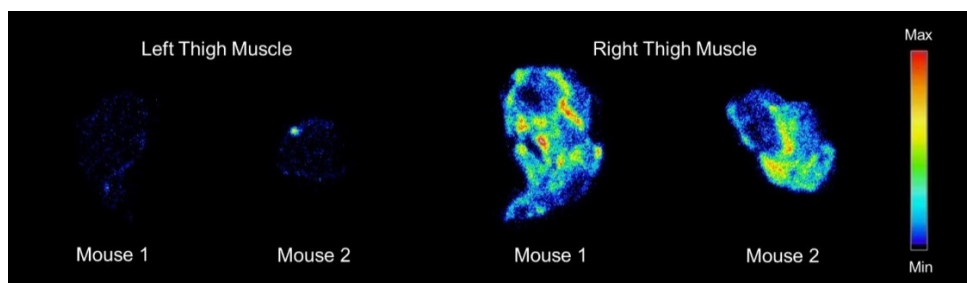


Figure 1.3.4 Representative images from ex vivo autoradiography of left and right thigh muscle sections (20 - 40 μm) from ^{64}Cu -1 in CD-1 mice, at 4 h post injection

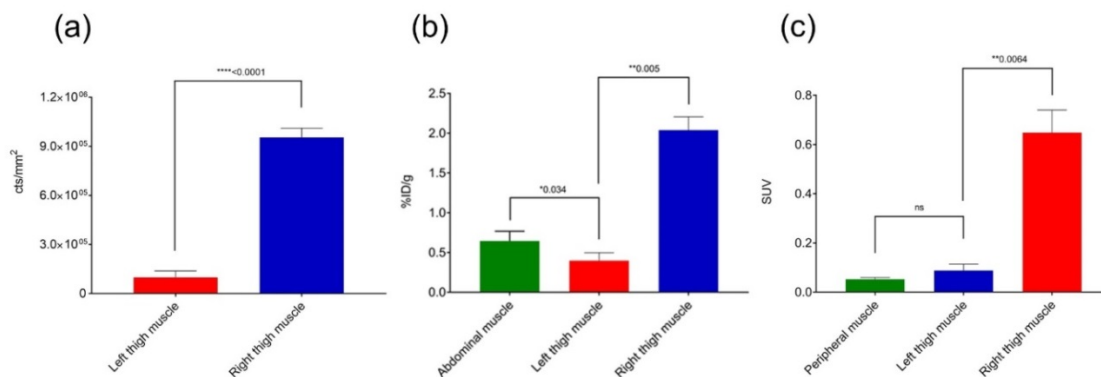


Figure 1.3.5 Comparisons of ⁶⁴Cu-1 uptake in CD-1 mice with an intramuscular infection (*E. coli*) in the right thigh at 4 h post injection. (a) Quantitative results (counts per mm²) of ⁶⁴Cu-1 in an ex vivo autoradiography study with left and right thigh muscle sections (20 - 40 μ m, n = 9 sections per muscle). (b) Abdominal vs. thigh muscle uptake of ⁶⁴Cu-1 in %ID/g. (c) SUV (standardized uptake value) calculations from in vivo imaging comparing peripheral and thigh muscle.

1.3.4 Conclusions

Lipopolysaccharide is the primary constituent of the outer membranes of Gram-negative bacteria, and the lipid A structure is well conserved among bacteria. Consequently, lipid A is a logical target for bacterial recognition. We have measured the K_d of the base structure of ceragenins for the lipid A portion of lipopolysaccharide as 0.59 μ M⁷, and the affinity of this structure for lipid A is greater than that of polymyxin B, the paradigm of small molecule binding of lipid A. The affinity of ceragenins for lipid A is consistent with measurements of interactions of the ceragenin base structure for intact cells; a labeled ceragenin was shown to preferentially associate with Gram-negative bacteria over Gram-positive bacteria and eukaryotic cells⁷. Translation of affinity of ceragenins to imaging of infection poses a challenge due to the complex environments provided by in vivo applications including higher numbers of eukaryotic cells relative to prokaryotes. Nevertheless, by conjugating ceragenins to NOTA and loading

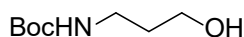
with ^{64}Cu , we have generated compounds that selectively label infected tissue in mice. These conjugates display the expected ability to bind ^{64}Cu while retaining affinity for bacteria. This affinity allows selective labeling of bacteria and may provide a means of identifying sites of infection in patients that display associated symptoms without indications of localized infection.

1.3.5 Experiment Section

General: Reagents were purchased from Aldrich Chemical Co. unless otherwise noted. Methylene chloride, THF, DMF, pyridine, and DMSO were dried by passage through a Glass Contour solvent drying system containing a cylinder of activated alumina. Silica gel was used for chromatography unless otherwise noted.

Instrumentation: ^1H and ^{13}C NMR spectra were recorded on a Varian Gemini 500 (500 MHz) spectrometer. Proton chemical shift were referenced to tetramethylsilane (TMS). Carbon chemical shifts were referenced to carbon resonance of solvents (CDCl_3 , CD_3OD). High resolution electron impact mass spectra (HR-MS) were obtained on a JOEL SX 102A spectrometer.

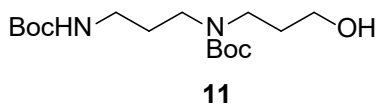
Experiment:



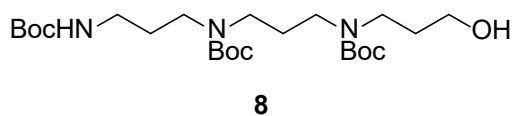
10

Compound 10. To a solution of 3-amino-1-propanol (20.64 g, 0.275 mol) in 200 mL of DCM, Boc₂O (60 g, 0.275 mol) was added in portion. The solution was stirred overnight. 45 g of the product was isolated through a column chromatography (SiO_2). The yield was 94%. ^1H NMR (CDCl_3 , 500 MHz) δ 4.822 (br, 1 H), 3.636-3.668 (m, 2 H), 3.275-3.299 (m, 2 H), 3.097 (br, 1

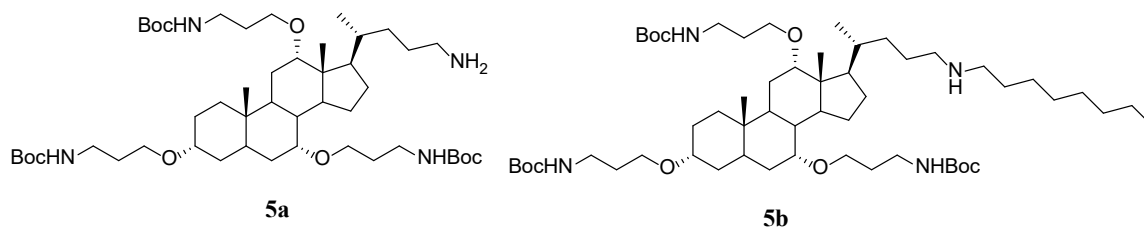
H), 1.633-1.677 (m, 2 H), 1.439 (s, 9 H); ^{13}C NMR (CDCl_3 , 125 MHz) δ 158.797, 59.391, 37.055, 33.122, 28.589; HRMS (ESI) calcd for $\text{C}_8\text{H}_{17}\text{NO}_3$ $[\text{M}+\text{H}]^+$: 176.1208, found: 176.1256.



Compound 11. To a solution of 10 (3.2 g, 18.3 mmol) in 20 mL of DCM, MsCl (2.4 g, 21 mmol) and Et₃N (2.12 g, 21 mmol) were added at 0 °C. The temperature was allowed to rise up to room temperature. The solution was stirred for 30 mins. Then, 10 mL of water was used to wash the solution. The aqueous layer was extracted with DCM three times. The combined organic layer was dried over Na₂SO₄. After the solvent was removed, 3-amino-1-propanol (10.32 g, 0.14mol) was added to dissolve the residue. The solution was stirred at 80 °C for 2 hrs. 3-amino-1-propanol was removed under vacuum. 50 mL of water was used to wash the solution. The aqueous layer was extracted with DCM three times. The combined organic layer was dried over Na₂SO₄. After removing the solvent, the residue was dissolved into 50 mL of DCM. Then, Boc₂O (4 g, 18.3 mmol) was added. The solution was stirred overnight. 4.8 g of the product was isolated through a column chromatography (SiO₂). The yield was 80%. ^1H NMR (CDCl_3 , 500 MHz) δ 3.475-3.054 (m, 8 H), 1.807-1.591 (m, 4 H), 1.413 (s, 9 H), 1.367 (s, 9 H); ^{13}C NMR (CDCl_3 , 125 MHz) δ 163.851, 158.797, 83.078, 80.677, 79.704, 66.490, 46.368, 44.971, 37.284, 28.445, 28.430, 28.414, 27.772, 27.753, 27.110, 22.257; HRMS (ESI) calcd for $\text{C}_{16}\text{H}_{32}\text{N}_2\text{O}_5$ $[\text{M}+\text{H}]^+$: 333.2311, found: 333.2316.

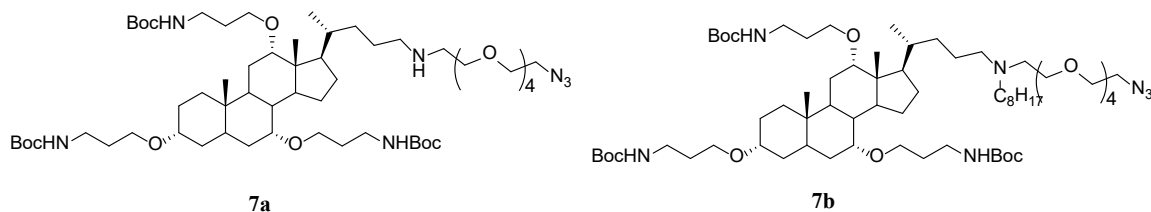


Compound 8. To a solution of **11** (4.8 g, 14.4 mmol) in 50 mL of DCM, MsCl (2.0 g, 17.5 mmol) and Et₃N (1.8 g, 17.5 mmol) were added at 0 °C. The temperature was allowed to rise up to room temperature. The solution was stirred for 30 mins. Then, 10 mL of water was used to wash the solution. The aqueous layer was extracted with DCM three times. The combined organic layer was dried over Na₂SO₄. After the solvent was removed, 3-amino-1-propanol (10.32 g, 0.14mol) was added to dissolve the residue. The solution was stirred at 80 °C for 2 hrs. 3-amino-1-propanol was removed under vacuum. 50 mL of water was used to wash the solution. The aqueous layer was extracted with DCM three times. The combined organic layer was dried over Na₂SO₄. After removing the solvent, the residue was dissolved into 50 mL of DCM. Then, Boc₂O (3.2 g, 15 mmol) was added. The solution was stirred overnight. 6.2 g of the product was isolated through a column chromatography (SiO₂). The yield was 81%. ¹H NMR (CDCl₃, 500 MHz) δ 4.822 (br, 1 H), 3.754-3.117 (m, 12 H), 3.097 (br, 1 H), 1.696-1.568 (m, 6 H), 1.477 (s, 9 H), 1.437 (s, 9 H); ¹³C NMR (CDCl₃, 125 MHz) δ 156.958, 156.436, 156.422, 80.541, 58.231, 44.158, 42.196, 37.658, 33.065, 31.310, 30.395, 28.827, 28.403, 28.383, 27.647; HRMS (ESI) calcd for C₂₄H₄₇N₃O₇ [M+H]⁺: 490.3414, found: 490.3468.



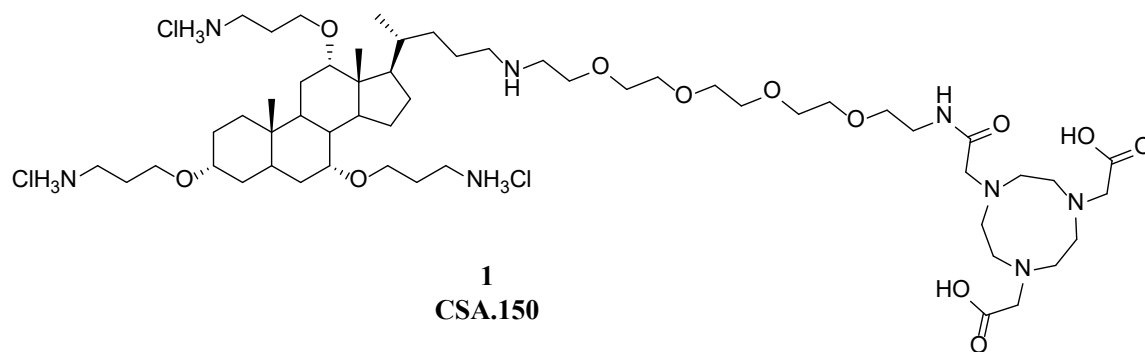
Compound 7a: To a solution of **5a** (4.67 g, 3.8 mmol) in acetonitrile (100 mL), potassium carbonate (1.5 g, 3.8 mmol) and **6** (1.45 g, 3.8 mmol) were added sequentially. The mixture was heated to reflux for 12 h. The mixture was allowed to cool to room temperature and water (50

mL) was added. The product was extracted with ethyl acetate (100 mL), and the extract was dried over sodium sulfate and concentrated under vacuum. Column chromatography (silica gel with dichloromethane/methanol: 20:1 as eluent) gave the desired azide as 2.8 g (64% yield) of a clear oil. ^1H NMR (CDCl_3 , 500 MHz): δ 4.79 (br, 1 H), 3.6-3.7 (m, 18 H), 3.03-3.58 (m, 22 H), 1.55-2.11 (m, 17 H), 1.43 (s, 27 H), 1.20-1.31 (m, 9 H), 0.98-1.03 (m, 2 H), 0.88-0.94 (m, 8 H), 0.69 (s, 3 H). ^{13}C NMR (CDCl_3 , 125 MHz): δ 158.02, 156.23, 156.07, 80.56, 79.26, 78.89, 78.63, 70.70, 70.67, 70.63, 70.61, 70.57, 70.52, 70.15, 70.02, 66.40, 65.76, 50.61, 47.78, 47.05, 46.15, 42.60, 41.88, 41.84, 39.68, 39.43, 38.64, 38.35, 35.66, 35.21, 34.91, 34.86, 33.16, 31.83, 30.57, 30.11, 29.69, 29.47, 29.27, 28.72, 28.61, 28.54, 28.48, 17.89, 14.11, 12.49. HRMS (ESI) calcd for $\text{C}_{59}\text{H}_{108}\text{N}_8\text{O}_{14}$ $[\text{M}+\text{H}]^+$: 1153.7985, found: 1153.8031.

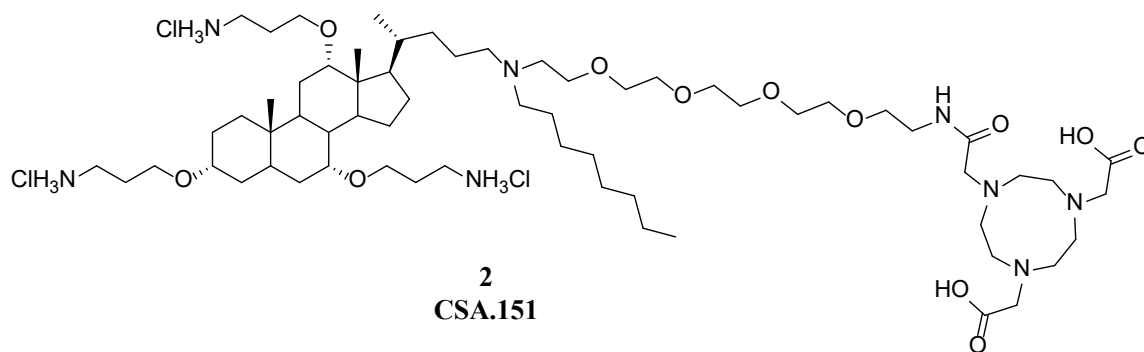


Compound 1: To a solution of **7a** (2.8 g, 2.4 mmol) in THF (50 mL) and water (17 mL), triphenyl phosphine (6.2 g, 24 mmol) was added. The mixture was stirred at room temperature for 12 h. The THF was removed under vacuum, and the resulting mixture was extracted with dichloromethane (3 x 50 mL). The combined extracts were dried over sodium sulfate and concentrated under vacuum. A silica gel plug, washed with dichloromethane/methanol: 20:1, was used to remove triphenylphosphine oxide and excess triphenylphosphine giving the desired amine in crude form as 1.8 g (73% yield) of a clear oil. To a solution of the amine (0.3 g, 0.27 mmol) and bis-BOC NOTA (0.11 g, 0.28 mmol) in DMF (20 mL), COMU (0.14 g, 0.33 mmol) and collidine (0.05 g, 0.416 mmol) were added. The mixture was stirred for 2 h. Water (20 mL)

was added, and the mixture was extracted with dichloromethane (3 x 50 mL). The combined extracts were dried over sodium sulfate and concentrated under vacuum. Column chromatography (silica gel with dichloromethane/methanol: 20:1 as eluent) gave the desired conjugate as 0.25 g (65% yield) of a clear oil. ^1H NMR (CDCl_3 , 500 MHz): δ 4.79 (br, 1 H), 3.6-3.7 (m, 18 H), 3.03-3.58 (m, 28 H), 2.2-2.4 (m, 12H), 1.55-2.11 (m, 17 H), 1.43 (s, 27 H), 1.39 (s, 18H), 1.20-1.31 (m, 9 H), 0.98-1.03 (m, 2 H), 0.88-0.94 (m, 8H), 0.69 (s, 3 H). ^{13}C NMR (CDCl_3 , 125 MHz): δ 158.02, 156.23, 156.07, 82.3, 81.18, 80.56, 79.26, 78.89, 78.63, 70.70, 70.67, 70.63, 70.61, 70.57, 70.52, 70.15, 70.02, 69.78, 69.66, 69.59, 69.51, 69.50, 69.45, 66.48, 66.47, 66.45, 66.40, 65.76, 50.61, 47.78, 47.05, 46.15, 42.60, 41.88, 41.84, 39.68, 39.43, 38.64, 38.35, 35.66, 35.21, 34.91, 34.86, 33.16, 31.83, 30.57, 30.11, 29.69, 29.47, 29.27, 28.78, 28.72, 28.61, 28.54, 28.48, 25.56, 17.89, 14.11, 12.49. HRMS (ESI) calcd for $\text{C}_{79}\text{H}_{145}\text{N}_9\text{O}_{19}$ $[\text{M}+\text{H}]^+$: 1525.0657, found:1525.0721. The conjugate (0.25 g) was dissolved in a solution of HCl in dioxane (4 M, 10 mL) and stirred at room temperature for 18 h. The solvent was removed under vacuum, and toluene (50 mL) as added. Removal of the toluene under vacuum (azeotropically drying the product) gave **1** (0.15 g, 91% yield) as a light yellow solid. ^1H NMR (CDCl_3 , 500 MHz): δ 4.79 (br, 1 H), 3.6-3.7 (m, 18 H), 3.03-3.58 (m, 28 H), 2.2-2.4 (m, 12H), 1.55-2.11 (m, 17 H), 1.20-1.31 (m, 9 H), 0.98-1.03 (m, 2 H), 0.88-0.94 (m, 8H), 0.69 (s, 3H). ^{13}C NMR (CDCl_3 , 125 MHz): δ 170.72, 158.02, 156.07, 80.56, 79.26, 78.89, 70.70, 70.67, 70.63, 70.61, 70.57, 70.52, 70.15, 70.02, 69.78, 69.66, 69.59, 69.51, 69.50, 69.45, 66.48, 66.47, 66.45, 66.40, 65.76, 50.61, 47.78, 47.05, 46.15, 42.60, 41.88, 41.84, 39.68, 39.43, 38.64, 38.35, 35.66, 35.21, 34.91, 34.86, 33.16, 31.83, 30.57, 30.11, 29.69, 29.51, 29.47, 29.35, 29.27, 28.78, 28.61, 28.54, 17.89, 14.11, 12.49. HRMS (ESI) calcd for $\text{C}_{56}\text{H}_{105}\text{N}_9\text{O}_{13}$ $[\text{M}+\text{H}]^+$: 1112.7832, found:1112.8031.

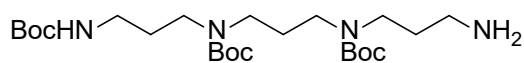


Compound 7b: Phenylcarbonate **6** (30 mg, 0.075 mmol) was added to a mixture of tris-Boc CSA-13 (**5b**) (73mg, 0.075 mmol) and potassium carbonate (21 mg, 0.15 mmol) in acetonitrile (3 mL). The mixture was heated to reflux for 12 h. Water (5 mL) was added after the reaction mixture had been cooled to room temperature. The resulting mixture was extracted with ethyl acetate (3 x 5 mL), and the combined organic extracts were dried over sodium sulfate. The solvent was removed under vacuum, and the product was purified via silica gel chromatography (5% methanol in dichloromethane as eluent). Compound **7b** was recovered as a clear oil (63 mg, 67% yield). ¹H NMR (CDCl₃, 500 MHz): δ 4.79 (br, 1 H), 3.6-3.7 (m, 18 H), 3.03-3.58 (m, 24 H), 1.55-2.11 (m, 17 H), 1.43 (s, 27 H), 1.20-1.31 (m, 21 H), 0.98-1.03 (m, 2 H), 0.88-0.94 (m, 11 H), 0.69 (s, 3 H). ¹³C NMR (CDCl₃, 125 MHz): δ 158.02, 156.23, 156.07, 80.56, 79.26, 78.89, 78.63, 70.70, 70.67, 70.63, 70.61, 70.57, 70.52, 70.15, 70.02, 66.40, 65.76, 50.61, 47.78, 47.37, 47.05, 46.15, 42.60, 41.88, 41.84, 39.68, 39.43, 38.64, 38.35, 35.66, 35.21, 34.91, 34.86, 33.16, 31.83, 30.57, 30.11, 29.69, 29.47, 29.27, 28.72, 28.61, 28.54, 28.48, 27.61, 27.04, 25.63, 23.31, 22.95, 22.87, 22.48, 17.89, 14.11, 12.49. HRMS (ESI) calcd for C₆₇H₁₂₄N₈O₁₄ [M+H]⁺: 1265.9237, found: 1265.9648.



Compound 2: To a solution of azide compound 7b (20 mg, 0.015 mmol) in THF (2mL) and H₂O (0.5 mL), triphenyl phosphine (40mg, 0.15 mmol) was added. The mixture was allowed to run for 12 h at room temperature. The THF was removed under vacuum, and the resulting mixture was extracted with dichloromethane (3 x 10 mL). The combined organic layers were dried over sodium sulfate and concentrated under vacuum. Column chromatography (silica gel with dichloromethane/methanol (0.05% ammonium hydroxide): 20:1 as eluent) gave 15 mg (85% yield) of the resulting amine product as a clear oil. The resulting amine (15 mg, 0.0125 mmol) and bis-BOC NOTA (5.2 mg, 0.0125 mmol) were dissolved in DMF (1 mL), COMU (6.5 mg, 0.015 mmol) and collidine (2.3 mg, 0.0188 mmol) were added. The mixture was stirred for 2 h. Water (2 mL) was added, and the mixture was exacted with dichloromethane (3 x 5mL). The combined extracts were dried over sodium sulfate and concentrated under vacuum. Column chromatography (silica gel with dichloromethane/methanol: 20:1 as eluent) gave the desired conjugate as 12 mg (63% yield) of a clear oil, which was treated with 3 mL of 4 M HCl in dioxane. The reaction was allowed to run for 18 hours at room temperature. The mixture solvent was removed under high vacuum to give the compound 2 (8mg,91% yield) as white solid HCl salt formation. (48% total yield) ¹H NMR (CDCl₃, 500 MHz): δ 4.79 (br, 1 H), 3.6-3.7 (m, 18 H), 3.03-3.58 (m, 30 H), 2.2-2.4 (m,12H), 1.52-2.11 (m, 19 H), 1.43 (s, 27 H), 1.39 (s, 18H), 1.20-1.31 (m, 19 H), 0.98-1.03 (m, 2 H), 0.88-0.94 (m, 11H), 0.69 (s, 3 H). ¹³C

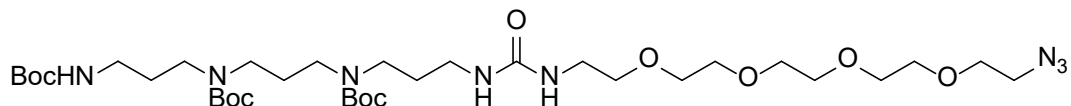
NMR (CDCl₃, 125 MHz): δ 173.2, 171.4, 158.02, 156.23, 156.07, 82.3, 81.18, 80.56, 79.26, 78.89, 78.63, 70.70, 70.67, 70.63, 70.61, 70.57, 70.52, 70.15, 70.02, 69.78, 69.66, 69.59, 69.51, 69.50, 69.45, 66.48, 66.47, 66.45, 66.40, 65.76, 50.61, 50.11, 47.78, 47.05, 46.15, 42.60, 41.88, 41.84, 39.68, 39.43, 38.64, 38.35, 35.66, 35.21, 34.91, 34.86, 33.16, 31.92, 31.83, 30.57, 30.11, 29.69, 29.47, 29.31, 29.28, 29.27, 28.78, 28.72, 28.61, 28.54, 28.48, 26.61, 25.56, 22.78, 17.89, 14.11, 14.10, 12.49. HRMS (ESI) calcd for C₆₄H₁₂₁N₉O₁₃ [M+H]⁺: 1225.6980, found: 1225.7132.



9a

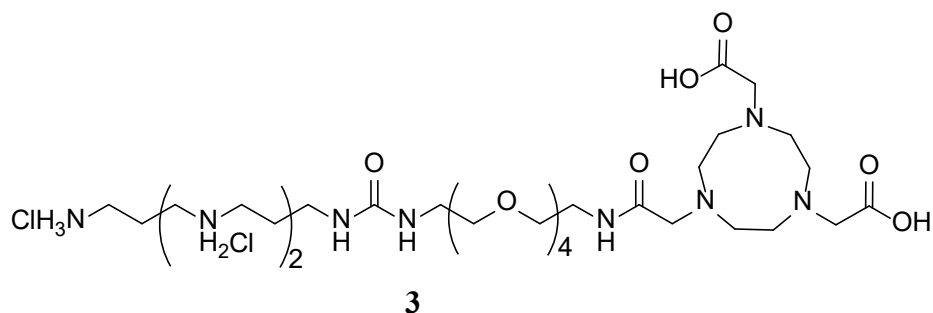
Compound 9a: To a solution of **8** (4.89 g, 10 mmol) in THF (100 mL), were added mesylchloride (1.2 g, 11 mmol) and triethylamine (1.2 g, 12 mmol) at 0 °C. The mixture was allowed to warm to room temperature over 30 min. Water (50 mL) was added, and the product was extracted using dichloromethane (3 x 50 mL). The combined extracts were dried over sodium sulfate, and solvents were removed under vacuum. After the solvent was removed, the oil was dissolved in DMSO (40 mL) and sodium azide (1.3 g, 20 mmol) was added, and the resulting mixture was stirred at 80 °C for 12 h. The mixture was cooled to room temperature and water (50 mL) and dichloromethane (100 mL) were added. The resulting organic solution was dried over sodium sulfate and concentrated under vacuum. The aqueous layer was extract with DCM three times and the combined organic phase was dried over Na₂SO₄. After dried off the solvent, the crude azide compound was treated with triphenyl phosphine (5.2g, 20 mmol) in THF (40 mL) and H₂O (10 mL), the mixture was allowed to run for 12 hours at room temperature. Then THF was removed, the aqueous layer was exacted with DCM (3×50 ml). The combined organic layer was dried over Na₂SO₄. 3.2g of the

target compound was isolated through a column chromatography. The yield was 68%. ^1H NMR (CDCl_3 , 400 MHz) δ 3.16-3.31 (m, 6H), 3.06 (m, 2H), 2.58 (m, 4H), 1.64 (m, 4H), 1.41 (s, 19H), 1.25-1.3 (m, 2H), 1.0-1.12 (m, 7H), 0.68 (t, 3H). ^{13}C NMR (CDCl_3 , 125 MHz) δ 156.81, 156.52, 79.81, 79.65, 79.58, 28.4, 27.16, 25.93, 24.41, 23.64, 22.65. HRMS (ESI) calcd for $\text{C}_{24}\text{H}_{48}\text{N}_4\text{O}_6$ $[\text{M}+\text{H}]^+$:489.3574, found:489.4132.



10a

Compound 10a: To a solution of **9a** (3.2 g, 6.5 mmol) in acetonitrile (30 mL) were added potassium carbonate (1.0 g, 7.6 mmol) and **6** (2.5 g, 6.5 mmol). The mixture was heated to reflux and stirred for 12 hrs. The mixture was allowed to cool to room temperature, and water (30 mL) was added. The product was extracted with ethylacetate (50 mL), and the resulting solution was dried over sodium sulfate. After chromatography (silica gel, 3% MeOH:DCM) 2.7 g of **10a** (55% yield). ^1H NMR (CDCl_3 , 400 MHz) δ 3.6-3.7 (m, 16 H), 3.47 (t, 2 H), 3.36 (t, 2 H), 3.16-3.31 (m, 6H), 3.06 (m, 2H), 2.58 (m, 4H), 1.64 (m, 6H), 1.41 (s, 15H), 1.25-1.3 (m, 2H), 1.0-1.12 (m, 7H), 0.68 (t, 3H) ^{13}C NMR (CDCl_3 , 125 MHz) δ 156.81, 156.52, 154.88, 79.81, 79.65, 79.58, 70.70, 70.67, 70.62, 70.61, 70.57, 70.31, 70.02, 69.85, 41.04, 28.35, 27.16, 24.41, 23.64, 22.65, 21.97. HRMS (ESI) calcd for $\text{C}_{35}\text{H}_{68}\text{N}_8\text{O}_{11}$ $[\text{M}+\text{H}]^+$:777.5008, found:777.5121.



Compound 3: To a solution of **10a** (2.5 g, 3.2 mmol) in THF (50 mL) and water (10 mL), was added triphenyl phosphine (2.6 g, 10 mmol). The mixture was stirred at room temperature for 12 h. The THF was removed under vacuum, and the remaining aqueous mixture was extracted with dichloromethane (3 x 50 mL). The combined extracts were dried over sodium sulfate, and the desired amine was recovered after chromatography (silica gel, 5% MeOH:DCM and 0.1% NH₄.OH) as 1.8 g (77% yield) of a clear oil. This amine (0.5 g, 0.66 mmol) and bis-Boc NOTA (0.27 g, 0.66 mmol), COMU (0.3 g, 0.7 mmol) and collidine (0.1 g, 0.82 mmol) were dissolved in DMF (20 mL). The mixture was stirred for 2 h, and cold water (20 mL) was added. The product was extracted with dichloromethane (3 x 50 mL), and the combined extracts were dried over sodium sulfate. The solvent was removed under vacuum, and after chromatography (silica gel, 3% MeOH:DCM), the desired amide was isolated as 0.45 g (61% yield) of a clear oil. ¹H NMR (CDCl₃, 400 MHz) δ 3.6-3.7 (m, 16 H), 3.47 (t, 2 H), 3.36 (t, 2 H), 3.16-3.31 (m, 12H), 2.9-3.1 (m, 12H), 3.06 (m, 2H), 2.58 (m, 4H), 1.64 (m, 4H), 1.43 (s, 27H), 1.41(s, 8H), 1.25-1.3 (m, 2H), 1.0-1.12 (m, 7H), 0.68 (t, 3H) ¹³C NMR (CDCl₃, 125 MHz) δ 170.71, 168.64, 159.47, 156.81, 156.52, 154.88, 81.18, 80.52, 79.81, 79.65, 79.58, 70.70, 70.67, 70.62, 70.61, 70.57, 70.31, 70.02, 69.85, 66.58, 66.53, 66.50, 66.46, 60.25, 58.06, 56.72, 51.10, 41.04, 28.42, , 27.16, 24.41, 23.64, 22.65, 21.97. HRMS (ESI) calcd for C₅₅H₁₀₅N₉O₁₆ [M+H]⁺:1149.7679, found:11149.7832. This amide (0.2 g) was dissolved in a solution of HCl in dioxane (4 M, 5 mL).

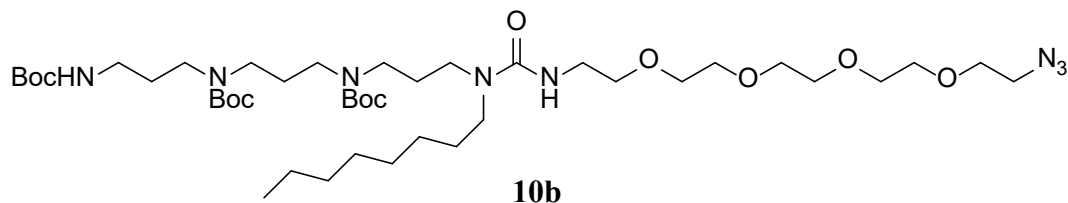
The mixture was stirred for 18 h, and solvent was removed under vacuum. Toluene (50 mL) was added to the resulting material and evaporated under vacuum to remove residual water. Compound **3** was isolated as a light yellow solid (0.12 g, 90% yield). ^1H NMR (D_2O , 400 MHz) δ 3.96 (m, 4 H), 3.85 (m, 2 H), 3.2-3.6 (m, 34H), 2.9-3.1 (m, 10 H), 1.98 (m, 2 H), 1.93 (m, 2H), 0.68 (t, 3H). ^{13}C NMR (D_2O , 125 MHz) δ 170.71, 168.64, 159.47, 71.51, 70.72, 69.71, 69.54, 69.41, 66.58, 66.53, 66.50, 66.46, 60.25, 58.06, 56.72, 51.10, 51.06, 46.71, 45.06, 44.63, 44.56, 44.30, 43.34, 43.27, 44.14, 39.90, 39.09, 36.49, 28.35, 27.16, 25.93, 24.41, 23.64, 22.65. HRMS (ESI) calcd for $\text{C}_{32}\text{H}_{65}\text{N}_9\text{O}_{10}$ $[\text{M}+\text{H}]^+$:736.4854, found:736.5023.



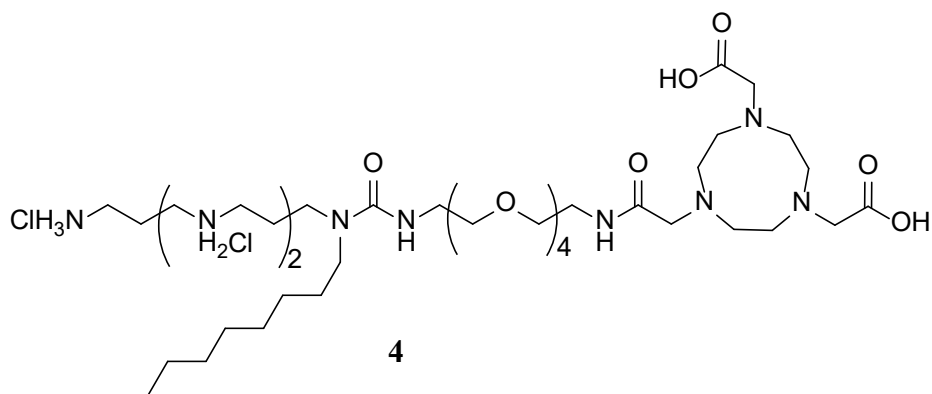
9b

Compound 9b: To a solution of **8** (4.89 g, 10 mmol) in THF (100 mL), were added mesylchloride (1.2 g, 11 mmol) and triethylamine (1.2 g, 12 mmol) at 0 °C. The mixture was allowed to warm to room temperature over 30 min. Water (50 mL) was added, and the product was extracted using dichloromethane (3 x 50 mL). The combined extracts were dried over sodium sulfate, and solvents were removed under vacuum. The resulting oil was dissolved in octyl amine (10 mL), and the resulting mixture was stirred at 80 °C for 1 h. The mixture was allowed to cool to room temperature, and water (50 mL) and dichloromethane (100 mL) were added. The layers were separated and the aqueous layer was extracted with dichloromethane (3 x 50 mL). The combined extracts were dried over sodium sulfate and concentrated under vacuum. After chromatography (silica gel, 3% MeOH:DCM and 0.1% NH_4OH), 4.6 g (78% yield) of the desired amine was isolated as a clear oil. ^1H NMR (CDCl_3 , 500 MHz) δ 3.16-3.31 (m, 8 H), 3.06 (m, 2 H), 2.58 (m, 4 H), 1.64 (m, 6 H), 1.41 (s, 27

H), 1.25-1.3 (m, 2 H), 1.0-1.12 (m, 10 H), 0.68 (t, 3 H) ^{13}C NMR (CDCl_3 , 125 MHz) δ 156.81, 156.52, 79.81, 79.65, 79.58, 28.4, 28.35, 27.16, 25.93, 24.41, 23.64, 22.65, 21.97, 13.42. HRMS (ESI) calcd for $\text{C}_{32}\text{H}_{64}\text{N}_4\text{O}_6$ $[\text{M}+\text{H}]^+$:848.6106, found:848.6183.



Compound 10b: To a solution of **9b** (4.6 g, 7.6 mmol) in acetonitrile (20 mL) were added potassium carbonate (3.0 g, 7.6 mmol) and **6** (2.9 g, 7.6 mmol). The mixture was heated to reflux and stirred for 12 h. The mixture was allowed to cool to room temperature, and water (30 mL) was added. The product was extracted with ethylacetate (50 mL), and the resulting solution was dried over sodium sulfate. After chromatography (silica gel, 3% MeOH: DCM) 3.8 g of **10b** (56% yield). ^1H NMR (CDCl_3 , 500 MHz) δ 3.6-3.7 (m, 16 H), 3.47 (t, 2 H), 3.36 (t, 2 H), 3.16-3.31 (m, 8 H), 3.06 (m, 2H), 2.58 (m, 4H), 1.64 (m, 6H), 1.41 (s, 27 H), 1.25-1.3 (m, 2 H), 1.0-1.12 (m, 10 H), 0.68 (t, 3 H). ^{13}C NMR (CDCl_3 , 125 MHz) δ 156.81, 156.52, 154.88, 79.81, 79.65, 79.58, 70.70, 70.67, 70.62, 70.61, 70.57, 70.31, 70.02, 69.85, 50.63, 41.04, 28.4, 28.35, 27.16, 25.93, 24.41, 23.64, 22.65, 21.97, 13.42. HRMS (ESI) calcd for $\text{C}_{43}\text{H}_{84}\text{N}_8\text{O}_{11}$ $[\text{M}+\text{H}]^+$:889.6260, found:889.6254.



Compound 4: To a solution of **10b** (3.8 g, 4.3 mmol) in THF (50 mL) and water (17 mL), was added triphenyl phosphine (2.3 g, 8.6 mmol). The mixture was stirred at room temperature for 12 h. The THF was removed under vacuum, and the remaining aqueous mixture was extracted with dichloromethane (3 x 50 mL). The combined extracts were dried over sodium sulfate, and the desired amine was recovered after chromatography (silica gel, 5% MeOH:DCM and 0.1% NH₄.OH) as 2.5 g (71% yield) of a clear oil. This amine (0.5 g, 0.58 mmol) and bis-Boc NOTA (0.24 g, 0.58 mmol), COMU (0.3 g, 0.7 mmol) and collidine (0.1 g, 0.82 mmol) were dissolved in DMF (20 mL). The mixture was stirred for 2 h, and water (20 mL) was added. The product was extracted with dichloromethane (3 x 50 mL), and the combined extracts were dried over sodium sulfate. The solvent was removed under vacuum, and after chromatography (silica gel, 3% MeOH:DCM), the desired amide was isolated as 0.40 g (55% yield) of a clear oil. ¹H NMR (CDCl₃, 500 MHz) δ 3.6-3.7 (m, 16 H), 3.47 (t, 2 H), 3.36 (t, 2 H), 3.16-3.31 (m, 14 H), 2.9-3.1 (m, 12 H), 3.06 (m, 2 H), 2.58 (m, 4 H), 1.64 (m, 6 H), 1.43 (s, 27 H), 1.41 (s, 18 H), 1.25-1.3 (m, 2 H), 1.0-1.12 (m, 10 H), 0.68 (t, 3 H). ¹³C NMR (CDCl₃, 125 MHz) δ 170.71, 168.64, 159.47, 156.81, 156.52, 154.88, 81.18, 80.52, 79.81, 79.65, 79.58, 70.70, 70.67, 70.62, 70.61, 70.57, 70.31, 70.02, 69.85, 66.58, 66.53, 66.50, 66.46, 60.25, 58.06, 56.72, 51.10, 50.63, 41.04, 28.4, 28.35, 27.16, 25.93, 24.41, 23.64, 22.65, 21.97, 13.42. HRMS (ESI) calcd for C₆₃H₁₂₁N₉O₁₆ [M+H]⁺:1260.8931, found:1260.9032. This amide (0.15 g) was dissolved in a solution of HCl in dioxane (4 M, 5 mL). The mixture was stirred for 18 h, and solvent was removed under vacuum. Toluene (50 mL) was added to the resulting material and evaporated under vacuum to remove residual water. Compound **4** was isolated as a light yellow solid (0.09 g, 90% yield). ¹H NMR (D₂O, 500 MHz) δ 3.96 (m, 4 H), 3.85 (m, 2 H), 3.2-3.6 (m, 36 H), 2.9-3.1 (m, 10 H), 1.98 (m, 2 H), 1.93 (m, 2 H), 1.0-1.12 (m, 10 H), 0.68 (t, 3 H). ¹³C NMR (D₂O, 125 MHz) δ 170.71, 168.64,

159.47, 71.51, 70.72, 69.71, 69.54, 69.41, 66.58, 66.53, 66.50, 66.46, 60.25, 58.06, 56.72, 51.10, 51.06, 50.83, 46.71, 45.06, 44.63, 44.56, 44.30, 43.34, 43.27, 44.14, 39.90, 39.09, 36.49, 31.04, 28.57, 28.35, 27.16, 25.93, 24.41, 23.64, 22.65, 21.97, 13.42. HRMS (ESI) calcd for $C_{40}H_{81}N_9O_{10} [M+H]^+$:848.6106, found:848.6183.

1.3.6 References

1. Arenholz, O. H.; Simmons, RL. Pancreatitis and other intraabdominal infections. In: *Simmons HRJ, editor. Surgical Infectious Disease*. 2nd ed. ed. Norwalk, CT: *Appleton & Lang*; **1988**, 605-46.
2. Pizzo, P.A. Evaluation of fever in the patient with cancer. *Eur. J. Cancer. Clin. Oncol.* **1989**, 25, 9-16.
3. Ferro-Flores, G.; Ocampo-Garcia, B. E.; Melendez-Alafort, L. Development of specific radiopharmaceuticals for infection imaging by targeting infectious micro-organisms. *Curr. Pharm. Des.* **2012**, 18, 1098-106.
4. Thomas, C.J.; Surolia, N.; Surolia, A. Surface plasmon resonance studies resolve the enigmatic endotoxin neutralizing activity of polymyxin B. *J. Biol. Chem.* **1999**, 274, 29624-29627.
5. Dürr, U. H. N.; Sudheendra, U.S.; Ramamoorthy, A. LL-37, the only human member of the cathelicidin family of antimicrobial peptides. *Biochim. Biophys. Acta.* **2006**, 1758, 1408-1425.
6. Isogai, E.; Isogai, H.; Takahashi, K.; Okumura, K.; Savage, P. B. Ceragenin CSA13 exhibits antimicrobial activity against cariogenic and periodontopathic bacteria. *Oral Microbiol. Immunol.* **2009**, 24, 170-172.
7. Ding, B.; Yin, N.; Liu, Y.; Cardenas-Garcia, J.; Evanson, R.; Orsak, R.; Fan, M.; Turin, G.; Savage, P. B. Origins of cell selectivity of cationic steroid antibiotics. *J. Am. Chem. Soc.* **2004**, 126, 13642-13648.
8. Bucki, R.; Sostarecz, A. G.; Byfield, F. J.; Savage, P. B.; Janmey, P. A. Resistance of the antibacterial agent ceragenin CSA-13 to inactivation by DNA of F-actin, and its activity in cystic fibrosis sputum. *J. Antimicrob. Chemother.* **2007**, 60, 535-545.

9. Hoppens, M. A.; Sylvester, C. B.; Qureshi, A. T.; Scherr, T.; Czaps, D. R.; Duran, R. S.; Savage, P. B.; Hayes, D. Ceragenin mediated selectively of antimicrobial silver nanoparticles. *ACS App. Mat. Interfaces*. **2014**, *6*, 13900-13908.
10. Hoppens, M. A.; Wheeler, Z. E. W.; Qureshi, A. T.; Hogan, K.; Wright, A.; Stanley, G. G.; Young, D.; Savage, P. B.; Hayes, D. Maghemite, silver, ceragenin conjugate particles for selective binding and contrast of bacteria. *J. Coll. Interface Sci*. **2014**, *413*, 167-174.
11. Lin, W.Y.; Chao, T.H.; Wang, S.J. Clinical features and gallium scan in the detection of post-surgical infection in the elderly. *Eur J. Nucl. Med. Mol. Imaging* **2002**; *29*, 371-375.
12. Rennen, H. J.; Boerman, O. C.; Oyen, W.J.; Corstens, F.H. Imaging infection/inflammation in the new millenium. *Eur J. Nucl. Med.* **2001**, *28*, 241-252.
13. Welling, M.; Feitsma, H. I.; Calame, W.; Pauwels, E.K. Detection of experimental infections with ^{99m}Tc-labeled monoclonal antibodies against TNF- α and interleukin-8. *Nucl. Med. Biol.* **1997**, *24*, 649-655.
14. Rao, P.S.; Pallela, V. R.; Vassileva-Belnikolovska, D.; Jungkind, D.; Thakur, M. L. A receptor-specific peptide for imaging infection and inflammation. *Nucl. Med. Commun.* **2000**, *21*, 1063-1070.
15. Welling, M.M.; Ferro-Flores, G.; Pirmettis, I., Brouwer, C. Current status of imaging infections with radiolabelled anti-infective agents. *Anti-Infective Agents Med. Chem* **2009**, *8*, 272-287.
16. Roohi, S.; Amir, N.; Ahmed, M.; Savage, P. B.; Saluhiddin, S. M.; Jehangir, M. J. Radioanal. Synthesis, quality control and biological evaluation of ^{99m}Tc labeled CSA-13. *Nuclear. Chem.* **2009**, *97*, 57-62.

17. Li, C.; Budge, L. P.; Driscoll, C. D.; Willardson, B. M.; Allman, G. W.; Savage, P. B. Incremental conversion of outer-membrane permeabilizers into potent antibiotics for Gram-negative bacteria. *J. Am. Chem. Soc.* **1999**, *121*, 931-940.
18. Kubíček, V.; Böhmová, Z.; Sevciková, R.; Vanek, J.; Lubal, P.; Poláková, Z.; Michalicová, R.; Kotek, J.; Hermann, P. NOTA complexes with copper(II) and divalent metal ions: Kinetic and thermodynamic studies. *Inorg. Chem.* **2018**, *57*, 3061-3072.
19. Skrubber, K.; Chaplin, K. J.; Phanstiel, O. IV. Synthesis and bioevaluation of macrocycle-polyamine conjugates as cell migration inhibitors. *J. Med. Chem.* **2017**, *60*, 8606-8619.

1.4 Maghemite, Silver, Ceragenin Conjugate Particles for Selective Binding and Contrast of Bacteria

1.4.1 Introduction

Interest in synthetic control, manipulation, and understanding of inorganic nanoparticles has increased alongside the enthusiasm, development and research in the biomedical field in recent years. Because of the wide variety of uses, such as in MRI contrast agents, CT contrast agents, thermal ablation targets, antimicrobials, and delivery platforms for RNA, DNA, peptides, fluorescent markers, and other small molecules, inorganic nanoparticles are being synthesized and studied regularly.¹⁻⁷ The highly specific organization of inorganic nanoparticles with reference to composition, morphology, resonance frequencies, shell thickness, and surface chemistries as well as their cost-effective and effortless bulk synthesis make them quintessential for these applications.⁸⁻¹⁰ Recently various hybrid nanoparticles have been developed to carry out multiple functions, such as in therapeutic treatment of disease.¹¹⁻¹²

One such inorganic nanoparticle that has been used clinically with great success as a T2 contrast agent for magnetic resonance imaging (MRI) were the superparamagnetic iron oxide nanoparticles (SPIONs). Products like Feridex, Resovist, and Combidex, which have been used in the diagnosis of spleen, liver, and bone marrow related ailments, contain SPIONs as the primary active component¹³. They may be coated in starch, dextran, silicones, polyethylene glycol, albumin, and many other hydrophilic surfactants and vary in size from 30 to 150 nm¹⁴. One characteristic shared among all MRI contrast agents is that they need to be paramagnetic, meaning they only possess a magnetic moment in the presence of a magnetic field.¹³

Of all inorganic nanoparticles, silver has proved to be an effective antimicrobial and therapeutic carrier agent, successfully deactivating bacteria through several different mechanisms.

This makes developing resistance very challenging for antimicrobials¹⁵. Silver Nanoparticles can serve as a reservoir for silver ions which bind to proteins causing cell death through structural modifications to the cell wall of bacteria and nuclear membranes. Toxicity is a common concern for all in vivo drug delivery applications. In a study by IlJe Yu et al., rats orally received between 30 and 1000mg/kg/day silver nanoparticles over 28-days to research silver toxicity. After exposure of 300 mg/kg/day, only minor liver damage was detected and there were no statistically significant differences in total erythrocyte numbers or ratios.¹⁶ In 2011, a similar study intravenously exposed rats to between 4 and 40 mg/kg of silver nanoparticles. It was found that exposure to under 10 mg/kg did not significantly affect platelet count, WBC count, RBC counts or hemoglobin and proved that such doses would not be dangerous, including no side-effects for biomedical applications¹⁷. Lately, silver has been incorporated into many products such as medical device coatings, wound dressings, dental resins, and washing machines due to its antimicrobial nature and biocompatibility at limited concentrations.^{2,10,18} Along with many other noble metal nanoparticles, Silver's robust functionalization chemistry, large surface area/volume ratio, readily tunable morphology, and ease of bulk synthesis offer an excellent vehicle for small molecule delivery¹⁹. Moreover, they offer decreased degradation of the therapeutic agent and high-density surface ligand attachment.²⁰⁻²²

Recently, studies have observed the antimicrobial characteristics of silver applied together with an array of other elements. Melaiye et al., encapsulated silver (i)-imidazole cyclophane gem-diol complexes in hydrophilic nanofibers and thereby developed a mechanism of implementing silver's antimicrobial characteristics to counter infections in burn wounds. The silver mats demonstrated to be an effective bacteria killer and exhibited an extended release of silver.²³ Similarly, within 30 in of application, silver organoalkoxysilane Nano membranes containing silver nanoparticles

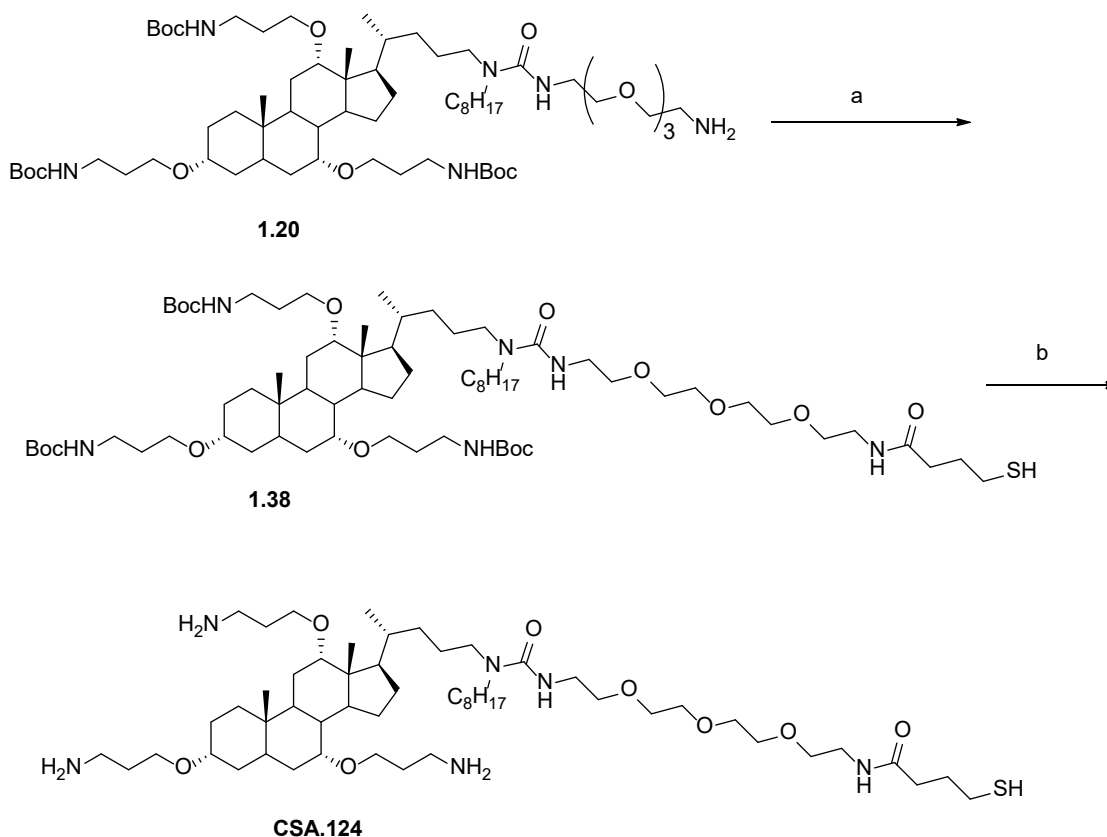
presented inhibition of *Bacillus anthracis*, *Escherichia coli*, *Staphylococcus aureus*, and *Brucella suis* and prevented any additional colonization.²⁴ Silver nanoparticles have also exhibited substantial antimicrobial tendencies through attachment to magnetic hybrid colloids containing an iron oxide core and a silica shell. Freed Ag⁺ ions rupture the bacterial membranes as silver nanoparticles bind to the bacteria, thus effectively destroying the bacteria.²⁵ Magnetic-silica Janus nanorods lined with silver nanoparticles was shown to be having magnetic sensitivity, biocompatible, and demonstrate antimicrobial activity in short-term as well as long-term timeframes.²⁶

Antimicrobial peptides, which are capable of circumventing traditional resistance mechanisms, are a promising means of controlling bacterial growth through membrane selectivity and novel modes of action; however, their high cost of bulk synthesis and weak structural stability in the presence of proteases are some of the constraints to the general clinical use of these peptides. Recent mimics of antimicrobial peptides, CSAs, or ceragenins have been produced which offer heightened stability and easy synthesis while mirroring the selectivity and antimicrobial characteristics of antimicrobial peptides. CSAs are shown to be effective against streptococcus mutans, *Porphyromonas* species and other periodontopathic bacteria as well as tobramycin-resistant *Pseudomonas aeruginosa*, vancomycin-resistant *S. aureus* (VRSA), and drug resistant strains of *Helicobacter pylori*.²⁷⁻²⁹ This proposal in this report contains a novel theragnostic conjugate nanoparticle displaying selective binding of bacteria, antimicrobial efficacy and T2 MRI negative contrast capability. The Diagnostic Antimicrobial Nanoparticles (DANs) mentioned incorporate the attributes of silver, SPIONs, and synthetic antimicrobial peptides, combining them into an individual spherical nanostructure. An array of diverse synthesis procedures provides the creation of a reduced silver shell, an iron oxide core, and CSA-124

surfactant. The synthetic mechanism and products are known to be developed through several methods: transmission electron microscopy (TEM), Fourier transform infrared spectroscopy (FT-IR), dynamic light scattering (DLS), inductively coupled plasma optical emission spectrometry (ICP-OES), High performance Liquid Chromatography-Electrospray Ionization tandem Time of Flight Mass Spectrometry (HPLC-ESI-TOF-MS), ultraviolet-visible spectroscopy (UV-VIS), and DC magnetization and susceptibility. This study's objective is to provide a feasible synthesis procedure that consistently synthesizes DANs and demonstrates the same selective diagnostic potential.

1.4.2 Synthesis of CSA-124

To generate the desired **CSA-124**, the key intermediate **1.20** described above was reacted with γ -thiobutyrolactone in presence of basic solution to form compound **1.38**. Deprotection of the remaining amines gave **CSA-124** (Scheme 1.4.1).



Scheme 1.4.1 Synthesis of CSA.124

Reagents: a) 4-Butyrolactone thiolan-2-one, NaHCO₃, MeOH, H₂O, 74% yield.; b) HCl/Dioxane, 91% yield.

1.4.3 Synthesis, Characteristic and Bioactivity of DANs

This study was accomplished by Dr. Hayes's group in Cain department of Biochemistry and Agricultural Engineering, Louisiana State University and LSU Agcenter. They synthesized the Diagnostic Antimicrobial Nanoparticles (DANs) and qualified characteristic and bioactivity using specific methods including Fourier transform infrared spectroscopy (FT-IR), Ultraviolet-Visible spectroscopy (UV-Vis), X-ray diffraction, Dynamic light scattering (DLS), Transmission electron microscopy (TEM), CSA quantification by high performance liquid chromatography-electrospray ionization tandem time of flight mass spectrometry (HPLC-ESI-TOF-MS),

Inductively coupled plasma optical emission spectrometry (ICP-OES), DC magnetization and susceptibility Contrast concentration dependence, Magnetic resonance imaging and Minimum inhibitory concentration.

1.4.4 Results and Discussion

The DANs synthesis is a multi-step procedure and is summarized in Figure.1.4.1. The key part of the DAN is an iron nanoparticle with a polyacrylic surface ligand (Fe-PAA) synthesized through thermal reduction of iron oxide in an organic solvent. After synthesis, the polyacrylic acid surfactant is improved with cysteamine through an ethyl-dimethyl-aminopropylcarbodiimide (EDC) chemistry reaction (depicted in Figure.1.4.2), resulting in a distal thiol group in the polyacrylic that will readily bind with gold and silver. The cysteamine “activated” product is then reacted with gold nanoparticles, or “seeds”, which incorporate with functionalized Fe-PAA through thiol linkages (33). This seeded surface with nucleation sites for silver reduction and shell formation results in a colloidal shell several nanometers thick. Finally, the CSA-124 is attached to the silver shell via its thiolated ethylene glycol side chain providing a uniform orientation of the compound with two primary amines on the distal portion of the molecular free to interact with the environment.

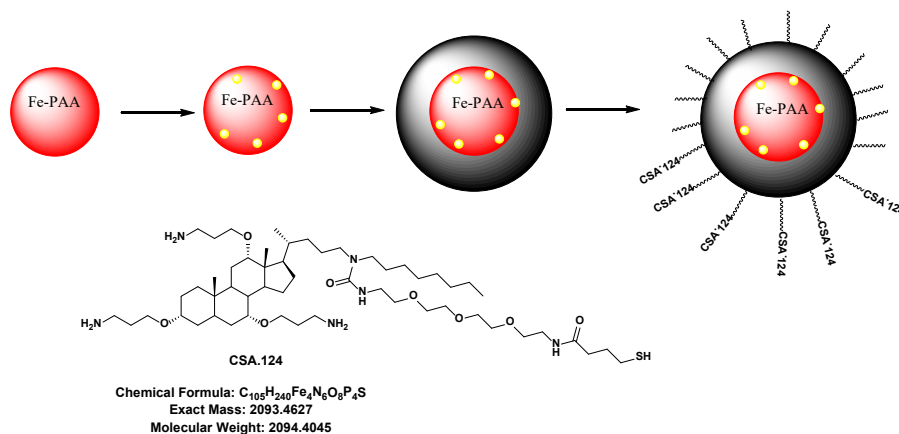


Figure.1.4.1 An overview of the synthesis process is exhibited. Fe-PAA NPs are synthesized; they are then functionalized and seeded with gold NPs. Silver ions from $AgNO_3$ are reduced onto the gold particles. Finally CSA-124 is bound to the surface of the silver shell.

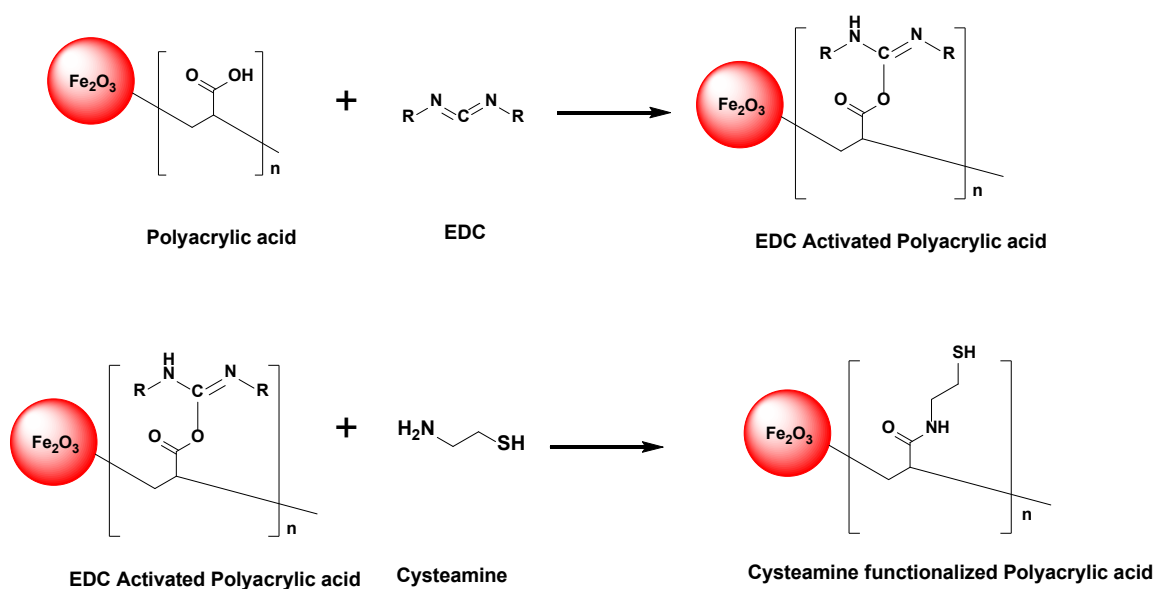


Figure.1.4.2 Functionalization schematic of the PAA surfactant through an EDC/Sulfo-NHS workup. Carboxylic acids are activated with EDC then functionalized with cysteamine, resulting in terminal thiols allowing for strong gold seed adhesion.

Functionalization of the iron with polyacrylic acid affords for a hydrophilic particle which is capable to increase colloidal solubility in the follow on aqueous reactions. Furthermore the PAA

surfactant affords a platform for gold seeding and colloidal shell formation. The functionalization procedure of PAA was optimized from the protocol Ken-Tye Yong et al. developed for the functionalization of carboxylate modified polystyrene beads.⁸ Firstly, the carboxyl groups of the PAA were activated by ethyl-dimethyl-aminopropylcarbodiimide (EDC) and N-hydroxysulfosuccinimide (Sulfo-NHS), and then reacted with the primary amine groups of cysteamine hydrochloride (CH), forming an amide bond linkage. An EDC/Sulfo-NHS workup is a well-established, moderate method for bonding molecules through their carboxylic and amine groups and has also been used in CA/BMPA-coating magnetic nanoparticles,³⁴ protein coupling³⁵, and protein film deposition.³⁶ Once bound to the NP surface, the cysteamine provided a primary thiol group that was ideal for the attachment of colloidal gold utilized in shell growth. The method of colloidal attachment of gold nanoparticles to the thiol-functionalized PAA and silver reduction was developed according to a method previously reported by Jackson and Halas⁹. In our modified procedure, silver from AgNO₃ was reduced onto the gold seed nucleation sites bound to the PAA through cysteamine. This method affords adequate control over shell thickness while sustaining colloidal stability in follow-on aqueous CSA functionalization reactions. The CSA functionalization reaction takes place immediately following silver shell reduction to add bulky surface groups offering steric hindrance and bound surface charges to reduce agglomeration of the finished particles. If surface functionalization is not conducted within hours of the silver reduction step, agglomeration of particles will occur rapidly. The composition of the nanoparticles was analyzed using FT-IR, ICP-OES, and UV-Vis. FT-IR was used to verify the addition of cysteamine to the carboxy terminus of the polyacrylic acid surfactant on the Fe-PAA NP. In this reaction, a carboxyl group is transformed into an amide bond (as seen in Figure 1.4.3). The FT-IR peaks for carboxyl and amide groups are normally found at 1780-1710 cm⁻¹

and 1690-1620 cm^{-1} , respectively³⁷. In the FT-IR spectra of Fe-PAA NPs in Figure.3a there is a clear peak at 1726 cm^{-1} indicative of the carboxyl group. In Figure.1.4.3 the 1726 cm^{-1} maxima peak is extremely reduced while a clear peak arises with a 1619 cm^{-1} maxima presenting that many, though not all, of the carboxyl groups have been transformed to amide.

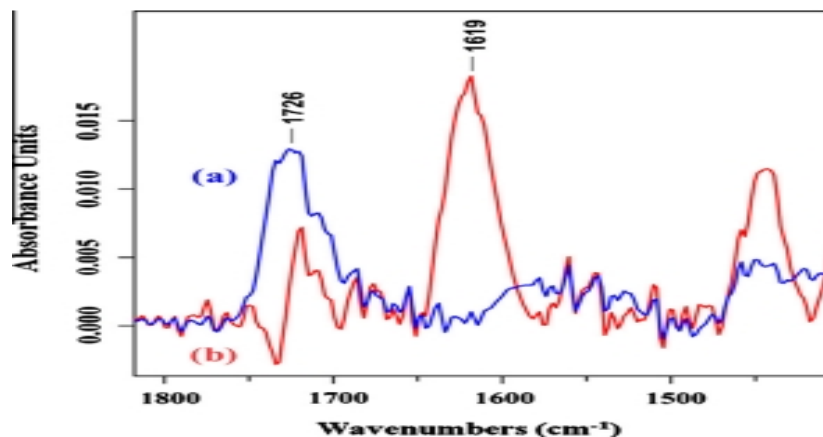


Figure.1.4.3 The FT-IR spectra shown indicate a shift in bond energy upon functionalization of Fe-PAA with cysteamine.

Using ICP-OES, concentrations of iron, gold, and silver were monitored during the whole synthesis process. With this information and the known sample volumes it was possible to track the mass balance of each element. ICP-OES data indicates that the compositions of DANs are 76.64% silver, 22.75% iron, and 0.61% gold. Based on the mass balance of iron, it was measured that the synthesis procedure from Fe-PAA NPs undergoing functionalization, gold seeding, and silver coating resulted in a 8.6% yield with the bulk of losses due to centrifugal purification. It is supposed that substituting magnetic separation for centrifugation during the purification process could minimize these losses. Iron was selected to be the element monitored for percent yield because it was the only element used in the first step and no introduced again throughout the process.

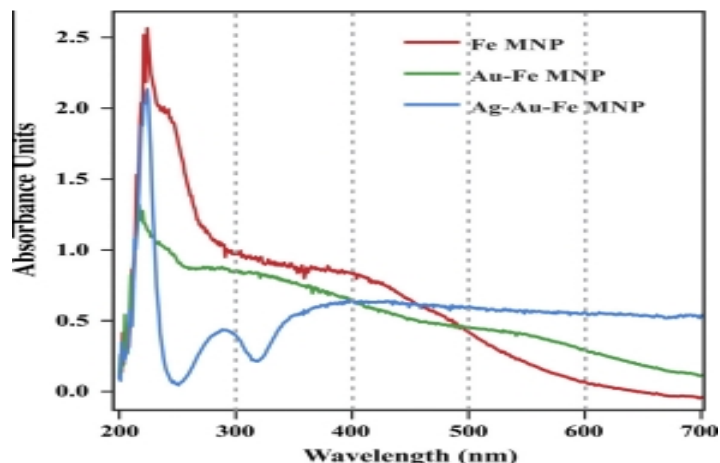


Figure.1.4.4 UV-Vis absorption spectra of DANs at different stages of development are shown. Series (a) shows Fe-PAA NP, (b) shows Au-Fe-PAA np, and (c) shows Ag- Fe-PAA.

UV-Vis spectroscopy was applied to monitor to process progress between steps. After NP-PAA functionalization, curve “a” in Figure 1.4.4 was obtained. This curve worked as a baseline or comparison point for subsequent determinations. Curve “b” stands for the UV-Vis spectra obtained after purification of gold seeded Fe-PAA NPs. This curve clearly varies the baseline curve and closely parallels the absorbance spectra of a gold NP control. The similarity between the Au-MNP an gold seed control curves demonstrates the assertion that gold seeds were successfully attached to the PAA coating of the iron NPs. Cure “c” describes the absorbance spectra obtained after silver was reduced onto the Au-Fe-PAA. As with the gold seeded NPs, the silver coated NPs curve is significantly different from both the previous curves and indicates the clear red shifting commonly associated with metal nanoshell synthesis.⁹This strongly demonstrates that a silver shell was successfully reduced onto the particle surface, thus supporting the ICP-OES findings.

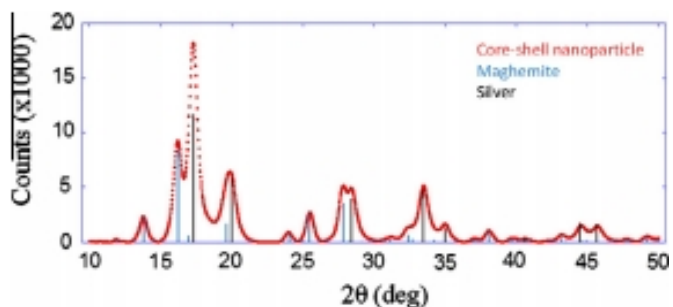


Figure.1.4.5. X-ray diffraction pattern of DAN core is representative of Silver and Maghemite.

To identify the exact structure of the DAN's iron oxide core, X-ray diffraction was employed. A powder diffraction pattern of the core-shell nanoparticles is displayed in Figure. 1.4.5. The reflections due to the iron oxide core are indicated as blue lines and the reflections due to the silver shell are indicated as black lines. The indicated reflections present that the iron oxide core is maghemite. This is compliance with the brown color of the core nanoparticles.

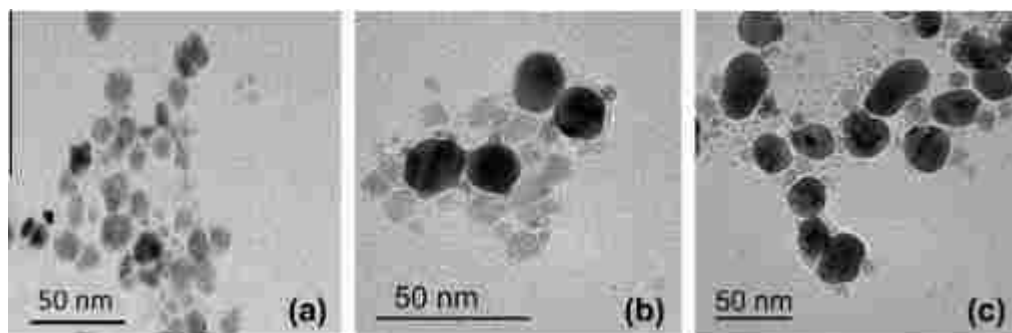


Figure 1.4.6 TEM images of the nanoparticles at three stages of development are shown: (a) Fe-PAA nanoparticle, (b) Au-Fe-PAA, and (c) Ag-Fe-PAA with CSA-124 surfactant.

The shape and size of nanoparticles at different stages of synthesis were measured using a combination of TEM and DLS. The TEM images displayed in Figure.1.4.6 indicates the growth of the nanoparticles as gold seeds were attached (Figure 1.4.6 b) and a silver shell was reduced

onto the Fe-PAA NP (Figure.1.4.6c). It is also obvious that the Fe-PAA NPs the growth of the nanoparticles as gold seeds were attached (Figure.1.4.6b) and a silver shell have a crude spherical morphology that became more regular and smooth as gold and silver were added in following processes.

Table 1.4.1 Nanoparticle diameters as determined by TEM.

Nanoparticle	Average diameter (nm)
Fe-PAA NP	9.4 ± 0.6
Au seeded Fe-PAA NP	20.5 ± 4.4
DAN	33.4 ± 6.1
Hydrodynamic diameters as determined by DLS	
Fe-PAA NP	45.6 ± 1.0
DAN	53.1 ± 1.2

Analysis of the TEM images with Advanced Metamorphic was used to determine nanoparticle size and is exhibited in Table 1.4.1. One sample t-test analysis of these values discovered that the diameter increase after gold seeding was not statistically significant ($P > 0.05$). Hydrodynamic diameters, as measured through DLS, are also included in Table 1.4.1. As expected from a relatively monodisperse product there is adequate agreement between the values generated from the TEM image and the DLS results. As the multi-step synthesis continues larger particles with larger hydrodynamic diameters are produced as a result of the addition of the silver coating and CSA-124 addition.

A standard curve of integrated peak area vs. CSA concentration was constructed using HPLC-ESI-TOF-MS in order to quantify the CSA bound to colloidal silver. CSA was then displaced

from the DAN surface and analyzed, again using HPLC-ESI-TOF-MS. The corresponding CSA concentration was measured to be 1.34 mg/L for a 500 uL sample, or 4.01×10^{14} CSA molecules. Using ICP-OES it was measured the same 500 uL sample with roughly 5.26×10^{12} DANs, thus we suggest there are on average 76.1 CSA-124 molecules bound to each DAN. As the packing density and uniformity of the CSA 124 surfactant layer is crucial to both particle stability and bacterial adhesion, future work will perform the optimization of this process. A hysteresis loop of the DANs is presented in Figure.1.4.7. The DAN magnetization was determined as a function of applied field from 0 to $\pm 90,000$ Oe. As seen in the picture, the magnetization of DANs increases rapidly with the applied field, tending toward saturation at fields >5000 Oe. The maximum magnetization is approximately 12 emu/g NP, which is 54 emu/g Fe. This value is consistent with the iron oxide T2 contrast agents currently in clinical use; Feridex and Combidex have magnetizations of 45 emu/g Fe and 61 emu/g Fe respectively ¹³. DAN magnetic moment was also assessed with respect to temperature and observed to have a slightly inverse relationship, however still maintained an adequate magnetic moment at physiological conditions, dropping less than 20% over a 300 K increase.

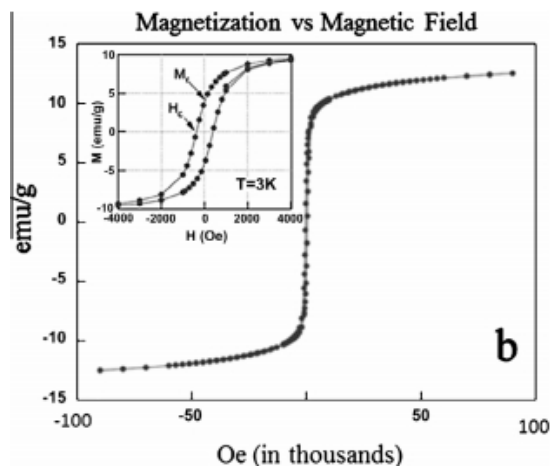


Figure.1.4.7 The hysteresis loop in graph (b) shows NP magnetization as a function of magnetic field.

This graph displays an expanded view of the low-field region of the magnetization in which a hysteresis is observed with a remnant magnetization, $M_r \sim 3.0$ emu/gm, and a coercive field, $H_c \sim 300$ Oe. The data indicates that the majority of the nanoparticles are paramagnetic and at least some subsets of the nanoparticles have a ferromagnetic component to their magnetization. This seems to be a result of the size distribution of the particles used in the iron core, some of which will be above the crucial transition size from superparamagnetic to ferromagnetic, roughly 10 nm^3 .

In Figure.1.4.8, a clear correlation is presented between nanoparticle concentration and MRI contrast, known as negative contrast. The paramagnetism of the NP's generates the relaxivity of nearby water molecules to drop, and a decrease in relaxivity causes lower pixel intensity. Using ImageJ, the pixel intensity of each tube was determined then plotted against particle concentration. On average, pixel intensity drops by 16.7 gray scale units for each additional ppm DAN. Figure.1.4.8 also displays the similar contrast of DANs and Fe-PAA Np presenting that the maghemite core is not compromised by the formation of the silver shell. In fact, DANs seem as though they may have slightly increased contrast ability. This can potentially be demonstrated

by Dr. Vuong et al. who proposed that surrounding a paramagnetic NP with a shell prevents it from directly coordinating with the select few neighboring water molecules but rather allows its impacts to be distributed over a greater surface area and thus affecting a greater number of water molecules. This causes a reduction of the relaxation time of a greater number of water molecules correlating with a greater negative contrast³⁹.

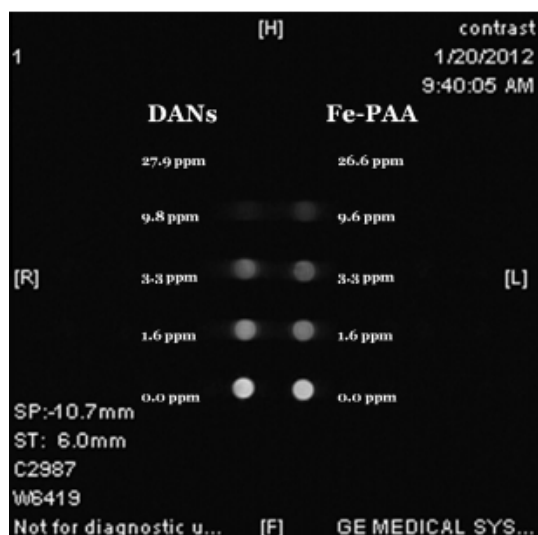


Figure.1.4.8 MRI of NPs dispersed in agarose at various concentrations (left). Graph of resulting pixel intensity for each sample concentration (right).

Determination of in vitro contrast of bacteria by DANs was evaluated by exposing *S. aureus* to DANs, filtering this mixture through a syringe filter, suspending this filter in a block of agarose, and imaging with MRI, seen in Image Figure.1.4.9c. Filter pores, 450 nm, were used to be large enough to allow DANs to pass unhindered yet retain all bacteria. As a negative control, *S. aureus* was also exposed to DANs without CSA-124, (Fe core with silver shell only) and filtered, Figure.1.4.9b. A positive control of total DAN capture using a 200 nm filter that captured bulk of the DAN's on the filter media can be seen in Figure.1.4.9a. As expected, Figure.1.4.9a displays

the greatest contrast, Figure.1.4.9b displays no contrast and Fig1.4.9c displays moderate contrast. This suggests that DAN attachment does take place, though the efficiency of the attachment is far below 100%. This may arise from variation in the particle CSA-124 functionalization. As described above the average functionality is 76.1 CSA/particle but distribution is currently unknown, as such, large numbers of particles may have little or no CSA attached. The images also suggest that DANs devoid of CSA do not adhere to the *S. aureus*, nor are they rapped in the filter. To assure the attachment of CSA-124 to the NP surface did not influence filter permeability, fully conjugated DANs in DI were filtered and also resulted in no contrast.

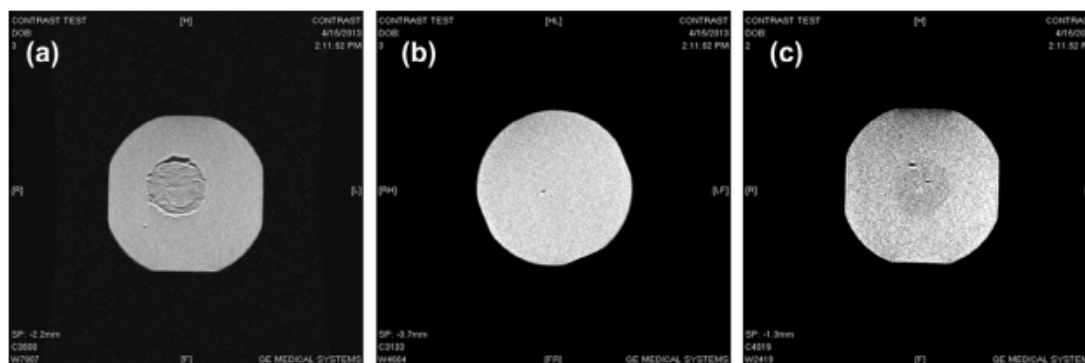


Figure 1.4.9 Magnetic resonance images of syringe filters suspended in agarose. Image (a) is a positive control, image (b) is a negative control, and image (c) is the treatment.

The minimum inhibitory concentration found for DANs indicates they are slightly more effective against *S. aureus* than *E. coli* at 12 ppm and 24 ppm respectively. Ruparelia et al. measured the average MIC of SNPs against four different strains of *E. coli* and three different strains of *S. aureus*⁴⁰. The MIC of SNPs against both *S. aureus* and *E. coli* was found to be 120 ppm. Our own MIC assay using the above protocol with cellulose stabilized-SNP was found to be 250 ppm. This makes DANs roughly ten times more effective against *S. aureus* and five times more effective against *E. coli* comparable with the results of Ruparelia et al.

1.4.5 Conclusions

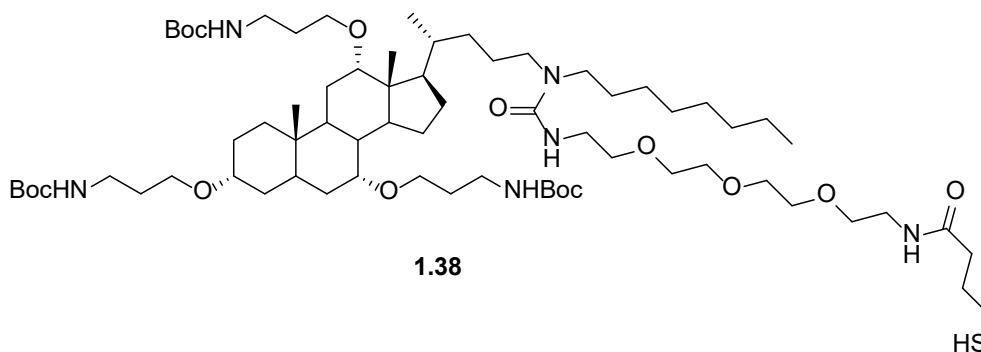
The results in this study demonstrate that the synthesis process described above successfully forms the desired iron containing, silver shell nanoparticle with a ceragenin monolayer surface functionalization. The FT-IR spectrums indicate the addition of a mercapto group to the Fe-PAA NP. ICP-OES supported the final product is comprised of 76.64% silver, 22.75% iron, and 0.61% gold with around 8% total yield. Both TEM and DLS results illustrate predictable growth of the particle with each additive process step. These results demonstrate that gold and silver were successfully deposited onto the Fe-PAA NPs, yielding a final nanoparticle of 32.474 ± 1.83 nm diameter and 53.053 ± 1.202 nm hydrodynamic diameter. Additionally, these particles were found to be predominantly paramagnetic and possess a strong magnetic moment of 54 emu/g Fe. These characteristics are representative of clinically adopted T2 MRI contrast agents, making DANs a good potential candidate for diagnostic application. MRI of DANs and maghemite core NPs at different concentrations indicate a 16.7 gray scale unit reduction in pixel intensity for each ppm DAN. DANs have also suggested an ability to adhere and contrast *S. aureus* in vitro. Finally, DANs have been exhibited to inhibit *S. aureus* at 12 ppm and *E. coli* at 24 ppm, five times more effectively than silver alone. The results presented in the report demonstrate DANs to be a potentially viable diagnostic contrast agent for treating deep tissue infection.

1.4.6 Experiment Section

General: Reagents were purchased from Aldrich Chemical Co. unless otherwise noted. Methylene chloride, THF, DMF, pyridine, and DMSO were dried by passage through a Glass Contour solvent drying system containing a cylinder of activated alumina. Silica gel was used for chromatography unless otherwise noted.

Instrumentation: ^1H and ^{13}C NMR spectra were recorded on a Varian Gemini 500 (500 MHz) spectrometer. Proton chemical shift were referenced to tetramethylsilane (TMS). Carbon chemical shifts were referenced to carbon resonance of solvents (CDCl_3 , CD_3OD). High resolution electron impact mass spectra (HR-MS) were obtained on a JOEL SX 102A spectrometer.

Experiment:



Compound 1.38 To a solution of **1.20** (1.2g, 1 mmol) in MeOH (10 mL) with stirring, 4-butyrothiolactone thiolan-2-one, 10 mL of Saturated NaHCO_3 solution were added respectively. The mixture was allowed to react overnight at room temperature. After dried off MeOH via rotavapor, the residue was filled with 20 mL of DI water and extracted with EtOAc (25 mL \times 3). After washing the combined organic phase with brine, the mixture was dried over Na_2SO_4 . 0.95g of the product was isolated through a column chromatography (SiO_2). The yield was 74%. ^1H NMR (CDCl_3 , 500 MHz): δ 5.63 (d, 1 H), 5.12 (br, 1 H), 4.8 (br, 1 H), 3.6-3.7 (m, 18 H), 3.03-3.58 (m, 26 H), 1.55-2.11 (m, 19 H), 1.43 (s, 29 H), 1.20-1.31 (m, 21 H), 0.98-1.03 (m, 2 H), 0.88-0.94 (m, 11 H), 0.69 (s, 3 H). ^{13}C NMR (CDCl_3 , 125 MHz): δ 158.67, 158.02, 156.23, 156.07, 80.56, 79.26, 78.89, 78.63, 70.70, 70.67, 70.63, 70.61, 70.57, 70.52, 70.15, 70.02, 66.40, 65.76, 47.78, 47.37, 47.05, 46.15, 42.60, 41.88, 41.84, 39.68, 39.43, 39.41, 38.64, 38.35, 35.66, 35.21, 35.01, 34.91, 34.86, 33.16, 31.83, 30.57, 30.11, 29.69, 29.47, 29.27, 28.72, 28.61,

1.4.7 References

1. Mahmoudi, M.; et al., *ACS Nano* , **2011**,5 (9), 7263–7276.
2. Kim, J.S.; et al., *Nanomed.-Nanotechnol. Biol. Med.* **2007**, 3 (1), 95–101.
3. Agasti, S.S.; et al., *J. Am. Chem. Soc.* **2009**, 131 (16) 5728-+.
4. O’Neal, D.P.; et al., *Cancer Lett.* **2004**, 209 (2), 171–176.
5. Cheng, K.; et al., *Circ. Res.* **2010**, 106 (10), 1570-U54.
6. Chertok, B.; et al., *Biomaterials.* **2008**, 29 (4) , 487–496.
7. Qureshi, A.T. et al., *Biomaterials.* **2013** ,34 (31), 7799–7810.
8. Yong, K. T. et al., *Colloids Surf. - Physicochem. Eng. Aspects.* **2006**, 290, 89–105.
9. Jackson, J.B.; Halas, N.J. *J. Phys. Chem. B.* **2001**, 105 (14), 2743–2746.
10. Pal, S.; Tak, Y. K.; Song, J. M. *Appl. Environ. Microbiol.* **2007**, 73, 1712–1720.
11. Chen,X.; Gambhir, S. *Acc. Chem. Res.* **2011**, 44, 841–1134.
12. Narayanan, S.; Sathy, B.N. Mony, U. M.; Koyakutty, S.V.; Menon, Nair, D. Biocompatible Magnetite/Gold Nanohybrid Contrast Agents via Green Chemistry for MRI and CT Bioimaging. *Applied Material Interfaces*, **2011**.
13. Koyakutty,S.; Nair, V.; Menon, D. Biocompatible Magnetite/Gold Nanohybrid Contrast Agents via Green Chemistry for MRI and CT Bioimaging. *Applied Material and Interfaces*, **2011**, 16, 2015-2023.
14. Na, H. B.; Song, I. C.; Hyeon, T. *Adv. Mater.* **2009**, 21 , 2133–2148.
15. Babes, L. et al., *J. Colloid Interface Sci.* **1999**, 212 , 474–482.
16. Becker, R. O. *Met.-Based Drugs.* **1999**, 6, 311.
17. Kim, Y. S. et al., *Inhalation Toxicol.* **2008**, 20 , 575–583.

18. Tiwari, D. K.; Jin, T. J. Behari, *Toxicol. Mech. Methods.* **2011**, 21, 13–24.
19. Jung, W. K. et al., *Appl. Environ. Microbiol.* **2008**, 74, 2171–2178.
20. Katz, E.; Willner, I.; *Angew. Chem. - Int. Ed.* **2004**, 43, 6042–6108.
21. Ghosh, P. et al., *Adv. Drug Deliv. Rev.* **2008**, 60, 1307–1315.
22. Seferos, D. S. et al. *Nano Lett.* **2009**, 9, 308–311.
23. Emerich, D. F.; Thanos, C.G. *Biomol. Eng.* **2006**, 23, 171–184.
24. Melaiye, A. et al., *J. Am. Chem. Soc.* **2005**, 127, 2285–2291.
25. Umar, S. et al., *Nanoscale Res. Lett.* **2013**, 8, 164.
26. Park, H. H. et al., *J. Mater. Chem. B.* **2013**.
27. Zhang, L. et al., *J. Mater. Chem.* **2012**, 22, 23741–23744.
28. Leszczynska, K. et al., *BMC Microbiol.* **2009**, 9.
29. Bucki, R. et al., *J. Antimicrob. Chemother.* **2007**, 60, 535–545.
30. Leszczynska, K. et al., *J. Appl. Microbiol.* **2011**, 110, 229–238.
31. Ling, M. M.; Wang, K. Y.; Chung, T. S.; *Ind. Eng. Chem. Res.* **2010**, 49, 5869–5876.
32. Andrews, J. M. *J. Antimicrob. Chemother.* **2011**, 48 (suppl 1), 5–16.
33. Wiegand, I. Hilpert, K. *R.E. Hancock, Nat. Protoc.* **2008**, 3, 163–175.
34. Brust, M. et al., *J. Chem. Soc. Chem. Commun.* **1994**, 7, 801–802.
35. Lattuada, M.; Hatton, T. A. *Langmuir.* **2007**, 23, 2158–2168.
36. Grabarek, Z. *J. Gergely, Anal. Biochem.* **1990**, 185, 131–135.
37. Tengvall, P. et al., *Colloids Surf. B - Biointerfaces* **2003**, 28, 261–272.
38. Merlic, C. *IR Absorption Table. WebSpectra* **2000**.
39. Dutz, S. et al., *J. Magn. Magn. Mater.* **2007**, 308, 305–312.
40. Vuong, Q. L. et al., *Adv. Healthcare Mater.* **2012**, 4, 502–512.

41. Ruparelia, J. P. et al., *Acta Biomater.* **2008**, *4*, 707–716.

1.5 Ceragenin Mediated Selectivity of Antimicrobial Silver Nanoparticles

1.5.1 Introduction

A major source of difficulty in infection treatment is the broad-spectrum activity of prescribed antibiotics. With the intent to eliminate pathogenic microbes, many antibiotics also kill or inhibit natural microbial flora.¹ Indigenous microbes assist in nutrient uptake and provide protection from colonization by pathogenic microorganisms. When these natural bacterial populations are compromised, opportunistic pathogens, such as *C. albicans*, *C. difficile*, and *S. aureus*, often hinder post-treatment recovery and necessitate additional treatment.¹⁻⁴ Selective antimicrobial agents seek to treat pathogenic infections while leaving the native microbes uncompromised.

Advances in inorganic nanoparticle chemistry have led to a substantial increase in the types and applications of nanoparticles.⁵⁻⁸ Nanoparticles can be manufactured from diverse materials into a variety of shapes, sizes, and surface chemistries. One particularly relevant use of nanoparticles is as vehicles for drug delivery.⁷ Nanoparticles offer a high surface area-to-volume ratio, allowing high drug carrying capacity, and can be made to target infected tissues for sustained drug delivery⁹⁻¹¹. Ligands associated with nanoparticles are also less susceptible to degradation than those free in solution¹¹. Additionally, amphiphilic molecules with thiol groups spontaneously assemble on noble metals like silver or gold.¹²⁻¹³ It has been shown that nanoparticles less than 200 nm in diameter are more likely to remain in circulation in vivo than nanoparticles larger than 200 nm.¹¹ Taken together, the composition, morphology, and surface

chemistry of nanoparticles is highly customizable, making them ideal candidates for selective antimicrobials.

Silver has long been known to possess antimicrobial properties and silver nanoparticles (SNPs) and other silver nanomaterial compositions have shown comparable antimicrobial properties.^{5,14-}

¹⁸ Currently, silver is employed as an antimicrobial in several products, including bandages, antibacterial gels, and catheters.¹⁹ Silver impacts microbial systems through disrupting multiple key cellular functions such as cell wall and nucleic acid synthesis, translation, protein folding, and membrane ion pumps. Without these crucial functions, microbial cell division inhibition or cell death often occurs. This combination of potent antimicrobial activity and limited patient cytotoxicity makes SNPs a favorable alternative to traditional antibiotics as a treatment for infections.

Natural cationic peptides show significant antimicrobial properties with low rates of resistance and various levels of selectivity. Many, however, are susceptible to protease activity, restricting their utility as standalone antibiotics *in vivo*.^{20, 21} CSA-124, a ceragenin used in this study, has been synthesized with a terminal thiol group, enabling specific covalent bonding to noble metals.

In this study, we present the synthesis of a CSA-124 conjugated SNP (CSA-SNP) with improved antimicrobial activity and physical selectivity for *S. aureus*. The composition and physical properties of the CSA-SNP are analyzed through the following: dynamic light scattering (DLS), transmission electron microscopy (TEM), inductively coupled plasma-optical emission spectrometry (ICP-OES), and liquid chromatography-electrospray ionization tandem mass spectrometry (LC-ESI-MS). The antimicrobial efficacy is determined with time-kill assays and standard minimum inhibitory concentration/minimum bactericidal concentration (MIC/MBC). Mammalian cytotoxicity of the CSA-SNP's is quantified with flow cytometry and live/dead

staining, and hemolytic characterization is analyzed via an ASTM standard. Physical selectivity is validated both quantitatively and qualitatively through laser trapping analysis and confocal microscopy.

1.5.2 Synthesis of CSA. 124

CSA.124 was readily to synthesize using the method described in Chapter 1.4.

1.5.3 Characteristic and Bioactivity of CSA-SNP

This study was accomplished by Dr. Hayes's group in Cain department of Biochemistry and Agricultural Engineering, Louisiana State University and LSU Agcenter. They qualified the CSA-SNP characteristic and bioactivity using specific methods including Conjugating silver nanoparticles with CSA-124, Dynamic light Scattering (DLS), Transmission Electron Microscopy (TEM), CSA quantification, Cytotoxicity Analysis, Hemolytic Characterization, Brightfield Imaging of Cell Morphology, Time-Kill Assay, Confocal Imaging, Image Analysis, Optical trapping and Minimum Inhibitory Concentration and Minimum Bactericidal Concentration.

1.5.4 Results and Discussion

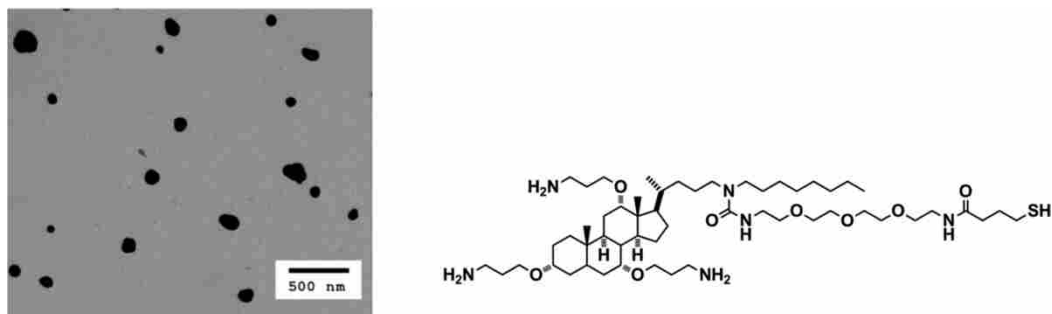


Figure 1.5.1 TEM of CSA-SNP (left) and CSA-124 structure (right).

Nanoparticle size was measured through TEM image analysis and DLS (Figure 1.5.1). These results are shown in Table 1.5.1. As expected, the hydrodynamic diameter determined via DLS is greater than the diameter determined via TEM in presence of solvated surfactant on the particle surface because the former is a weight-average technique. It is also noteworthy that the hydrodynamic diameter increased as the positively charged CSA-124 molecules were added to the system, indicating self-assembly on the nanoparticle surface. Whereas precise size and distribution of CSA-SNPs are not crucial in these experiments, they are relevant to colloidal stability and in vivo biocompatibility. Larger particles are more likely to precipitate from solution, potentially irreversibly aggregating and increasing apparent size.

Table 1.5.1 Nanoparticle Characterization

Parameter	HPC-SNP	CSA-SNP
SNP diameter via TEM analysis (nm)	68 ± 18	64 ± 38
Hydrodynamic diameter (nm)	81.9 ± 9.4	102.2 ± 2.3
Zeta potential (mV)	-18.23 ± 0.83	-8.34 ± 1.05

Besides, nanoparticles possessing a diameter greater than 200 nm are more liable to activate the complement system and thus be cleared from the circulatory system.³⁴ Nanoparticles with a diameter under 100 nm are capable of penetrating blood vessel pores, and NPs under 20 nm can access interstitial spaces.¹¹ This characteristic has been termed the enhanced permeability and retention (EPR) effect.^{35, 36}

As anticipated, the nanoparticle obtains positive charge after the addition of CSA, due to the three ammonium groups on CSA-124 in neutral media. This data sustains the fact that CSA was successfully conjugated to the nanoparticle surface. It is also significant because the nature of the surface charge also affects the nanoparticles' in vitro and in vivo interactions. When particles have a moderately neutral charge, they will be more likely to agglomerate, resulting in shorter shelf lives, a lower solubility threshold, and an increased probability of removal from in vivo circulation.³⁷ Once in the body, nanoparticles are sensitive to opsonization, recognition, and removal by the mononuclear phagocyte system (MPS). In a general way, neutral to negatively charged nanoparticles with hydrophilic polymer surfaces exhibit prolonged circulation times.³⁴

A high quality of the CSA-SNP is easy to conjugate with noble metal nanoparticle. CSA-124 has been specifically prepared with a thiol-terminated polyethylene glycol side chain that favorably binds to noble metals. The SmartSilverAS silver nanoparticles, from this point termed as SNPs, used for this procedure are stabilized with hydroxypropyl cellulose (HPC), which affords the nanoparticles with high solubility in aqueous and organic alcohol solvent systems and increases biocompatibility. Due to CSA-124 has greater thermodynamic and steric stability than HPC on the surface of the SNPs, CSA-124 spontaneously displaces a portion of the HPC molecules.

For the quantification of CSA-124 bound to the SNP surface, we first built a standard curve of integrated peak area versus known CSA concentration using HPLC-ESI-TOF-MS. The CSA was displaced from the SNP surface using DTT; the particles were separated by centrifugation and analyzed using HPLC-ESI-TOF-MS. The corresponding CSA concentration was measured to be 1.5 mg/L for a 500 μ L sample, or 4.52×10^{14} CSA molecules. Using ICP-OES and estimates of particle size from TEM, we measured the same 500 μ L sample contained 1.32×10^{11} SNPs, and

thus, we come to conclusion that there are on average 3424 CSA-124 molecules bound to each SNP³⁸.

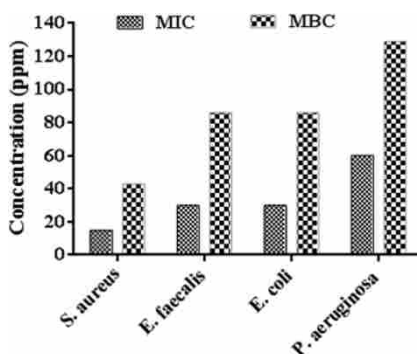


Figure 1.5.2 MIC and MBC of CSA-SNP against various bacteria.

The antimicrobial results for the minimum inhibitory concentration (MIC) and minimum bactericidal concentration (MBC) are illustrated in Figure 1.5.2. As the chart indicates, CSA-SNPs demonstrate similar efficacy against *S. aureus* (MIC 15 ppm), *E. faecalis* and *E. coli* (MIC 30 ppm), and *P. aeruginosa* (MIC 60 ppm). Our own measurement of the MIC of SNPs was obtained using the same protocol as above and found to be roughly 250 ppm for both *S. aureus* and *E. coli*. Whereas this study demonstrates that a CSA-SNP conjugate is a more potent antimicrobial than an SNP alone, it does not attempt to illustrate the mechanistic roles of each component, as potential mechanisms of each have previously been published. Although SNPs have been demonstrated to disrupt cell wall synthesis, membrane ion pumps, translation, and nucleic acid synthesis,^{5,14-17,25,39} antimicrobial properties of CSA have been attributed to membrane disruption through depolarization and permeabilization. It is also noteworthy; Kim et al. reported that SNPs alone inhibited *E. coli* 10 times more effectively than *S. aureus*, suggesting the CSA may impart SNPs with some mechanism of selectivity.¹⁴ Further evidence of physical selectivity was provided by confocal imaging of cocultures of these bacteria. Statistical

analysis using MATLAB demonstrated that CSA-SNPs were more likely to be near *S. aureus* than *E. coli*. This could result in part to electrostatic attraction between the cationic CSA and the negatively charged peptidoglycan, which Gram-positive bacteria express in much greater quantities.⁴⁰ It has been well demonstrated that various cell types present different membrane constituents to its surrounding environment, which affects how the cell responds to extracellular foreign bodies, a concept known as cell vision. This phenomenon influences the surface binding, cellular uptake, and internal fate of nanoparticles and in part explains the drastic differences in NP response among different cell types.^{41,42} Further antimicrobial characterization was given through a time-Kill study, depicted in Figure 1.5.3.

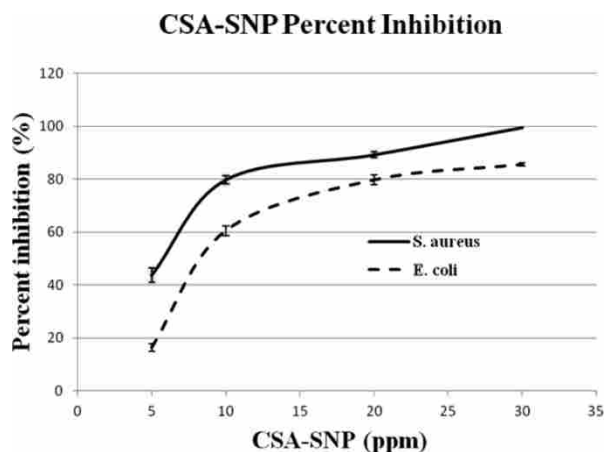


Figure 1.5.3 Time –kill assay showing increased inhibition of *S. aureus* versus *E. coli* due to CSA-SNPs. Percent inhibition is with respect to unexposed live controls.

As described in Figure 1.5.3, minimal inhibition is seen at 5 ppm, and efficacy increases as concentration increases. Note that inhibition results of the time-kill assay change slightly from those of the MIC, as this was a 4 h study and MIC is a 24 h study. The results of the time-kill

assay echo those of the MIC/MBC in that *S. aureus* depicts increased sensitivity to CSA-SNPs compared to *E. coli*.

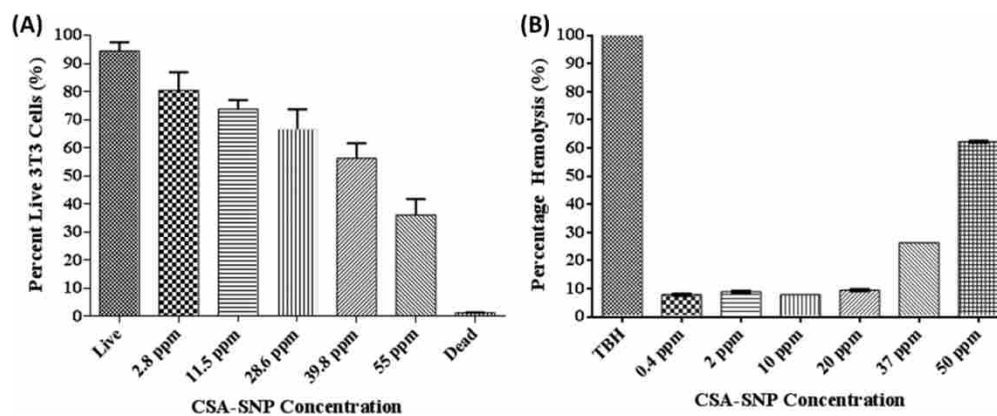


Figure 1.5.4 (A) Cytotoxicity of CSA-SNPs. (B) Hemolytic activity of CSA-SNPs.

The concentration dependent toxicity of CSA-SNPs to mouse 3T3 fibroblasts was measured by cell treatment followed by flow cytometry and is shown in Figure 1.5.4. The CSA-SNPs display very limited toxicity below 39.8 ppm and reach the 50% viability threshold at ~ 50 ppm. The differences between the live control and the 39.8 and 55 ppm samples were observed to be significant by one-way ANOVA with Bonferroni's posttest ($p < 0.05$). The hemolytic assay displays nearly identical results with increasing hemolysis at 37.5 ppm and slightly over 50% hemolysis occurring at 50 ppm. The differences between the TBH, 37 ppm, and 50 ppm samples were observed to be significant from all other samples as determined by one-way ANOVA with Bonferroni's posttest ($p < 0.05$). These findings suggest about a 3-fold difference between MIC and EC_{50tox} for *S. aureus* and 3T3 cells, respectively. Simultaneous testing of SNPs alone presented little cytotoxicity up to 200 ppm. This result is supported by the work of Jain et al., who reported that the IC_{50} for SNPs against Hep G2 cells to be 251 ppm. These findings suggest that CSA-SNPs are approximately 5 times more toxic to 3T3 cells than SNPs alone⁴³.

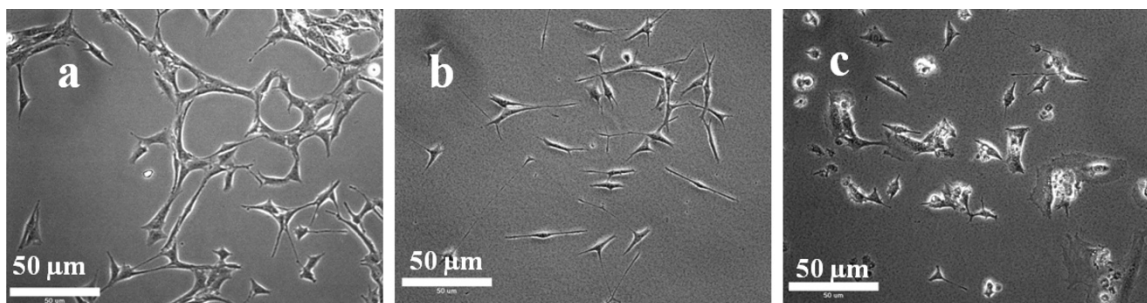


Figure 1.5.5 Bright-field images of 3T3 fibroblasts that received (a) 0 ppm of CSA-SNP, (b) 15 ppm of CSA-SNP, and (c) 37 ppm of CSA-SNP.

The cytotoxic effects of CSA-SNPs were also qualitatively evaluated via bright-field imaging. In Figure 1.5.5a, the representative spindle morphology of healthy 3T3 fibroblast cells can be found. In Figure 1.5.5b, representing the MIC of *S. aureus* at 15 ppm of CSA-SNP, the cells seem to have slightly reduced size but retain their characteristic spindle morphology. CSA-SNP at 37 ppm results in stark contrast in cell morphology indicative of cytotoxicity. These results are compliance with those from the hemolysis and flow cytometry studies.

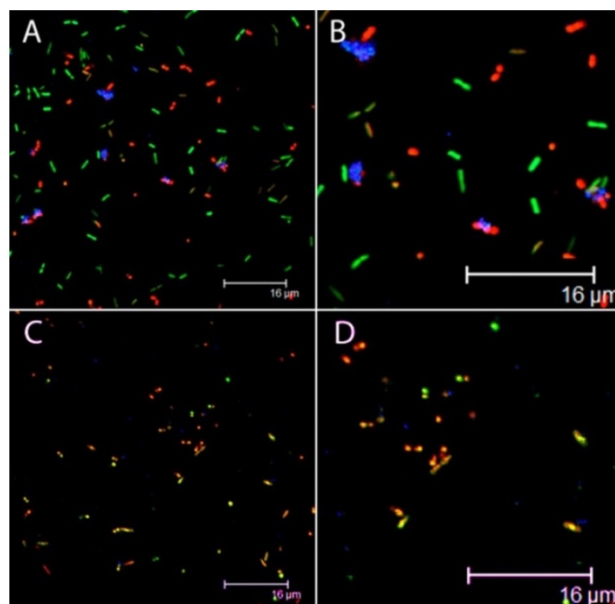


Figure 1.5.6 confocal imaging of (red) *S. aureus*, (green) *E. coli*, and (blue) nanoparticles. (A and B) CSA-SNPs and (C and D) unmodified SNPs. (B and D) Enlarged segments of A and C, respectively.

Qualitative image analysis of the confocal overlays (Figure 1.5.6) illustrates that the CSA-SNPs are distributed spatially closer to *S. aureus* cells than to *E. coli* cells. Analysis of these images presents the closest *S. aureus* and *E. coli* to each SNP; histograms and simple statistics are shown in Figure 1.5.7 and Table 1.5.2, respectively.

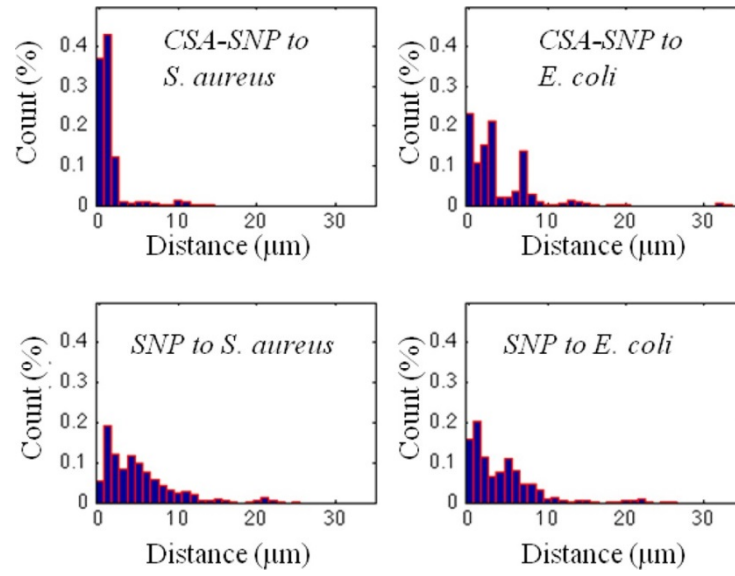


Figure 1.5.7 Histograms of (top) experimental and (bottom) negative control distances from SNPs to (left) *S. aureus* and (right) *E. coli*.

Table 1.5.2 Statistics from Quantitative Image Analyses

Samples	av distance from NP to cell (μm)
CSA-SNP to <i>S. aureus</i>	1.283 ± 1.994
CSA-SNP to <i>E. coli</i>	3.489 ± 3.883
SNP (neg. control) to <i>S. aureus</i>	4.864 ± 4.393
SNP (neg. control) to <i>E. coli</i>	3.991 ± 4.165

Table 1.5.2 demonstrates the distribution of distances for both experimental and negative control groups. The difference in average distance between CSA-SNP and *S. aureus* versus CSA-SNP and *E. coli* is statistically significant, as is the difference in average distance between the CSA-SNP treatment samples and the SNP negative control samples (two-way t test, $p < 0.05$). More than 70% of the CSA-SNPs are within 2 μm of an *S. aureus* cell, while less than 40% of CSA-SNPs are within 2 μm of an *E. coli* cell. CSA-SNPs, on average, are closer to *S. aureus* than to *E. coli*. The standard deviations show less dispersion among the CSA-SNP to *S. aureus* data than the CSA-SNP to *E. coli* data. Ripley's K-function clustering analysis shows that the CSA-SNPs are spatially clustered, particularly on shorter scales.

The negative control data indicate no significant difference between the SNP to *S. aureus* distance and the SNP to *E. coli* distance. This is distinguished by large standard deviations for both negative control groups. Nevertheless, statistically, the mean CSA-SNP to *S. aureus* distance is significantly different from SNP to *S. aureus* average distance. Selectivity was then qualitatively explained on the scale of single cells through video observation and optical trapping technology. Optical trapping has the capability to manipulate small living biological objects, such as single bacterial cells, as well as inanimate particles. The infrared wavelength is minimally invasive to living cells. The optical trapping at a cellular level affords insight into biological interactions. Thus, optical trapping of CSA-SNP and *S. aureus* was conducted to further investigate the interactions and potential selectivity.

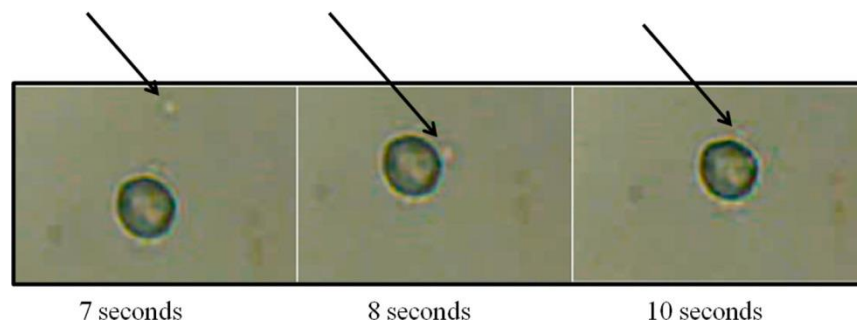


Figure 1.5.8 *S. aureus* (indicated with arrows) adhering to CSA functionalized MP.

An optical trap was used to indicate the adhesion of CSA-MP to *S. aureus* (Figure 1.5.8). A single bacterium was trapped in one specific trap, and CSA-MP was simultaneously trapped in another trap. The bacteria were then allowed to touch and reside for several seconds, and then the two traps were removed. The result indicated the *S. aureus* remained attached and could not be displaced by the force of the optical trap. The video indicates that three separate bacteria can attach and bind to one CSA functionalized particle. Repeated trials showed that interactions generally formed within periods of <2 s. As a control, the procedure was repeated with nanoparticles lacking CSA-124 surfactant. The nanoparticles without CSA-124 did not reveal adhesion to *S. aureus*, even when extending the residence time beyond 10 s.

1.5.5 Conclusions

Since Silver was approved by the FDA in the 1920s⁴³, it has been applied clinically as a broad-spectrum antimicrobial. Recent research demonstrates that there are many drawbacks to broad-spectrum antimicrobials including longer recover times, increased risk of further infection, and higher incidence of drug resistance. The data presented indicate that the antimicrobial qualities of silver can be supplemented via conjugation with selective ligands such CSA-124. Whereas SNPs alone have an MIC of 120 ppm against *S. aureus*, CSA-SNPs present an MIC of 15 and 30 ppm

toward *S. aureus* and *E. faecalis*, respectively, and an MIC of 30 and 60 ppm toward *E. coli* and *P. aeruginosa*, respectively. This study further demonstrates that the functionalization of CSA to the nanoparticle surface imparts spatial selectivity in favor of *S. aureus* over *E. coli*; nevertheless, spatial selectivity does not necessarily imply antimicrobial selectivity. These findings were further supported through MATLAB analysis of confocal images, presenting that while in coculture, 70% of CSA-SNPs were within 2 μm of an *S. aureus* cell while less than 40% were within 2 μm of an *E. coli* cell. Video images of laser captured nanoparticle interactions with both bacteria also indicate clear selectivity for the Gram-positive *S. aureus* over the Gram-negative *E. coli*.

1.5.6 References

1. Guarner, F.; Malagelada, J.R. *Gut Flora in Health and Disease Lancet*. **2003**, *361*, 512–519.
2. Kelly, C. P.; Pothoulakis, C.; LaMont, J. T. *Clostridium difficile Colitis. N. Engl. J. Med.* **1994**, *330* (4), 257–262.
3. Bignardi, G. Risk Factors for Clostridium difficile Infection. *J.Hosp. Infect.* **1998**, *40* (1), 1.
4. Eckert, R.; He, J.; Yarbrough, D. K.; Qi, F.; Anderson, M. H.; Shi, W. Targeted Killing of Streptococcus mutans by a Pheromone-Guided “Smart” Antimicrobial Peptide. *Antimicrob. Agents Chemother.* **2006**, *50* (11), 3651–3657.
5. Travan, A.; Pelillo, C.; Donati, I.; Marsich, E.; Benincasa, M.; Scarpa, T.; Semeraro, S.; Turco, G.; Gennaro, R.; Paoletti, S. Noncytotoxic Silver Nanoparticle–Polysaccharide Nanocomposites with Antimicrobial Activity. *Biomacromolecules.* **2009**, *10* (6), 1429–1435.
6. Pal, S.; Tak, Y. K.; Song, J. M. Does the Antibacterial Activity of Silver Nanoparticles Depend on the Shape of the nanoparticle? A study of the Gram-Negative Bacterium *Escherichia coli*. *Appl. Environ. Microbiol.* **2007**, *73*, 1712–1720.
7. Yih, T.; Al-Fandi, M. Engineered Nanoparticles as Precise Drug Delivery Systems. *J. Cell. Biochem.* **2006**, *97*, 1184–1190.
8. Minichin, R. F.; Martin, D. J. *Mini-review: Nanoparticles for Molecular Imaging-An Overview.* *Endocrinology* **2010**, *151*, 474–481.
9. Singh, R.; Lilard, J. W., Jr. Nanoparticle-Based Targeted Drug Delivery. *Exp. Mol. Pathol.* **2009**, *86*, 215–223.

10. Gelperina, S.; Kisich, K.; Iseman, M. D.; Heifets, L. The potential advantages of Nanoparticle Drug Delivery Systems in Chemotherapy of Tuberculosis. *Am. J. Respir. Crit. Care Med.* **2005**, *172*, 1487-1490.
11. Emerich, D. F.; Thanos, C. G. The Pinpoint Promise of Nanoparticle-Based Drug Delivery and Molecular Diagnosis. *Biomol. Eng.* **2006**, *23*, 1171-184.
12. Love, J. C.; Estroff, L. A.; Kriebel, J. K.; Nuzzo, R. G.; Whitesides, G. M. Self-Assembled Monolayers of Thiolates on Metals as a Form of Nanotechnology. *Chem. Rev.* **2005**, *105*, 1103-1170.
13. Brown, P. K.; Qureshi, A. T.; Moll, A. N.; Hayes, D. J.; Monroe, W. T. Silver nanoscale Antisense Drug Delivery System for Photoactivated Gene Silencing. *ACS Nano.* **2013**, *7*, 2948-2959.
14. Kim, J. S.; Kuk, E.; Yu, K. N.; Kim, J.-H.; Park, S. J.; Lee, H. J.; Kim, S. H.; Park, Y. K.; Park, Y. H.; Hwang, C. Y. Antimicrobial Effects of silver Nanoparticles. *J. Nanomed. Nanotechnol.* **2007**, *3*, 95-101.
15. Lok, C.-N.; Ho, C.-M.; Chen, R.; He, Q.-Y.; Yu, W.-Y.; Sun H.; Tam, P. K.-H.; Chiu, J.-F.; Che, C.-M. Silver Nanoparticles: Partial Oxidation and Antibacterial Activities. *J. Biol. Inorg. Chem.* **2007**, *12*, 527-534.
16. Baker, T. B.; McFall, R. M.; Shoham, V. Current Status and Future Prospects of Clinical Psychology Toward a Scientifically Principled Approach to Mental and Behavioral Health Care. *Psychol. Sci. Public Interest.* **2009**, *9*, 67-103.
17. Aymonier, C.; Schlotterbeck, U.; Antonietti, L.; Zacharias, P.; Thomann, R.; Tiller, J. C.; Mecking, S. *Chemical Communications.* **2002**, No. 24, 3018–3019.

18. Gibbins, B.; Warner, L. The role of antimicrobial silver Nanotechnology. *Med. Device Diagn. Ind.* **2005**, *1*, 1-2.
19. Silver, S.; Phung, L. T.; Silver, G. Silver as Biocides in Burn and Wound Dressings and Bacterial Resistance to Silver Compounds. *J. Ind. Microbiol. Biotechnol.* **2006**, *33*, 627-634.
20. Hancock, R.; Patrzykat, A. Clinical Development of Cationic Antimicrobial Peptides: From Natural to Novel Antibiotics. *Curr. Drug Targets: Infect. Disord.* **2002**, *2*, 79-83.
21. Zasloff, M. Antimicrobial Peptides of Multicellular Organisms. *Nature* **2002**, *415*, 389-395.
22. Eband, R. M.; Eband, R. F.; Savage, P. B. Cergenins (Cationic Steroid Compounds), A novel class of antimicrobial agents. *Drug News Perspect.* **2008**, *21*, 307-311.
23. Chin, J. N.; Jones, R. N.; Sader, H. S.; Savage, P. B.; Rybak, M. J. Potential Synergy Activity of the novel Ceragenin, CSA-13, Against Clinical Isolates of *Pseudomonas aeruginosa*, Including Multidrug resistant *P. aeruginosa*. *J. Antimicrob. Chemother.* **2008**, *61*, 365-370.
24. Leszczynska, K.; Namiot, A.; Fein, D. E.; Wen, Q.; Namiot, Z.; Savage, P. B.; Diamond, S.; Janmey, P. A.; Buci, R. Bactericidal Activities of the Cationic Steroid CSA-13 and the Cathelicidin Peptide LL-37 Against *Helicobacter pylori* in Simulated Gastric Juice. *BMC Microbiol.* **2009**, *9*, 187.
25. Chin, J. N.; Rybak, M. J.; Cheung, C. M.; Savage, P. B. Antimicrobial Activities of Ceragenins Against Clinical Isolates of Resistant *Staphylococcus aureus*. *Antimicrob. Agents Chemother.* **2007**, *51*, 1268-1273.
26. Leszczynska, K.; Namiot, D.; Byfield, F. J.; Cruz, K.; Zendzian-Piotrowska, M.; Fein, D. E.; Savage, P. B.; Diamond, S.; McCulloch, C.A.; Janmey, P. A. Antibacterial Activity of the Human Host Defence Peptide LL-37 and Selected Synthetic Cationic Lipids Against Bacteria

Associated with Oral and Upper Respiratory Tract Infections. *Antimicrob. Agents Chemother.* **2013**, *68*, 610-618.

27. Standard Test Method for Analysis of Hemolytic Properties of Nanoparticles. In *International Committee for Standardization in Haematology*; ASTM international: West Conshohocken, PA, 1979; Vol. E2524-08.

28. Andrews, J. M. Determination of Minimum Inhibitory Concentrations. *Antimicrob. Agents Chemother.* **2001**, *48*, 5-16.

29. Wiegand, I.; Hilperk, K.; Hancock, R. E. Agar and Broth Dilution Methods to Determine the Minimal Inhibitory Concentration (MIC) of Antimicrobial Substances. *Nat. Protoc.* **2008**, *3*, 163-175.

30. seligy, B.; Rancourt, J. Antibiotic MIC/MBC analysis of Bacillus-Based Commercial Insecticides: Use of Bioreduction and DNA-Based Assays. *J. Ind. Microbiol. Biotechnol.* **1999**, *22*, 565-574.

31. de Nooijer, L. J.; Duijnste, I.; Van der Zwaan, G. Nowel Application of MTT Reduction: A viability Assay for Temperate Shallow- Water Benthic Foraminifera. *J. Foraminiferal Res.* **2006**, *36*, 195-200.

32. Taylor, P.; Schoenknecht, F.; Sherris, J.; Linner, E. Determination of minimum Bactericidal Concentrations of Oxacillin for *Staphylococcus aureus*: Influence and Significance of Technical Factors. *Antimicrob. Agents Chemother.* **1983**, *23*, 142-150.

33. Isenberg, H. D., Ed. *Clinical Microbiology Procedures Handbook*; ASM Press: Washington, DC, **2007**.

34. Perry, J.; Reuter, K. G.; Kai, M. P.; Herlihy, K. P.; Jones, S. W.; Luft, J. C.; Napier, M. E.; Bear, J. E.; DeSimone, J. M. PEGylated Print Nnaoparticles: The Impact of PEG Density on

Protein Binding, Macrophage Association Biodistribution, and Pharmacokinetics. *Nano Lett.* **2012**, *12*, 5304-5310.

35. Agasti, S. S.; Chompoosor, A.; You, C. C.; Ghosh, P.; Kim, C. K.; Rotello, V. M. Photoregulated Release of Caged Anticancer Drugs from Gold Nanoparticles *J. Am. Chem. Soc.* **2009**, *131*, 5728-5729.

36. Chertok, B.; Moffat, B. A.; David, A. E.; Yu, F.; Bergemann, C.; Ross, B. D.; Yang, V. C. Iron oxide nanoparticles as a Drug Delivery Vehicle for MRI Monitored Magnetic Targeting of Brain Tumors. *Biomaterials* **2008**, *29*, 487-496.

37. Moghadam, B. Y.; Hou, W. C.; Corredor, C.; Westerhoff, P.; Posner, J. The role of nanoparticle surface functionality in the disruption of model cell membranes. *Lanmuir* **2012**, *28*, 16318-16326.

38. Brown, P. K.; Qureshi, A. T.; Moll, A. N.; Hayes, D. J.; Monroe, W. T. Silver Nanoscale Antisense Drug Delivery System for Photoactivated Gene Silencing. *ACS Nano* **2013**, *7*, 2948-2959.

39. Ding, B.; Guan, Q.; Walsh, J. P.; Boswell, J. S.; Winter, T. W.; Winter, E. S.; Boyd, S. S.; Li, C.; Savage, P. B. Correlation of the Antibacterial Activities of Cationic Peptide Antibiotics and Cationic Steroid Antibiotics 1. *J. Med. Chem.* **2002**, *45*, 663-669.

40. Morones, J. R.; Elechiguerra, J. L.; Camacho, A.; Holt, K.; Kouri, J. B.; Ramirez, J. T.; Yacaman, M. J. The bactericidal Effect of Silver Nanoparticles. *Nanotechnology* **2005**, *16*, 2346.

41. mahmoudi, M.; Laurent, S.; Shokrgozar, M. A.; Hosseinkhani, M. Toxicity Evaluations of Superparamagnetic Iron Oxide Nanoparticles: Cell "Vision" Versus Physicochemical Properties of Nanoparticles. *ACS Nano* **2011**, *5*, 7263-7276.

42. Laurent, S.; Burtea, C.; Thirifays, C.; Hafeli, U. O.; Mahmoudi, M. Crucial Ignored Parameters on Nanotoxicology: The Importance of Toxicity Assay Modifications and “Cell Vision”. *PLoS One*. **2012**, *7*, e29997.
43. Jain, J.; Arora, S.; Rajwade, J. M.; Omay, P.; Khandelwal, S.; Paknikar, K. M. Silver nanoparticles in Therapeutics: Development of an Antimicrobial Gel Formulation for Topical Use. *Mol. Pharmaceutics* **2009**, *6*, 1388-1401.

Chapter 2

Structural Improvement and Synthesis of Cyclopentenone Prostaglandins

2.1 Introduction

2.1.1 Prostaglandins

Prostanoids are natural subclass of eicosanoids, or signaling molecules, generated mainly from metabolic oxidation of arachidonic acid (AA).¹⁻³ They are unsaturated carboxylic acids with 20-carbon atoms in their skeleton. They are divided into two types: prostaglandins (PGs), which contain a cyclopentane ring, and thromboxanes, which contain a cyclohexane ring.⁴

PGs were first found by Euler et al. in 1930s and first characterized in 1950s.^{5,6} As shown in Figure 2.1, every prostaglandin is named with the prefix 'PG' followed by a letter A-K depending on the nature and position of the substituents on the cyclopentane ring. Furthermore, a numerical subscript (1-3) is used to denote the total number of double bonds in the hydrocarbon substituents. A Greek subscript (α or β) is used with the PGF series to describe the stereochemistry of the hydroxyl group on C9. A key feature of prostaglandins is the five membered ring encompassing C8 to C12.

covalent adducts with nucleophilic residues, such as cysteine in proteins through Michael addition, as shown in Figure 2.2. CyPGs are biologically generated from unsaturated fatty acids, such as arachidonic acid from membrane-bound phospholipids via the action of phospholipases and linolenic acid from the diet via the action of elongase. These unsaturated fatty acids can be converted into different PGs enzymatically and non-enzymatically. The enzymatic pathway in fact is the metabolism via cyclooxygenases (COXs) to produce PGH_1 and PGH_2 . PGH_2 is further transformed to PGE_2 and PGD_2 by different prostaglandin synthases. The non-enzymatic pathway is the epimerization of isoprostanes to produce PGE_2 and PGD_2 . Finally, these parent PGs are dehydrated or undergo an albumin-dependent pathway to yield cyPGs (such as PGA_2 and 15d-PGJ_2).⁹⁻¹³ Since the unsaturated carbonyl group in the cyclopentenone ring is reactive, cyPGs react with nucleophilic groups (such as thiol or amino groups) in amino acid residues of proteins by Michael's addition, resulting in alterations of protein function.¹⁴⁻¹⁷

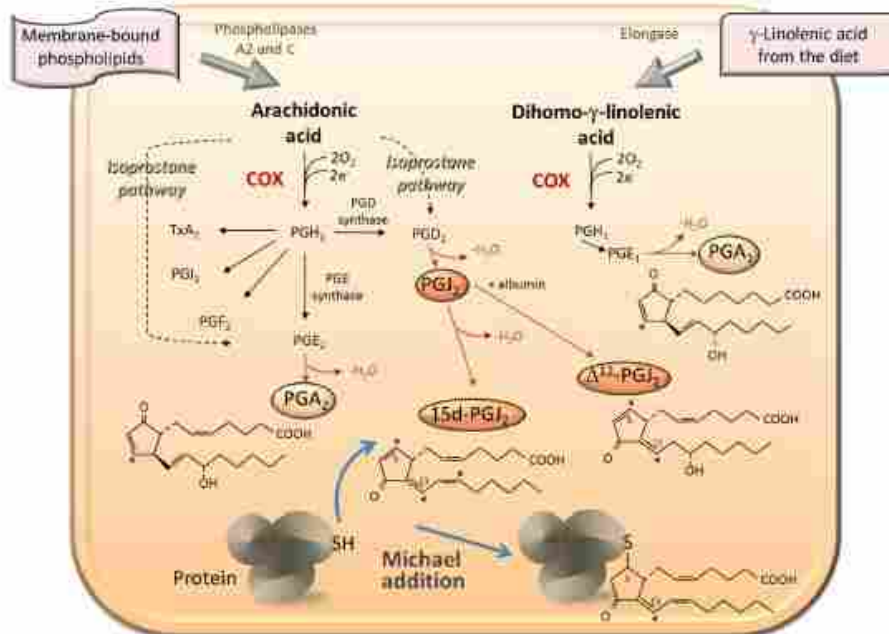


Figure 2.2 Formation of cyPGs and covalent binding to proteins through Michael addition. Adapted from ref[8].

2.1.2 Functions of Cyclopentenone Prostaglandins

Due to their α,β -unsaturated carbonyl group, can easily form Michael adducts with free nucleophilic groups, cyPGs are potent bioactive lipid mediators and have important roles in the resolution of inflammation and the regulation of cell proliferation and cellular redox status (tumorigenesis). As a result, cyPGs possess three main potentially therapeutic properties: anti-inflammatory, antiproliferative and antiviral.

2.1.3 Regulation of Inflammation

CyPGs play an essential role in the regulation of the inflammation response through their ability to covalently modify the related key proteins. CyPGs are present at low levels in normal conditions and get increased in situations of chronic inflammation, especially when associated with COX-2 expression. Recent researchers suggested that cyPGs play a protective role in pathophysiological process and considered potentially useful drug-candidates. CyPGs are generated in the defense mechanisms and then participate in the resolution of inflammation. They act as a switch between inflammatory factor and pro-resolving mediator, reduce the activity of pro-inflammatory transcription factors, such as nuclear factor kappa B (NF- κ B) and activator protein 1 (AP-1), and are involved in modification of proteins involved in inflammatory resolution. Martínez et al. illustrated how 15d-PGJ₂ displayed a biphasic effect on cell activation of mesangial cells to cytokine stimulation. In detail, 15d-PGJ₂ led to an amplification of NO and iNOs with nanomolar concentrations in the early stages of the inflammatory response and inhibited proinflammatory gene expression with micromolar concentrations during late stages.¹⁸ Fernandez-Bustamante et al. demonstrated that 15d-PGJ₂ contributed in counteracting ongoing lung inflammation in early endogenous conditions but also worked as an early biomarker of lung

inflammation.¹⁹ Pe´rez-Sala et al. identified a novel site binding site for 15d-PGJ₂ with the AP-1 that contributes to the cellular response to pro-inflammatory agents.²⁰

2.1.4 Antiproliferative Activity and Antitumoral Activity

CyPGs, such as 15d-PGJ₂, suppress proliferation of cancer cells, induce apoptosis in various cancer cells and show great potential antitumor activity due to their involvement in inhibition of transcription factor AP-1 or activation of peroxisome proliferator activated receptor gamma (PPAR γ). Kim et al. reported 15d-PGJ₂ inhibited the bone loss that is associated with breast cancer as well as bone metastasis and estrogen deficiency caused by cancer.²¹ Ciucci et al. demonstrated 15d-PGJ₂ induced inhibition of constitutive I κ B-kinase and NF- κ B activities in ER-negative breast cancer cells.²² PGA and analogues also inhibited DNA synthesis and proliferation of tumor cells substantial potently. They were able to inhibit the proliferation of tumor cells in vitro, including melanoma and leukemia cells.²³⁻²⁵ Garzón et al. demonstrated that PGAs potently activate heat shock factor (HSF) and induce the transcription of heat shock protein 70 (Hsp70) due to their electrophilic nature. These effects have been verified to correlate with the antiproliferative actions of PGA₁.^{26, 27} Pavithra et al. proposed PGA₂ also had an antiproliferative effect, inducing the binding of Hsp 70 to the 5'-UTR of the mRNA of tumor suppressor SMAR1, and leading to an increase in SMAR1 protein levels.²⁸

2.1.5 Antiviral Properties

CyPGs have been reported to have antiviral activity against poliovirus, Sendai and HIV virus via their interactions with the cells or the targets.²⁹⁻³² Santoro et al. found several cyPGs displayed antiviral effects and inhibited viral replication factors, such as NF- κ B.²⁹ Suzuki et al demonstrated Δ^7 -PGA₁ methyl ester and PGA₁ methyl ester reacted with thiol nucleophiles via covalent modification to inhibit cell growth.³⁰ Hayes et al. illustrated that, PGA₁ and PGA₂

inhibited the replication of HIV-1 in infected human monocyte-derived macrophages and reduced the replication of HIV in lately infected U1 cells³¹, due to electrophilic groups in cyPGs. Kalantari et al. reported cyPGs directly inhibited HIV-1 proteins via covalently direct bindings.³³

2.1.6 Synthesis of Cyclopentenone Prostaglandins

To further understand the relationships between the chemical structures and the extraordinary bioactivities of cyPGs, organic synthesis of cyPGs and analogues greatly facilitated the evaluation of their activities in diverse biological systems and exploration of their applications in pathophysiological and pharmacological fields.

As shown in Figure 2.1, cyPGs have a cyclopentenone ring as the key point, and two side chains with three or four stereo-centers, including the α -chain containing carboxy group (C-1 to C-7) and the ω -chain containing hydroxyl group (C-13 to C-20). Based on these chemical structures of cyPGs, total synthesis could be completed with Djuric's strategy.³⁴ The core cyclopentenone ring was synthesized with certain substitutes in appropriate positions as one of the side chains, then the second chain (α - or ω -side chain) was introduced in a following step. Last, 1,4-addition of the ω -chain on the appropriate Cyclopentenone was done, followed by in situ trapping with the required α component as the electrophile gave the target molecule.

Egger et al. explored the synthesis of 15d-PGJ₂ in their previous research.³⁵⁻³⁷ They utilized the 1, 5-pentanediol as the initial reagent, protected one of the alcohols, left the other subjected to oxidation to yield aldehyde. They obtained the cyclopentanone after several following steps, installation of ω -side chain, removed protecting group of the ether, and finally stepwise oxidized the alcohol to acid to complete the synthesis.

Considering this previous research, we used inexpensive glycols as the initial reactants and follow the main strategy mentioned above to carry out cyPGs synthesis, especially the PGA and analogues.

2.2 Synthesis and Modification of Cyclopentenone Prostaglandins

2.2.1 The Target Cyclopentenone Prostaglandin to Synthesize and Modify

Recently, Egger and co-workers evaluated the activity of EI and EC (Figure 2.3) in reducing the secretion of proinflammatory cytokines IL-6 and IL-12 by dendritic cells in response to a TLR4 agonist. EC has been identified as the most active compound. Furthermore, another similar cyclopentenone prostaglandin, 15d-PGJ₂(Figure 2.3) is reported as the anti-inflammatory prostaglandin. This cyclopentenone prostaglandin also exhibits extraordinary biological activity in the modulation of inflammatory and apoptotic process. Due to their high bioactivity, EC was chosen as a target compound of cyclopentenone prostaglandin to synthesize and modify.

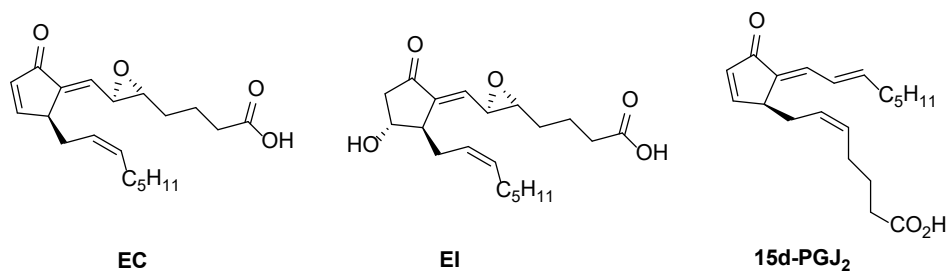
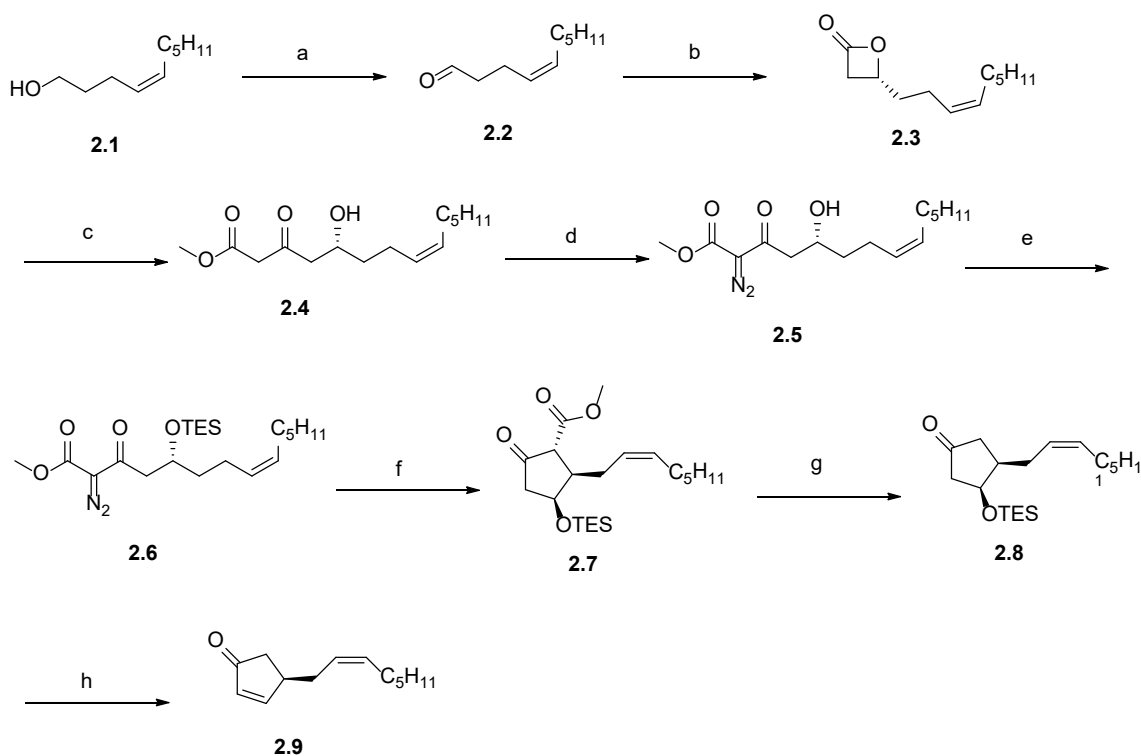


Figure 2.3 Structure of EC, EI and 15d-PGJ₂

2.2.2 Synthesis of EC

In 2005, Jung and Kobayashi developed the total synthesis of EC in 20 steps with 0.19% total yield and 14 steps with 0.13% total yield respectively, using chiral cyclopentadiene as starting material. In 2013, Egger and co-workers completed total synthesis of EC in just 11 steps with up to 5.4% total yield. Two years later, Lu developed an efficient synthetic route for EC ester in 8

steps with 10% total yield. We followed Egger's synthetic strategy of the total synthesis of EC in our study using (*Z*)-dec-4-en-1-ol as starting material.

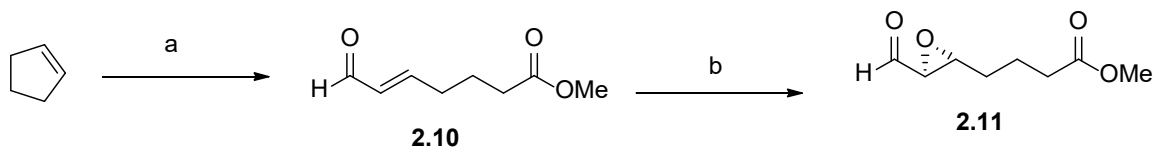


Scheme 2.1 Synthesis of compound **2.9**

Reagents: a) Oxalyl chloride, TEA, DMSO, 87%; b) LiClO₄, TMS-quinidine, Acetyl chloride, DIPEA, 61%; c) *n*-BuLi, Diisopropylamine, Methyl acetate, THF, 74%; d) 4-Acetamidobenzensulf-only azide, TEA, DCM, 96%; e) TESCl, DMF, 88%; f) Rh₂(s-PTAD)₄, DCM, 59%; g) NaCl, DMSO, 140 °C, 65%; h) DBU, DCM, 93%;

The first step was a classic swern oxidation to form corresponding aldehyde **2.2**, which was converted to β-lactone **2.3** in 61% yield and 92% ee, as determined by SFC analysis. Opening of compound **2.3** with methyl acetate enolate afforded β-ketoester **2.4** in 74% yield. Compound **2.4** was subjected to sequential diazotization providing compound **2.5**, which was protected by TESCl to form compound **2.6**. Rh-catalyzed C-H insertion reaction using [Rh₂(OAc)₄] gave the cyclized product resulting from insertion into the homoallylic C-H bond. This tartgent compound

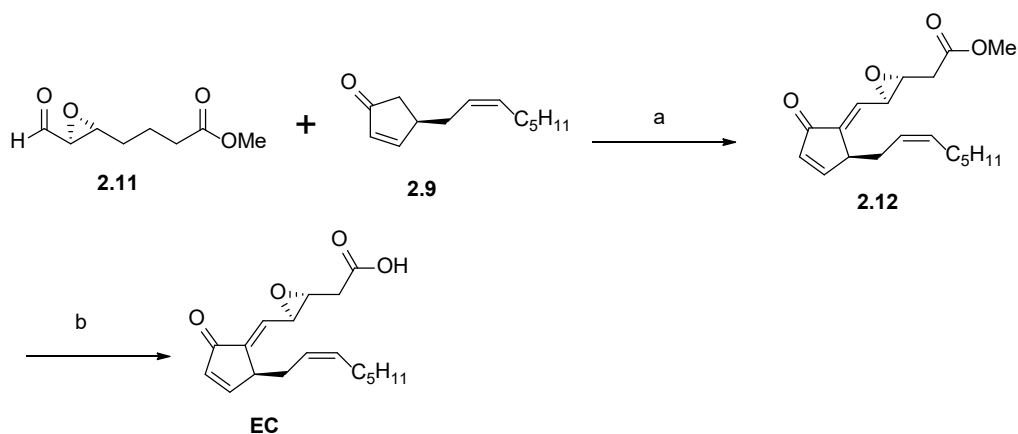
2.7 was obtained as a 4:1 mixture of diastereomers as determined by analysis of the crude NMR spectra, which indicated a preference of the desired C11-C12 cis product. Decarboxylation of Compound 2.7 gave compound 2.8, which was treated with DBU to form the key intermediate compound 2.9.



Scheme 2.2 Synthesis of compound 2.11

Reagents: a) i) O_3 , $NaHCO_3$, MeOH/DCM, $-78\text{ }^\circ\text{C}$ then TEA, Ac_2O , PhH, $0\text{ }^\circ\text{C}$; ii) $Ph_3PCHCHO$, toluene, $70\text{ }^\circ\text{C}$, 55%; b) (S)-2-(diphenyl[(trimethylsilyl)oxy]pyrrolidine), H_2O_2 , DCM, RT, 51%.

To prepare the side chain part, we started with cyclopentene and underwent ozone oxidation and Wittig reaction to form compound 2.10. Epoxidation of hydrogen peroxide gave the corresponding compound 2.11 as a synthetic side chain block.



Scheme 2.3 Synthesis of EC

Reagents: a) i) $\text{LiN}(\text{SiMe}_3)_2$, THF, $-78\text{ }^\circ\text{C}$; ii) MeSO_2Cl , TEA, DCM, $-78\text{ }^\circ\text{C}$, then Al_2O_3 , DCM, RT, 64%; b) Novozyme (lipase on acrylic resin), PBS, 70%.

Within compound **2.9** and compound **2.11** in hands, installation of the C8 side chain of cyclopentenyl ring was performed with a modification of a procedure by Kobayashi, involving the aldol addition of these two key intermediate, followed by a *trans*-selective elimination to form dienone **2.12**. Enzymatic hydrolysis of the methyl ester in PBS gave the target acid EC.

2.2.3 Modification and Synthesis of Cyclopentenone Prostaglandin

Modification of cyclopentenone prostaglandin

Since we successfully synthesized the most active cyclopentenone prostaglandin in reducing the secretion of pro-inflammatory cytokines IL-6 and IL-12 by dendritic cells in response to a TLR4 agonist, several similar structural cyclopentenone prostaglandins were designed and synthesized (Figure 2.4).

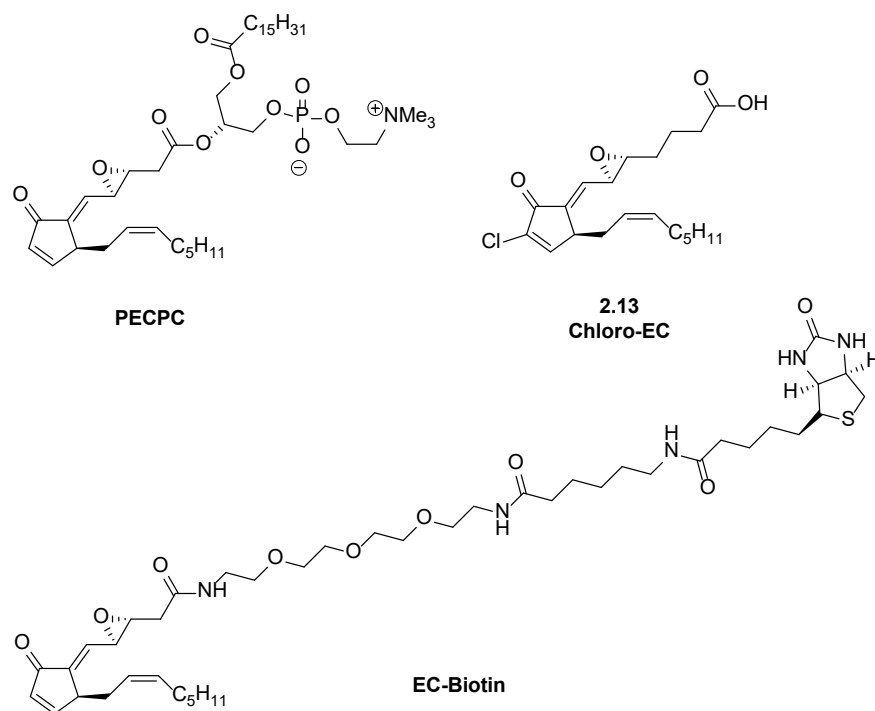
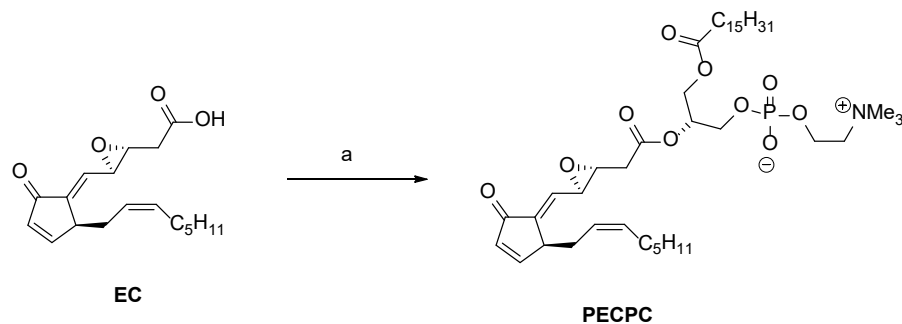


Figure 2.4 Structure of derivatives of EC

As one of oxidized phospholipids (OxPLs), PECPC (shown in **Figure 2.4**) has been shown to act as an anti-inflammatory agent in reducing the secretion of the pro-inflammatory cytokines IL-6 and IL-12. According to the cyclopentenone prostaglandins structural specification, we induced one chlorine element at position 2 to design a new cyclopentenone prostaglandin **2.12** (shown in **Figure 2.4**). Otherwise, we designed and synthesized one new EC derivative called EC-Biotin, which was modified through coupling with Biotin mediated by a PEG linkage chain. We proposed these modifications could possibly to improve bioactivity as anti-inflammatory agents due to increasing nucleophilicity of molecule and be easy to identify as a biomarker during metabolic activities.

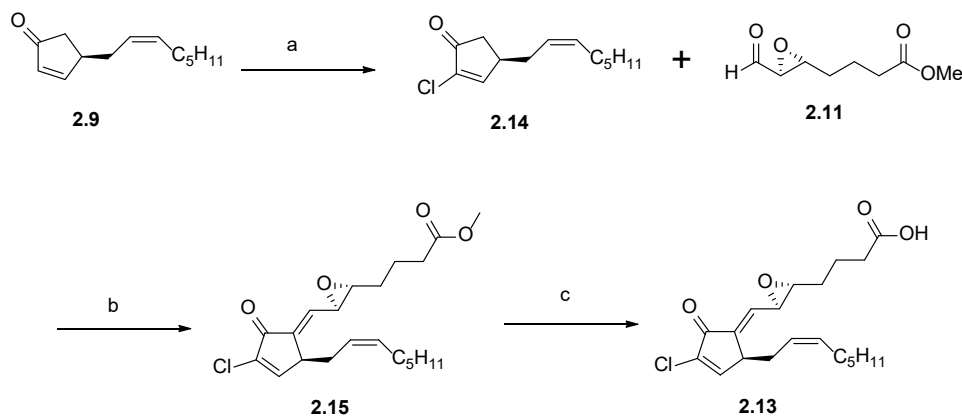
Synthesis of designed cyclopentenone prostaglandins



Scheme 2.4 Synthesis of PECPC

Reagents: a) 2,4,6- Cl₃C₆H₂COCl, DMAP, lyso-PC, CHCl₃, 59%.

To synthesize PECPC, we used EC as starting material, followed an esterification reaction with lyso-pc to form the target product.

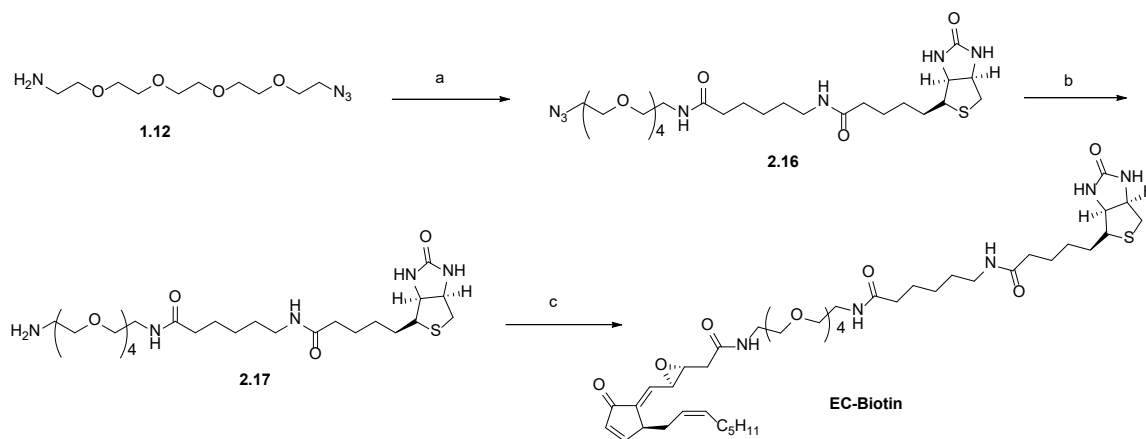


Scheme 2.5 Synthesis of Compound 2.13

Reagents: a) m-CPBA, DMF/HCl, DMF, 63%; b) i) LiN(SiMe₃)₂, THF, -78 °C; ii) MeSO₂Cl, TEA, DCM, -78 °C, then Al₂O₃, DCM, RT, 61%; c) Novozyme (lipase on acrylic resin), PBS, 68%.

To synthesize compound 2.13, we used the key intermediate 2.9 as starting material. The compound 2.9 was treated with m-CPBA in the 6.6 M of DMF/HCl solution at 0 °C to give compound 2.14. With this key intermediate 2.14 in hands, the same synthetic pathway as

synthesis of EC mentioned in scheme 2.3 was conducted to form successfully the target compound **2.13**.



Scheme 2.6 Synthesis of EC-Biotin

Reagents: a) Biotin.OSu.X, TEA, DCM, 90%; b) Zn, AcOH, MeOH, THF, 88%; c) EC, EDCl, HOBt, CHCl₃, 92%.

Compound **1.12** was treated with Biotin.OSu.x in presence of basic condition to obtain coupling product Compound **2.16**. Reduction of Zn afforded the corresponding amine **2.17**, which was underwent a peptide coupling reaction to form the EC-Biotin.

2.3 Study of Bioactivities of EC and Its Derivatives in Reducing Secretion of Pro-inflammatory Cytokines IL-6 and IL-12

EC and its derivatives were sent to Dr. Freigang's Group in Institute for Integrative Biology, ETH Zurich for their bioactivities in reducing secretion of pro-inflammatory cytokines IL-6 and IL-12 respectively.

2.4 Results and Discussion

The preliminary bioactivity of EC in reducing secretion of pro-inflammatory cytokines IL-12 had been accomplished in Dr. Feigang group (Figure 2.3).

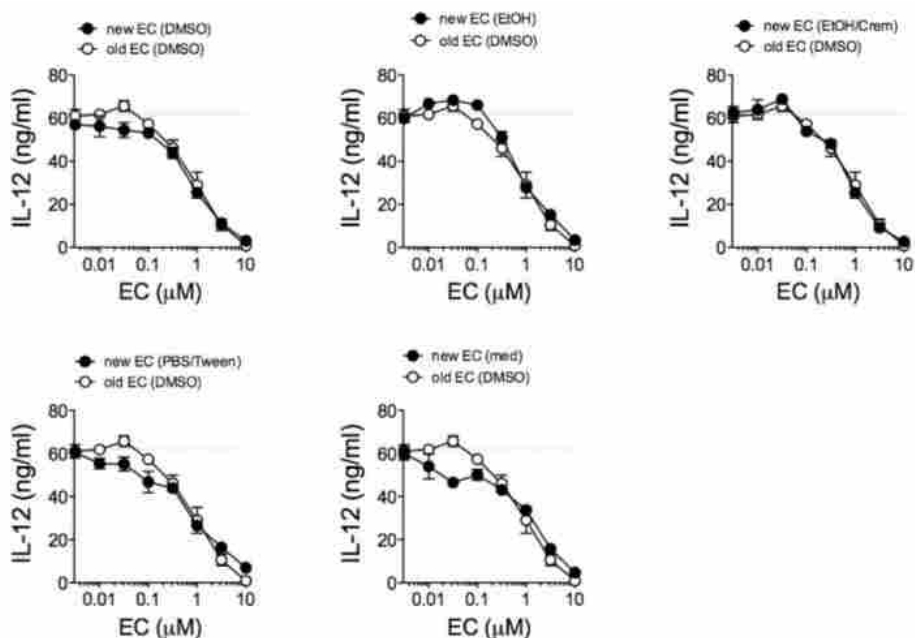


Figure 2.3 Effect in Reducing Secretion of Pro-inflammatory Cytokines IL-12.

As expected, the fresh EC elicited a strong effect in the inhibitory of secretion of pro-inflammatory cytokines IL-12. Figure 2.3 indicated that various concentrations of EC, range from 0.01 μM to 10 μM , inhibited the secretion of pro-inflammatory cytokines IL-12. In the experiment, we also qualified the inhibitory effect of EC in reducing the secretion of pro-inflammatory cytokines IL-12 using different solvent such as EtOH, DMSO, Med, PBS/ tween and EtOH/Crem. They showed a similar and strong inhibitory effect. In Figure 2.3, we observed a dose-dependent decrease in the secretion of the pro-inflammatory cytokines IL-12. Further investigation of the inhibitory effect of other derivatives will be conducted in the due course.

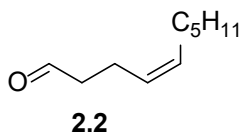
2.5 Conclusions

In general, we successfully prepared the cyclized oxidized phospholipids PECPC and the corresponding free carboxylic acids EC in our lab. We also were managed to synthesize two designed derivatives in an effective and efficient route. The route we developed provides Chloro-EC in 13 steps (0.88% yield) and EC-Biotin in 15 steps (0.99% yield), respectively. As the most bioactive compound in reducing the secretion of pro-inflammatory cytokines IL-6 and IL-12, EC was investigated for the inhibitory effect in various concentrations and in several solvent systems. Further studies on inhibitory of secretion of pro-inflammatory cytokines IL-6 and IL-12 for derivatives are in progress.

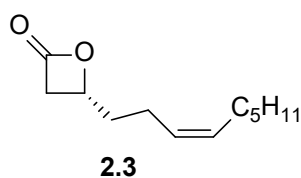
2.6 Experiment Section

General: Reagents were purchased from Aldrich Chemical Co. unless otherwise noted. Methylene chloride, THF, DMF, pyridine, and DMSO were dried by passage through a Glass Contour solvent drying system containing a cylinder of activated alumina. Silica gel was used for chromatography unless otherwise noted.

Instrumentation: ^1H and ^{13}C NMR spectra were recorded on a Varian Gemini 500 (500 MHz) spectrometer. Proton chemical shift were referenced to tetramethylsilane (TMS). Carbon chemical shifts were referenced to carbon resonance of solvents (CDCl_3 , CD_3OD). High resolution electron impact mass spectra (HR-MS) were obtained on a JOEL SX 102A spectrometer.

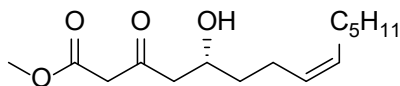


Compound 2.2 To a solution of oxalyl chloride(1.82 mL, 20.8 mmol, 1.30eq.) in DCM (30 mL) at -78 °C, was added over a period of 10 min a solution of DMSO (3.0 mL, 41.6 mmol, 2.6 eq) in DCM (5 mL). The mixture was stirred for 30 min and then a solution of (z)-dec-4-en-1-ol (3 mL, 16 mmol, 1.00eq) in DCM (20 mL) was added. The mixture was stirred at -78 °C for 2 h, then a solution of TEA (10 mL, 64 mmol, 4.00eq) in DCM (5 mL) was added and the mixture stirred for another 45 min at -78 °C, before it was allowed to reach room temperature. The mixture was treated with water (15 mL) and the layers were separated. The aqueous layer was extracted with DCM (3X 10 mL) and the combined organic layers were washed with brine (25 mL), dried over Na₂SO₄, filtered and concentrated in vacuo. Purification by flash column chromatography (SiO₂, pentane/Et₂O, 10:1) gave aldehyde 2.2 (2.0g, 158 mmol, 87% yield) as a colorless oil. TLC: R_f=0.64 (hexane/EtOAc, 5:1, Vanillin). ¹H NMR (400 MHz, CDCl₃): δ= δ 9.77(t, J = 1.6Hz, 1H), 5.48-5.38 (m, 1H), 5.37-5.28 (m, 1H), 2.52-2.44 (m, 2H), 2.41-2.38 (q, J= 7.1 Hz, 2H), 1.40-1.23 (m, 6H), 0.88 (t, J= 6.9Hz, 3H). ¹³C NMR (100 MHz, CDCl₃): δ= δ 202.39, 131.89, 127.14, 44.00, 31.64, 29.38, 27.34, 20.23, 14.19, HRMS (ESI) calcd for C₁₀H₁₈O [M+H]⁺: 155.1436, found: 155.1434.



Compound 2.3 To a 100mL-flask equipped with a big stirring bar and dried lithium perchlorate (2.2g, 2.1 mmol, 3.00 eq) was added Et₂O (20 mL), followed by a solution of TMS-quinidine (0.35g, 0.9 mmol, 0.12 eq) in DCM (30 mL). The mixture was stirred at room temperature until a clear solution has formed and then cooled to -78 °C before i-Pr₂NEt (3.0 mL, 17.3 mmol, 2.50 eq) was added, followed by a solution of decenal 2-2 (1.0g, 7.0 mmol, 1.00 eq) in DCM (15 mL). A

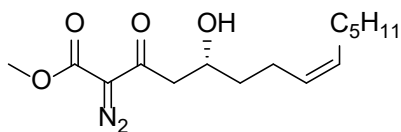
solution of acetyl chloride (1 mL, 14 mmol, 2.50 eq) in DCM (2X 3 mL) was then added over 4h via a syringe pump and the mixture kept stirring at -78 °C for 8 h. After full consumption of the starting material, the now yellow, turbid reaction mixture was quenched at -78 °C with Et₂O (10 mL) and then allowed to reach room temperature, before it was filtered through a pad of silica, that was afterwards carefully washed with Et₂O (3 X 15 mL). The filtrate was concentrated in vacuo and the crude material purified by flash column chromatography (SiO₂, pentane/Et₂O, 5:1) to give lactone **2.3** (0.78 g, 43 mmol, 61% yield, 93% ee) as a colorless oil. TLC: R_f=0.41 (Hexane/EtOAc, 3:1, Vanillin). ¹H NMR (400 MHz, CDCl₃): δ= δ 5.55-5.22 (m, 2H), 4.60- 4.43 (m, 1H), 3.51 (dd, J=16.3Hz, 5.8 Hz, 1H), 3.08 (dd, J=16.3Hz, 5.8 Hz, 1H), 2.19 q, J=7.3 Hz, 2H), 2.11- 1.89 (m, 3H), 1.40-1.23 (m, 6H), 0.88 (t, J= 6.9Hz, 3H). ¹³C NMR (100 MHz, CDCl₃): δ= δ 168.33, 132.17, 127.10, 70.89, 43.06, 34.84, 31.64, 29.38, 27.34, 20.23, 14.19, HRMS (ESI) calcd for C₁₂H₂₀O₂ [M+H]⁺: 196.1463, found: 196.1460.



2.4

Compound 2.4 To a solution of diisopropylamine (2 mL, 14 mmol, 3.90eq.) in THF (10 mL) was added at -78 °C n-butyllithium (1.6M in hexane, 9 mL, 13.8 mmol, 3.77 eq) and the mixture stirred for 15 min at -78 °C. Then at -78 °C a solution of methyl acetate (1 mL, 13.7 mmol 3.77 eq) in THF (5 mL) was added dropwise and the mixture stirred for another 20 min at that temperature. A solution of lactone **2.3** (0.7g, 3.6 mmol, 1.00 eq) in THF (5 mL) was added and the mixture kept stirring at -78 °C for 15 h. after consumption of the starting material the

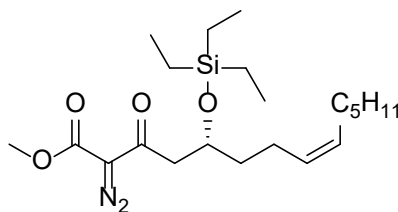
reaction was quenched with a saturated aqueous solution of NH_4Cl (7 mL). The layers were separated and the aqueous extracted with EtOAc (3 X 10 mL). The combined organic layers were washed with brine, dried over Na_2SO_4 , filtered and concentrated in vacuo. Purification by flash column chromatography (SiO_2 , hexane/EtOAc, 10:1 to 3:1 gradient) gave the ketoester **2.4** (0.7g, 28.0 mmol, 74% yield) as a 14:1 mixture together with its tautomer as a pale yellow oil. TLC: $R_f=0.34$ (hexane/EtOAc, 4:1, Vanillin). ^1H NMR (400 MHz, CDCl_3): δ 12.15 (s, 1H), 5.46-5.26 (m, 2H), 4.09 (m, 1H), 4.02-3.93 (m, 2H), 3.74 (s, 3H), 3.70 (s, 2H), 3.64 (s, 1H), 3.49 (s, 2H), 2.75 (d, $J=3.3\text{Hz}$, 3H) 2.72- 2.64 (m, 2H), 2.63 (d, $J=8.5\text{Hz}$, 3H), 2.20- 2.08 (m, 2H), 2.03 (q, $J=6.7\text{ Hz}$, 2H), 1.66-1.51 (m, 1H), 1.40-1.23 (m, 7H), 0.88 (t, $J= 6.9\text{Hz}$, 3H). ^{13}C NMR (100 MHz, CDCl_3): δ 203.58, 175.75, 167.46, 131.20, 128.65, 90.99, 69.15, 52.60, 51.39, 49.80, 43.01, 36.45, 31.64, 29.38, 27.34, 23.40, 22.72, 14.19, HRMS (ESI) calcd for $\text{C}_{15}\text{H}_{26}\text{O}_4$ $[\text{M}+\text{Na}]^+$: 293.1723, found: 293.1727



2.5

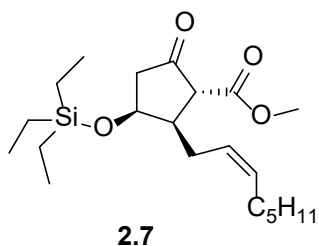
Compound 2.5 To a solution of ketoester **2.4** (6.98 g, 25.8 mmol, 1.00 eq.) in MeCN (200 mL.) at 0 °C was added sequentially 4-acetamidobenzenesulfonyl azide (8.31g 33.6 mmol, 1.30 eq) and Et_3N (7.26 mL, 5.16 mmol, 2.00 eq). The mixture was allowed to warm to room temperature and stirred for 5.5 h. The reaction mixture became turbid during that time and was filtered through a plug of celite before it was concentrated in vacuo. The residue was taken up in DCM (80 mL) and filtered again through a plug of celite. The solvent was removed in vacuo and the residue purified by flash column chromatography (SiO_2 , hexane/ EtOAc, 7:1) to yield the

diazo compound (7.39g, 24.8 mmol, 96%) as yellow oil. TLC: $R_f=0.53$ (hexane/EtOAc, 4:1, Vanillin, UV). ^1H NMR (400 MHz, CDCl_3): $\delta= \delta$ 5.41-5.26 (m, 2H), 4.11- 4.01 (m, 1H), 3.81 (s, 3H), 3.08- 2.97 (m, 2H), 2.90 (dd, $J = 17.2\text{Hz}$, 1H), 2.20- 2.08 (m, 2H), 2.00 (q, $J=6.7\text{ Hz}$, 2H), 1.64-1.41 (m, 2H), 1.36-1.18 (m, 6H), 0.85 (t, $J= 6.9\text{Hz}$, 3H). ^{13}C NMR (100 MHz, CDCl_3): $\delta= \delta$ 192.87, 161.72, 130.88, 128.65, 67.71, 52.60, 46.90, 46.86, 36.45, 31.64, 29.38, 27.34, 23.40, 22.72, 14.19, HRMS (ESI) calcd for $\text{C}_{15}\text{H}_{24}\text{N}_2\text{O}_4$ $[\text{M}+\text{Na}]^+$: 319.1634, found: 319.1628.

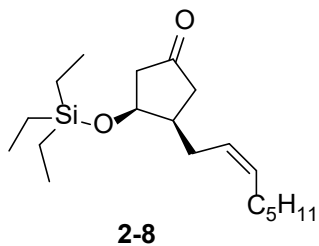


2.6

Compound 2.6 To a solution of the diazo compound **2.5** (3.39g 11.4 mmol, 1.00 eq.) at 0 °C was added imidazole (1.55g, 22.8 mmol, 2.00 eq.) and triethylchlorosilane (2.9 mL, 17.3 mmol, 1.51 eq.) The mixture was allowed to warm to room temperature and stirred for 3h. Then the reaction mixture was diluted with Et_2O (150 mL) and washed with water (400 mL). The organic layer was dried over Na_2SO_4 , filtered and concentrated in vacuo. Purification by flash column chromatography (SiO_2 , Hexane/EtOAc, 10:1) gave the TES-protected diazo compound **2.5** (4.0g, 11.18 mmol, 88%) as yellow oil. TLC: $R_f=0.65$ (hexane/EtOAc, 5:1, Vanillin, UV). ^1H NMR (400 MHz, CDCl_3): $\delta= \delta$ 5.401-5.30 (m, 2H), 4.31-4.20 (m, 1H), 3.83 (s, 3H), 3.15 (dd, $J = 15.5$, 7.2 Hz, 1H), 2.92 (dd, $J=15.5\text{Hz}$, 1H), 2.18- 1.97 (m, 4H), 1.61-1.48 (m, 2H), 1.39-1.18 (m, 6H), 0.99- 0.81 (m, 12H), 0.58 (q, $J = 7.9\text{ Hz}$, 6H). ^{13}C NMR (100 MHz, CDCl_3): $\delta= \delta$ 191.03, 161.78, 130.56, 129.13, 68.88, 52.30, 47.42, 38.15, 31.69, 29.53, 27.34, 23.40, 22.72, 14.19, 6.99, 5.10 HRMS (ESI) calcd for $\text{C}_{21}\text{H}_{38}\text{N}_2\text{O}_4\text{ Si}$ $[\text{M}+\text{Na}]^+$: 433.2493, found: 433.2498.

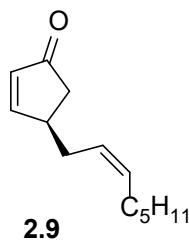


Compound 2.7 To a solution of $\text{Rh}_2(\text{S-PTAD})_4$ (170 mg, 0.109 mmol, 0.01 eq) in DCM (200 mL) at reflux was added a solution of TES-protected diazo compound 2.6 (4.48g 10.9 mmol, 1.00 eq.) in DCM (30 mL.). The mixture was stirred at reflux for 20 min and then allowed to cool to room temperature. The reaction mixture was concentrated in vacuo and purified by flash column chromatography (SiO_2 , Hexane/ Et_2O , 10:1) to yield cyclic ketoester **2.7** (2.5g, 7.75 mmol, 59%) in a 9:1 mixture of diastereomers as yellow oil. TLC: $R_f=0.29$ (hexane/ Et_2O , 4:1, Vanillin, UV). ^1H NMR (400 MHz, CDCl_3): δ = δ 12.24 (s, 1H), 5.58-5.25 (m, 2H), 4.45 (t, $J=3.8\text{Hz}$, 1H), 3.71 (s, 3H), 3.64 (s, 3H), 3.15 (dd, $J = 11.6\text{Hz}$, 1H), 2.81-2.67 (m, 2H), 2.65-2.53 (m, 1H), 2.50 (dd, $J= 18.0, 4.2\text{ Hz}$, 1H), 2.44- 2.33 (m, 2H), 2.31- 2.18 (m, 1H), 2.01 (q, $J= 7.0\text{ Hz}$, 2H), 1.39-1.18 (m, 6H), 0.93 (t $J = 7.9\text{ Hz}$, 9H), 0.87 (t, $J = 7.0\text{ Hz}$, 3H), 0.59 (q, $J = 7.8\text{ Hz}$, 6H). ^{13}C NMR (100 MHz, CDCl_3): δ = δ 210.20, 170.18, 132.28, , 126.17, 69.90, 57.71, 52.30, 49.46, 47.93, 31.69, 29.53, 27.34, 26.99, 22.72, 14.19, 6.99, 4.97. HRMS (ESI) calcd for $\text{C}_{21}\text{H}_{38}\text{O}_4\text{ Si}$ $[\text{M}+\text{Na}]^+$: 405.2432, found: 405.2438.



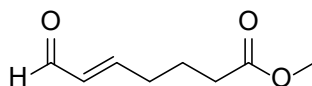
Compound 2.8 A solution of cyclic β -ketoester **2.7** (2.69 g, 7.05 mmol, 1.00 equiv.) and sodium chloride (12.36 g, 211 mmol, 30 equiv.) in degassed DMSO (100 mL) was immersed

into an oil bath pre-heated to 140 °C and stirred for 30 min. Then the mixture was allowed to cool to room temperature and diluted with water (900 mL). It was extracted with EtOAc (3 x 250 mL) and the combined organic layers were dried over MgSO₄, filter and concentrated in vacuo. Purification by flash column chromatography (SiO₂, Hexane/EtOAc, 98:2) allowed the separation of the cis-substituted cyclopentenone (1.49 g, 4.59 mmol, 65% yield). TLC: R_f = 0.71 (Hexane/EtOAc, 5:1, Vanillin). ¹H NMR (400 MHz, CDCl₃): δ = 5.51-5.28 (m, 2H), 4.49-4.35 (m, 1H), 2.43-1.92 (m, 9H), 1.43-1.18 (m, 6H), 0.95 (t, J = 7.9 Hz, 9H), 0.89 (t, J = 7.0 Hz, 3H), 0.59 (q, J = 7.8 Hz, 6H). ¹³C NMR (100 MHz, CDCl₃): δ = 217.76, 132.28, 126.17, 71.66, 49.46, 43.69, 41.17, 31.69, 29.53, 27.51, 27.49, 22.72, 14.19, 6.99, 4.97. HRMS (ESI) calcd for C₁₉H₃₆O₂ Si [M]⁺: 324.2485, found: 324.2483.



Compound 2.9 To a solution of the cis-substituted cyclopentenone (1.21 g, 3.73 mmol, 1.00 equiv.) in CH₂Cl₂ (35 mL) at 0 °C was added 1,8-Diazabicyclo[5.4.0]undec-7-ene (5.60 mL, 37.2 mmol, 9.97 equiv.) and the mixture allowed to warm to room temperature. The layer was separated and the aqueous was extracted with DCM (3 x 50 mL). The combined organic layers were washed with brine, dried over Na₂SO₄, filtered and concentrated in vacuo. In order to remove the residue silanol the mixture was azeotroped with toluene (5 x 15 mL). Purification by flash column chromatography (SiO₂, hexane/EtOAc, 7:1) gave cyclopentenone 2-8 (667 mg, 3.47 mmol, 93% yield) as a pale yellow oil. TLC: R_f = 0.52 (Hexane/EtOAc, 5:1, Vanillin, UV).

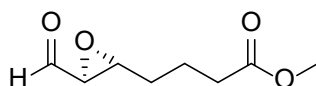
^1H NMR (400 MHz, CDCl_3): δ = 7.62 (dd, J =5.6, 2.5 Hz, 1H), 6.16 (dd, J =5.6, 2.0 Hz, 1H), 5.60-5.26 (m, 1H), 3.04-2.96 (m, 1H), 2.51 (dd, J =18, 6.4 Hz, 1H), 2.39-2.11 (m, 2H), 1.43-1.18 (m, 6H), 0.87 (t, J = 7.9 Hz, 3H). ^{13}C NMR (100 MHz, CDCl_3): δ = 209.98, 168.13, 134.19, 133.01, 125.17, 41.57, 40.65, 32.08, 31.62, 29.36, 27.51, 22.72, 14.19, HRMS (ESI) calcd for $\text{C}_{13}\text{H}_{20}\text{O}$ $[\text{M}]^+$: 192.1509, found: 192.1508.



2.10

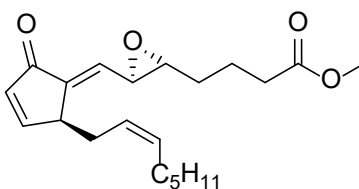
Compound 2.10 A solution of cyclopentene (10.34 mL, 113 mmol, 1.00 equiv.) and NaHCO_3 (3.00 g, 35.7 mmol, 0.32 equiv.) in MeOH (46 mL) and DCM (225 mL) at $-78\text{ }^\circ\text{C}$ was ozonized until a blue color persisted for 5 min. Then the solution was bubbled with N_2 until the blue color disappeared and allowed to warm to room temperature. Then the mixture was diluted with benzene (150 mL) and concentrated to 65 mL. It was treated at $0\text{ }^\circ\text{C}$ with Et_3N (31.4 mL, 225 mmol, 2.00 equiv.) and Ac_2O (21.28 mL, 225 mmol, 2.00 equiv.) for 1.5 h. The mixture was washed with NaHCO_3 and dried over Na_2SO_4 , filtered and concentrated in vacuo to yield crude aldehyde as colorless oil (11.64 g, 89.3 mmol, 79%). (7.09 g, 54.5 mmol, 1.00 equiv.) of the crude product was added to a solution of 2-(triphenylphosphoranylidene) acetaldehyde (34.82 g, 114 mmol, 2.10 equiv.) in toluene (150 mL) and the mixture stirred at $70\text{ }^\circ\text{C}$ for 12 h. Then it was cooled to room temperature, poured onto petrol ether (300 mL) and stirred until a clear yellow solution formed. It was filtered and the filtrate concentrated in vacuo. Purification by flash column chromatography (SiO_2 , hexane/EtOAc, 3:1) gave the enal (4.67 g, 29.9 mmol, 55% yield) as a pale yellow oil in a 5:1 E/Z mixture. TLC: R_f = 0.38 (Hexane/EtOAc, 3:1, Vanillin,

UV). ^1H NMR (400 MHz, CDCl_3): δ = 9.50 (d, J = 7.8 Hz, 1H), 6.81 (dt, J = 15.3, 6.7 Hz, 1H), 6.12 (dd, J = 15.7, 7.8 Hz, 1H), 3.67 (s, 3H), 2.38 (dt, J = 14.0, 7.2 Hz, 4H), 1.85 (p, J = 7.4 Hz, 2H). ^{13}C NMR (100 MHz, CDCl_3): δ = δ 193.94, 173.45, 157.13, 133.63, 51.80, 33.26, 32.01, 23.12. HRMS (ESI) calcd for $\text{C}_8\text{H}_{12}\text{O}_3$ $[\text{M}+\text{Na}]^+$: 179.0679, found: 179.0685.



2.11

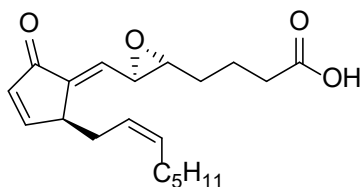
Compound 2.11 To a solution of enal **2.10** (1.9 g, 12.17 mmol, 1.00 equiv.) and (s)-2-(diphenyl((trimethylsilyl)oxy)methyl)-pyrrolidine (0.396 g, 1.217 mmol, 0.10 equiv.) in CH_2Cl_2 at 0 °C was added H_2O_2 (30% aqueous solution, 1.615 mL, 15.82 mmol, 1.30 equiv.) and the mixture stirred at RT for 5 h. To the reaction mixture were added saturated aqueous solutions of NaHCO_3 and $\text{Na}_2\text{S}_2\text{O}_3$ (1/1 (v/v), 30 mL) and the mixture stirred for 30 min. Then the layers were separated and the aqueous extracted with CH_2Cl_2 (3 x 50 mL). The combined organic layers were dried over MgSO_4 , filtered and concentrated in vacuo. Purification by flash column chromatography (SiO_2 , $\text{CH}_2\text{Cl}_2/\text{MeOH}$ 98:2) gave epoxy aldehyde **2.11** (1.07 g, 12.17 mmol, d.r.: 10:1, E/Z, 51% yield, 92% ee) as a colorless oil. TLC: R_f = 0.23 (Hexane/EtOAc, 5:1, Vanillin). ^1H NMR (400 MHz, CDCl_3): δ = 9.00 (d, J = 6.2 Hz, 1H), 3.67 (s, 3H), 3.24 (ddd, J = 6.2, 4.3, 2.0 Hz), 3.14 (dd, J = 6.2, 2.0 Hz, 1H), 2.38 (dt, J = 14.0, 7.2 Hz, 2H), 1.88- 1.73 (m, 3H), 1.71- 1.59 (m, 1H). ^{13}C NMR (100 MHz, CDCl_3): δ = δ 198.25, 173.45, 58.96, 56.36, 51.80, 33.26, 30.67, 21.27. HRMS (ESI) calcd for $\text{C}_8\text{H}_{12}\text{O}_4$ $[\text{M}+\text{Na}]^+$: 195.0628, found: 195.0638.



2.12

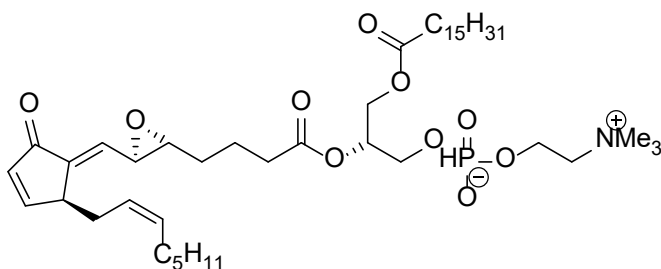
Compound 2.12 To a solution of LHMDS (503 mg, 3.01 mmol, 1.20 equiv.) in THF (10 mL) at $-78\text{ }^{\circ}\text{C}$ was added a solution of cyclopentenone **2.9** (482 mg, 2.50 mmol, 1.00 equiv.) in THF (2 x 3 mL) and the mixture stirred for 30 min. Then a solution of epoxy aldehyde 2-10 (863 mg, 5.01 mmol, 2.00 equiv.) in THF (2 x 4 mL) was added and the mixture stirred at $-78\text{ }^{\circ}\text{C}$ for 1.5 h. The reaction was quenched at $-78\text{ }^{\circ}\text{C}$ with a saturated, aqueous solution of NH_4Cl (25 mL) and the layers were separated. The aqueous layer was extracted with ether (3 x 40 mL) and the combined organic layers were washed with brine, dried over Na_2SO_4 , filtered and concentrated in vacuo. The crude product and the co-spotting aldehyde X. without further purification the mixture was dissolved in CH_2Cl_2 (20 mL) and treated at $-78\text{ }^{\circ}\text{C}$ with Et_3N (2.1 mL, 15.05 mmol, 6.00 equiv.) and methanesulfonyl chloride (0.59 mL, 7.52 mmol, 10.00 equiv.). The mixture was vigorously stirred at room temperature for 18 h and then filtered through a plug of celite. Then the mixture was concentrated in vacuo and purified by flash column chromatography (SiO_2 , hexane/ EtOAc , 4:1 to 3:1 gradient) to give the dienone **2.12** (445 mg, 1.29 mmol, 64% yield) as a yellow oil. TLC: $R_f = 0.58$ (Hexane/ EtOAc , 2:1, Vanillin, UV). ^1H NMR (400 MHz, CDCl_3): $\delta = 7.54$ (ddd, $J = 6.0, 2.6, 0.9$ Hz, 1H), 6.35 (dd, $J = 6.0, 1.8$ Hz, 1H), 6.19 (dt, $J = 8.2, 1.1$ Hz, 1H), 5.60 - 5.45 (m, 1H), 5.41 - 5.26 (m, 1H), 3.65 (s, 3H), 3.39 (dd, $J = 8.2, 2.1$ Hz, 1H), 2.99 (ddd, $J = 6.4, 4.0, 2.1$ Hz, 1H), 2.64 - 2.47 (m, 1H), 2.44 - 2.25 (m, 3H), 2.05 - 1.92 (m, 2H), 1.90 - 1.71 (m, 3H), 1.68 - 1.49 (m, 2H), 1.43 - 1.18 (m, 6H), 0.87 (t, $J = 7.9$ Hz, 3H). ^{13}C NMR (100 MHz, CDCl_3): $\delta = 195.87, 173.59, 162.05, 141.24, 134.59, 133.52, 131.06, 124.53, 60.03, 55.05,$

51.78, 43.45, 33.59, 32.02, 31.67, 31.37, 29.34, 27.48, 22.69, 21.49, 14.20. HRMS (ESI) calcd for $C_{21}H_{30}O_4 [M+Na]^+$: 369.2036, found: 369.2030.



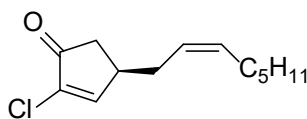
EC

EC. To a solution of methyl ester **2.12** (80 mg, 0.231 mmol, 1.00 equiv.) in THF (1 mL) and aqueous phosphate buffer pH 7 (4 mL) at room temperature was added Novozyme (30 mg) and the mixture stirred for 1h. The mixture was filtered through a plug of cotton and the filtrate treated with EtOAc (10 mL). The layers were separated and the pH of the aqueous layer was carefully adjusted to pH 5 using 0.1 M HCl. Then the aqueous layer was extracted with EtOAc (3 x 10 mL) and the combined organic layers were dried over Na_2SO_4 , filtered and concentrated in vacuo. Purification by flash column chromatography (SiO_2 , hexane/EtOAc/MeOH, 4:1:1) gave EC (54 mg, 0.162 mmol, 70% yield) as a pale yellow oil. TLC: $R_f = 0.4$ (Hexane/EtOAc/MeOH, 4:1:1, Vanillin, UV). 1H NMR (400 MHz, $CDCl_3$): $\delta = 7.54$ (ddd, $J = 6.0, 2.6, 0.9$ Hz, 1H), 6.35 (dd, $J = 6.0, 1.8$ Hz, 1H), 6.19 (dt, $J = 8.2, 1.1$ Hz, 1H), 5.60-5.45 (m, 1H), 5.41-5.26 (m, 1H), 3.69-3.64 (m, 1H), 3.39 (dd, $J = 8.2, 2.1$ Hz, 1H), 3.01-2.98 (m, 1H), 2.64-2.47 (m, 1H), 2.45 (t, $J = 6.0$ Hz, 2H), 2.32 (dt, $J = 15.2, 8.3$ Hz, 1H), 1.98 (q, $J = 7.2$ Hz, 2H), 1.90-1.71 (m, 3H), 1.68-1.49 (m, 1H), 1.43-1.18 (m, 6H), 0.87 (t, $J = 7.9$ Hz, 3H). ^{13}C NMR (100 MHz, $CDCl_3$): $\delta = 195.87, 177.41, 162.05, 141.24, 134.59, 133.52, 131.06, 124.53, 60.03, 55.05, 43.45, 33.59, 32.02, 31.67, 31.37, 29.34, 27.48, 22.69, 21.49, 14.20$. HRMS (ESI) calcd for $C_{20}H_{28}O_4 [M-H]^-$: 331.1910, found: 331.1910.



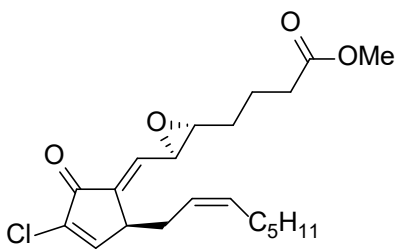
PECPC

PECPC To a solution of EC (17.9 mg, 0.052 mmol, 1.00 equiv.) in CHCl_3 (2.5 mL) at room temperature was added 2,4,6-trichlorobenzoyl chloride (84 μL , 0.538 mmol, 10.0 equiv.), N,N-dimethyl-4-aminopyridine (66 mg, 0.54 mmol, 10.0 equiv.) and lyso-PC (80 mg, 0.162 mmol, 3.00 equiv.) and the mixture stirred at room temperature for 3 h. The reaction mixture was concentrated in vacuo and purified by flash column chromatography (SiO_2 , DCM/MeOH/ H_2O , 80:20:0 to 80:18:2 gradient) to give PECPC (30 mg, 0.037 mmol, 69% yield) as a pale yellow oil. TLC: $R_f=0.16$ (MeOH, Vanillin, UV). ^1H NMR (400 MHz, CDCl_3): $\delta=$ 7.54 (dd, $J=6.0, 2.6, 0.9$ Hz, 1H), 6.35 (dd, $J=6.0, 1.8$ Hz, 1H), 6.14 (dt, $J = 8.2, 1.1$ Hz, 1H), 5.60-5.45 (m, 1H), 5.41-5.26 (m, 1H), 5.24 – 5.15 (m, 1H), 4.44 -4.26 (m, 3H), 4.12 (dd, $J = 12.0, 7.0$ Hz, 1H), 3.99- 3.91 (m, 2H), 3.80 (s, 3H), 3.69-3.64 (m, 1H), 3.35 (d, $J = 10.1$ Hz, 10H), 3.01- 2.98 (m, 1H), 2.51 (dd, $J = 13.4, 6.5$ Hz, 1H), 2.42- 2.21 (m, 6H), 2.00- 1.90 (m, 2H), 1.79 (s, 2H), 1.68- 1.49 (m, 3H), 1.23 (s, 30H), 0.87 (t, $J = 7.9$ Hz, 6H). ^{13}C NMR (100 MHz, CDCl_3): $\delta=$ δ 195.87, 173.64, 172.48, 162.05, 141.24, 134.59, 133.52, 131.06, 128.22, 124.53, 71.15, 71.07, 66.60, 63.00, 55.05, 54.62, 43.45, 34.04, 33.81, 32.02, 31.67, 31.37, 29.34, 29.78, 29.66, 29.63, 29.48, 29.45, 29.42, 29.30, 27.48, 25.00, 22.81, 22.69, 21.49, 14.20, 14.18. HRMS (ESI) calcd for $\text{C}_{44}\text{H}_{76}\text{NO}_{10}\text{P}$ $[\text{M}+\text{Na}]^+$: 832.5099, found: 832.5111.



2.14

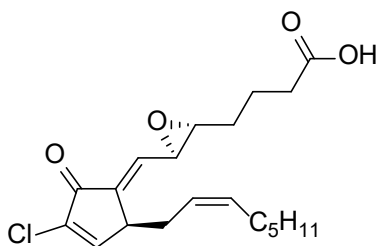
Compound 2.14 To a solution of **2.9** (1.92g, 10 mmol) in dry DMF (20 mL), m-CPBA (2.0g, 12 mmol) was added at 0 °C. The mixture was allowed to stir for 30 min at the same temperature. 6.6 M HCl/DMF solution (20 mL) was added slowly and the mixture was allowed to stir for another 1 hour. After the temperature reached to room temperature, Na₂SO₃ solution was used to quench the reaction. 40 mL of EtOAc was added and the mixture was transferred to a separated funnel. The aqueous phase was extracted with EtOAc 20 mL × 3 and the combined organic layers were dried over Na₂SO₄, filtered and concentrated in vacuo. Purification by flash column chromatography (SiO₂, hexane/EtOAc, 6:1) gave **2.14** (1.4 g, 6.3 mmol, 63%) as a pale yellow oil. ¹H NMR (400 MHz, CDCl₃): δ= 7.62 (dd, J=5.6, 2.5 Hz, 1H), 5.60-5.26 (m, 1H), 3.04-2.96 (m, 1H), 2.51 (dd, J=18, 6.4 Hz, 1H), 2.39-2.11(m, 2H), 1.43-1.18 (m, 6H), 0.87 (t, J = 7.9 Hz, 3H). ¹³C NMR (100 MHz, CDCl₃): δ= δ 193.25, 142.33, 134.19, 132.11, 125.17, 41.57, 40.65, 32.08, 31.62, 29.36, 27.51, 22.72, 14.19, HRMS (ESI) calcd for C₁₃H₁₉ClO [M]⁺: 227.1124, found: 227.1532.



2.15

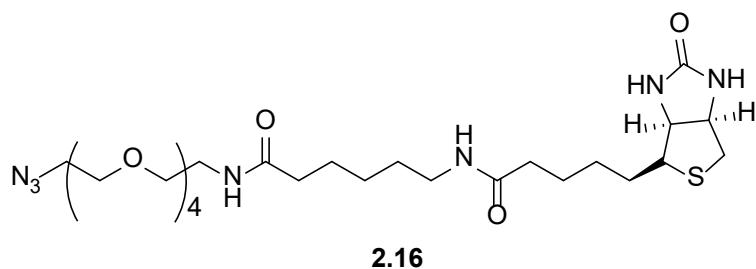
Compound 2.15 To a solution of LHMDS (503 mg, 3.01mmol, 1.20 equiv.) in THF (10 mL) at -78 °C was added a solution of cyclopentenone **2.14** (565 mg, 2.50 mmol, 1.00 equiv.) in THF

(2 x 3 mL) and the mixture stirred for 30 min. Then a solution of epoxy aldehyde **2.10** (863 mg, 5.01 mmol, 2.00 equiv.) in THF (2 x 4 mL) was added and the mixture stirred at -78 °C for 1.5 h. The reaction was quenched at -78 °C with a saturated, aqueous solution of NH₄Cl (25 mL) and the layers were separated. The aqueous layer was extracted with ether (3 x 40 mL) and the combined organic layers were washed with brine, dried over Na₂SO₄, filtered and concentrated in vacuo. The crude product and the co-spotting aldehyde X. without further purification the mixture was dissolved in CH₂Cl₂ (20 mL) and treated at -78 °C with Et₃N (2.1 mL, 15.05 mmol, 6.00 equiv.) and methanesulfonyl chloride (0.59 mL, 7.52 mmol, 10.00 equiv.). The mixture was vigorously stirred at room temperature for 18 h and then filtered through a plug of celite. Then the mixture was concentrated in vacuo and purified by flash column chromatography (SiO₂, hexane/EtOAc, 3:1) to give the dienone **2.15** (566 mg, 1.52 mmol, 61% yield) as a yellow oil. TLC: R_f = 0.51 (Hexane/EtOAc, 2:1, Vanillin, UV). ¹H NMR (400 MHz, CDCl₃): δ = 7.54 (dd, J = 6.0, 2.6, 0.9 Hz, 1H), 6.19 (dt, J = 8.2, 1.1 Hz, 1H), 5.60-5.45 (m, 1H), 5.41-5.26 (m, 1H), 3.65 (s, 3H), 3.39 (dd, J = 8.2, 2.1 Hz, 1H), 2.99 (ddd, J = 6.4, 4.0, 2.1 Hz, 1H), 2.64-2.47 (m, 1H), 2.44-2.25 (m, 3H), 2.05-1.92 (m, 2H), 1.90-1.71 (m, 3H), 1.68- 1.49 (m, 2H), 1.43-1.18 (m, 6H), 0.87 (t, J = 7.9 Hz, 3H). ¹³C NMR (100 MHz, CDCl₃): δ = δ 185.27, 173.59, 162.05, 145.34, 134.59, 133.52, 131.06, 124.53, 60.03, 55.05, 51.78, 43.45, 33.59, 32.02, 31.67, 31.37, 29.34, 27.48, 22.69, 21.49, 14.20. HRMS (ESI) calcd for C₂₁H₂₉ClO₄ [M+Na]⁺: 403.1754, found: 403.2030.

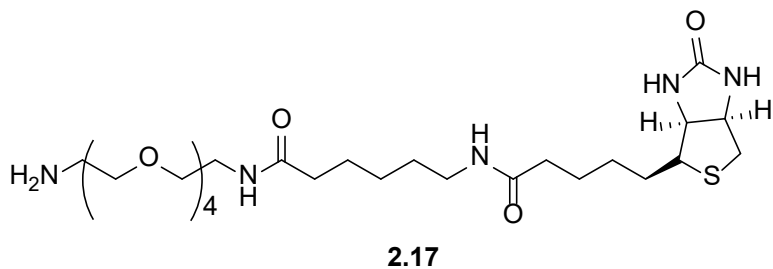


2.13

Compound 2.13 To a solution of methyl ester **2.15** (88 mg, 0.231 mmol, 1.00 equiv.) in THF (1 mL) and aqueous phosphate buffer pH 7 (4 mL) at room temperature was added Novozyme (30 mg) and the mixture stirred for 1h. The mixture was filtered through a plug of cotton and the filtrate treated with EtOAc (10 mL). The layers were separated and the pH of the aqueous layer was carefully adjusted to pH 5 using 0.1 M HCl. Then the aqueous layer was extracted with EtOAc (3 x 10 mL) and the combined organic layers were dried over Na₂SO₄, filtered and concentrated in vacuo. Purification by flash column chromatography(SiO₂, hexane/EtOAc/MeOH, 4:1:1) gave Chloro-EC (40 mg, 0.162 mmol, 68% yield) as a pale yellow oil. TLC: R_f= 0.38 (Hexane/EtOAc/MeOH, 4:1:1, Vanillin, UV). ¹H NMR (400 MHz, CDCl₃): δ= 7.54 (dd, J=6.0, 2.6, 0.9 Hz, 1H), 6.19 (dt, J = 8.2, 1.1 Hz, 1H), 5.60-5.45 (m, 1H), 5.41-5.26 (m, 1H), 3.69-3.64 (m, 1H), 3.39 (dd, J = 8.2, 2.1 Hz, 1H), 3.01- 2.98 (m, 1H), 2.64-2.47 (m, 1H), 2.45 (t, J = 6.0 Hz, 2H), 2.32 (dt, J = 15.2, 8.3 Hz, 1H), 1.98 (q, J = 7.2 Hz, 2H), 1.90-1.71 (m, 3H), 1.68- 1.49 (m, 1H), 1.43-1.18 (m, 6H), 0.87 (t, J = 7.9 Hz, 3H). ¹³C NMR (100 MHz, CDCl₃): δ= δ 187.27, 177.41, 162.05, 141.24, 134.59, 133.52, 131.06, 124.53, 60.03, 55.05, 43.45, 33.59, 32.02, 31.67, 31.37, 29.34, 27.48, 22.69, 21.49, 14.20. HRMS (ESI) calcd for C₂₀H₂₇O₄Cl [M-H]⁻: 365.1598, found: 365.1621.

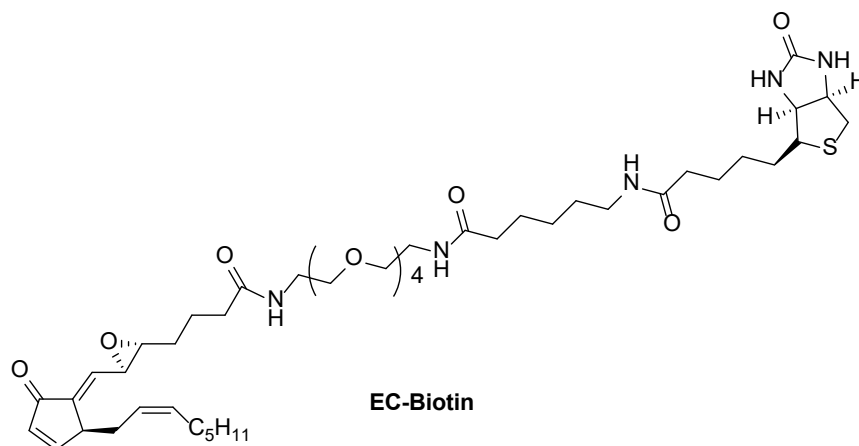


Compound 2.16 To a solution of Compound **1.12** (2.62 g, 10 mmol, 1.0 eq) in 50 mL of DCM, Biotin.OSu.X (4.5g, 10 mmol, 1.0 eq) and TEA (1.5g, 15 mmol, 1.5 eq). The mixture was allowed to stir for 2 hours at room temperature. 40 mL of DI water was added to quench the reaction and the mixture was transferred to a separate funnel. The aqueous phase was extracted with DCM (30 mL \times 3). The combined organic layer was dried over Na₂SO₄ and concentrated in vacuo. Purification by flash column chromatography gave compound 2.16 (5.4g, 9 mmol, 90% yield). ¹H NMR (400 MHz, CDCl₃): δ = 4.4-4.8 (m, 4H), 3.2-3.7 (m, 19H), 2.8-3.2 (m, 2H), 2.24 (m, 4H), 1.3-1.7 (m, 12H) 1.2 (m, 2H). ¹³C NMR (100 MHz, CDCl₃): δ = δ 174.5, 173.4, 164.3, 71.2, 70.8, 70.2, 63.8, 62.6, 55.6, 48.4, 41.3, 41.0, 38.9, 37.1, 36.5, 29.3, 28.4, 25.7, 25.2, 25.1, 24.4. HRMS (ESI) calcd for C₂₆H₄₇N₇O₇S [M+H]⁺: 602.3258, found: 602.3803.



Compound 2.17 To a solution of Compound **2.16** (5.4 g, 9 mmol, 1.0 eq) in 50 mL of THF and MeOH (v/v=1:1), 5 mL of AcOH and 5g of Zn were added respectively. The mixture was sonicated at room temperature for 1 hour. The organic solvent was removed in high vacuo and 50 mL of saturated NaHCO₃ was added to the residue. The aqueous phase was extracted with

DCM (50 mL \times 3) and the combined organic layer was dried over Na₂SO₄ and concentrated in high vacuum. Purification by flash column chromatography gave compound 2.17 (4.5g, 7.8 mmol, 88% yield) as a white solid. ¹H NMR (400 MHz, CDCl₃): δ = 4.4-4.8 (m, 4H), 3.2-3.7 (m, 19H), 2.8-3.2 (m, 4H), 2.24 (m, 4H), 1.3-1.7 (m, 10H) 1.2 (m, 2H). ¹³C NMR (100 MHz, CDCl₃): δ = δ 174.5, 173.4, 164.3, 71.2, 70.8, 70.2, 63.8, 62.6, 55.6, 41.8, 41.3, 41.0, 38.9, 37.1, 36.5, 29.3, 28.4, 25.7, 25.2, 25.1, 24.4. HRMS (ESI) calcd for C₂₆H₄₉N₅O₇S [M+H]⁺: 576.3353, found: 576.3521.



Compound EC-Biotin.X To a solution of EC (0.32 g, 1 mmol, 1.0 eq) in 10 mL of DCM, EDC (0.23g, 1.2 mmol, 1.2 eq) and HOBt (0.22g, 1.2 mmol, 1.2 eq) were added. The mixture was allowed to stir for 1 hour at room temperature. The amine 2.17 (0.57g, 1.0 mmol, 1.0 eq) was added in 5 mL of DCM. The reaction was stirred overnight at room temperature. 15 mL of DI water was added and the aqueous layer was extracted with DCM (10 mL \times 3). The combined organic layer was wash with 20 mL of brine, dried over Na₂SO₄ and concentrated in high vacuum. Purification by flash column chromatography gave EC-Biotin.X (0.79g, 92% yield) as a white solid. ¹H NMR (400 MHz, CDCl₃): δ = 7.54 (ddd, J=6.0, 2.6, 0.9 Hz, 1H), 6.35 (dd, J=6.0,

1.8 Hz, 1H), 6.19 (dt, J = 8.2, 1.1 Hz, 1H), 5.60-5.45 (m, 1H), 5.41-5.26 (m, 1H), 4.4-4.8 (m, 4H), 3.2-3.7 (m, 20H), 3.39 (dd, J = 8.2, 2.1 Hz, 1H), 2.8-3.2 (m, 6H), 2.45 (t, J = 6.0 Hz, 2H), 2.32 (dt, J = 15.2, 8.3 Hz, 1H), 2.24 (m, 4H), 1.98 (q, J = 7.2 Hz, 2H), 1.90-1.71 (m, 3H), 1.3-1.7 (m, 17H) 1.2 (m, 2H), 0.87 (t, J = 7.9 Hz, 3H). ¹³C NMR (100 MHz, CDCl₃): δ = 195.87, 174.5, 173.4, 172.41, 164.3, 162.05, 141.24, 134.59, 133.52, 131.06, 124.53, 71.2, 70.8, 70.2, 63.8, 62.6, 60.03, 55.6, 55.05, 43.45, 41.8, 41.3, 41.0, 38.9, 37.1, 36.5, 33.59, 32.02, 31.67, 31.37, 29.34, 29.3, 28.4, 27.48, 25.7, 25.2, 25.1, 24.4, 22.69, 21.49, 14.20. HRMS (ESI) calcd for C₄₆H₇₅N₅O₁₀S [M+H]⁺: 890.5235, found: 890.5632.

2.7 References

1. Harris, S.G. et al. Prostaglandins as modulators of immunity. *Trends Immunol.* **2002**, *23*, 144–150.
2. Wada, M. et al. Enzymes and receptors of prostaglandin pathways with arachidonic acid-derived versus eicosapentaenoic acid-derived substrates and products. *J. Biol. Chem.* **2007**, 22254–22266
3. Levin, G. et al. Differential metabolism of dihomo-g-linolenic acid and arachidonic acid by cyclo-oxygenase-1 and cyclo-oxygenase-2: implications for cellular synthesis of prostaglandin E1 and prostaglandin E2. *Biochem. J.* **2002**, *365*, 489–496.
4. Buczynski, M.W.; Dumlao, D.S.; Dennis, E.A. Thematic review series: proteomics. An integrated omics analysis of eicosanoid biology. *J. Lipid Res* **2009**, *50*, 1015–1038.
5. Von Euler, U.S. To the knowledge of the pharmacological effects of native secretions and extracts of male accessory glands, Naunyn Schmiedebergs. *Arch Pharmacol* **1934**, *175*, 78–84.
6. Collins, P.W.; Djuric, S.W.; Synthesis of therapeutically useful prostaglandin and prostacyclin analogs. *Chem Rev* **1993**, *93*, 1533–1564.
7. Fukushima, M.; Kato, T.; Narumiya, S. *Adv. Prostaglandin Thromboxane Leukot. Res.*, **1989**, *19*, 415–418.
8. Oeste, C. L.; Dolores, P-S. Modification of cysteine residues by cyclopentenone prostaglandins: interplay with redox regulation of protein function. *Mass Spectrom. Rev.*, **2014**, *33*, 110–125.
9. Funk, C. D. Prostaglandins and leukotrienes: Advances in eicosanoid biology. *Science* **2001**, *294*, 1871–1875.

10. Gao, L.; Zackert, W. E.; Hasford, J. J.; Danekis, M.E.; Milne, G. L.; Remmert, C.; Reese, J.; Yin, H.; Tai, H. H.; Dey, S. K. Porter NA, Morrow JD. Formation of prostaglandins E2 and D2 via the isoprostane pathway: A mechanism for the generation of bioactive prostaglandins independent of cyclooxygenase. *J Biol Chem* **2003**, *278*, 28479–28489.
11. Shibata, T.; Kondo, M.; Osawa, T.; Shibata, N.; Kobayashi, M.; Uchida, K. 15-Deoxy-Delta 12,14-prostaglandin J2. A prostaglandin D2 metabolite generated during inflammatory processes. *J Biol Chem* **2002**, *277*, 10459–10466.
12. Ziboh, V. A.; Miller, C. C.; Cho, Y. Metabolism of polyunsaturated fatty acids by skin epidermal enzymes: Generation of antiinflammatory and antiproliferative metabolites. *AmJ Clin Nutr* **2000**, *71*, 361–366.
13. Levin, G.; Duffin, K. L.; Obukowicz, M. G.; Hummert, S. L.; Fujiwara, H.; Needleman, P. Raz, A. Differential metabolism of dihomo-gamma-linolenic acid and arachidonic acid by cyclooxygenase-1 and cyclo-oxygenase-2: Implications for cellular synthesis of prostaglandin E1 and prostaglandin E2. *Biochem J* **2002**, *365*, 489–496.
14. Mossner, E.; Iwai, H.; Glockshuber, R.; Influence of the pK(a) value of the buried, active-site cysteine on the redox properties of thioredoxin-like oxidoreductases. *FEBS Lett* **2000**, *477*, 21–26.
15. Pérez-Sala, D. Electrophilic eicosanoids: signaling and targets, *Chem. Biol. Interact.* **2011**, *192*, 96–100.
16. Santoro, M.G.; Crisari, A.; Benedetto, A.; Amici, C. Modulation of the growth of a human erythroleukemic cell line (K562) by prostaglandins: antiproliferative action of prostaglandin A, *Cancer Res.* **1986**, *46*, 6073–6077.

17. Wiley, M.H.; Feingold, K.R.; Grunfeld, C.; Quesney-Huneeus, V.; Wu, J. M. Evidence for cAMP-independent inhibition of S-phase DNA synthesis by prostaglandins, *J. Biol. Chem.* **1983**, *258*, 491–496.
18. Alma, E.; Martínez, F. J.; Sánchez-Gómez, B.; Díez-Dacal, C.L.; Oeste; Dolores, P.S. 15-Deoxy- $\Delta^{12,14}$ -Prostaglandin J₂ exerts pro- and anti-inflammatory effects in mesangial cells in a concentration-dependent manner. *Inflammation & Allergy - Drug Targets*, **2012**, *11*, 58-65.
19. Fernandez-Bustamante, A.; Klawitter, J.; Wilson, P.; Elkins, N. D. Amanda Agazio, Takahiro Shibata, Koji Uchida, Uwe Christians, and John E. Repine. Early increase in alveolar macrophage prostaglandin 15d-PGJ₂ precedes neutrophil recruitment into lungs of cytokine-insufflated rats. *Inflammation* **2013**, *36*, 1030-1040.
20. Pe´rez-Sala, D.; Cernuda-Morollo´n, E.; and Javier Can˜ada, F. Molecular Basis for the Direct Inhibition of AP-1 DNA Binding by 15-Deoxy- $\Delta^{12,14}$ -prostaglandin J₂. *J Biol Chem* **2003**, *278*, 51251-51260.
21. Kim, K. R.; Kim, H.; Sun, J.; Lee, K.; Ma, G. T.; Park, K. K.; Chung, W. Y. 15-deoxy-Delta (12,14)-prostaglandin J₂ inhibits osteolytic breast cancer bone metastasis and estrogen deficiency-induced bone loss. *PLOS ONE* **2015**, *168*, 122764–122772.
22. Ciucci, A.; Gianferretti, P.; Piva, R.; Guyot, T.; Snape, T. J.; Roberts, S. M.; Gabriella Santoro, M. Induction of apoptosis in estrogen receptor-negative breast cancer cells by natural and synthetic cyclopentenones: role of the I κ B kinase/nuclear factor- κ B pathway. *Mol Pharmacol* **2006**, *70*, 1812–1821.
23. Bregman, M.D.; Funk, C.; Fukushima, M. Inhibition of human melanoma growth by prostaglandin A, D, and J analogues, *Cancer Res.* **1986** *46*, 2740–2744.
24. Kato, T.; Fukushima, M.; Kurozumi, S.; Noyori, R. Antitumor activity of delta 7-

- prostaglandin A1 and delta 12-prostaglandin J2 in vitro and in vivo, *Cancer Res.* **1986**, *46*, 3538–3542.
25. Sasaki, S.; Niimi, M. Akiyama, T. Tanaka, A. Hazato, S. Kurozumi, S. Fukushima, M. Fukushima, Antitumor activity of 13,14-dihydro-15-deoxydelta7-prostaglandin-A1-methyl ester integrated into lipid microspheres against human ovarian carcinoma cells resistant to cisplatin in vivo, *Cancer Res.* **1999**, *59*, 3919–3922.
26. Garzón, B.; Gayarre, J.; Gharbi, S. ; Díez-Dacal, B.; Sánchez-Gómez, F. J. ; Timms, J. F.; Pérez-Sala, D. A biotinylated analog of the anti-proliferative prostaglandin A1 allows assessment of PPAR-independent effects and identification of novel cellular targets for covalent modification, *Chem. Biol. Interact.* **2010**, *183*, 212–221.
27. C. Amici, L.; Sistonen, M.G.; Santoro, R.I.; Antiproliferative prostaglandins activate heat shock transcription factor, *Proc. Natl. Acad. Sci. USA* **1992** *89*, 6227–6231.
28. Pavithra, L.; Sreenath, K.; Singh, S. ; Chattopadhyay, S. Heat-shock protein 70 binds to a novel sequence in 50 UTR of tumor suppressor SMAR1 and regulates its mRNA stability upon prostaglandin A2 treatment. *FEBS Lett.* **2010**, *584*, 1187–1192.
29. Santoro, M.G. Antiviral activity of cyclopentenone prostanoids. *Trends Microbiol.* **1997**, *5*, 276–281.
30. Suzuki, M.; Mori, M.; Niwa, T.; Hirata, R.; Furuta, K.; Ishikawa, T.; Noyori, R. Chemical Implications for Antitumor and Antiviral Prostaglandins: Reaction of Δ^7 -Prostaglandin A1 and Prostaglandin A1 Methyl Esters with Thiols. *Journal of the American Chemical Society* **1997**, *119*, 2376-2385.
31. Hayes, M. M.; Lane, B. R.; King, S. R.; Markovitz, D. M.; Coffey, M. J. Peroxisome

proliferator-activated receptor gamma agonists inhibit HIV-1 replication in macrophages by transcriptional and post-transcriptional effects, *J. Biol. Chem.* **2002**, *277*, 16913–16919.

32. Santoro, M.G. Antiviral activity of cyclopentenone prostanoids. *Trends Microbiol.* **1997**, *5*, 276–281.

33. Kalantari, P.; Narayan, V.; Henderson, A.J.; Prabhu, K. S. 15-Deoxy-Delta12,14-prostaglandin J2 inhibits HIV-1 transactivating protein, Tat, through covalent modification. *FASEB J.* **2009**, *23*, 2366–2373.

34. Collins, P. W.; Djuric, S. W. Synthesis of therapeutically useful prostaglandin and prostacyclin analogs. *Chem. Rev.* **1993**, *93*, 1533-1564.

35. Egger, J.; Bretscher, P.; Freigang, S.; Kopf, M.; Carreira, E. M. Synthesis of epoxyisoprostanes: effects in reducing secretion of pro-inflammatory cytokines IL-6 and IL-12. *Angew. Chem., Int. Ed.* **2013**, *52*, 5382-5385.

36. Egger, J.; Bretscher, P.; Freigang, S.; Kopf, M.; Carreira, E. M. Discovery of a highly potent anti-inflammatory epoxyisoprostane-derived lactone. *J. Am. Chem. Soc.* **2014**, *136*, 17382-17385.

37. Egger, J.; Fischer, S.; Bretscher, P.; Freigang, S.; Kopf, M.; Carreira, E. M. Total synthesis of prostaglandin 15d-PGJ2 and investigation of its effect on the secretion of IL-6 and IL-12. *Org. Lett.* **2015**, *17*, 4340–4343.

Chapter 3

Modification and Synthesis of Derivatives of Ribityllumazines: Potential Antigens for Activation of MAIT Cells

3.1 Introduction

3.1.1 Mucosal-Associated Invariant T (MAIT) Cells

Mucosal-Associated Invariant T (MAIT) Cells, a subset of homogenous T cell, were first found in 1999 by Tilloy et al.¹ They are unique innate-like T cells, that are surprisingly abundant in human beings, up to 10% of the total circulating T cells, and are distributed throughout blood, mesenteric lymph nodes, and gastrointestinal mucosa.² In humans, MAIT cells consist of a semi-variant T cell receptor (TCR) α -chain, V α 7.2 (TRAV1-2), joined to J α 33 (TRAJ33), paired with a limited array of TCR β -chains (predominantly V β 2 or V β 13, i.e. TRBV6 or TRBV20) and are activated by means of their $\alpha\beta$ T-cell antigen receptors.¹ MAIT cells express the semi-invariant T cell receptor and are restricted by the evolutionarily conserved major histocompatibility complex (MHC) related protein 1, MR1, which is ubiquitously expressed in human cells and a necessity for *in vivo* development.¹⁻⁶ Interestingly, MR1 alone can't activate MAIT cells; it needs the cooperation of a critical ligand--vitamin B metabolites--to achieve the activation, which will be discussed in detail in the following section.⁷⁻¹¹

Different from conventional T cells, MAIT cells have the innate ability to detect and respond to infections.^{11, 12} The roles of MAIT cells in human health and disease are not clear, but they have been shown to have unique antibacterial function and phenotype. MAIT cells play a key role in host defense against bacterial and fungal infection as well as in human autoimmune diseases such as inflammatory bowel disease (IBD), multiple sclerosis (MS), systemic lupus erythematosus, and also cancer.^{3,4,13-21} For example, Sugimoto et al. demonstrated that

populations of MAIT cells from fibromyalgia patients were lower than that of healthy donors, which implies analysis of MAIT cells may provide a more objective standard for the diagnosis of fibromyalgia syndrome and other related diseases, including rheumatoid arthritis and spondyloarthritis.²⁰ Serriari et al. illustrated that MAIT cells are activated in patients with inflammatory bowel diseases (IBD) and accumulated in the inflamed mucosa, which suggests MAIT cells are immune players in IBD and helpful to the understanding of IBD pathophysiology.¹⁵ Miyazaki et al. explored the character of MAIT cells in multiple sclerosis (MS) patients and suggested MAIT cells may have a disease-suppressive role and regulate the immune system to prevent MS.¹⁴ Meierovics et al. utilized a murine model of pulmonary infection to investigate the kinetics and function of murine MAIT cell responses in the lungs *in vivo* and found MAIT cells can initiate mucosal immunity in early phases but also contribute to pulmonary immune responses in the later phases of infection.²²

3.1.2 Activation of MAIT Cells

Previous studies have demonstrated that there are two pathways for the activation of MAIT cells, as shown in Figure 3.1. One is TCR-dependent activation, and the other is TCR-independent cytokine activation.^{3, 23-26} In the TCR-independent situation, MAIT cells are triggered by cytokines produced by infected cells, including interleukin-12 (IL-12), IL-15, IL-18 and IL-7, as well as release of anti-bacterial effector molecules, including cytokines and cytolytic products.²⁴ In the TCR-dependent situation, the MAIT cells are activated through T-cell receptor $\alpha\beta$ chain (TCR- $\alpha\beta$) binding with the MR1-ligand, which is vitamin B metabolites presented on MR1. The MAIT/T Cell then may produce cytokines and cytolytic products that are related to the regulation of inflammation or result in local proliferation and apoptosis which may result in

shaping the TCR repertoire.²⁵The primary challenge is the identification of the MR1-restricted antigens and recent research points to the characterization of these special kinds of antigens.

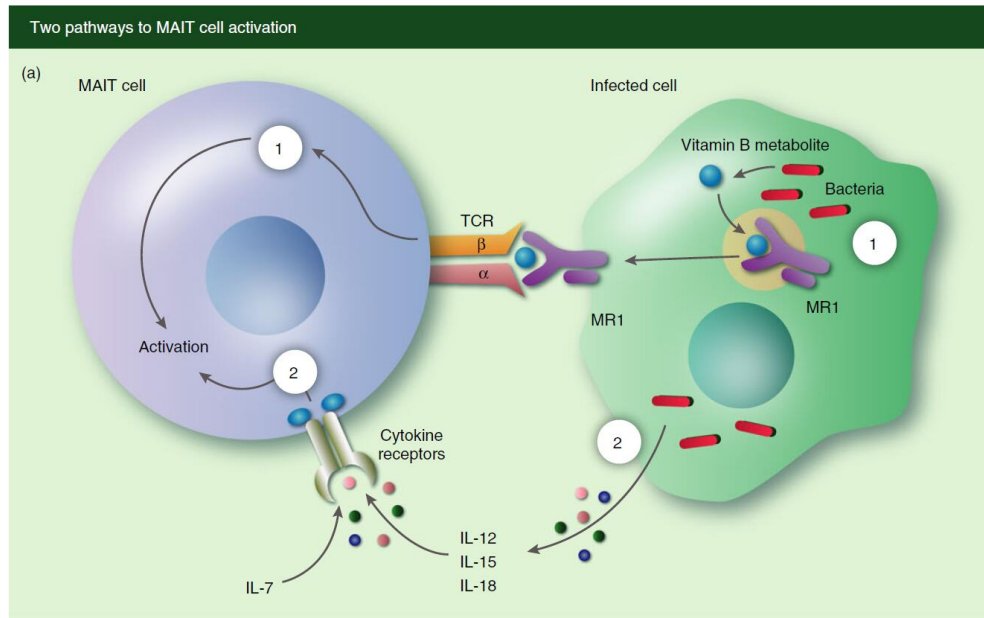


Figure 3.1 Mucosal-associated invariant T (MAIT) cell activation pathways with infected cells surroundings. (1) TCR-dependent MAIT cell activation (2) TCR-independent MAIT cell activation (Adapted from reference [26])

Godfrey et al. elucidated that MAIT cells are activated by a wide range of microorganisms, including diverse strains of bacteria and some yeast species, which all contain the riboflavin (vitamin B2) synthetic pathway. Conversely, MAIT cells are not activated by *S. pyogenes* or *E. faecalis*, which lack the riboflavin synthetic pathway.²⁹ Kjer-Nielsen et al. identified the ligands that bind MR1 and confirmed these ligands are responsible for the response of MAIT cells to a wide range of bacteria.⁸ They observed 6-formyl pterin (6-FP), a vitamin B9 metabolite, bound to MR1 and stabilized this molecule, but were unable to stimulate the MAIT cells. Considering the culture supernatant *S. typhimurium* could activate MAIT cells, the ligand herein should have the ability to activate MAIT cells. They analyzed and confirmed this kind of ligand should be

reduced to 6-hydroxymethyl-8-D-ribityllumazine (rRL-6-CH₂OH), a metabolic by-product of riboflavin (vitamin B₂) metabolism. Furthermore, they synthesized compounds derived from riboflavin metabolism, 7-hydroxy-6-methyl-8-d-ribityllumazine (RL-6-Me-7-OH) and 6, 7-dimethyl-8-d-ribityllumazine (RL-6,7-diMe) and found these compounds could also stimulate primary MAIT cells in MRI-dependent manners. These findings are consistent with the results illustrated in previous studies^{3,4} -the riboflavin synthesis pathway is a key point in the activation of MAIT cells.⁸

Sakala et al. further utilized MR1/ribityllumazine (RL, bacterial vitamin B₂ metabolites) tetramers to stimulate mouse MAIT cells and investigated the importance of the subsets of MAIT cells in antimycobacterial immunity and the mechanisms of how MAIT cells provided early protection against mycobacterial infection.²⁷

Corbett et al. illustrated the early unstable intermediates in bacterial riboflavin synthesis, 5-(2-oxoethylideneamino)-6-D-ribitylaminouracil (5-OE-RU) and 5-(2-oxopropylideneamino)-6-D-ribitylaminouracil (5-OP-RU), and gave identical results in the activation of MAIT cells as rRL-6-CH₂OH. These unstable intermediates can undergo dehydration upon ring closure to convert to stable, isolatable lumazines, including RL-6,7-diMe, which have been verified to activate MAIT cells.²⁸

3.1.3 MR1–Antigen Structures

Which kinds of small molecules can work as ligands for MR1? Among these ligands, what is the real MR1-restricted antigen in living organisms? To explore these questions, let us begin with some deep insight into MR1 and its ligands.

The overall structure of human MR1 adopts a standard binary MHC-I fold, shown in Figure 3.2, and comprises of a α 1- α 2 cleft and a α 3 sheet, both non-covalently associated with the

β_2 microglobulin (β_2m) subunit. The $\alpha 1$ - $\alpha 2$ cleft in fact contains two long α -helices at the top of the β_2m (structurally similar to the HLA-A2 and CD1d) and is proven to be the MR1 antigen-binding center. The MR1 still has its unique characteristics, and its central cleft is not suited to accept the peptide- or lipid-based antigens like HLA-A2 or CD1d. There are some morphological features of MR1 that may be explanations for this particular pheromone, shown in Figure 3.3. Firstly, the $\alpha 1$ - $\alpha 2$ central cavity of MR1 is about 760\AA^3 -much smaller than that of classical MHC-I molecules. This suggests bigger lipid-like ligands are not fit for the MR1 cavity. Secondly, different from that of HLA-A2 or CD1d, MR1 contains both basic (arginine and lysine) and hydrophobic (aromatic residues in tryptophan, tyrosine and phenylalanine) residues, and is mostly solvent exposed, while the HLA-A2 is mostly polar and solvent exposed, which is the primary reason that it is suited for binding peptides. Furthermore, the CD1d cleft is hydrophobic and shielded from solvent. Thirdly, the end of the MR1 cavity doesn't have a small opening portal and is mostly closed because of a large number of bulky side chains occupied in/by the cleft.

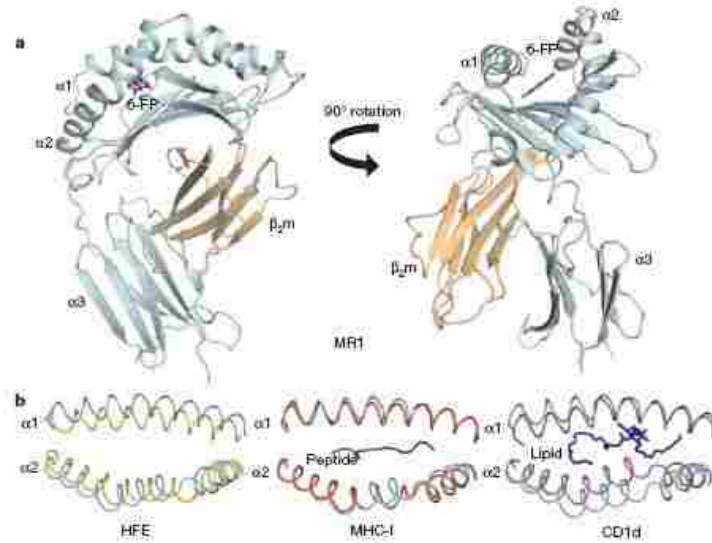


Figure 3.2 Overview of the crystal structure of MR1–antigen complex. a, Structure of MR1. b, Overlay of the $\alpha 1$ and $\alpha 2$ helices using the residues within the antigen-binding cleft of MR1 with HFE (left), MHC-I (middle, HLA-A2) and CD1d (right). MR1 is in cyan; HFE is in yellow; MHC-I is in red; CD1d is in magenta. Adapted from reference[8].

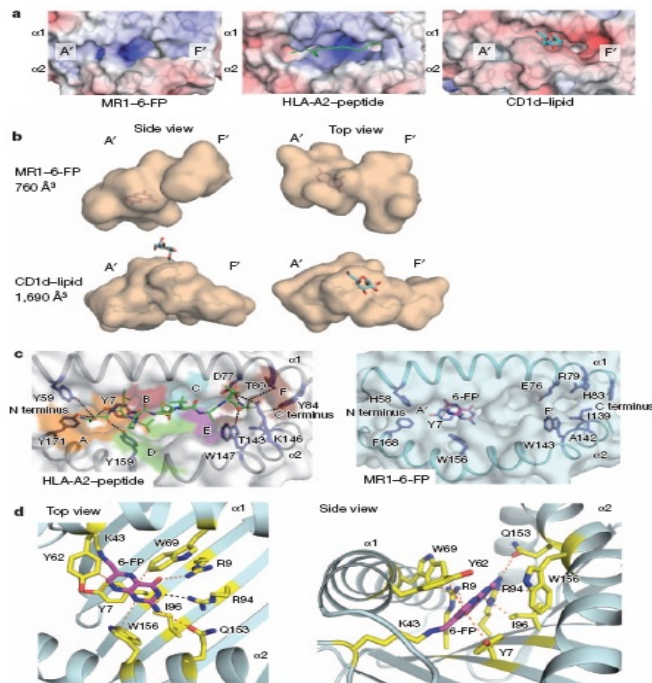


Figure 3.3 Comparison of MR1, MHC-I and MHC-I-like binding clefts. Adapted from reference[8]. a, Electrostatic surface of MR1, HLA-A2 and CD1d antigen-binding clefts. Peptide, green; lipid, cyan. A' and F' are binding

pockets within CD1d. b, Side (left) and top (right) views of MR1–6-FP and CD1d– α -galactosylceramide. c, Left, peptide interaction with HLA-A2 residues; right, corresponding MR1 residues. Six pockets (A–F) of MHC-I, colored in orange, red, cyan, green, magenta and brown, respectively; peptide is in green. The surface in b and c is transparent to show 6-FP binding. d, Top (left) and side (right) views of MR1–6-FP. MR1 residues that contact 6-FP are in yellow. H-bond and van der Waals interactions are shown in black- and red-dashed lines, respectively. MR1 is in cyan; 6-FP is in magenta.

Considering the aromatic and basic residues, the MR1-antigen cavity should have one overall basic charge. Considering its smaller size, the ligands fit for this special cavity should be small molecules with polar residues and potentially negative charge. As mentioned in the previous papers, 6-FP, RL-6,7-diMe, RL-6-Me-7-OH, rRL-6-CH₂OH all meet these requirements and present a structural scaffold for binding of MR1, shown in Figure 3.4.

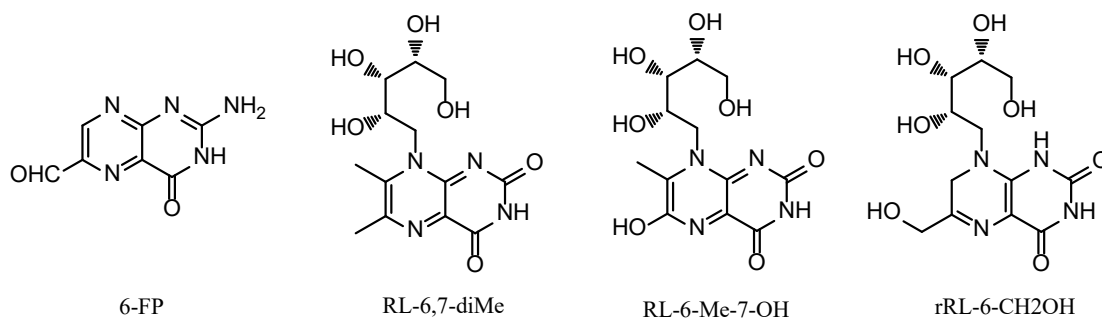


Figure 3.4 Structures of 6-FP, RL-6,7-diMe, RL-6-Me-7-OH, rRL-6-CH₂OH

3.1.4 Synthesis of Ligands of MR1

To better understand the functions of MAIT cells in human beings, organic synthesis of antigens that align with MR1 to stimulate MAIT cells is an essential assistance to facilitate further research.

The antigens for MR1 have been proved to be related to the riboflavin-based metabolites and are ribityllumazine derivatives. The synthesis of these potential antigens has been carried out in some previous papers. Plaut, E. et al. focused on the synthesis of substituted lumazines and demonstrated how to use 4-chlorouracil to easily prepare lumazines.³⁰⁻³²

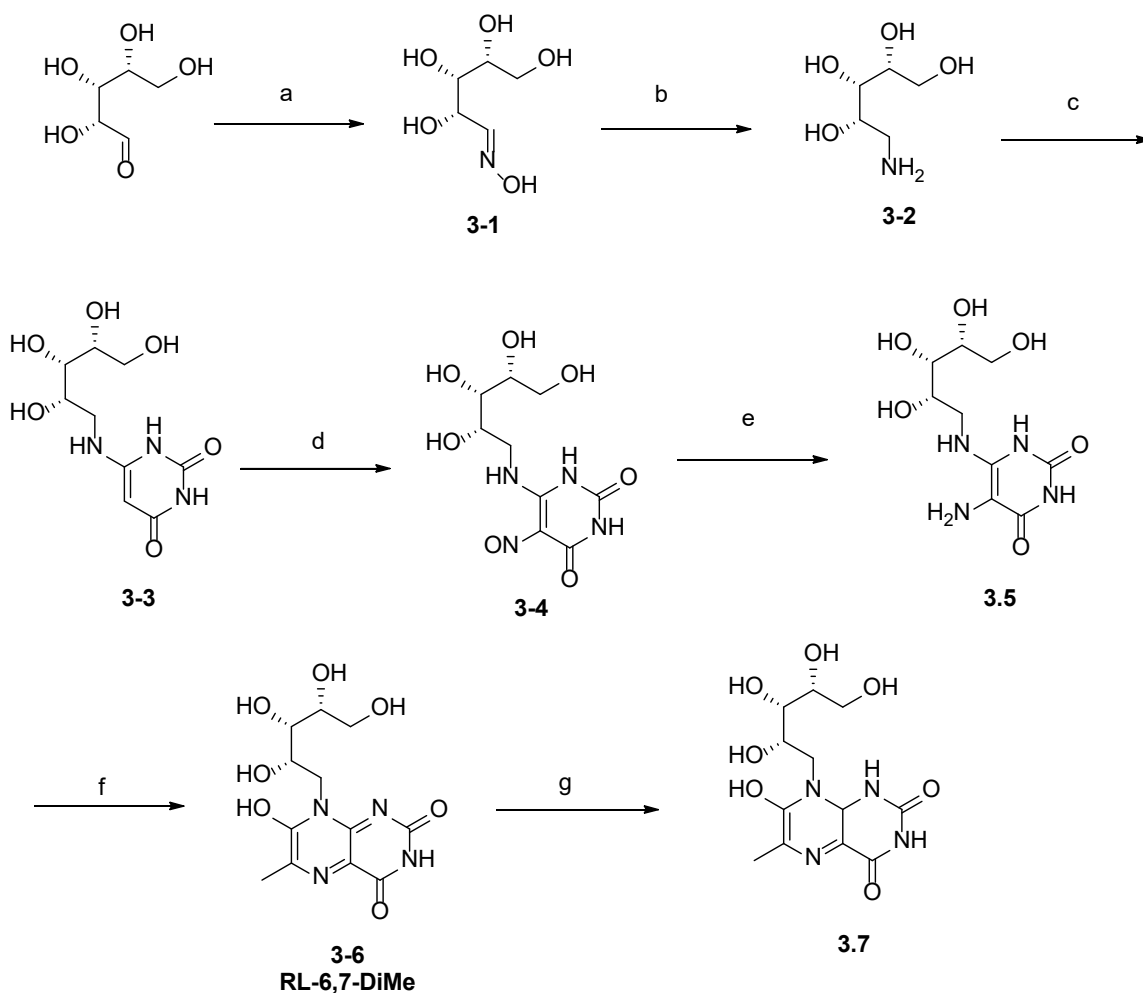
3.2 Synthesis of Ligands of MR1

To better understand the functions of MAIT cells in human beings, organic synthesis of antigens that aligned with MR1 to stimulate MAIT cells is an essential assistance to facilitate the further research.

The antigens for the MR1 have been proved to being related with the riboflavin-based metabolites and are the ribityllumazine derivatives. The synthesis of these potential antigens has been carried out in some previous papers. Plaut, G. W. E. et al. focused on the synthesis of substituted lumazines and demonstrated how to use 4-chlorouracil to easily prepare lumazines.³⁰⁻

³²

In our study, synthesis of derivatives of ribityllumazine was first to investigate. We selected RL-6,7-DiMe (Structure shown in Figure 3.4) as our synthetic target product and proposed one synthetic route for RL-6,7-DiMe and ribityllumazine (See Scheme3.1).



Scheme 3.1 Proposed synthetic pathway for RL-6,7-DiMe and ribityllumazines

Reagents: a) Hydroxylamine hydrochloride, NaOMe. 64.4% yield. b) PtO₂, AcOH, MeOH, H₂/ 50 PSI. 59.5% yield. c) 4-chloropyrimidine-2,4(1H,3H)-dione, H₂O, Refluxing. 56% yield. d) Sodium nitrite, 50 °C. 65% yield. e) KOH, Sodium hydrosulfite, H₂O. 61% yield. f). pyruvic acid sodium salt, HCl, H₂O. 22.6% yield. g) Sodium hydrosulfite, PBS. 31.6% yield.

D-(-) Ribose was used as starting material, treated with hydroxylamine in presence of NaOMe to afford **compound 3-1**. Catalytic hydrogenation reduction of compound **3-1** using PtO₂ gave

the corresponding amine **3-2**, which coupled with 4-chloropyrimidine-2,4(1H,3H)-dione in presence of boiling water to provide compound **3-3**. Oxidation by Sodium nitrite in presence of acidic solution gave compound **3-4**, which underwent a reduction by Sodium hydrosulfite under basic condition to form the amine **3-5**. The key step in the whole synthetic strategy was conducted through coupling compound **3-5** with pyruvic acid to provide the important the compound **3-6**. Rearrangement of **3-6** using Sodium hydrosulfite in the PBS solution gave the target compound **3-7**.

3.3 Results

Two target compounds **3.7** and **3.6** (RL-6,7-DiMe) were sent for investigation of their bioactivities.

3.4 Collusions

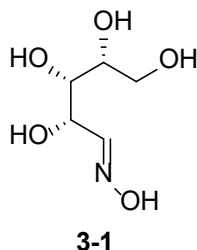
Since we successfully synthesized two compounds using our proposed pattern, further synthesis of ribityllumazine derivatives can be accessed. Once we have results of bioactivities of compound **3.7** and **3.6**, further synthesis and modification will be employed.

3.5 Experiment Section

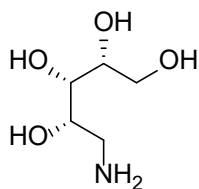
General: Reagents were purchased from Aldrich Chemical Co. unless otherwise noted. Methylene chloride, THF, DMF, pyridine, and DMSO were dried by passage through a Glass Contour solvent drying system containing a cylinder of activated alumina. Silica gel was used for chromatography unless otherwise noted.

Instrumentation: ^1H and ^{13}C NMR spectra were recorded on a Varian Gemini 500 (500 MHz) spectrometer. Proton chemical shift were referenced to tetramethylsilane (TMS). Carbon chemical shifts were referenced to carbon resonance of solvents (CDCl_3 , CD_3OD). High

resolution electron impact mass spectra (HR-MS) were obtained on a JOEL SX 102A spectrometer.

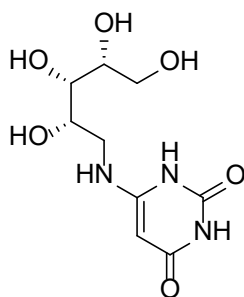


Compound 3.1 Hydroxylamine hydrochloride (5.90 g, 84.9 mmol, 2.34 equiv.) was dissolved in MeOH (dry, 40 mL) and stirred at room temperature. 2 drops of phenolphthalein (1%, solution in EtOH) was added to mixture. Then a solution of NaOMe (4.75 g, 88 mmol, 2.45 equiv.) in MeOH (40 mL) was added slowly to the suspension, upon with a white precipitate formed. When the reaction stayed pink for 1 min, addition of base (NaOMe) was halted. The mixture was stirred for several mins and filtered to remove slats. The filtrate was transferred to a round bottom flask (250 mL) and warmed to 70 °C. Then D-(-) Ribose (5.45g, 36.3 mmol, 1.00 equiv.) was added to reaction in small portions. The mixture was allowed to stir at 70 °C until the sugar had completely dissolved (5-10 min) and cooled down to room temperature. The product 3-1 (3.86 g, 23.4 mmol, 64.4%) was precipitated from solution after keeping the mixture at fridge overnight. TLC: $R_f=0.38$ ($\text{CHCl}_3/\text{MeOH}/\text{NH}_4.\text{OH}$ 12:9:4, CAM). ^1H NMR (400 MHz, D_2O): $\delta=$ 7.45 (m, 1H), 6.86 (m, 1H), 5.08 (m, 1H), 4.42 (m, 1H), 3.81-3.65 (m, 6H), 3.64-3.61 (m, 2H) ^{13}C NMR (100 MHz, CDCl_3): $\delta=$ δ 153.2, 152.8, 74.6, 74.3, 73.1, 72.7, 71.1, 67.3, 64.4, 64.1. HRMS (ESI) calcd for $\text{C}_5\text{H}_{11}\text{NO}_5$ $[\text{M}+\text{Na}]^+$: 188.0637, found: 188.0548.



3-2

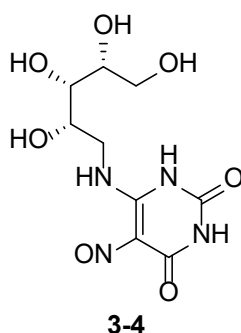
Compound 3.2 The compound **3-1** (2.86g, 17.3 mmol, 1.00 equiv.) was diluted with glacial AcOH (10 mL) and MeOH (10 mL), and PtO₂ (100mg) was added. The mixture was hydrogenated with shaking on a parr apparatus at 50 PSI for 36h at room temperature. The mixture was then filtered to remove the catalyst. The filtrate was concentrated in vacuo and purified by flash column chromatography (SiO₂, CHCl₃/MeOH/NH₄.OH 12:9:4) to give the white solid compound **3-2** (1.56g, 10.3 mmol, 59.5%). TLC: R_f=0.18 (CHCl₃/MeOH/NH₄.OH 12:9:4, CAM). ¹H NMR (400 MHz, D₂O): δ= 3.70-3.65 (m, 2H), 3.58 (m, 1H), 3.45 (m, 1H), 3.41 (m, 1H), 2.72 (m, 1H), 2.64 (m, 1H) ¹³C NMR (100 MHz, CDCl₃): δ= δ 73.2, 72.4, 72.0, 63.1, 42.1. HRMS (ESI) calcd for C₅H₁₃NO₄ [M+H]⁺: 152.0845, found: 152.0923.



3-3

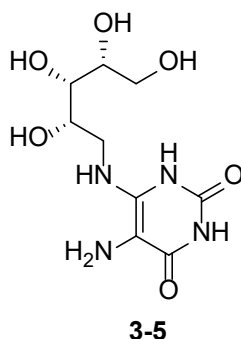
Compound 3.3 6-D-Ribitylamino-2,4(1H,3H)-dione compound **3-3** was prepared by a modification of the method of Maley and Plaut as follows. To a solution of D-ribitylamine (1.56g, 10.3 mmol, 1.00 equiv.) in 25 mL DI water, 4-chloropyrimidine -2,4(1H,3H)-dione (1.5g,

5.6 mmol, 0.5 equiv) was added. The reaction was allowed to reflux for 12 h with stirring. Then the mixture was cooled to room temperature and poured into 150 mL MeOH with stirring. After being allowed to stand in fridge overnight, the precipitate was collected, dried, and recrystallised from acetic acid-ethnaol (4:1) to give the target compound 3-3 as colourless crystals (810mg, 3.1 mmol, 56%). TLC: $R_f=0.32$ ($\text{CHCl}_3/\text{MeOH}/\text{NH}_4.\text{OH}$ 12:9:4, CAM, UV). ^1H NMR (400 MHz, D_2O): $\delta=$ 5.52 (s, 1H), 3.70-3.65 (m, 2H), 3.58 (m, 1H), 3.45 (m, 1H), 3.41 (m, 1H), 2.72 (m, 1H), 2.64 (m, 1H) ^{13}C NMR (100 MHz, CDCl_3): $\delta=$ δ 175.2, 170.2, 162.3, 98.1, 73.2, 72.4, 72.0, 63.1, 42.3. HRMS (ESI) calcd for $\text{C}_9\text{H}_{15}\text{N}_3\text{O}_6$ $[\text{M}+\text{H}]^+$: 262.0961, found: 262.1011.

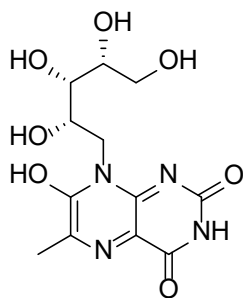


Compound 3.4 To a solution of compound 3-3 (458 mg, 1.75 mmol, 1.00 equiv.) in 5 mL DI water, sodium nitrite (360 mg, 5.26 mmol, 3.00 equiv) was added. The mixture was adjusted to pH 4.3 with several drops of Acetic acid slowly, and was allowed to warm at 50 °C for 30 min. The reaction was allowed to cool down to room temperature and dry off the solvent in high vacuum. Purification by flash column chromatography (SiO_2 , $\text{CHCl}_3/\text{MeOH}/\text{NH}_4.\text{OH}$ 12:9:4) to give the target product 3-4 (189 mg, 65% yield) as a red sold. TLC: $R_f=0.28$ ($\text{CHCl}_3/\text{MeOH}/\text{NH}_4.\text{OH}$ 12:9:4, CAM, UV). ^1H NMR (400 MHz, D_2O): $\delta=$ 3.70-3.65 (m, 2H), 3.58 (m, 1H), 3.45 (m, 1H), 3.41 (m, 1H), 2.72 (m, 1H), 2.64 (m, 1H) ^{13}C NMR (100 MHz,

CDCl₃): δ= δ 165.6, 140.8, 140.3, 78.5, 73.2, 72.4, 72.0, 63.1, 42.1. HRMS (ESI) calcd for C₉H₁₄N₄O₇ [M+H]⁺: 291.0862, found: 292.0921.

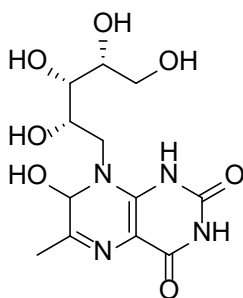


Compound 3.5 To a solution of compound **3-4** (100 mg, 0.344 mmol, 1.0 equiv.) in 4 mL DI water with stirring, was adjusted to pH 5.8 by the addition a few drops of 2N KOH solution and heated on a boiling oil bath. To the hot reaction, sodium hydrosulfite (200 mg, 1.2 mmol, 3.5 equiv) was added. The clear red solution turned pale yellow within 5 min. The mixture was allowed to cool down to room temperature and dry off water by high vacuum. Purification by flash column chromatography (SiO₂, CHCl₃/MeOH/NH₄.OH 12:9:4) to give the target product **3-5** (58 mg, 0.21 mmol, 61.1%) as a yellow sold. TLC: R_f=0.12 (CHCl₃/MeOH/NH₄.OH 12:9:4, CAM, UV). ¹H NMR (400 MHz, D₂O): δ= 3.70-3.65 (m, 2H), 3.58 (m, 1H), 3.45 (m, 1H), 3.41 (m, 1H), 2.72 (m, 1H), 2.64 (m, 1H) ¹³C NMR (100 MHz, CDCl₃): δ= δ 165.6, 140.8, 140.3, 94.5, 73.2, 72.4, 72.0, 63.1, 42.4. HRMS (ESI) calcd for C₉H₁₆N₄O₆ [M+H]⁺: 277.1070, found: 277.1321.



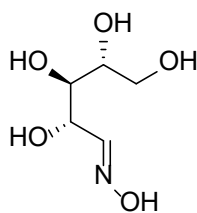
3-6

Compound 3.6 To a solution of compound **3-5** (250 mg, 0.9 mmol, 1.0 equiv.) in 4 mL DI water with stirring, pyruvic acid sodium salt (1.8g, 16.3 mmol, 18.0 equiv.) was added. The mixture was adjusted to pH 4.5 by addition a few drops of 2N HCl solution carefully. Then the reaction was allowed to heat up to 80 °C in an oil bath for 20 min. After cool down to room temperature, the solvent was dried off by high vacuum. Purification by flash column chromatography (SiO₂, CHCl₃/MeOH/NH₄.OH 12:9:4) to give the target product **3-6** (67 mg, 0.21mmol, 22.6%) as a yellow solid. TLC: R_f=0.24 (CHCl₃/MeOH/NH₄.OH 12:9:4, CAM, UV). ¹H NMR (400 MHz,D₂O): δ= 3.70-3.65 (m, 2H), 3.58 (m, 1H), 3.45 (m, 1H), 3.41 (m, 1H), 2.96 (s, 3H), 2.72 (m, 1H), 2.64 (m, 1H) ¹³C NMR (100 MHz, CDCl₃): δ= δ 181.4, 162.3, 161.2, 156.3, 131.2, 85.3, 73.2, 72.4, 72.0, 63.1, 42.1. HRMS (ESI) calcd for C₁₂H₁₆N₄O₇ [M+Na]⁺: 351.0917, found: 351.1044.



3-7

Compound 3.7 To a solution of compound **3-6** (180 mg, 0.55 mmol, 1.0 equiv.) in 5 mL PBS buffer solution (pH = 7.4), sodium hydrosulfite (400 mg, 2.74 mmol, 5.0 equiv.) was added with stirring. The mixture was allowed to stir at room temperature for 1 h. After the solvent was dried off by high vacuum, purification by flash column chromatography (SiO₂, CHCl₃/MeOH/NH₄.OH 12:9:4) to give the target product **3-7** (55 mg, 0.17, 31.1%) as a yellow sold. TLC: R_f=0.25 (CHCl₃/MeOH/NH₄.OH 12:9:4, CAM, UV). ¹H NMR (400 MHz,D₂O): δ= 4.81 (m, 1H), 3.70-3.65 (m, 2H), 3.58 (m, 1H), 3.45 (m, 1H), 3.41 (m, 1H), 2.72 (m, 1H), 2.64 (m, 1H) ,1.95 (s, 3H). ¹³C NMR (100 MHz, CDCl₃): δ= δ 164.4, 162.3, 157.2, 156.3, 86.7, 85.3, 73.2, 72.4, 72.0, 63.1, 45.9. HRMS (ESI) calcd for C₁₂H₁₈N₄O₇ [M+H]⁺: 331.1175, found: 331.1182.



3-8

Compound 3.8 Hydroxylamine hydrochloride (3.0 g, 43 mmol, 2.34 equiv.) was dissolved in MeOH (dry, 40 mL) and stirred at room temperature. 2 drops of phenolphthalein (1%, solution in EtOH) was added to mixture. Then a solution of NaOMe (2.4 g, 44 mmol, 2.45 equiv.) in MeOH (40 mL) was added slowly to the suspension, upon with a white precipitate formed. When the reaction stayed pink for 1 min, addition of base (NaOMe) was halted. The mixture was stirred for several mins and filtered to remove slats. The filtrate was transferred to a round bottom flask (250 mL) and warmed to 70 °C. Then D-(-) Xylose (2.8 g, 18 mmol, 1.00 equiv.) was added to reaction in small portions. The mixture was allowed to stir at 70 °C until the sugar had completely dissolved (5-10 min) and cooled down to room temperature. The product **3-8** (2.8 g, 16.9 mmol, 94.2%) was precipitated from solution after keeping the mixture at fridge overnight.

TLC: $R_f=0.38$ ($\text{CHCl}_3/\text{MeOH}/\text{NH}_4.\text{OH}$ 12:9:4, CAM). ^1H NMR (400 MHz, D_2O): $\delta=$ 7.51 (m, 1H), 6.88 (m, 1H), 4.96 (m, 1H), 4.36 (m, 1H), 3.79-3.69 (m, 6H), 3.63 (m, 2H) ^{13}C NMR (100 MHz, CDCl_3): $\delta=$ δ 153.8, 153.2, 73.5, 73.3, 73.0, 72.5, 71.3, 67.0, 64.4, 64.1. HRMS (ESI) calcd for $\text{C}_5\text{H}_{11}\text{NO}_5$ $[\text{M}+\text{Na}]^+$: 188.0637, found: 188.0589.

3.6 References

1. Tilloy, F.; Treiner, E.; Park, S. H.; Garcia, C.; Lemonnier, F.; de la Salle, H. et al. An invariant T cell receptor chain defines a novel TAP-independent major histocompatibility complex class Ib-restricted/T cell subpopulation in mammals. *J Exp Med* **1999**, *189*, 1907–21.
2. Treiner, E. Lantz O. CD1d- and MR1-restricted invariant T cells: of mice and men. *Curr Opin Immunol* **2006**, *18*, 519–26.
3. Le Bourhis, L.; Martin, E.; Péguillet, I.; Guihot, A.; Froux, N.; Coré, M. et al. Antimicrobial activity of mucosal-associated invariant T cells. *Nat Immunol* **2010**, *11*, 701–8.
4. Gold, M. C.; Eid, T.; Smyk-Pearson, S.; Eberling, Y.; Swarbrick, G. M.; Langley, S. M. et al. Human thymic MR1-restricted MAIT cells are innate pathogen-reactive effectors that adapt following thymic egress. *Mucosal Immunol* **2013**, *6*, 35–44.
5. Gapin, L. Where do MAIT cells fit in the family of unconventional T cells? *PLoS Biol* **2009**, *7*(3), 70.
6. Young, M.H.; et al. MAIT cell recognition of MR1 on bacterially infected and uninfected cells. *PLoS ONE* (2013) *8*(1): 53789.
7. Huang S, et al. Evidence for MR1 antigen presentation to mucosal-associated invariant T cells. *J Biol Chem* **2005**, *280*(22), 21183–21193.
8. Kjer-Nielsen L, et al. MR1 presents microbial vitamin B metabolites to MAIT cells. *Nature* **2012**, *491*, 717–723.
9. Reantragoon, R.; Corbett, A.J.; Sakala, I. G.; Gherardin, N. A.; Furness, J. B.; Chen, Z. et al. Antigen-loaded MR1 tetramers define T cell receptor heterogeneity in mucosal-associated invariant T cells. *J Exp Med* **2013**, *210*, 2305–20.

10. Eckle, S. B.G.; Birkinshaw, R. W.; Kostenko, L.; Corbett, A. J.; McWilliam, HEG. Reantragoon, R. et al. A molecular basis under pinning the T cell receptor heterogeneity of mucosal-associated invariant T cells. *J Exp Med* **2014**, *211*, 1585–1600.
11. Gold, M. C.; Ehlinger, H. D.; Cook, M. S.; Smyk-Pearson, S. K.; Wille, P. T.; Ungerleider, R. M. et al. Human innate Mycobacterium tuberculosis-reactive alpha- beta TCR+ thymocytes. *PLoS Pathog* **2008**, *4*, e39.
12. Gold, M. C.; Eid, T.; Smyk-Pearson, S.; Eberling, Y.; Swarbrick, G. M.; Langley, S. M. et al. Human thymic MR1-restricted MAIT cells are innate pathogen-reactive effectors that adapt following thymic egress. *Mucosal Immunol* **2013**, *6*, 35–44.
13. Cho, Y-N.; Kee, S-J.; Kim, T-J.; Jin, H. M.; Kim, M-J.; Jung, H-J.; Park, K-J.; Lee, S-J.; Lee, S-S.; Kwon, Y-S.; Kee, H. J.; Kim, N.; Park, Y-W.; Mucosal-associated invariant T cell deficiency in systemic lupus erythematosus. *J Immunol* **2014**, *193*, 3891–3901.
14. Miyazaki, Y.; Miyake, S.; Chiba, A.; Lantz, O.; Yamamura, T. Mucosal-associated invariant T cells regulate Th1 response in multiple sclerosis. *Int Immunol* **2011**, *23*, 529–535.
15. Serriari, N-E.; Eoche, M.; Lamotte, L.; Lion, J.; Fumery, M.; Marcelo, P.; Chatelain, D.; Barre, A.; Nguyen-Khac, E.; Lantz, O.; Dupas, J-L.; Treiner, E. Innate mucosal-associated invariant T (MAIT) cells are activated in inflammatory bowel diseases. *Clin Exp Immunol* **2014**, *176*, 266–274.
16. Treiner, E.; Liblau, R. S. Mucosal-associated invariant T cells in multiple sclerosis: the Jury is still out. *Front Immunol* **2015**, *6*, 503.
17. Carolan, E.; Tobin, L. M.; Mangan, B. A; Corrigan, M.; Gaoatswe, G.; Byrne, G. et al. Altered distribution and increased IL-17 production by mucosal-associated invariant T cells in adult and childhood obesity. *J Immunol* **2015** *194*, 5775–5780.

18. Magalhaes, I.; Pingris, K.; Poitou, C.; Bessoles, S.; Venteclef, N.; Kiaf, B. et al. Mucosal-associated invariant T cell alterations in obese and type 2 diabetic patients. *J Clin Invest* **2015** *125*, 1752–62.
19. Kim, J. C.; Jin, H. M.; Cho, Y.N.; Kwon, Y. S.; Kee, S.J.; Park, Y. W. Deficiencies of circulating mucosal-associated invariant T cells and natural killer T cells in patients with acute cholecystitis. *J Korean Med Sci* **2015** *30*, 606–611.
20. Sugimoto, C.; Konno, T.; Wakao, R.; Fujita, H.; Fujita, H.; Wakao, H. Mucosal-associated invariant T cell is a potential marker to distinguish fibromyalgia syndrome from arthritis. *PLoS One* **2015**, *10*, e0121124.
21. Hinks, T. S.; Zhou, X.; Staples, K. J.; Dimitrov, B. D. Manta, A. Petrossian T, et al. Innate and adaptive T cells in asthmatic patients: relationship to severity and disease mechanisms. *J Allergy Clin Immunol* **2015**, *136*, 323–333.
22. Meierovics, A.; Yankelevich, W. J. C.; Cowley, S. C. MAIT cells are critical for optimal mucosal immune responses during in vivo pulmonary bacterial infection. *P Natl Acad Sci USA*, **2013**, *110*, 3119-3128.
23. Gold, M.C.; Cerri, S.; Smyk-Pearson, S.; Cansler, M. E.; Vogt, T. M.; Delepine, J. et al. Human mucosal associated invariant T cells detect bacterially infected cells. *PLoS Biol* **2010**, *8*, e1000407.
24. Ussher, J. E.; Bilton, M.; Attwod, E.; Shadwell, J.; Richardson, R.; de Lara, C. et al. CD161⁺⁺ CD8⁺ T cells, including the MAIT cell subset, are specifically activated by IL-12⁺ IL-18 in a TCR-independent manner. *Eur J Immunol* **2014**, *44*, 195–203.

25. Sattler, A. Dang-Heine, C.; Reinke, P.; Babel, N. IL-15 dependent induction of IL-18 secretion as a feedback mechanism controlling human MAIT-cell effector functions. *Eur J Immunol* **2015**, *45*, 2286–2298.
26. Wong, E. B.; Ndung'u, T.; Kasprowicz, V. O. The role of mucosal-associated invariant T cells in infectious diseases. *Immunology* **2017**, *150*, 45-54.
27. Sakala, I. G.; Kjer-Nielsen L, E.; Wang, X.; Blazevic, A.; Liu, L. et al. Functional heterogeneity and antimycobacterial effects of mouse mucosal-associated invariant T cells specific for riboflavin metabolites. *J Immunol* **2015**, *195*, 587–601.
28. Corbett, A. J.; Eckle, S. B.; Birkinshaw, R.W.; Liu, L.; Patel, O.; Mahony, J. Z.; Chen, R.; Reantragoon, B.; Meehan, H. Cao. et al. T-cell activation by transitory neo-antigens derived from distinct microbial pathways. *Nature* **2014**, *509*, 361–365.
29. Godfrey, D. I.; Rossjohn, J. ; McCluskey, J. Fighting infection with your MAITs. *Nature Immunol.* **2010**, *11*, 693–695.
30. Maley, G. F.; Plaut, G. W. E. The Isolation, Synthesis, and Metabolic Properties of 6,7-Dimethyl-8-ribityllumazine, *J. Biol. Chem.* **1959**, *234*, 641-647.
31. Winestock, C. H.; Plaut, G. W. E. Synthesis and Properties of Certain Substituted Lumazines. **1961**, *26*, 4456-4462.
32. Plaut, G. W. E.; Smith, C. M.; Alworth, W. L. Biosynthesis of water-soluble vitamins. *Annu. Rev. Biochem.* **1974**, *43*, 899–922.

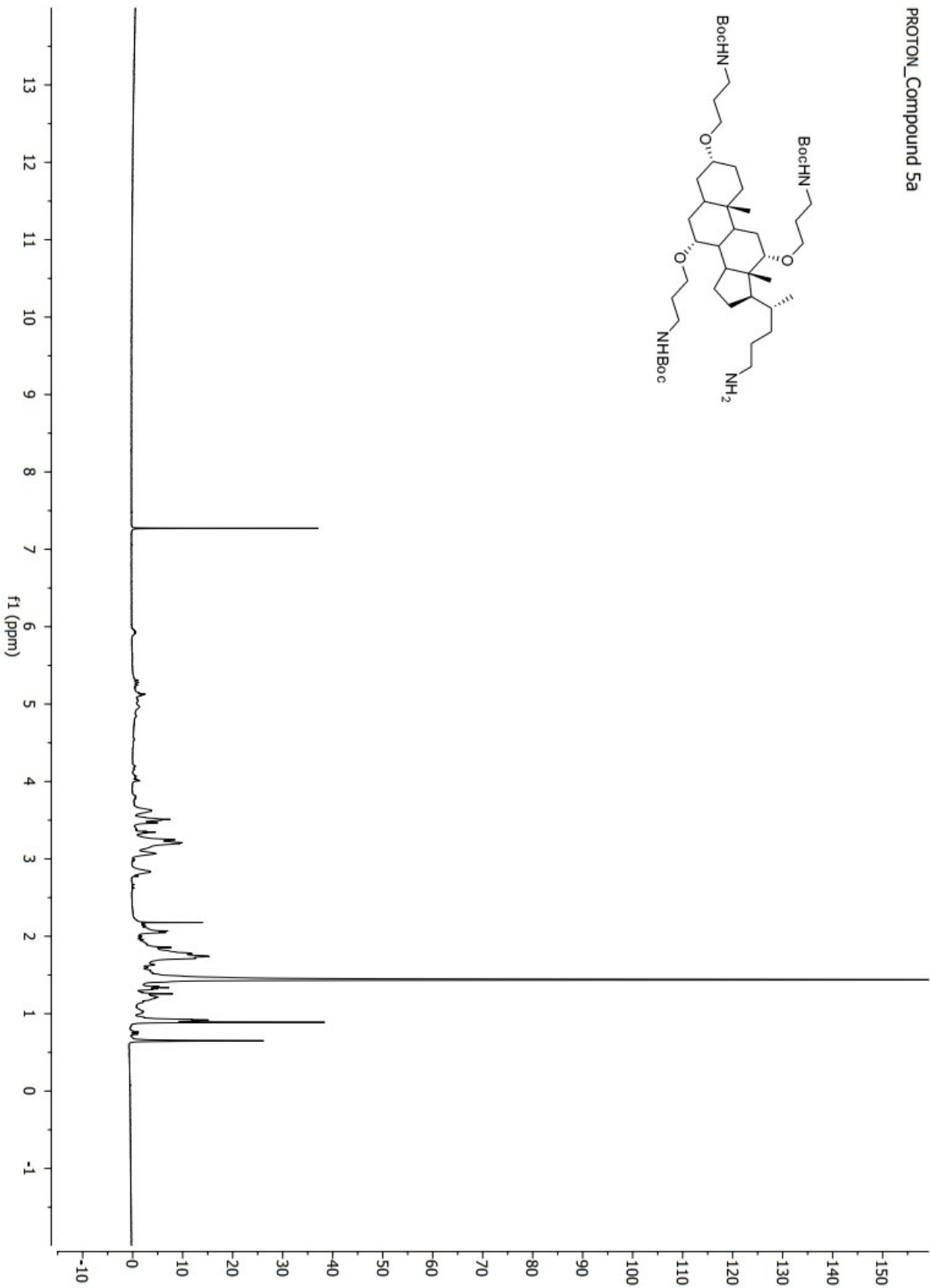
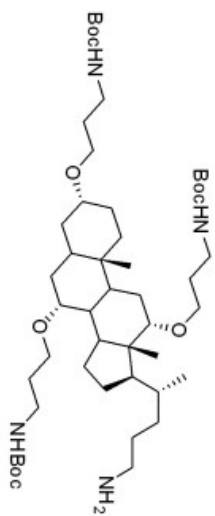
Appendix A:

List of abbreviation

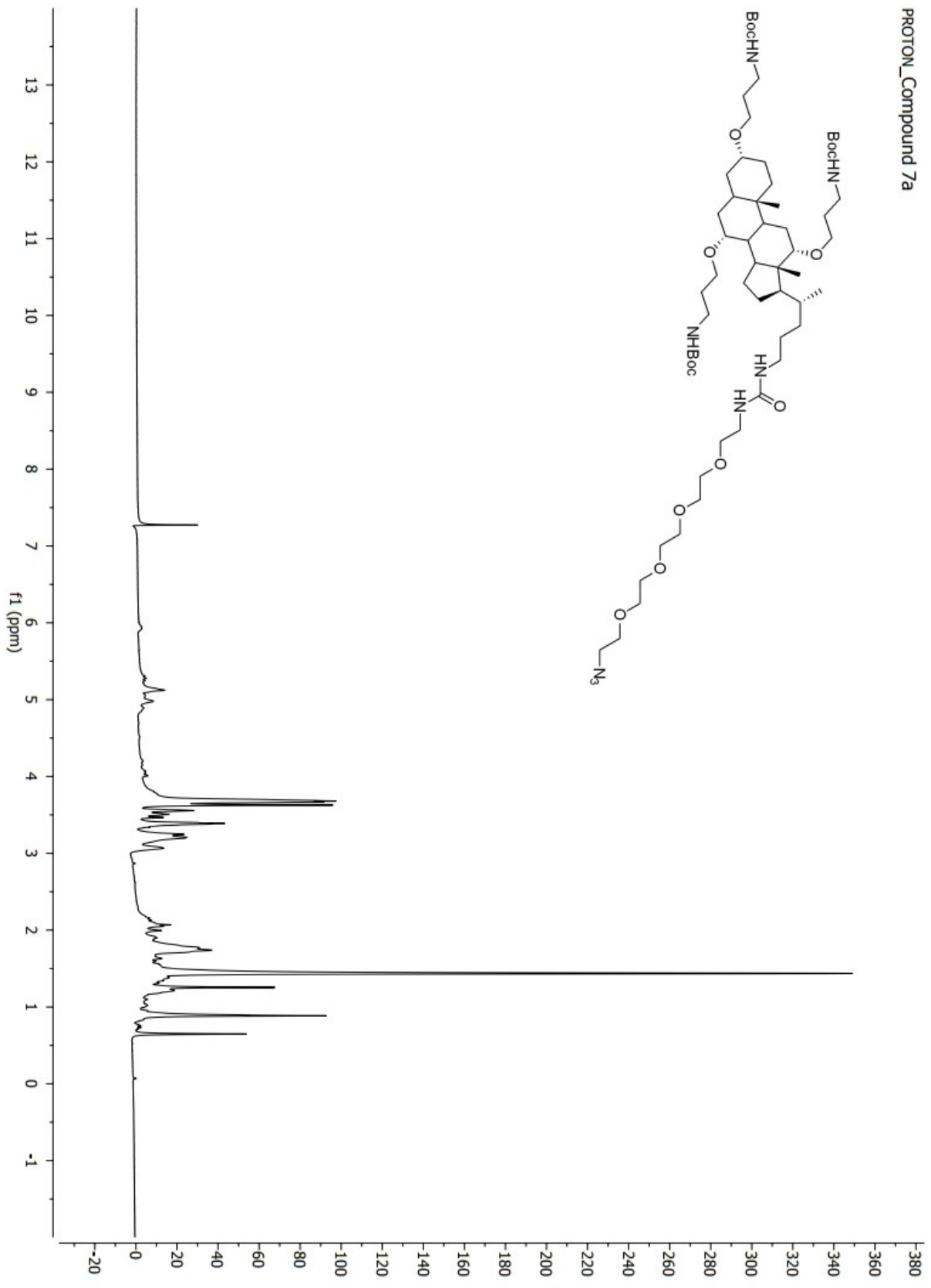
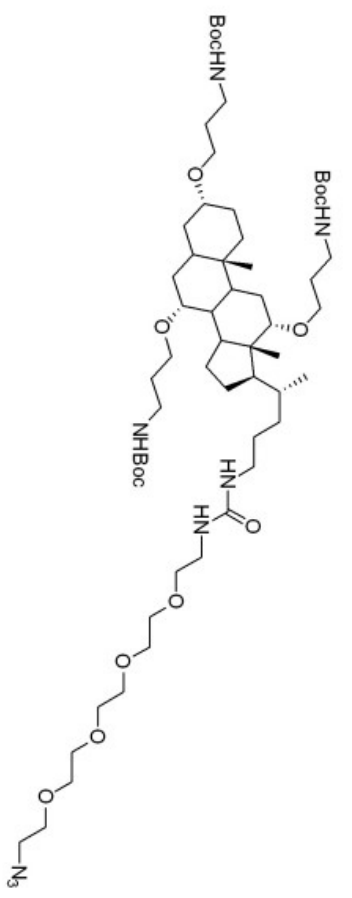
9-BBN	9-Borabicyclo[3.3.1]nonane solution
AcOH	Acetic acid
Ac ₂ O	Acetic anhydride
Boc	tert-Butoxycarbonyl
Boc ₂ O	Di-tert-butyl dicarbonate
CH ₃ CN	Acetonitrile
DCM	Dichloromethane
DMF	Dimethylformamide
DMAP	Dimethylaminopropylamine
DMSO	Dimethyl sulfoxide
DLS	Dynamic light scattering
EDCI	1-Ethyl-3-[3-(dimethylamino)propyl]-carbodiimide hydrochloride
EtOAc	Ethyl acetate
Fmoc	9-Fluorenylmethoxycarbonyl
FT-IR	Fourier-transform Infrared Spectroscopy
HPC	Hydroxypropyl Cellulose
HOBt	Hydroxybenztriazole
ICP-OES	Inductively Coupled Plasma - optical emission spectrometry
KHMDS	Potassium bis(trimethylsilyl)amide
OM	Outer Membrane LPS Lipopolysaccharide
PEC	Positron Emission Tomography
Ph ₃ P	Triphenylphosphine
LPS	Lipopolysaccharide
MAIT Cells	Mucosal-Associated Invariant T Cells
MsCl	Methanesulfonyl chloride
MRI	Magnetic Resonance Imaging
MIC	Minimum Inhibitory Concentration
MBC	Minimum Bactericidal Concentration
MeOH	Methanol
NOTA	1, 4, 7-Triazacyclononane-1,4-bis-tert-butyl acetate-7-acetic acid
Tr	Tryl
THF	Tetrahydrofuran
p-TsOH	p-Toluenesulfonic acid
TEM	Transmission Electron Microscopy
TCR	T cell Receptor
SPECT	Single Photon Emission Computed Tomography
SNPs	SmartSilverAS Silver Nanoparticles
COMU	(1-Cyano-2-ethoxy-2-oxoethylideneaminoxy)dimethylamino-morpholino-carbenium hexafluorophosphate

Appendix B:
NMR Spectra

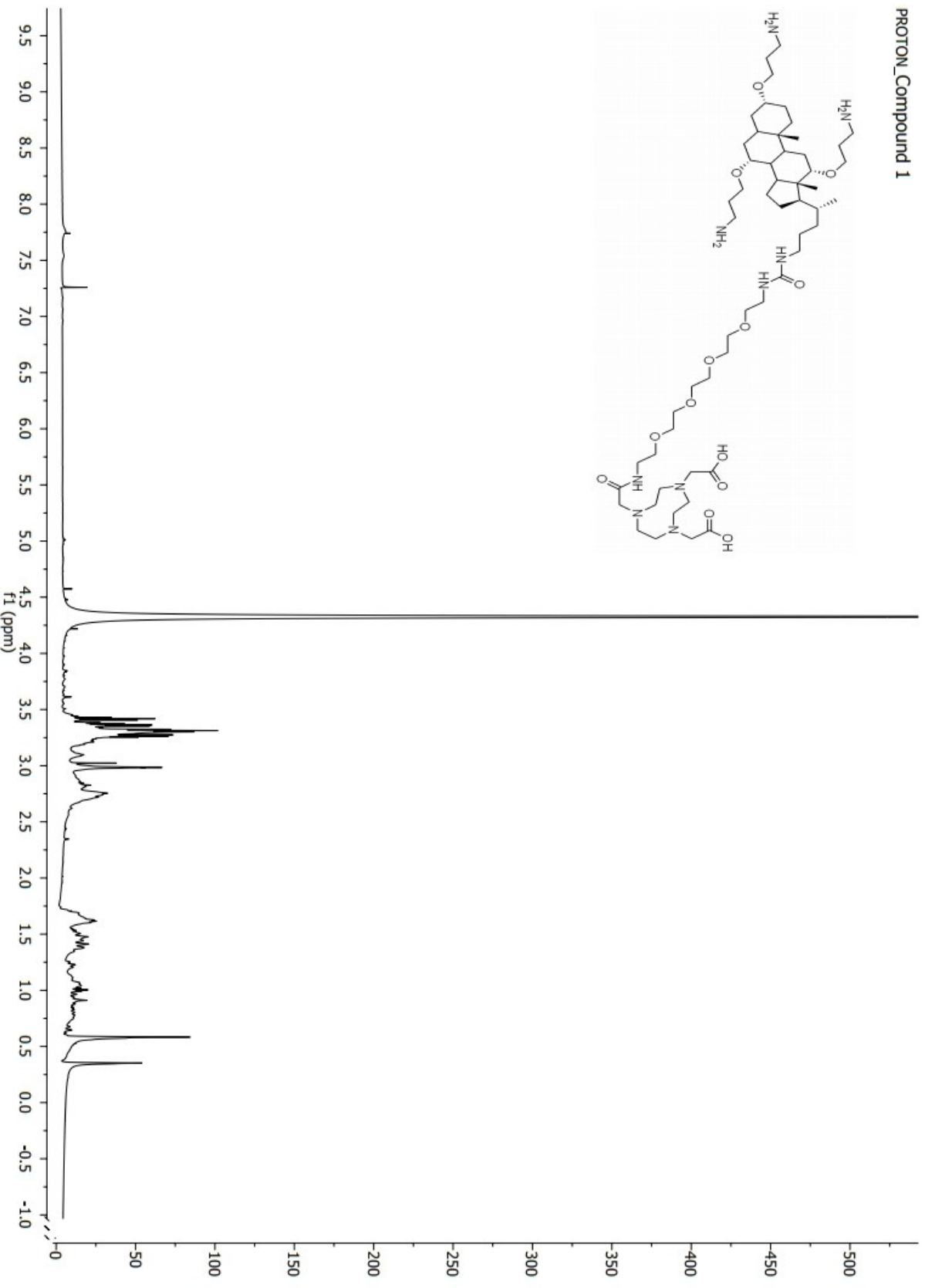
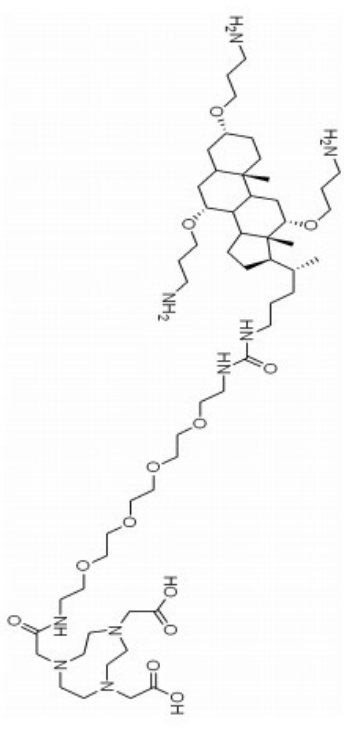
PROTON_Compound 5a



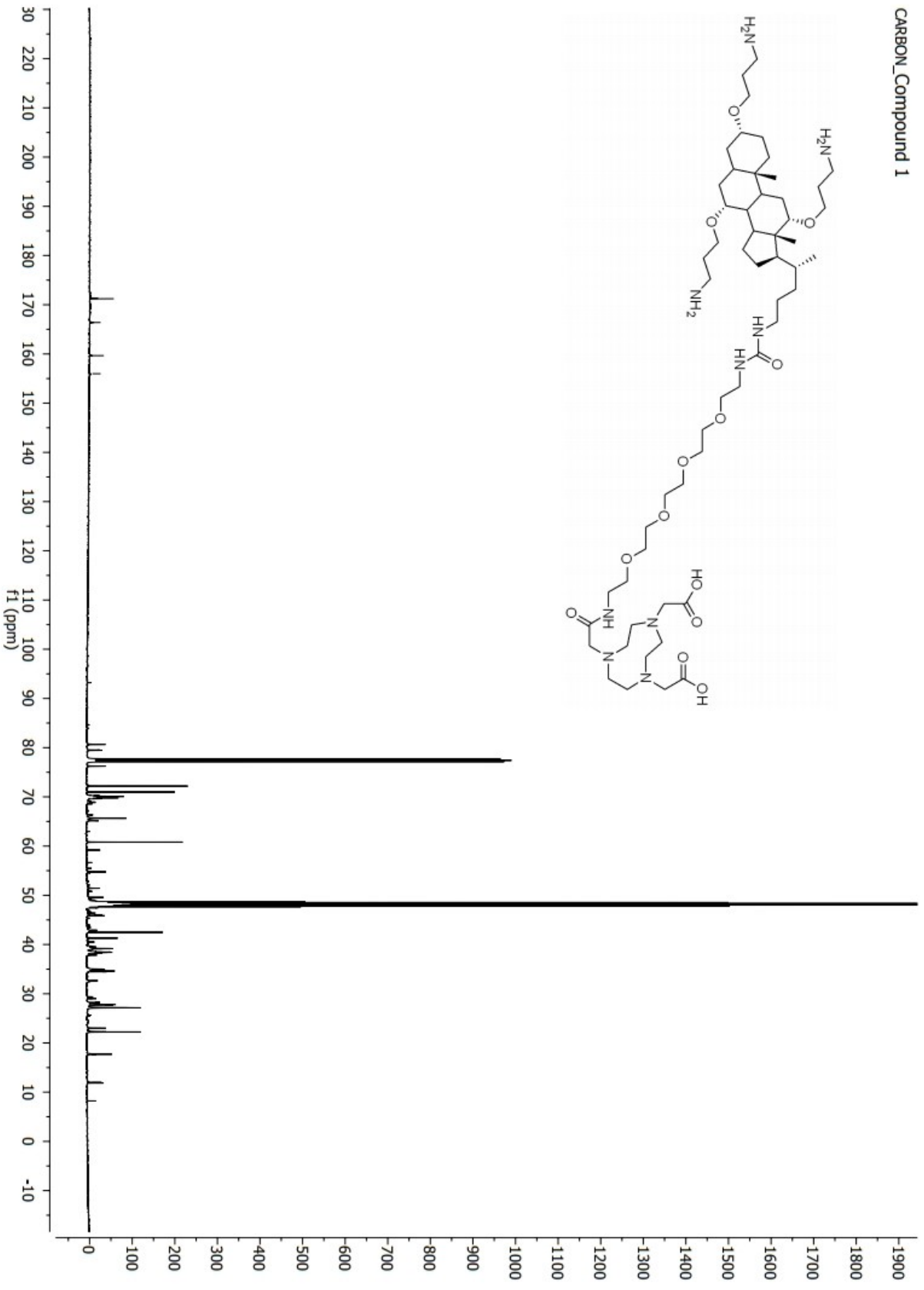
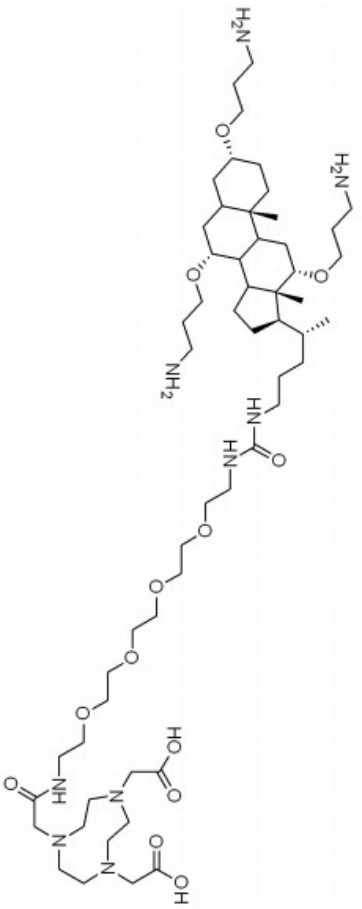
PROTON_Compound 7a



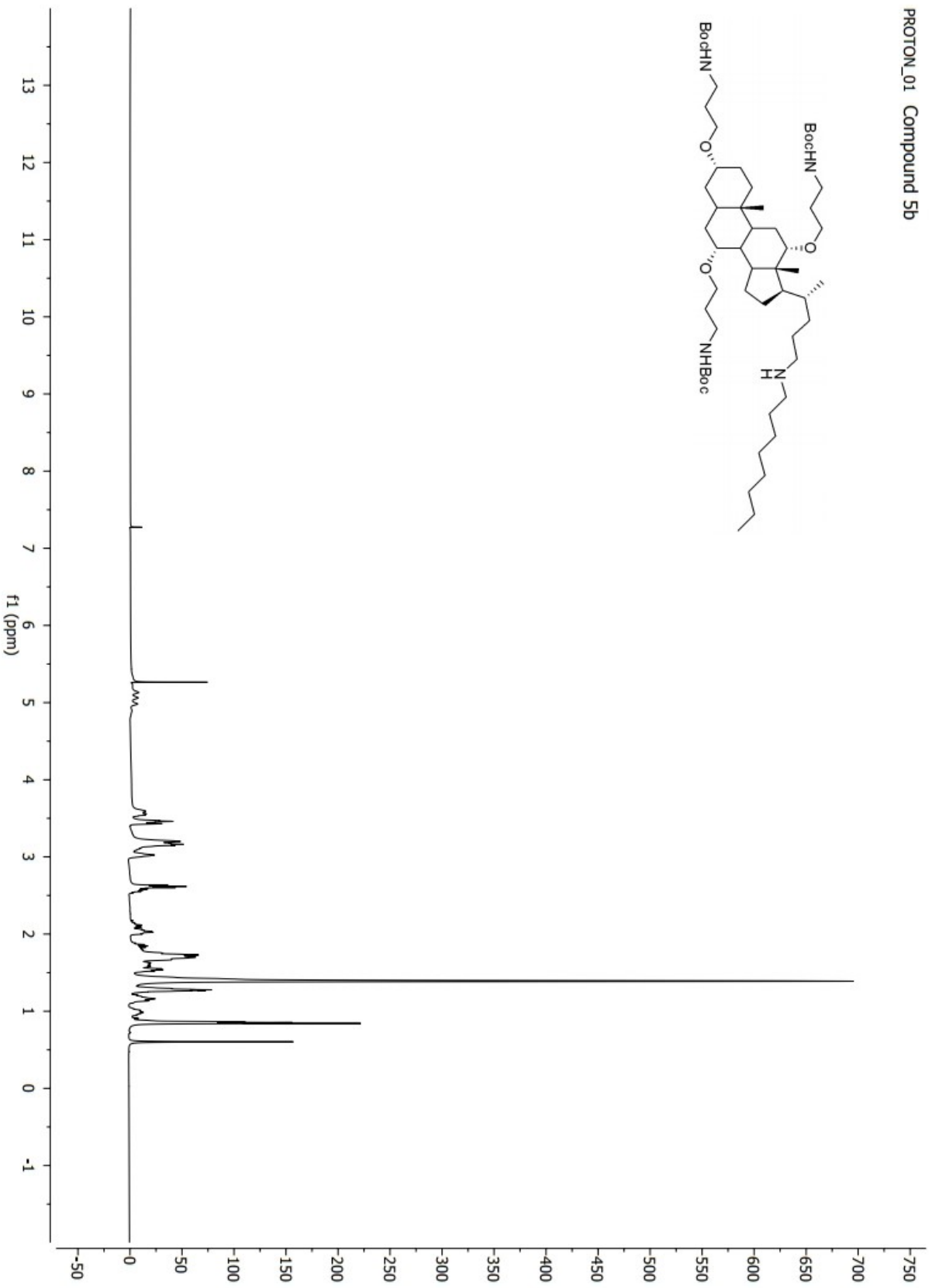
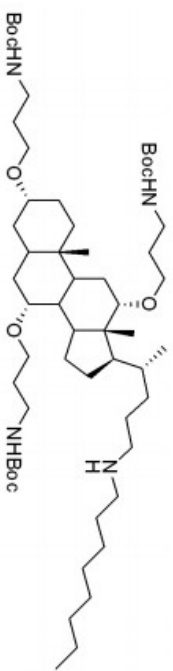
PROTON_Compound 1



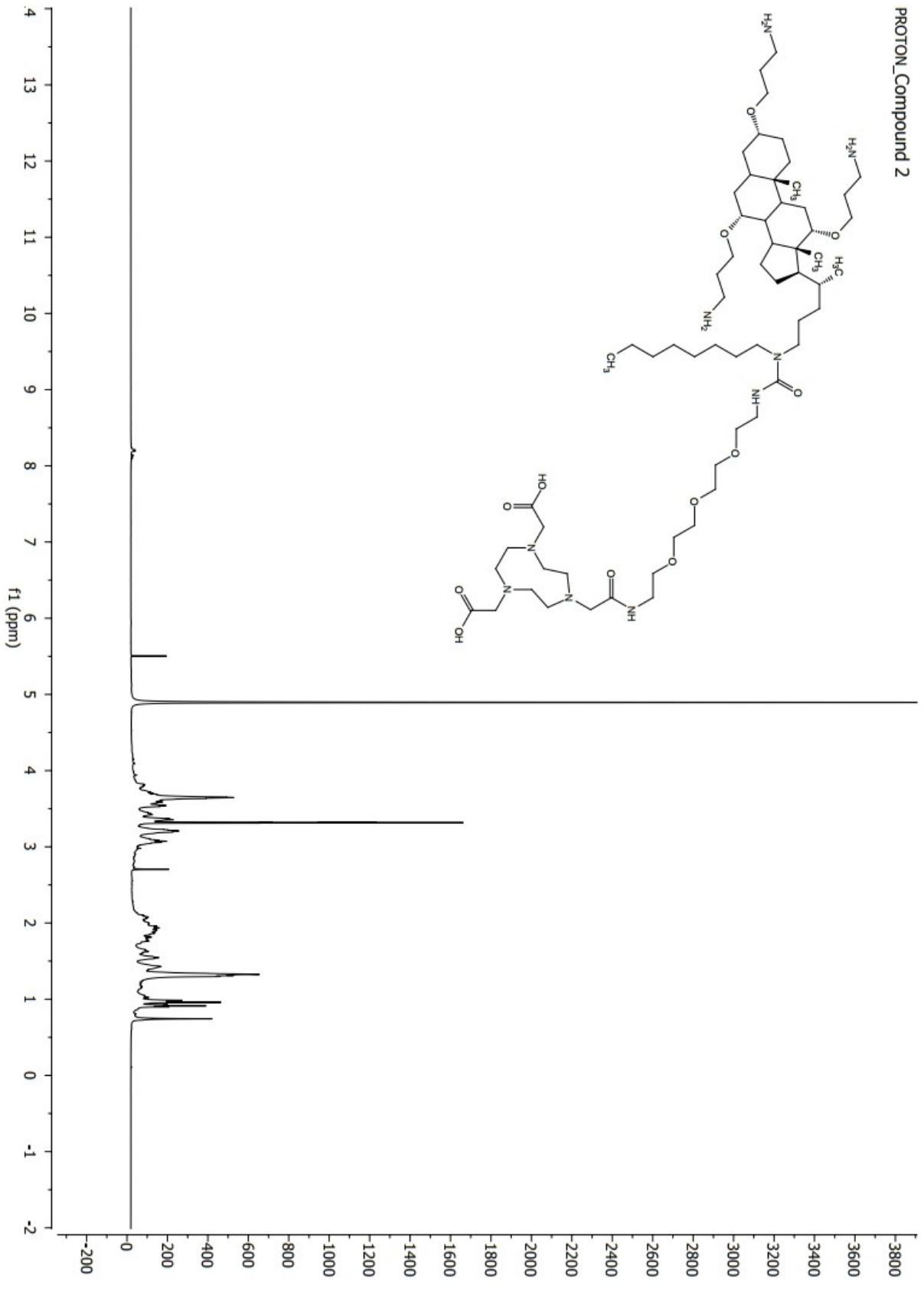
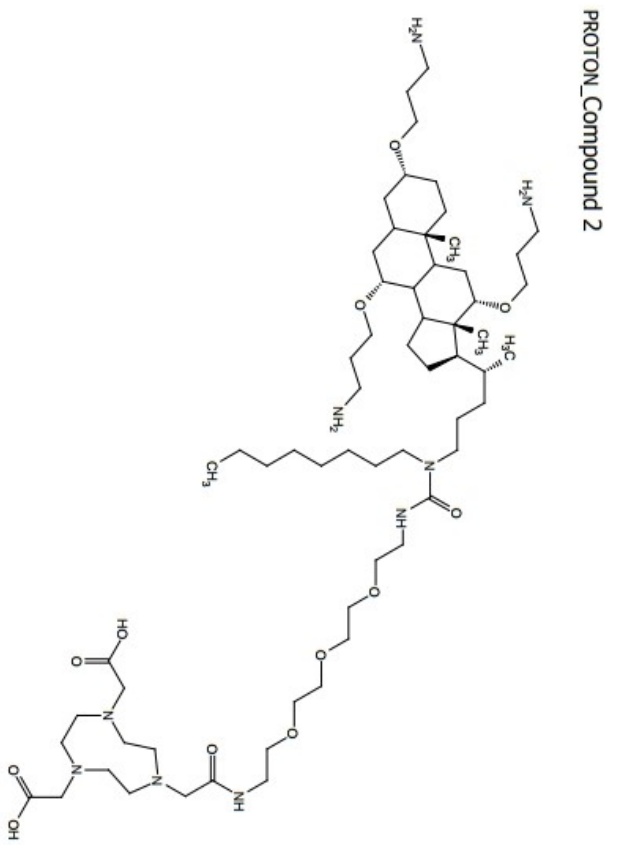
CARBON_Compound 1



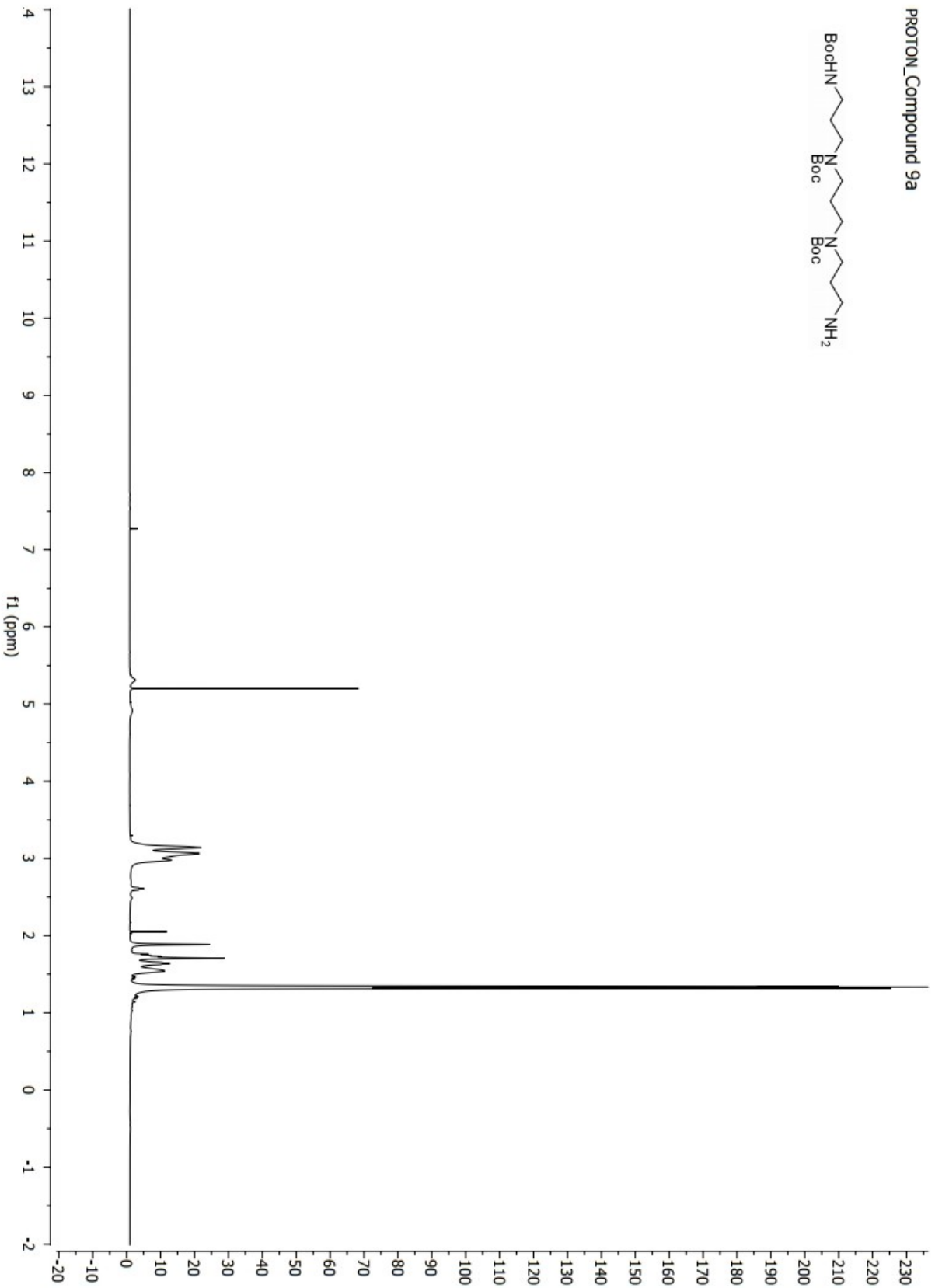
PROTON_01 Compound 5b



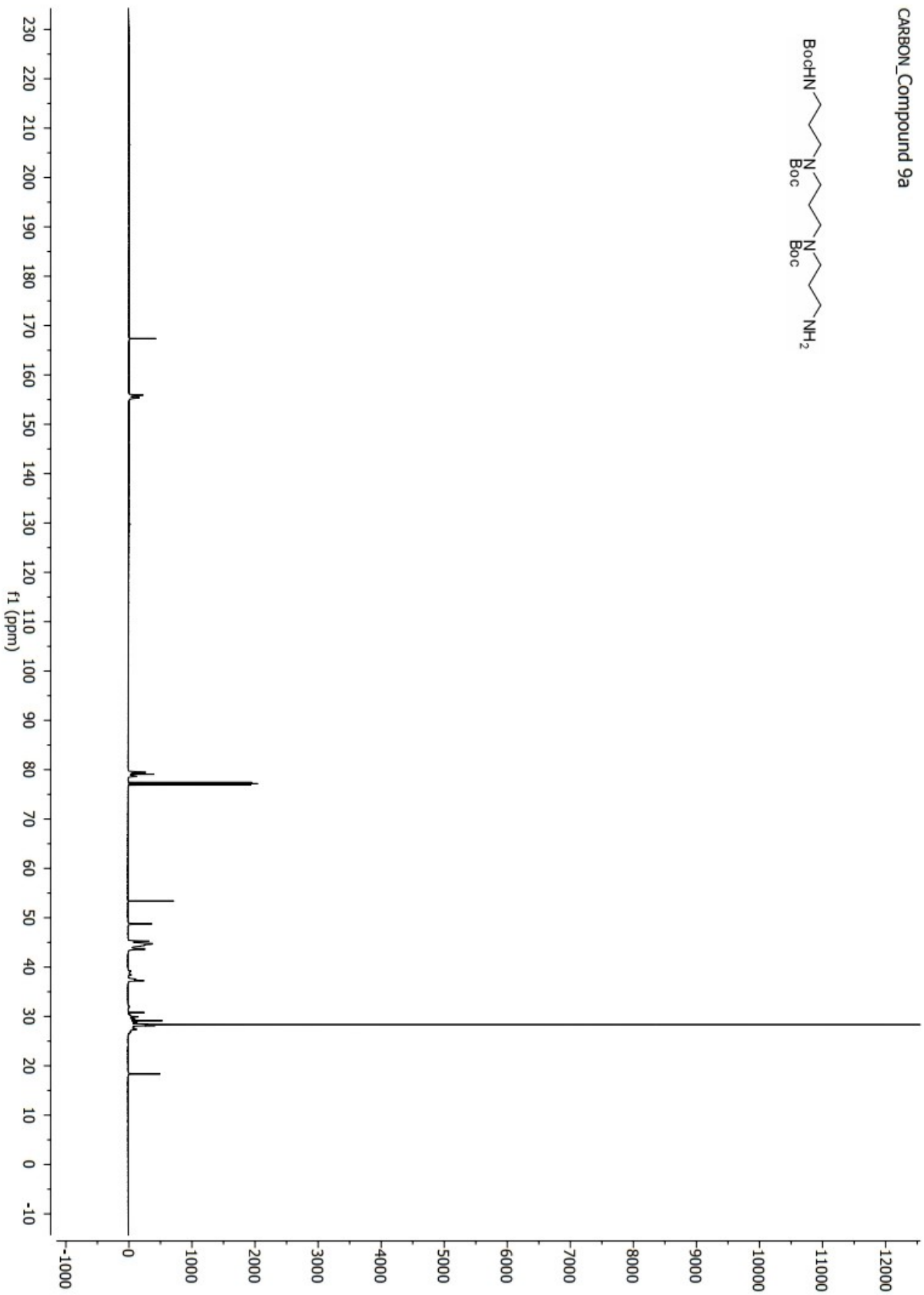
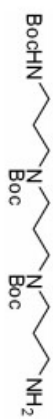
PROTON_Compound 2



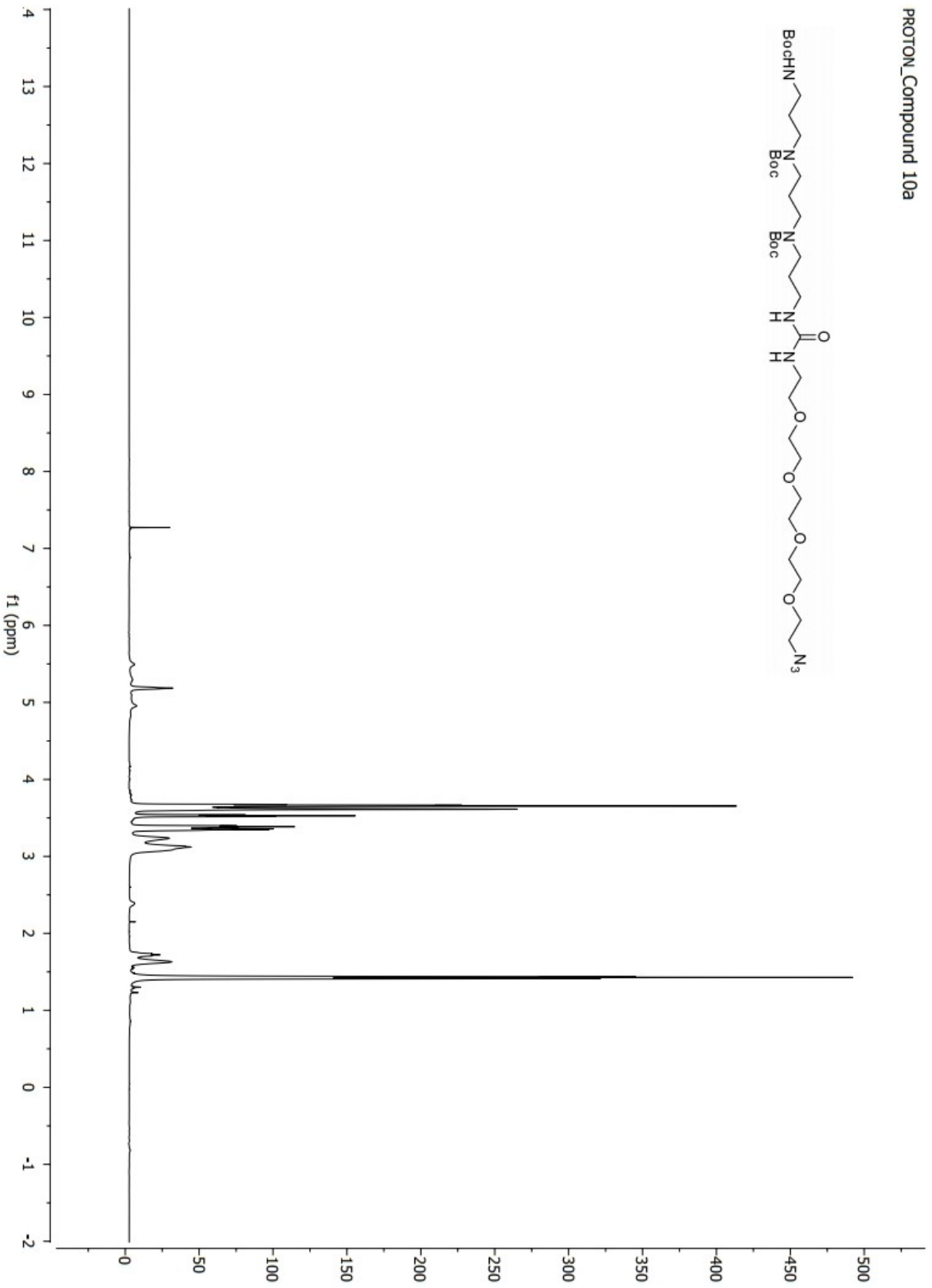
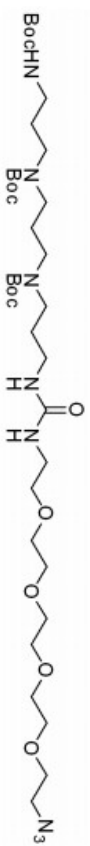
PROTON_Compound 9a



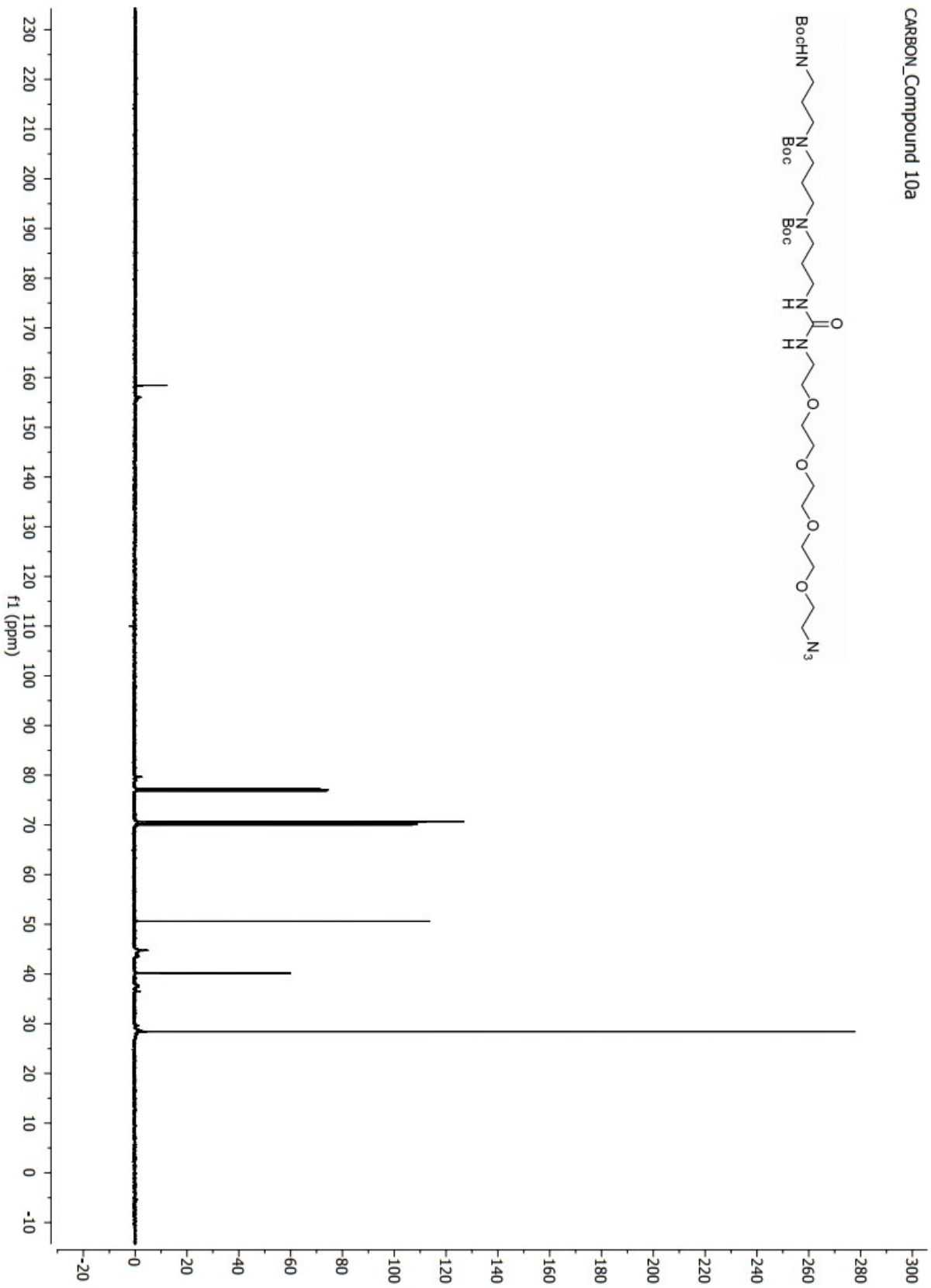
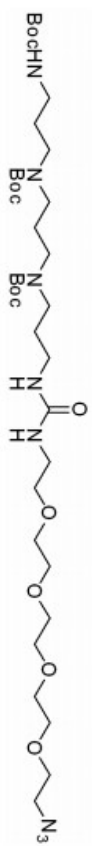
CARBON_Compound 9a



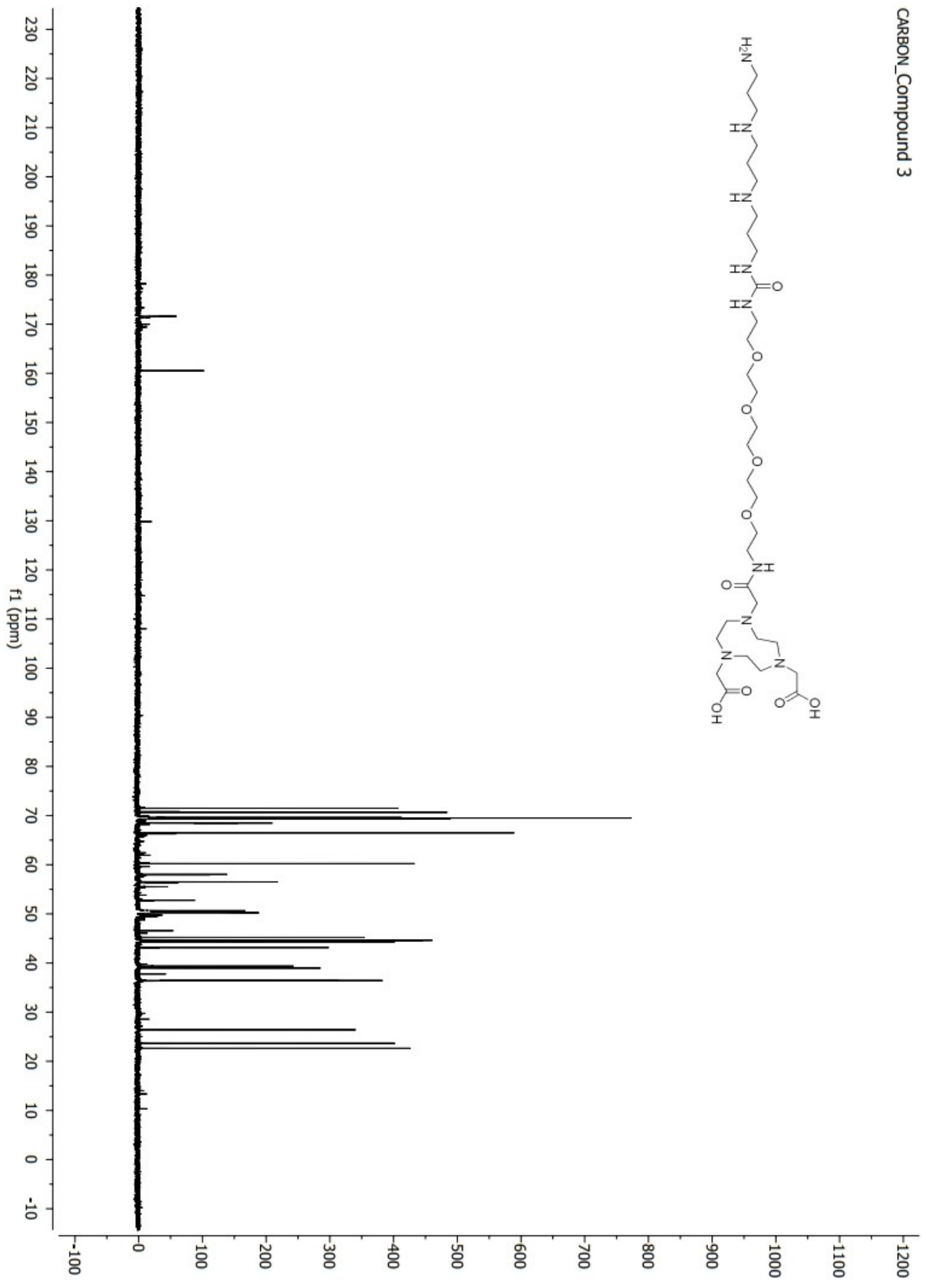
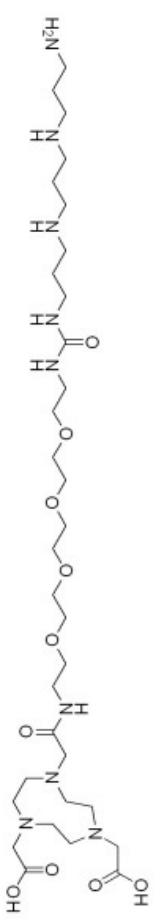
PROTON_Compound 10a



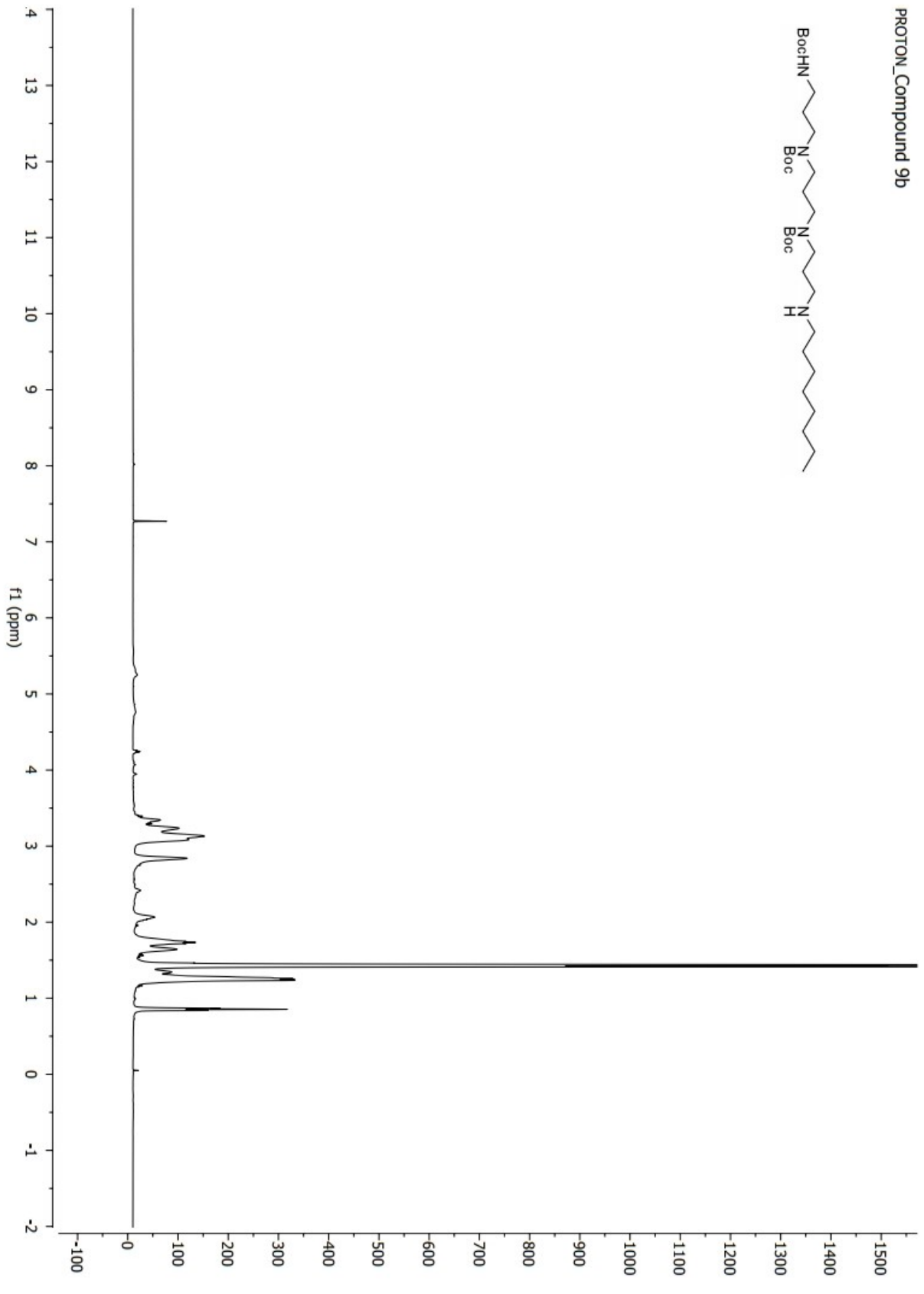
CARBON_Compound 10a



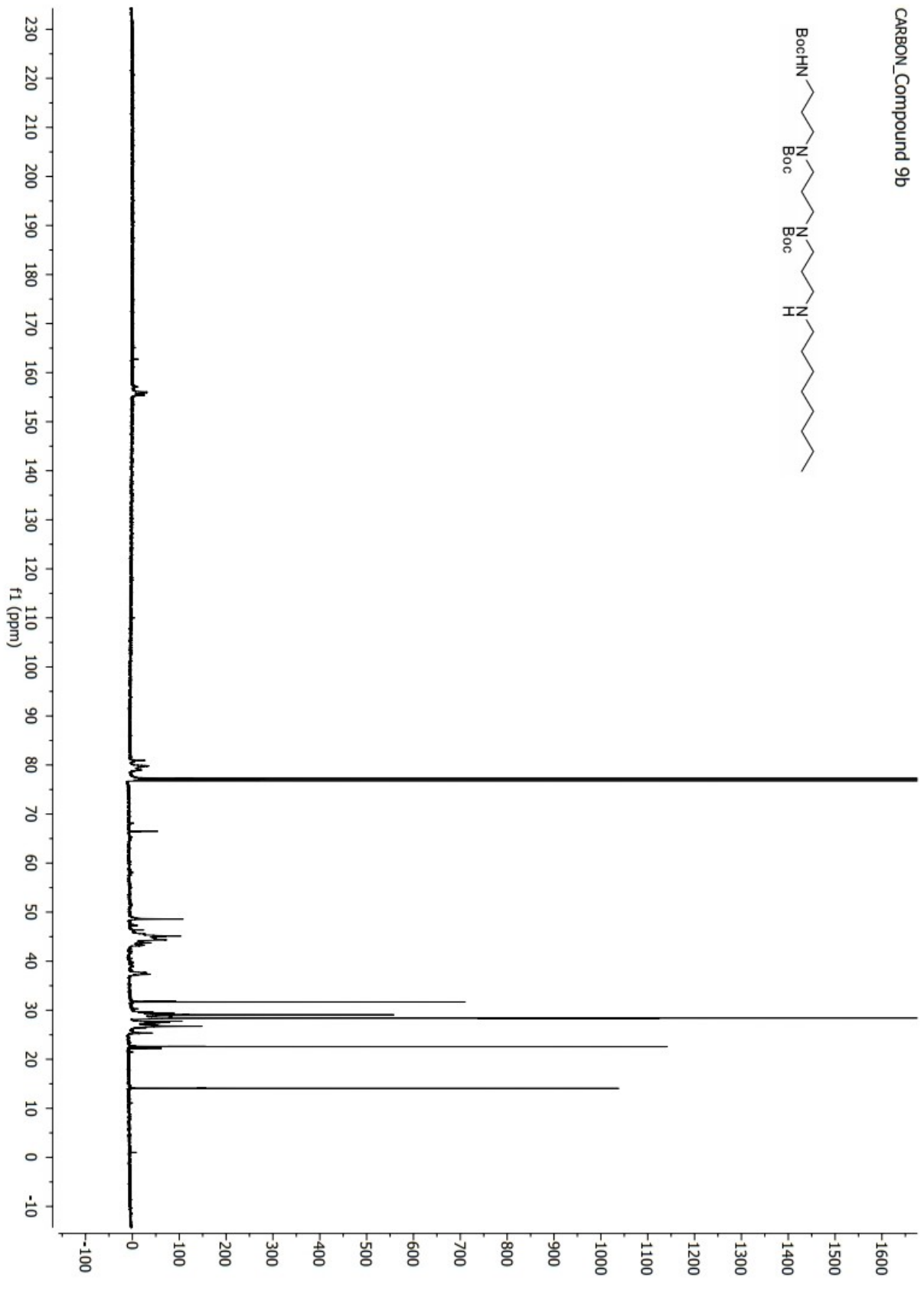
CARBON_Compound 3



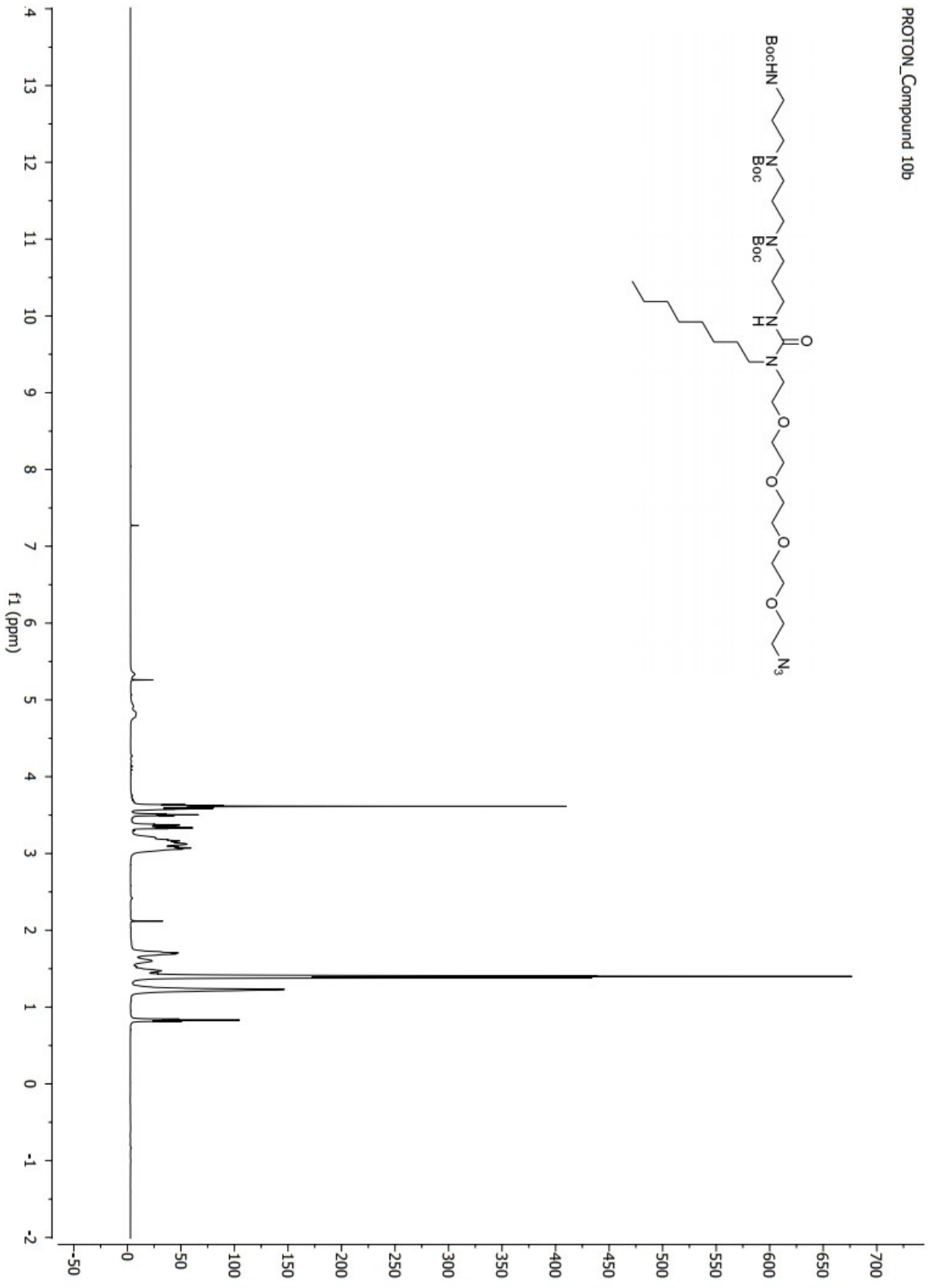
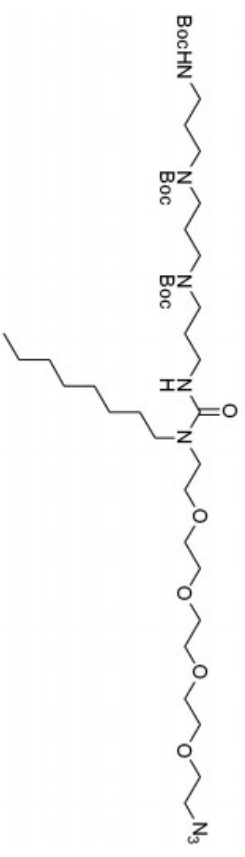
PROTON_Compound 9b



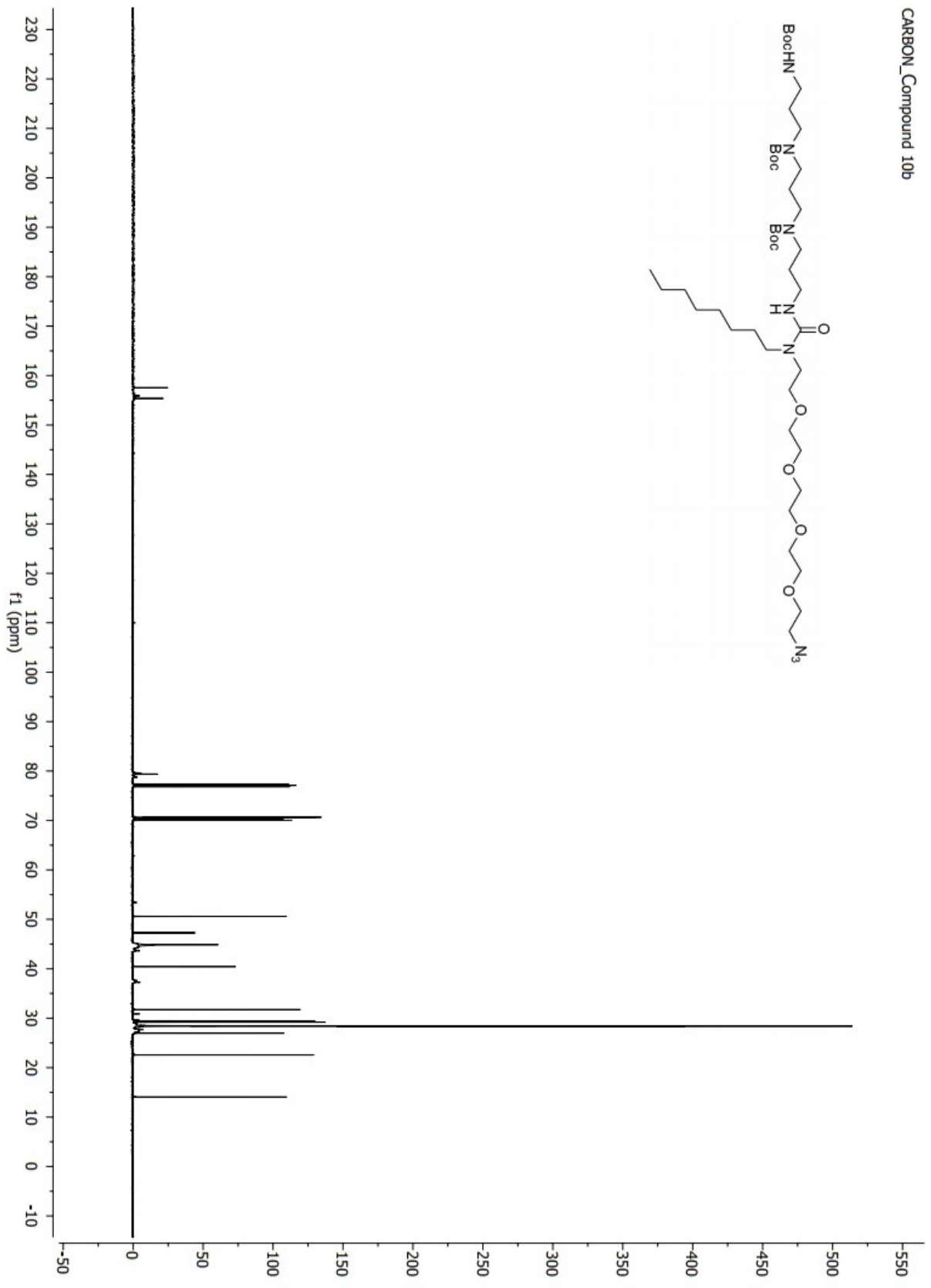
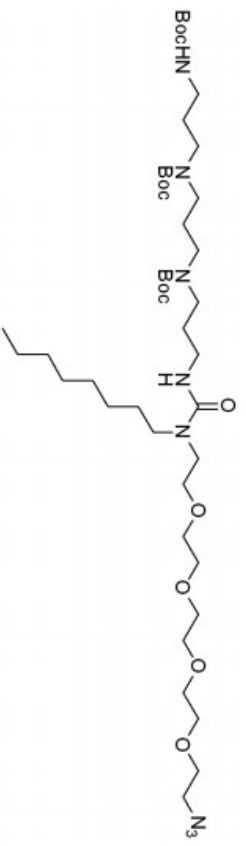
CARBON_Compound 9b



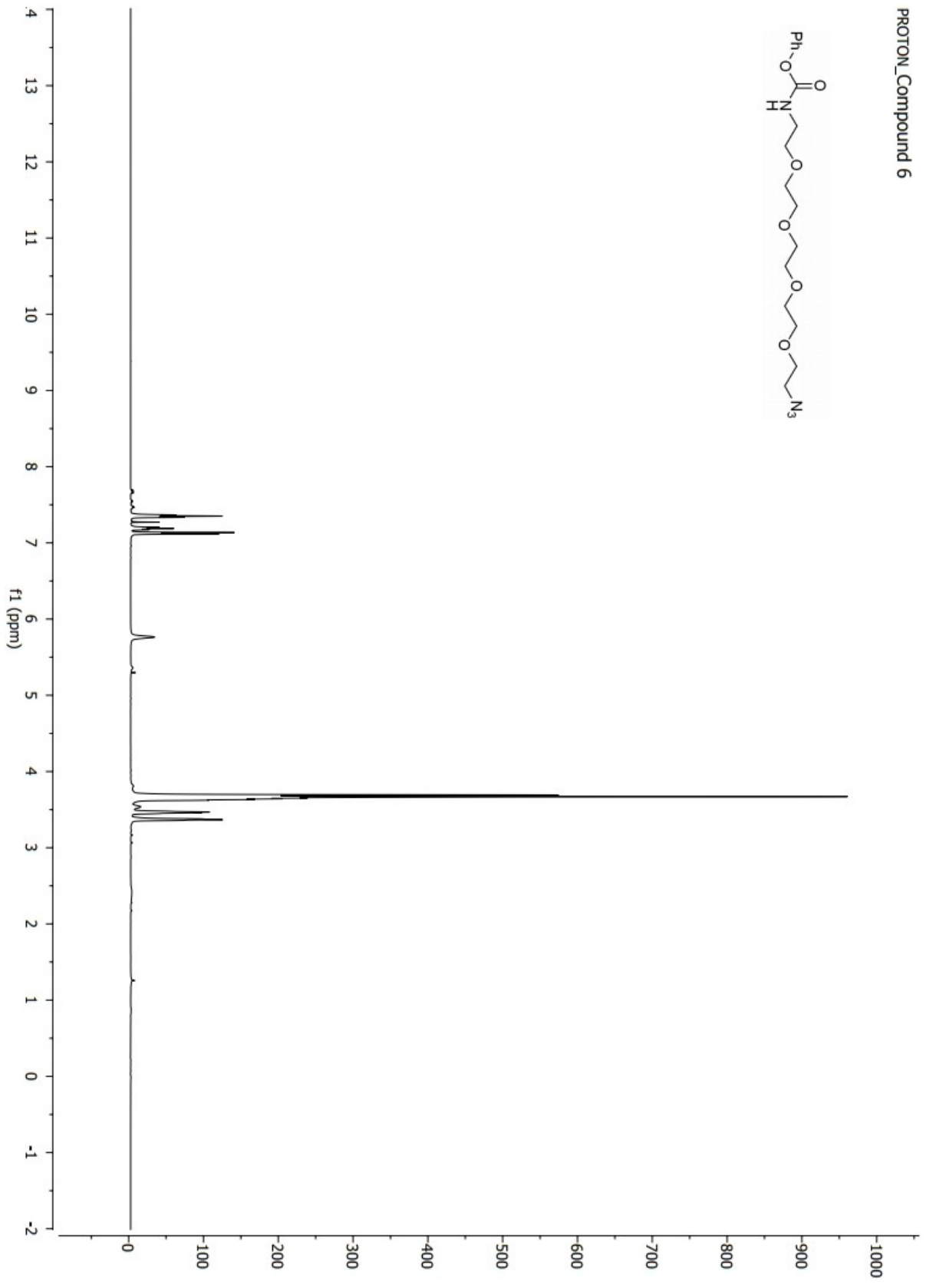
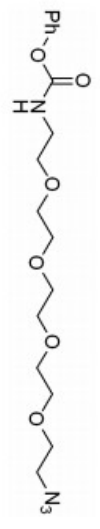
PROTON_Compound 10b



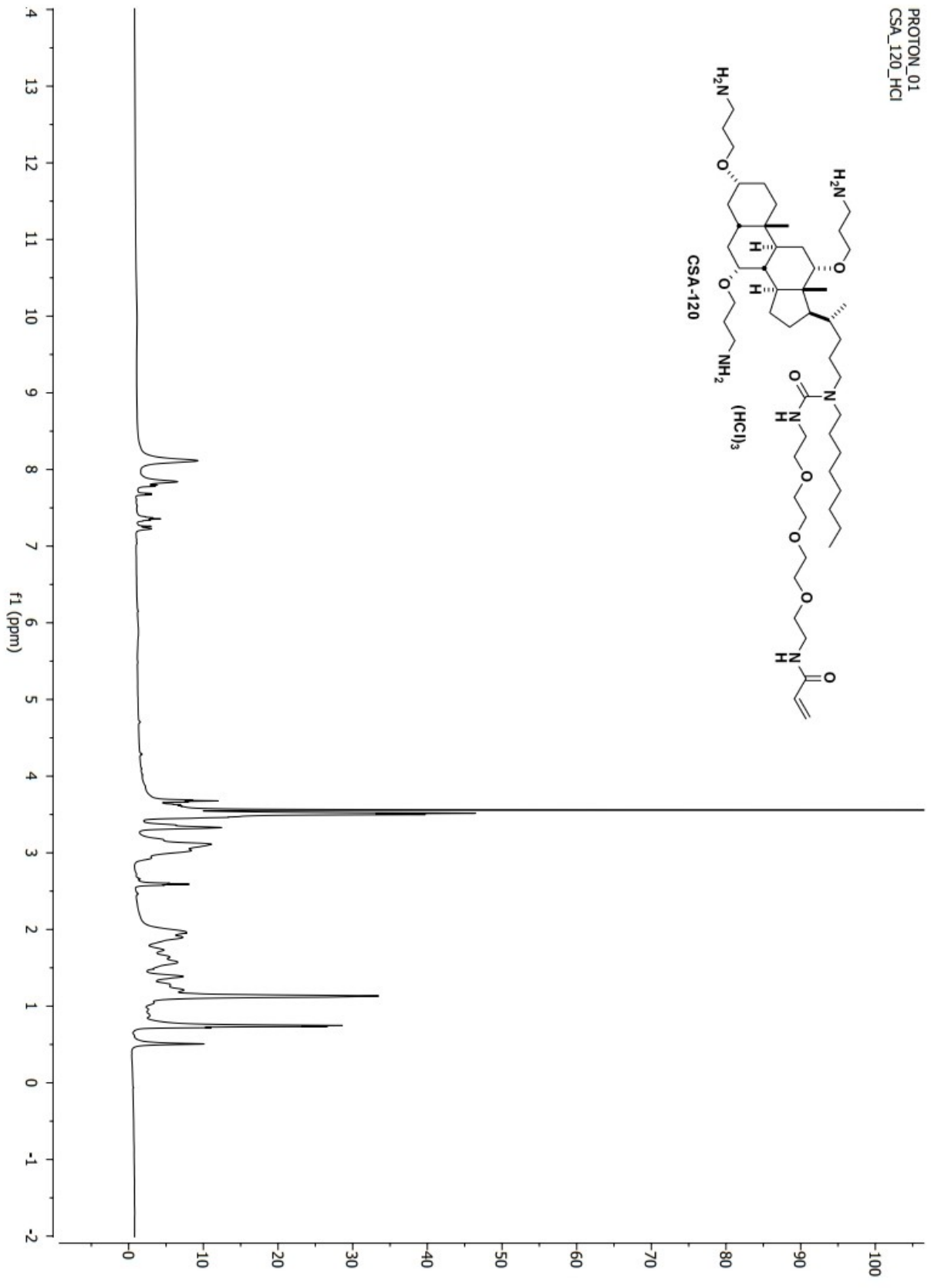
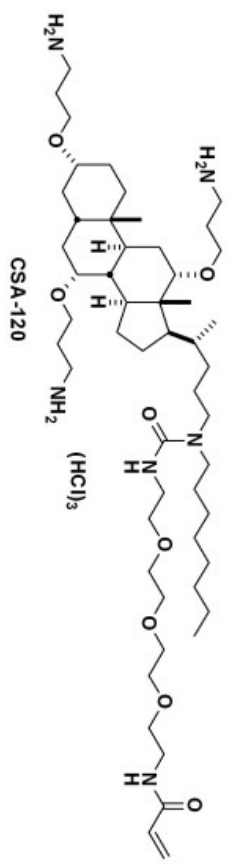
CARBON_Compound 10b



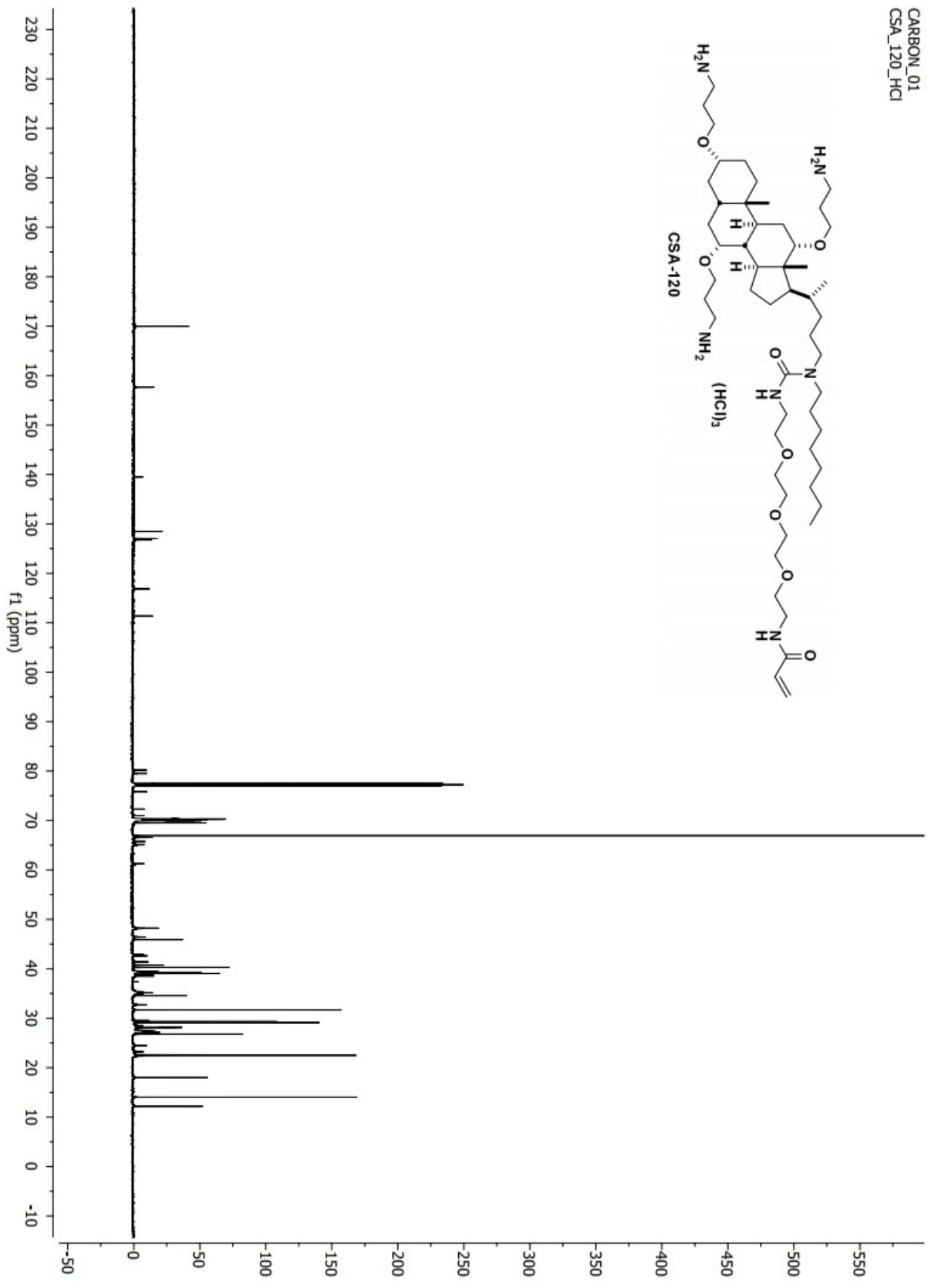
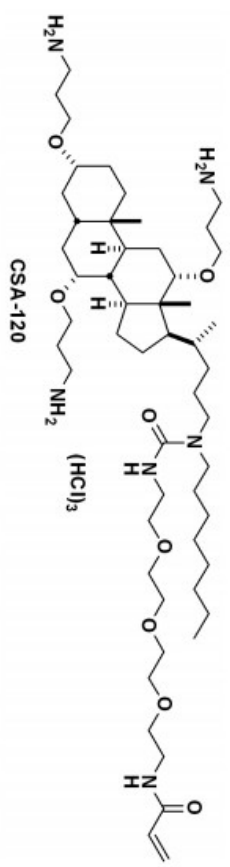
PROTON_Compound 6



PROTON_01
CSA_120_HCl



CARBON_01
CSA_120_HCl



PROTON_01
CSA_124

